THE UNIVERSITY OF MANITOBA

APPLICATION OF THE CONCEPT OF ELECTROMAGNETIC INVERSE BOUNDARY CONDITIONS TO THE PROFILE CHARACTERISTICS INVERSION OF CONDUCTING SHAPES

by

HARINDER PAL SINGH AHLUWALIA

A THESIS

SUBMITTED TO THE FACULTY OF GRADUATE STUDIES

IN PARTIAL FULFILMENT OF THE REQUIREMENTS FOR THE DEGREE

OF DOCTOR OF PHILOSOPHY

DEPARTMENT OF ELECTRICAL ENGINEERING

WINNIPEG, MANITOBA R3T 2N2

October 1973

APPLICATION OF THE CONCEPT OF ELECTROMAGNETIC INVERSE BOUNDARY CONDITIONS TO THE PROFILE CHARACTERISTICS INVERSION OF CONDUCTING SHAPES

by

Harinder Pal Singh Ahluwalia

A dissertation submitted to the Faculty of Graduate Studies of the University of Manitoba in partial fulfillment of the requirements of the degree of

DOCTOR OF PHILOSOPHY

ABSTRACT

The inverse problem of scattering, also known as profile inversion, is encountered in many areas of Science, e.g. Quantum Mechanics, Electromagnetic Theory, Geophysics, Roentgenology, etc. Regardless of the particular measurement techniques and the wavelength band, the mathematical problems encountered are similar in that they result in the inversion of associated integro-differential equations or of equivalent formulations.

In the presented study, the inverse problem of electromagnetic scattering is treated using the novel concept of inverse boundary conditions. The target characteristics of unknown two- and three-dimensional scatterers need to be determined from the knowledge of the incident and the scattered fields, given everywhere in the vicinity of the scatterer, assuming that the laws governing the interaction satisfy the Leontovich or scalar boundary conditions. The novel set of inverse boundary conditions (IBCs), resulting from the inversion of the Leontovich boundary conditions, is employed to recover the electrical size, the surface locus $S_0(\underline{r})$ and the averaged local surface impedance $\eta(\underline{r})$ directly from the total near field expressions which are assumed to be given in the Sommerfeld region so that they can be computed everywhere. Of particular importance is the cognizance that a set of exact independent necessary and not *locally* but *globally* sufficient inverse boundary conditions (IECs) exists and is required to uniquely resolve the electromagnetic inverse problem of scattering by conducting shapes.

The analysis is verified by numerical computation for cylindrical and spherical mono- and two-body configurations assuming arbitrarily polarized plane wave incidence. Coordinate transformation and analytic continuation techniques, well established for circular cylindric wave functions, are employed to recover the characteristic parameters for those regions of the scattering surface which lie within the minimum circle enclosing the scatterers. Three-dimensional analytic continuation is introduced to verify the applicability of the novel set of IBCs to the most general three-dimensional configurations. The theoretical analysis of analytic continuation and two-body scattering in two- and three-dimensions is supplemented, where particular emphasis is laid on an analysis of errors which are caused by coordinate origin displacement, series truncation, numerical quadrature and measurement uncertainty of Fourier coefficients.

The presented results demonstrate that the inversion of the conducting multibody problem can uniquely be resolved thus proving the importance of the novel *Ansatz* (IBCs) introduced to the inverse theory of electromagnetic scattering. As a by-product, the direct scattering solutions to the two-cylinder and two-sphere problems with impedance boundary conditions have been obtained. A novel truncation approach for employing vector wave functions in analytic continuation based on the concept of inverse boundary conditions has been proposed which should also be of relevance to direct scattering problems.

In essence, the hypothesis is set forth that an entirely new approach

to the general inverse problem of scattering must be undertaken in case that more than one of the many characteristics are to be determined simultaneously. Namely, the *Ansatz* of exact independent necessary not *locally* but *globally* sufficient inverse boundary conditions, whose existence has been uniquely proved for the electromagnetic case, could open up new avenues of attaining deeper insight into inverse problems in other areas of Science.

RÉSUMÉ

Le problème inverse de la diffusion se recontre dans de nombreuses disciplines scientifiques telles que la mécanique quantique, l'électromagnétisme, la géophysique, la Roentgénologie, etc... Quelles que soient le techniques de mesure et les longueurs d'onde considerées, les problèmes mathématiques rencontrés sont communs du fait qu'ils résultent d'une inversion des équations integro-différentielles associées ou de formulations équivalentes.

Dans la présente étude, le problème inverse de la diffusion électromagnétique est traité, en utilisant le nouveau concept de conditions inverses de passage. Les caractéristiques de cible de diffuseurs inconnus à deux ou trois dimensions doivent être déterminées à partir des champs incidents et diffusés connus au voisinage du diffuseur en supposant que les lois d'interaction satisfont les conditions de passage de Léontovich ou scalaires. Le nouvel ensemble de conditions de passage (IBCs), résultant de l'inversion des conditions de passage de Léontovich, est utilisé pour retrouver la dimension électrique, la forme de la surface diffusante $S_0(\underline{r})$ et la valeux moyenne locale de l'impédance de surface $\eta(\underline{r})$ directement à partir des expressions du champ proche total qui sont supposées données dans la région de Sommerfeld telles qu'elles puissent être calculées de partout. Il est trés important de noter l'existence d'un ensemble de conditions inverses de passage exactes, indépendantes et globalement (non localement) suffisantes (IBCs) qui sont nécessaires pour donner une solution

unique au problème inverse de la diffusion par corps conducteurs.

L'analyse est verifiée par calcul numérique dans le cas d'un ou deux cylindres ou sphères, en supposant une onde plane de polarisation arbitraire. Les techniques de transformation de coordonnées et la détermination analytique de proche en proche bien établies pour une fonction d'onde cylindrique circulaire sont utilisées pour retrouver les parametres caractéristiques pour les régions de la surface diffusante qui se trouvent à l'intérieur du plus petit cercle entourant les diffuseurs. Une détermination de proche en proche à trois dimensions est introduite pour vérifier l'applicabilité du nouvel ensemble de conditions de passage inverses (IBCs) au cas le plus général, celui d'une configuration à trois dimensions. L'analyse théorique du calcul de proche en proche et la diffusion par deux corps à deux ou trois dimensions est suppléée lorsque l'on attache une importance particulière à l'analyse des erreurs dues à un déplacement d'origine des coordonnées, une troncature de série, une quadrature numérique et à une mesure incertaine des coefficients des séries de Fourier.

Les résultats présentés prouvent que l'inversion du problème du conducteur multi corps a une solution unique prouvant ainsi l'importance du nouveau concept (IBCs) introduit dans la théorie inverse de la diffusion électromagnétique. En résultat secondaire, les solutions de la diffusion directe pour les problèmes des deux cylindres et des deux sphères avec une impédance aux conditions de passage, ont été obtenues. Une nouvelle approche de troncature pour utiliser une fonction

d'onde vectorielle dans la détermination de proche en proche, basée sur le concept des conditions de passage inverses a été proposée; elle serait également en rapport avec les problèmes de diffusion directe.

Par nature même, l'hypothèse est posée selon laquelle une approche entièrement nouvelle du problème inverse de la diffusion doit être engagée dans le cas où plus d'une des nombreuses caractéristiques doivent être déterminées simultanément. En particulier, le concept de conditions inverses de passage, exactes, indépendantes, nécessaires et globalement (non localement) suffisantes, dont l'existence a été démontrée être unique dans le cas de la diffusion électromagnétique, pourrait ouvrir de nouvelles voies à une meilleure approche du problème inverse de la diffusion dans d'autres domaines de la Science.

ZUSAMMENFASSUNG

Das inverse Problem der Streuung spielt in vielen, wenn nicht gar allen Fachgebieten der Naturwissenschaft eine zunehmend bedeutendere Rolle, wie z.B. in den Fachbereichen der Quantenmechanik, der elektromagnetischen Theorie, der Geophysik, der Röntgenologie, u.s.w. Wenn man von den partikulären Meßtechniken und dem Wellenlängenbereich absieht, sind die auftretenden mathematischen Probleme ähnlich, indem diese die Inversion der assoziierten Integrodifferentialgleichungen oder entsprechend gleichwertiger Ausdrücke verlangen.

In der vorliegenden Arbeit wird das inverse Problem der elektromagnetischen Streuung mittels des Ansatzes inverser Randbedingungen behandelt. Im besonderen sollen die charakteristischen Eigenschaften von zwei- und drei-dimensionalen Streukörpern von den gegebenen einfallenden und gestreuten Feldern bestimmt werden wobei vorausgesetzt wird, daß das gebeugte Feld überall bekannt ist, und daß die Randbedingungen der Leontowitsch oder skalaren Impedanzbedingung genügen. Der neue Satz von inversen Randbedingungen, der von der Inversion der Leontowitsch Bedingung abgeleitet wurde, wird angewandt um die elektrische Größe, die Oberflächengestalt $S_0(\underline{r})$, und die durchschnittliche örtliche Oberflächenimpedanz $\eta(\underline{r})$ unmittelbar vom gesamten Nahfeld zu bestimmen, das im Sommerfeldschen Bereiche als bekannt und berechenbar vorausgesetzt wurde. Von besonderer Bedeutung ist die Erkenntnis, daß ein Satz exakter, von einander unabhängiger, notwendiger und *nicht örtlich* jedoch *global genügender* inverser Randbedingungen (IBCs)

existiert und notwendig ist um das inverse Problem der elektromagnetischen Streuung von leitenden Streukörpern eindeutig zu lösen.

Die theoretische Untersuchung wird durch numerische Rechnungen für kreiszylindrische und kugelförmige Ein- und Zwei-Körperstreuung für beliebig polarisierten Planarwellen-Einfall nachgeprüft. Methoden der Koordinatentransformation und der analytischen Fortsetzung, die für kreiszylindrische Wellenfunktionen hinreichend begründet sind, werden angewandt um die charakteristischen Eigenschaften auch jener Bereiche zu bestimmen, die im kleinsten den Streukörpern umschriebenen Kreise liegen. Drei-dimensionale analytische Fortsetzung wird eingeführt um die Anwendbarkeit des neuen Satzes der inversen Randbedingungen für drei -dimensionale Streukörper allgemeiner, kontinuierlich gekrümmter Oberflächengestalt nachzuprüfen. Die theoretischen Untersuchungen der neueingeführten Methoden der zwei- und drei- dimensionalen analytischen Fortsetzung und der Mehrkörperstreuung wird durch numerische Berechnungen ergänzt. Eine Untersuchung der unvermeidlich impliziten Rechenfehler, die durch Koordinatentransformation, numerische Quadratur, Begrenzung der Reihenordnung der Vektorwellenentwicklung und durch Meßunschärfe der Fourier Koeffizienten hervorgerufen werden, wurde mit besondener Sorgfalt durchgeführt.

Die erhaltenen Ergebnisse zeigen, daß die Inversion der leitenden Mehrkörperstreuung eindeutig gelöst werden kann, was die Bedeutung des angewandten, neuen Ansatzes zum inversen Problem der elektromagnetischen Streuung vortrefflichst beweist. Weiterhin werden neue

Lösungen zum direkten Problem der Streuung von zwei kreisförmigen Zylindern und von zwei Kugeln, deren Oberflächenbeschaffenheiten die skalare Impedanzbedingungen erfüllen, angeführt. Eine neue Behandlung des Problems der impliziten Fehlerberechnung für die Anwendbarkeit von Vektorwellfunktionen wird eingeführt, die auf dem Ansatz der inversen Randbedingungen beruht und somit auch von Bedeutung für das direkte Streuungsproblem sein sollte.

Im wesentlichen wird die Hypothese aufgestellt, daß ein ganz neuer Angriff des allgemeinen inversen Problems der Streuung unternommen werden muß, falls mehr als nur eine der vielen charakteristischen Eigenschaften gleichzeitig gefunden werden soll. Nämlich, der Ansatz von exakten, von einanden unabhängigen, notwendigen, *nicht örtlich* so jedoch *global genügenden* inversen Randbedingungen, deren Existenz für den elektromagnetischen Wellenbereich eindeutig bewiesen wurde , könnte neue Wege öffnen um ein bessere Einsicht in inverse Probleme anderer Fachbereiche zu erhalten.

ACKNOWLEDGEMENTS

I wish to express my sincere gratitude to my advisor Dr. Wolfgang M. Boerner for his invaluable guidance, encouragement and interest throughout this project. The motivation for presented work arose from Dr. Boerner's work which was carried out under the supervision of Dr. V.H. Weston at the University of Michigan, Radiation Laboratory. I cannot thank my advisor enough for his willingness and enthusiasm during our many discussions and his genuine interest in his students.

I am also indebted to Dr. S.K. Sen, Dr. K.C. Kao and Dr. L. Shafai, the members of my advisory committee,for their guidance and direction during my Ph.D. program.

Special thanks are due to Professor Vaughan H. Weston who refereed this thesis and whose pioneer work in the field of inverse scattering generated the presented study.

The financial support provided by the University of Manitoba and particularly by the National Research Council of Canada in terms of an NRC Fellowship is gratefully acknowledged.

Last but not the least, I am particularly appreciative of the tireless efforts of Mrs. Shirley Clubine who readily agreed to type this material and who devoted long hours to typing; and of Ms. Adrienne Belusic for reading the manuscript.

H P S Ahluwalia

Harinder P.S. Ahluwalia

TABLE OF CONTENTS

LIST OF FIGURES

List of Figures cont.

List of Figures cont.

List of Figures cont.

LIST OF TABLES

LIST OF SYMBOLS

Unless otherwise stated, the symbols most commonly used in this thesis have the following meaning.

Greek Alphabet:

$\alpha,\beta,\theta,\theta_r,\theta_1,\theta_2,\phi_1,\phi_2$	Polar angles
$\alpha_i(m,n)$, $\beta_i(m,n)$	Translated interior expansion coefficients for TM and TE modes
$\alpha_e(m,n)$, $\beta_e(m,n)$	Translated exterior expansion coefficients for TM and TE modes
$\alpha_{mn}^{\mu\nu}$	Expansion coefficients for scalar addition theorem, defined by (5.4.5c)
α_t	Propagation constant
$\gamma(x)$	Characteristic function of the target
γ_j	Measured quantity
Γ	Reflection coefficient
$\Gamma(k)$	Defined by (1.3.7)
δ	Skin depth in the conductor
$\varepsilon_0,\varepsilon$	Permittivitty of free space and body material respectively
ε	Eccentricity, total equivalent error vector, a small number
ε_i	Defined by (4.2.9)
η	Surface impedance of scatterer
$\nabla\eta$	Spatial variation of η
κ	$= (2\omega/c)\,\hat{j}$
κ_u, κ_v	Principal curvatures

λ	Wavelength
λ_n	Eigenvalues
μ_0, μ	Permeability of free space and body material respectively
μ,ν	Summation indices
$\xi = 1/\eta$	Surface admittance
ρ	Electrical size (radius), the smallest radius of curvature
$\rho(\kappa)$	Field cross-section
σ	Conductivity, radar cross-section
ϕ_0	Coordinate translation angle
$\chi(x)$	Density function
ψ	Wave function, phase angle of surface impedance
ψ_ν $(\nu = 1,2,3,4)$	Roots of (3.4.14)
ψ_0	Root of (3.4.16)
ω	Angular frequency

Latin Alphabet (Upper Case)

A	Discrete form of operator T
$A_{mn}^{\mu\nu}$, $B_{mn}^{\mu\nu}$	Translation coefficients defined by (5.4.5a) and (5.4.5b) respectively
$A_\sigma(m,n)$, $B_\sigma(m,n)$	TM and TE scattering coefficients for sphere $\sigma = 1,2$ in the presence of $\sigma' = 2,1 \neq \sigma$
$_{ii'}A_n$ and $_{ii'}B_n$	are defined by (4.2.15) and (4.2.21)
$C(m,n)$, $D(m,n)$	Sums of translated TM coefficients $\alpha_1(m,n)$, $\alpha_2(m,n)$ and TE coefficients $\beta_1(m,n)$, $\beta_2(m,n)$ respectively

$C(\kappa)$	Aperture function
$C(x)$	Spatial distribution function
$\underline{D}$	A vector normal to the body surface
D_r^v	Defined by (1.2.6)
E	Energy of particle
$\underline{E}_i$	Incident electric field vector
$\underline{E}_s$	Scattered electric field vector
$\underline{E} = \underline{E}_i + \underline{E}_s$	Total electric field vector
$E^s_{\theta_c}$	θ - component of $\underline{E}_s$
$E^s_{\phi_c}$	ϕ - component of $\underline{E}_s$
$F(r)$	Linear combination of γ_j 's
G	Gaussian curvature
$\underline{\underline{G}}_0$	Free space dyadic Green's function
$\underline{\underline{G}}_{1s}$	Dyadic Green's function of the first kind for scattered field
$\underline{\underline{G}}_1 = \underline{\underline{G}}_0 + \underline{\underline{G}}_{1s}$	Entire Green's function
$G_j(r)$	Data kernel
$\underline{H}_i$	Incident magnetic field vector
$\underline{H}_s$	Scattered magnetic field vector
$\underline{H} = \underline{H}_i + \underline{H}_s$	Total magnetic field vector
$\underline{K}_e$	Effective magnetic surface current
$\underline{K}_m$	Effective electric surface current
K_{e_u} , K_{e_v}	u and v components of $\underline{K}_e$
K_{m_u} , K_{m_v}	u and v components of $\underline{K}_m$

$K(\hat{n})$	Gaussian curvature
$\underline{M}_{o_{mn}}$, $\underline{N}_{o_{mn}}$	Hansen's spherical vector wave functions
M	Number of digits used in expansion coefficients
N	Refractive index of the body
N	Order of truncation
N_ℓ, N_u	Lower and upper truncation bounds
Q_1	Min $\{(\underline{E}x\underline{E}^*)\cdot(\underline{E}x\underline{E}^*)\}$
Q_2	Min $\{\underline{E}\cdot\underline{H}\}$
Q_3	Min $\{\lvert E_{inc}\rvert-\lvert E_{scat}\rvert\}$
QH_1	Min$\{(\underline{H}x\underline{H}^*)\cdot(\underline{H}x\underline{H}^*)\}$
QH_2	Min $\{\underline{H}\cdot\underline{E}\}$
QH_3	Min $\{\lvert\underline{H}_{inc}\rvert-\lvert\underline{H}_{scat}\rvert\}$
R_n^m	Defined by (5.2.6)
S	Standing wave ratio
S_{P_n}	Loci of Min {Y2} or Min {Q1}
S_{q_n}	Loci of Min {Y1}
S_n^m	Defined by (5.2.6)
U_i^{TM}, V_i^{TE}	TM and TE components of scattered field potential
U_i^{tot} , V_i^{tot}	Total TM and TE field potentials respectively
V(r)	Potential energy
V, V_0	Potentials
Z_0	Intrinsic impedance of free-space

Latin Alphabet (Lower Case)

a_i	Radius of ith cylinder
$a(m,n,\mu,\nu,p)$	Coefficients of linearized expansion (A3.1)
a_{mn}, b_{mn}	TM and TE expansion coefficients
$\hat{a}_x, \hat{a}_y, \hat{a}_z$	Unit vectors in rectangular coordinate system x, y and z
$\hat{a}_r$, $\hat{a}_\theta$, $\hat{a}_\phi$	Unit vectors in spherical system r, θ and ϕ
$\hat{a}_1$, $\hat{a}'_1$, $\hat{a}_2$, $\hat{a}'_2$, $\hat{b}_2$, $\hat{b}'_2$	Unit vectors
a', b'	Principal axes of an ellipse
${}_i a_n$, ${}_i b_n$	TM and TE scattering coefficients, respectively, of cylinder i(= 1,2) in the presence of cylinder i'(= 2,1) $\neq$ i(= 1,2)
c	Velocity of light
c_n, d_n	Sums of translated coefficients ${}_1 a'_n$, ${}_2 a'_n$ and ${}_1 b'_n$, ${}_2 b'_n$ respectively
f(x)	Function to be retrieved from observed data
g(x)	Far-field pattern function
$\hat{j}$	Unit vector specifying the aspect
$k = \frac{2\pi}{\lambda}$	Wave number
$k_n^{(1)}(x) =$	$(1/x)\ \frac{d}{dx}\ [x\ h_n^{(1)}(x)]$
k(x,y)	Data kernel
l,m,n,p	Summation indices
m(r)	Property to be determined
$\hat{n}$	Outward unit normal to the scatterer

$\hat{n}_0$	Receiver direction
$\underline{p}$	A vector in the direction of receiving point
$p_1(m,n)$, $q_1(m,n)$	Multipole coefficients of the incident field
r,z	Parameters of the two-dimensional scatterer
r'	Distance between observation point and translated origin
r_a	Radius of minimum circle enclosing the body or equivalent sources
r_b	Radius of maximum circle for interior analytic continuation
r_{ab}, r_0	Coordinate translation distance
r,r_1,r_2,s	Distance between two points
u,v	Real and imaginary parts of surface impedance η
x,y	Discrete form of $f(x)$ and $g(x)$ respectively
x_1,x_2,x_3	Coordinate axes of 3-D orthogonal system

INTRODUCTION

The field of inverse scattering encompasses a variety of problems including the classic problem of target identification. Curiosity of man to perceive remote objects resulted in the invention of the telescope. The necessity to detect distant hostile objects during World War II was responsible for the rapid development of radar at a pace which never ceases to amaze those who work in this field. In the period of a few years radar technology was brought from a laboratory concept to a mature discipline resulting in equipment which has had a significant effect on the past defense research work. The sophistication of some of the radar systems is such that in addition to their conventional functions they can be used for estimating target shape. With the advent of Doppler-radar, sonar operated systems, Fourier optics and aperture synthesis, it is now possible to localize and attain a good resolution of otherwise remote objects.

Barton [11], who analysed radar returns from Sputnik II, was the first to report successful shape estimate. Since the military has been impressed by the possibility of building practical shape estimating radar systems, most of the work in this field is classified. However, Brindley [29] has disclosed some of the results of the United States Air Force manual radar signature analysis program. Bates [15] has discussed the question regarding what constitutes the minimum radar system with which meaningful estimates can be made of the shape of any artificial satellite which has not been designed either to cooperate with

or to confuse the radar system.

There has been a very limited activity in the field of inverse scattering in electromagnetics, which is directed towards the goal of target identification. No one has yet succeeded in determining the actual shape, size and the material constituents of remote objects. Part of the reason for the slow development in inverse scattering is the complexity of the problem which involves very accurate measurements of the far field. Many scientists are not yet convinced about the uniqueness of the solution, which might be obtained by inverting measured data. Taking all these problems into consideration, any contribution to this field will be of great help in achieving the ultimate goal of practical target identification.

With this aim in mind the inverse scattering problem has been treated in this work using the concept of inverse scattering boundary conditions for the profile characteristics inversion of perfectly and imperfectly conducting shapes. Starting with simple canonical shapes, viz, cylinder and sphere, it has been shown how the method can be extended to the more complicated two-body cases which assimilate general curved bodies. To recover the em fields in the cavity regions, analytic continuation methods have been employed. It is shown how the concept of profile inversion can be exploited to study the truncation errors in field expansions.

chapter one

SURVEY OF LITERATURE

1.1 THE PROBLEM OF PROFILE INVERSION

Profile inversion is a very generalized concept. In many areas of physical science, fundamental functions that define or describe a physical medium are computed from experimental data through a differential equation and the reconstruction of the basic function or some of its properties constitutes the general class of inverse problems. In other words, the study of inverse problems consists in the development of mathematical techniques to obtain information on the cause of scattering from the parameters that are measured in a scattering experiment. The direct scattering problem of any kind is defined as the problem of predicting the scattered quantities given the incident quantities, the relevant description of the scatterer and given the appropriate laws governing the interaction. The direct problem is normally more amenable to solution than the inverse problem due to the absence of both data limitations and experimental errors in the former. In most inversion problems it is important to deduce the spatial variation (radial height etc.) of the fundamental function from the experimental data, hence the inclusion of the term profile. The inverse problem is encountered in many disciplines of science and engineering and a comprehensive treatment of the problem in various fields is given in Ref.[89]. Since similar techniques may apply to various fields, it is considered worth-while to give a brief account of inverse problems in the related fields.

1.2 INVERSE PROBLEMS IN RELATED FIELDS

1.2.1 INVERSE PROBLEM IN QUANTUM MECHANICS

In the framework of quantum mechanics major attention has been given to the case of non-relativistic particle interacting via a potential, with a scattering center or equivalently, that of two particles interacting through a potential depending on their relative distance. It is well known in quantum mechanics that the scattering of particles by a potential field is completely determined by the asymptotic form of the wave functions at infinity. In accordance with Heisenberg's idea it is precisely the asymptotic behavior of the wave functions that has physical meaning[1]. The question therefore naturally arises as to whether it is possible to reconstruct the potential from the knowledge of the wave function at infinity [1,42,90,104]. In general, the problem is more complex and difficult than those in the other disciplines.

The scattering of spinless particles is described by the time independent Schrödinger equation which in appropriate units reads

$$[-\nabla^2 + V(r)]\psi = E\psi \qquad (1.2.1)$$

Where ∇^2 is Laplace's operator in three dimensions, E is the energy of the particle and V(r) is the potential energy assumed to be spherically symmetric and rapidly decreasing to zero at large r. Ref.[90]

Now the transformation kernel may be obtained through a fundamental integral equation

$$K(V, V_0, r, r') = f(V, V_0, r, r') - \int_0^r K(V, V_0, r, \rho)\, f(V, V_0, \rho, r')\rho^{-2} d\rho \qquad (1.2.7)$$

obtained by analogy with the Gelfand-Levitan equation. Therefore, the inverse problem is completely solved when $f(V, V_0, r, r')$ is known. For description of other methods, e.g. JWKB method, Newton-Sabatier method etc., review papers[104, 89] may be consulted.

1.2.2 GEOPHYSICAL INVERSE PROBLEM

The geophysical inverse problem is concerned with the inversion of seismic data to obtain profiles of parameters which describe the earth's interior (e.g. permeability or conductivity of earth's crust). Suppose we have made measurements of the magnetic field of the earth. What does this tell us about the magnetization of surface rocks? Or given a set of normal mode frequencies (the frequencies of free oscillation of the earth observed after the largest earth quake), we will like to find the density and seismic velocities as a function of radius.

The most general theory for handling seismological inverse problems is the Backus and Gilbert method [5,6,7] which starts with the following general equation [94]

$$\gamma_j = \int_0^a m(r)\, G_j(r)\, dr \qquad j = 1, 2, \ldots N \qquad (1.2.8)$$

where $m(r)$ is the property and $G_j(r)$ is called the data kernel, one for each observation γ_j which are first assumed to be error-free. In order to localize the information to points within the earth, Backus and Gilbert use a linear combination of γ_j's to obtain the following final expression

$$L = \int_0^a F(r)\, m(r)\, dr \qquad (1.2.9)$$

If $F(r)$ can be chosen as a Dirac-delta function centered at r_o, then L would simply be $m(r_o)$, i.e. the property we want at the position r_o. Backus and Gilbert's theory provides information about the uncertainty in the models developed and also supplies a method of carrying out adjustments to the model of the conductivity structure to systematically bring the calculated response into satisfactory agreement with the observed data, rather than having to rely on inspired guess work.

Bailey[8] found a direct method whereby the conductivity structure is reproduced from em data through the solution of a nonlinear integro-differential equation which requires precise data on a continuum of frequencies from zero to infinity. Although Bailey's method is impractical, it presents an important uniqueness proof and thus has provided the assurance that, in general, the true conductivity structure of the earth's crust can be recovered from geomagnetic variations. Starting from data given by Banks [9], a new conductivity structure was derived by Parker [95] who also studied its uniqueness. He

generalized a procedure derived by Banks and applied his cross-spectral techniques making a considerable contribution to the geophysical inverse problem. Though the Backus-Gilbert theory can be generalized for non-linear problems as well [95], the Monte Carlo technique [145] is often used for this case.

1.2.3 PASSIVE ATMOSPHERIC SOUNDING

Inverse problems are also encountered in passive atmospheric sounding. In this case measurement of the emitted terrestrial (planetary) or reflected solar radiation is made as a function of wavelength (visible, ultraviolet, infra-red), look angle and atmospheric optical depth using ground based airborne or space borne systems. The data thus obtained is inverted to yield the vertical structure of several atmospheric parameters, including temperature, ozone, water vapor and trace constituents. Like other inversion problems the difficulties are both mathematically and numerically oriented and the ultimate choice of the best method for a particular application may not be based on accuracy but is restricted normally by available resources, quantity of experimental data, and *a priori* knowledge [72, 99].

1.2.4 ACTIVE RADAR SOUNDING

In contrast to the passive sounding techniques, active sounding is concerned with measurement of reflected and/or scattered radiation from the atmosphere arising from man-made probing sources i.e. active

radar experiments [35, 73]. Both monostatic and bistatic configurations with pulse and continuous wave techniques are in use as well as acoustic and electromagnetic radars. The data are inverted to yield vertical profiles of wind speed and direction, turbulence, precipitation, refractive index structure, particulate concentrations and gaseous molecule concentrations. Active remote sounding is a rapidly growing research field and great technological advances leading to sophisticated sounding techniques have been made in recent years.

Active radar sounding, both monostatic and bistatic, but at wavelengths such that the probing signals are negligibly affected by the atmosphere but are reflected by the ionosphere, is used for the study of the structure of ionospheric layers. Pulse or amplitude sounding of the ionosphere are employed, i.e. only the time delay characteristics of the radar echoes are used [56,96,74]. More sophisticated techniques using e.g. phase, direction of arrival or polarization have appeared in the literature but have not found extensive application [73].

1.3 INVERSE PROBLEMS IN E.M. THEORY

1.3.1 TRANSMISSION LINE THEORY

In transmission line theory inverse scattering is distinguished by its one-dimensional character and the fact that the waves propagate along the line in two directions from left to right and from right to left. In a lossless case the transmission line equations can be

written as

$$\frac{dV}{dZ} = i\omega L(Z)I \qquad (1.3.1)$$

$$\frac{dI}{dZ} = i\omega C(Z)V \qquad (1.3.2)$$

If $r(\omega)$ and $\rho(\omega)$ represent the left and right amplitude reflection coefficients, and $t(\omega)$ and $\tau(\omega)$ the corresponding transmission coefficients, then a matrix of these four coefficients is called the scattering matrix for the system. In the inverse scattering problem some part of the scattering matrix, usually the reflection coefficient $r(\omega)$, is given and $L(Z)$ and $C(Z)$ or their equivalents are required to be determined [46, 61]. Techniques used are those developed in quantum mechanics with slight modification [89].

1.3.2 TARGET IDENTIFICATION

The inverse scattering problem which we are interested in pertains to recovering the relavent quantities (e.g. material constituents and the shape) describing the scatterer, from the given incident field and measured scattered field, when the laws (e.g. Maxwell's equations) governing the interaction are assumed to be known. The study also involves the determination of whether this problem is uniquely solvable for incomplete input data, e.g. various permutations of incomplete bistatic aspect angles, incomplete monostatic aspect angles, incomplete frequency, monochromatic data only, incomplete polarization matrix, amplitude data only, and scattered far field data only. Also of

interest is the inverse scattering problem for which there is some *a priori* information about the scatterer such as, the conductivity of the scatterer is infinite or that the geometry of the problem is of axial symmetry.

1.3.3 Solution of Inverse Scattering Problem

The scattered magnetic field at a point can be written as [4]

$$\underline{H}_s \Big|_p = \frac{1}{4\pi} \iint_S (\hat{n} \times \underline{H}) \times \nabla \left(\frac{e^{-jkr}}{r} \right) dA \qquad (1.3.3)$$

and its far field approximation can be written as

$$\underline{H}_s = \frac{jk}{4\pi r_1} e^{-jkr_1} \iint_S [(\hat{n} \times \underline{H}) \times \hat{a}_1] \, e^{-jk(\underline{\rho} \cdot \hat{a}_1)} dA \qquad (1.3.4)$$

where the symbols used are explained in Fig.1.1.

The exact solution of the inverse problem would be obtained if (1.3.3) can be inverted. But,let alone equation (1.3.3), even the solution to equation (1.3.4) has not been carried out conclusively. The inversion techniques described in the literature concern physical optics and geometric optics [39],subject in both cases to severe restrictions.

In their introductory notes related to em inverse scattering, Altman et al [4] consider the following three cases:

(1) If the body is known to be flat and if the scattered field falls within a small solid angle, then the body shape may be related to the two-dimensional Fourier transform of the scattered field as a function of angle.

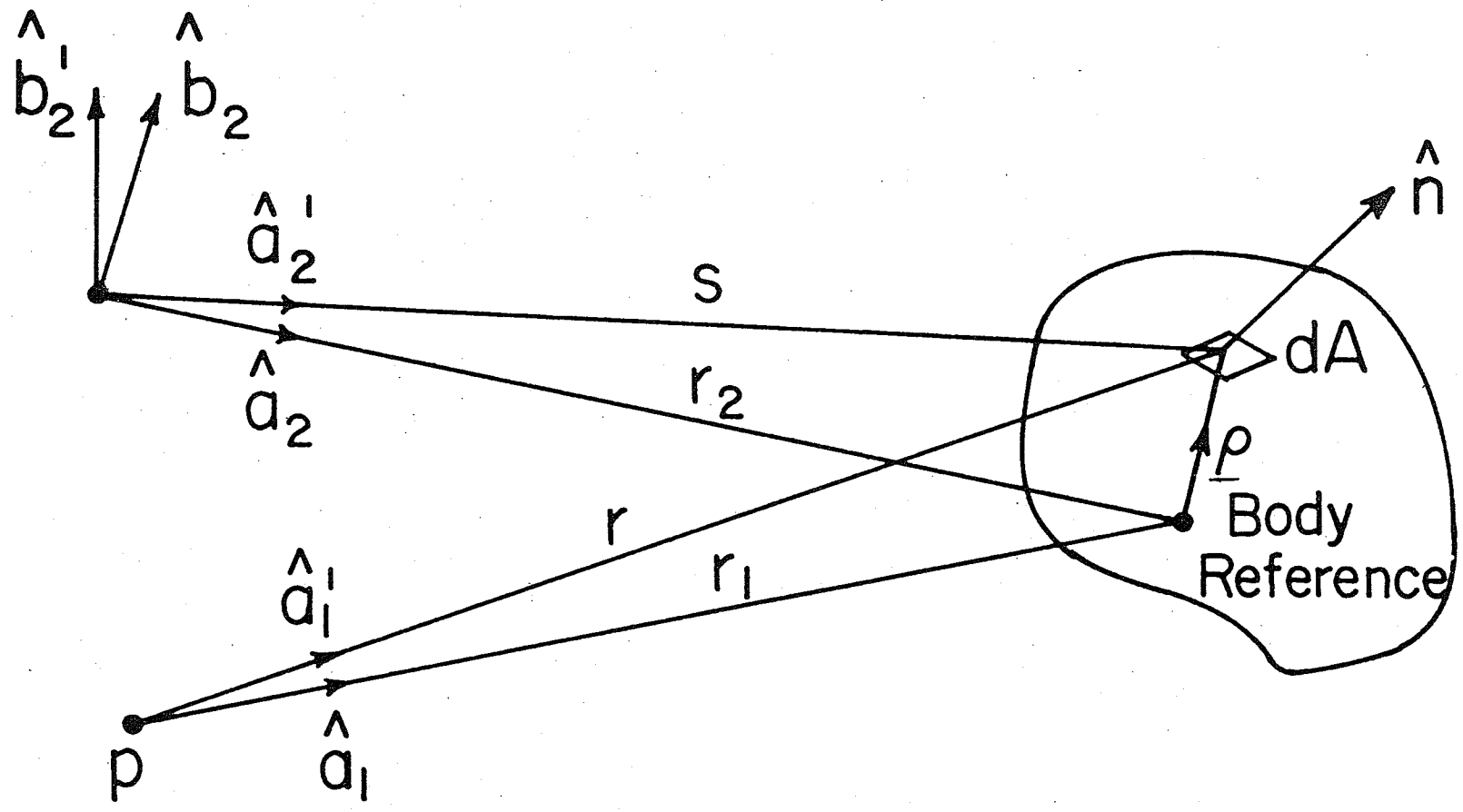

Fig. I.I Bistatic Symbols and Reference Directions.

Starting from the physical optics approximation, which assumes that for a perfectly conducting scatterer the current on the illuminated portion of the scatterer is $2n \times \underline{H}^i$ and on the shadow side it is zero, they show that the form function is the Fourier transform of the scattered field. The result is applicable only to singly-curved surfaces.

(2) If the target is known to be a doubly-curved convex body of revolution whose axis of symmetry has been determined in space, then the generatix of the body surface may be obtained from the radar cross-section as a function of the aspect angle.

(3) If the body is known to be a singly-curved body of revolution whose axis of symmetry has been determined in space, then the body surface may be determined by the application of the stationary phase method for the azimuthal direction and the Fourier transform method for the longitudinal direction.

No numerical verification for the above methods has been encountered. The basic principles of various methods are discussed below.

1.3.4 PHYSICAL OPTICS INVERSE SCATTERING

A general three-dimensional electromagnetic vector inverse identity based on the physical optics approximation [27] has been developed by Bojarski [19 , 20]. It states that if $\gamma(x)$ is the characteristic function of the target (i.e. $\gamma = 1$ inside the target and $\gamma = 0$ outside) and $\Gamma(\kappa)$ can be obtained by measurement of the back-scattered em far field at a frequency $\omega = (c/Z)|\kappa|$, then $\gamma(x)$ and $\Gamma(\kappa)$ are

a Fourier transform pair where $\kappa = (2\omega/c)\hat{j}$, ω is the frequency, $\hat{j}$ is a unit vector specifying the aspect. The identity can be expressed as

$$\gamma(x) = \frac{1}{(2\pi)^3} \int_{-\infty}^{\infty} e^{i\kappa x}\, \Gamma(\kappa)\, d^3\kappa \qquad (1.3.5)$$

or

$$\gamma(x) = \frac{1}{2\pi^{5/2}} R_e \int_{-\infty}^{\infty} e^{i\kappa x}\, \frac{\rho(\kappa)}{\kappa^2}\, d^3\kappa \qquad (1.3.6)$$

with

$$\Gamma(\kappa) = \sqrt{4\pi}\ \frac{\rho(\kappa)+\rho^*(-\kappa)}{\kappa^2} \qquad (1.3.7)$$

which clearly requires complete scattering information, namely knowledge of $\rho(\kappa)$ over all κ space, i.e. all frequencies and all aspect angles.

In actual practice $\rho(\kappa)$ is known only for an incomplete finite portion of the κ space, viz, a κ-space aperture consisting of a limited (finite) frequency band. For this situation the three-dimensional inverse problem can be reduced to the three-dimensional non-singular convolution integral equation (a Fredholm IE of the first kind)[19, 20],

$$a(x) * \gamma(x) = g(x) \qquad (1.3.8)$$

where

$$g(x) = \frac{1}{(2\pi)^3} \int_C e^{i\kappa x}\, \Gamma(\kappa)\, \omega(\kappa)\, d^3\kappa \qquad (1.3.9)$$

$a(x)$ is the Fourier transform of $A(\kappa)$ defined as

$$A(\kappa) = C(\kappa)\, \omega(\kappa) \qquad (1.3.10)$$

with aperture function $C(\kappa) = \begin{cases} 1 & \text{for } \kappa \text{ for which } \Gamma(\kappa) \text{ is known} \\ 0 & \text{if } \Gamma(\kappa) \text{ is not known} \end{cases}$

and $\omega(\kappa)$ is the aperture function subject to the condition

$$\int_{-\infty}^{\infty} |A(\kappa)| \, d^3\kappa < \infty \qquad (1.3.11)$$

The integral equation (1.3.10) can be solved numerically by a variety of existing techniques. Several closed-form solutions of this equation for apertures of specific geometry have been obtained by Lewis [67,68] and Bojarski [19]. Bojarski [19] also shows that a three-dimensional density plot of $\chi(x)$ represents the smeared geometrical image of the surface of the scatterer, the spatial extent of the smearing being the spatial extent, $C(x)$ - the resolution. This method alleviates all the objections to the so called radar imaging technique by the application of em inverse scattering theory, based on direct scattering theory (and not based on the heuristic model of a spatially extended scatterer as a fictitious ensemble of identifiable, stationary, non-interactive, non-dispersive, isotropic point scatterers). It therefore avoids the problems of converting radar images to geometrical images by side stepping and avoiding the radar image altogether and addressing itself to the problem of generating actual geometrical images directly from the radar data.

1.3.5 GEOMETRIC OPTICS INVERSE SCATTERING

This method is based on the inversion of the geometric optics radar

cross section equation given by [63],

$$\sigma(\theta,\phi) = \frac{R(\theta/2)}{4G(\theta/2,\phi)} \tag{1.3.12}$$

where σ is the radar scattering cross section, R is the energy reflection coefficient and G is the gaussian curvature. For a perfectly conducting scatterer the monostatic radar cross section is given by [130]

$$\sigma(u) = \pi G^{-1}(u) \tag{1.3.13}$$

where u describes the direction of the incident plane wave. The gaussian curvature G(u) at the specular point is given by

$$G^{-1}(u) = \frac{r[1+(dr/dZ)^2]^2}{d^2r/dZ^2} \tag{1.3.14}$$

Weiss[130]obtains the following two parametric equations which are also derived in [4] and [63], [Fig. 1.2]

$$r(u) = \{ \frac{1}{\pi} \int_0^u \sigma(u) \sin 2u \, du \}^{1/2} \tag{1.3.15}$$

$$Z(u) = \frac{1}{\pi} \int_0^u \frac{\sigma(u)}{r(u)} \sin^2 u \, du \tag{1.3.16}$$

Keller [63] treats various cases, e.g. 1) two-dimensional case with an incident field due to a line source, 2) a three-dimensional case of a reflecting surface of revolution with a plane wave incident along the axis of revolution or with a point source located on the axis. The results obtained for these cases are tabulated in Keller's paper[63]. The general case of arbitrary smooth convex closed surface in three-

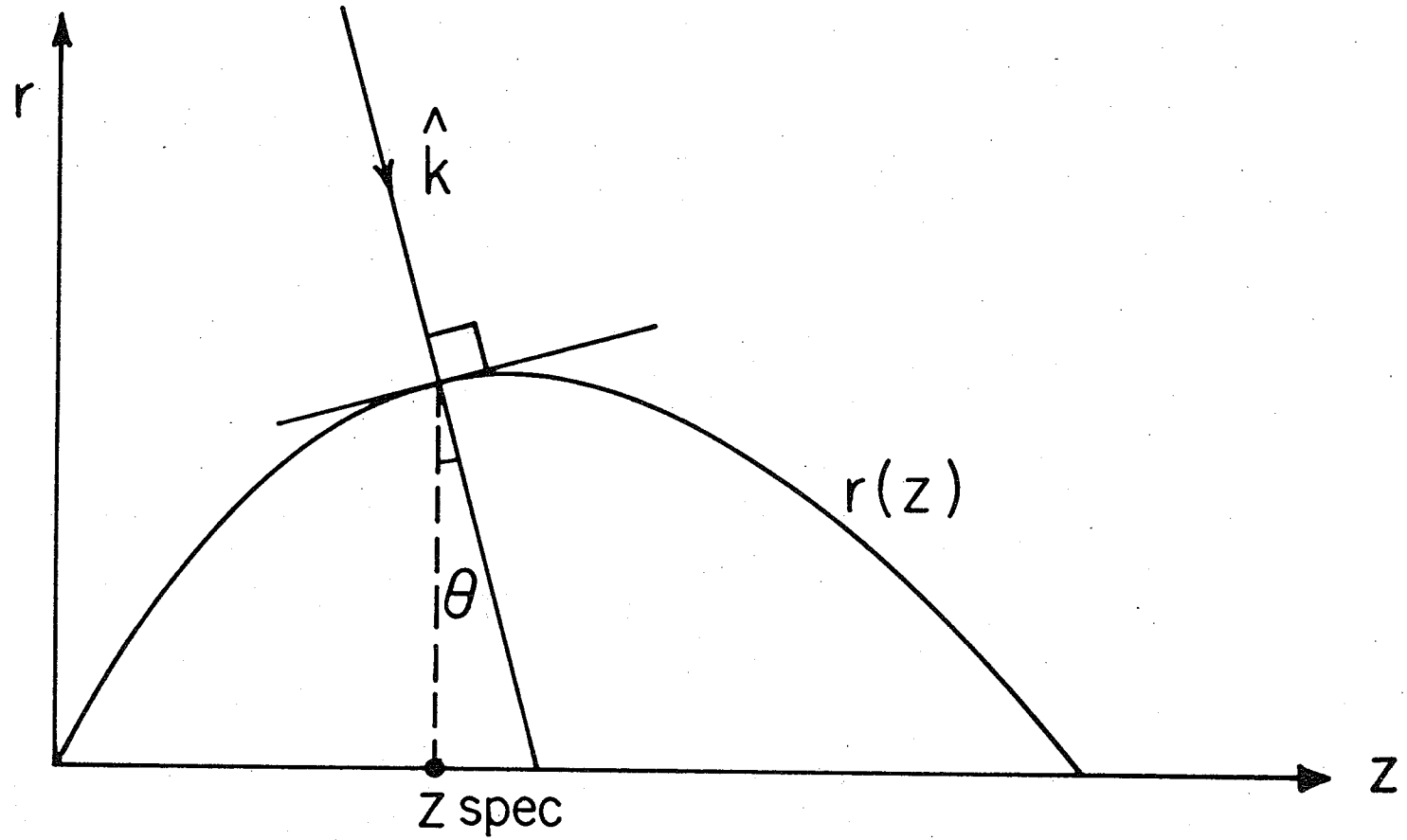

Fig. I.2 Geometric Optics inverse scattering geometry.

dimensional space is reduced to Minkowski's problem and it is shown that the data provided by equation (1.3.12) do not suffice to determine the shape of the reflector nor any part of it. But if two functions $\sigma_+(\theta,\phi)$ and $\sigma_-(\theta,\phi)$ are given, corresponding to two incident waves coming from opposite directions and if R is also known, then (1.3.12) determines G over the complete Minkowski's sphere and the inverse problem has a unique solution [91].

Weiss [130] applies equations (1.3.15) and (1.3.16) to a number of axi-symmetric bodies (e.g. prolate and oblate spheroids, cone, cylinder with a circular cap) for which exact cross-section results are available. Results presented in that paper are designed to demonstrate the bounds on size and shape which can be determined. The correct shape tends to be closer to the vertical polarization result (smaller of the radar cross section results) and this polarization difference is more pronounced for lower ka values ($ka = 5$). Doubly-curved bodies of size $k\ell \geq 2.5$ can be determined fairly accurately by this technique. Though the direct scattering equation (1.3.13) does not apply to the case of a singly curved body (because of the zero gaussian curvature the geometric optics result predicts an infinite radar cross section), the results indicate that a large class of such bodies can be quite accurately inverted. The reason for this apparent anomaly is that the inverse procedure involves the integral of the radar cross section. Therefore, this singularity is removed.

Geometrical optics approach has also been used by Vandenberghe and

Boerner [121]. Their approach is based on the fact that smooth and convex shaped scatterers of identical curvature about the monostatic direction give rise to identical far scattered field magnitude in the high frequency case. They developed an iterative averaging procedure with the intent to recover unknown local radii of curvature of remote scatterers about the specular point which are in fair agreement with exact values for elliptical cylindrical scatterers employed by them for computation. Since the knowledge of the near field and its phase is not required, the method is very useful for practical application. It should, however, be pointed out here that for curve-fitting, some additional information on the relative phase differences between only the monostatic directions of various measurement domains must also be recovered. Furthermore, the method is applicable only in the high frequency case.

1.4 APPLICATION OF PULSE TECHNIQUES FOR TARGET IDENTIFICATION

Since more information may be obtained by transient analysis than from steady state results, pulse techniques offer a convenient method for target identification. The behavior of the leading wavefront of a scattered pulse usually contains information about the composition of the body, whereas the behavior of the trailing return of a scattered pulse is related to the shape of the body and its radii of curvature.

Freedman shows [44] that if a body is illuminated by a modulated pulsed wave, the directly scattered radiation at a field point in the

lit region is composed of a number of discrete signals. These components are generated by certain discontinuities associated with the projection of the scattering body, with their magnitude proportional to the discontinuity size and phase depending on the total associated path. Weston et al [135] point out the necessity of using short pulse measurements to separate out the signals from the various scattering centers. They investigate the use of short pulse data to determine the properties of uniformly coated conducting bodies where the main attention is paid to the illuminated portion of smooth, convex bodies at high frequencies.

Kennaugh and Moffat [64] suggest that the impulse response waveform of a target is a concept that replaces sets of numbers for a target by a useful characteristic function. This function is simple in form, related to the geometrical properties of the target and permits extrapolation to new configurations. Furthermore, knowing this function only approximately for a target, it is possible to predict the reflectivity as a function of frequency or signal waveform. They illustrate the nature and utility of impulse response waveforms for specific cases. Pulse techniques are also studied in some of the papers (e.g. [150,151]) in a special issue of the Proceedings of the IEEE on 'Radar Reflectivity' (August, 1965) and in [152].

Various other papers based on pulse response methods are reviewed by Vandenberghe in [122] where he also cites signature comparison methods used by Defence Departments and scattering matrix measurement techniques.

He also mentions the case in which the scattering geometry is non-stationary. In this case, the translatory vector, giving the direction of spinning, a vector determining spinning rate and a third vector, outlining the direction and rate of tumbling, have to be specified in terms of a stationary fixed time space reference system [4].

Graf investigates the relationship between the Doppler frequency spectrum and the structure of a rotating body in a recent report [47]. He shows that analysis of the intensities in the Doppler frequency [37] spectra permits conclusions to be drawn on the shape of the body. By appropriately processing the complex Doppler spectra, it is possible to get a highly resolved image of the object as seen from the direction of the axis of rotation. Both the procedures are treated theoretically and are confirmed by experiments with microwaves of 3.2 cm wavelength.

1.5 EXACT SOLUTION OF ELECTROMAGNETIC INVERSE PROBLEMS

In contrast with the approximate methods of previous sections which employ either geometric or physical optics approximations, the exact methods are based on a rigorous treatment of Maxwell's equations. A series of technical reports on inverse scattering have been published by Weston and his associates at the University of Michigan. In [139], they introudce the concept of equivalent sources originally analysed by Saunders [105], Weyl [143], Wilcox [146] and Müller [85,86] for vector and scalar cases. The concept of equivalent sources pertains to

the assumption that the scattered field may be thought of as arising from a set of equivalent sources on or within the body if the surface of the body is infinitely differentiable; and is important in the inverse scattering studies since the radii of the minimum convex surface which encloses the equivalent sources is related to the convergence of any expansion technique utilized to derive the near scattered field of the target from the observed far field. As Weston points out [134], from a practical stand point, when a finite set of measurements is made, the scattered field has to be approximated by a finite sum, and the knowledge of the domain of convergence is important for estimating the errors in the scattered field in the vicinity of the surface. This was ignored by Bates [14] when he assumed that the absolute value of the sum of an infinite series of terms of order ε was less than ε, where ε is a small parameter. Weston et al[139] also show that the plane wave representation converges part way inside smooth, convex portions of the body, thus establishing the concept that the minimum convex shape enclosing the equivalent sources often may be inside the actual scattering body. For non-magnetic and imperfectly conducting bodies, it is shown that the exact total field inside the body could be represented in terms of the plane wave expansion involving the far field quantities. This representation involves an appropriate split up of the far field data and a fundamental problem still exists to uniquely determine the split up from the knowledge of the far field data alone. This indicates the need of additional information, perhaps the knowledge of the complete scattering matrix for all frequencies. The boundary condition $\underline{E} \times \underline{E}^{*} = 0$, which is applicable

for the case of perfectly conducting bodies, is introduced. They also suggest the use of the monostatic bistatic theorem due to Kell to determine the material characterisitcs of the scatterer. Kell's theorem[62]states that for sufficiently smooth bodies, the bistatic cross section for the transmitter direction $\underline{k}$ and receiver direction $\hat{n}_0$ is equal to the monostatic cross section for the transmitter-receiver direction $(\underline{k} + \hat{n}_0)$ with $\underline{k} \neq 0$ in the limit of vanishing wavelengths. It is shown that two polarization measurements of the cross-section at one non-zero bistatic angle (back-scattering) determines the reactive surface impedance $\eta = u + iv$, apart from the sign of the imaginary part, where such surfaces would correspond to poor conductors or absorber-coated conductors. However, the case where the ratio of the bistatic monostatic cross-section is unity for both polarizations, only yields $u = 0$. The method has not been verified numerically and no estimate of accuracy for the value of η is given.

An inversion technique which reproduces the radial variation of the dielectric constant in a dielectric target from its microwave scattering pattern is presented by Fedotowsky et al [43]. The numerical feasibility of this method has been illustrated by applying it to experimentally measured scattering patterns. They have developed inversion criteria which show that details in a target, much smaller than the wavelength, cannot be reproduced.

As relates to the general inverse problem of em diffraction, another relevant inverse identity, derived by Weston and Boerner [136,137]

and based on an integral equation given by Barrar and Dolph [10], must be mentioned. This inverse identity proves that the total field produced by a plane wave incident upon a scattering object can be expressed at all points in space as the sum of the incident field and the Fourier transform of a quantity which is related to the scattering matrix requiring data over the entire frequency range and can be written as

$$E(\underline{x},\underline{k}) = E_i(\underline{x},\underline{k}) + \frac{1}{(2\pi)^{3/2}} \int_{-\infty}^{\infty} \frac{e^{j\underline{p}\cdot\underline{x}}}{p^2-k^2} \overleftrightarrow{T}(\underline{p},\underline{k})\cdot d\underline{p} \qquad (1.4.1)$$

where $-\infty < \underline{p} < \infty$, $\underline{k}$ represents the direction of the incident wave and $\overleftrightarrow{T}(\underline{p},\underline{k})$ is a measurable function proportional to the far scattered field in the direction $\underline{p}$ related to the scattering matrix. It should be noted that Weston's identity is general, i.e. holds also for the conducting case. Furthermore, the obtained results lend themselves to the construction of synthetic Fourier transform holograms [80],[113] and thus may open up new avenues of attacking the inverse problem of em scattering. A similar identity was earlier derived by Moses [83].

The inverse boundary condition $\underline{E} \times \underline{E}^* = 0$ was verified numerically in [137], where spheres of different radii were identified with an additional boundary condition $|\underline{E}_i| - |\underline{E}_s| = 0$ which is based on the physical optics approximation. It is proved that $\underline{E} \times \underline{E}^* = 0$ is a necessary but not sufficient condition, but the physical optics condition ($|\underline{E}_i| - |\underline{E}_s| = 0$) is a necessary and sufficient condition, though it is valid only in the limit of high frequency. Their results

also indicate that it is possible to determine those portions of the prolate spheroid which lie within the minimum sphere enclosing the body but outside the sphere enclosing the equivalent sources. Imbriale and Mittra [54, 55] also demonstrate that the knowledge of the incident field and the scattered far fields, at one frequency, is sufficient to determine the size, shape and location of a perfectly conducting scatterer. The natural boundary condition for a perfectly conducting body (i.e. the tangential electric field component is zero) is used to determine closed surfaces. Methods of analytic continuation for the two-dimensional case are used to obtain exterior and interior expansions in order to determine convex as well as concave portions of the scatterer. They reconstruct circular and elliptic cylinders, strips and two cylinders. Though the method represents a useful analytic continuation technique for the two-dimensional case, the reconstructed surfaces for the treated cases do not match very well with the targets used, except for the case of a circular cylinder. They also touch upon the subject of determining the scatterer when the far field pattern is known in a limited sector. The mean square error is minimized between the observed values and its series representation by using Rosenbrock's rotating coordinate system method [100]. Effects of noise in the far field on reconstruction of the targets is demonstrated by introducing different levels of noise (error) in the calculated coefficients.

The question as to what information about the body can be recovered, if the scattering matrix (phase and amplitude) is known only over an angular sector and is measured in the far field is studied by Weston

and Boerner in [136]. Employing spherical vector wave functions, they show that the near field representation can be determined by matrix inversion for rotationally symmetric scatterers with end-on incidence. The recovery process involves instability and a definite loss of accuracy because of inversion of a matrix to recover the coefficients. This problem has been studied in some detail by Boerner and Vandenberghe for rotationally symmetric bodies [25,26]. They show that for the spherical case the optimum distribution for the polar θ dependence of the N measurement aspect angles involved in the associated determinant is given by the N zeros of the optimization function [25]

$$O_N^m(U_r) = \frac{1}{(1-U_r^2)^{\frac{m-1}{2}}} P_{N+m-1}^{m-1}(U_r) \qquad (1.4.2)$$

with

$$U_r = \frac{X_r - (\cos\alpha+\cos\beta)/2}{|(\cos\alpha-\cos\beta)/2|} \quad , \quad X_r = \cos\theta_r \qquad (1.4.3)$$

α and β define the polar sector to which the measurements are confined and P_N^m represent associated Legendre's polynomials. A similar but simpler equation holds for cylindrical case [26].

It is shown in [25] analytically that the unknown expansion coefficients can be recovered with standard double-precision matrix inversion techniques to the degree of accuracy dictated only by any suitable measurement technique . To achieve a non-singular matrix inversion a novel, determinate optimization procedure for the measurement aspect angles is derived and proved for the cylindrical case in [26] and the spherical case

in [25]. In both cases it is also shown that the electrical radius ka of a perfectly conducting cylinder or a sphere can be directly recovered from a finite number of contiguous expansion coefficients. Furthermore, relationships between contiguous expansion coefficients of both electric and magnetic type result which are relevant to the general inverse problem since the scattered field can be uniquely expressed in terms of only one set of expansion coefficients associated with either the electric or magnetic vector wave functions. Vandenberghe and Boerner [123] also show that for an elliptical cylinder the characteristic parameters of the ellipse i.e. the principal axes a' and b' and the eccentricity ε, can be directly recovered from the expansion coefficients associated with circular cylindrical wavefunctions. Similarly the characteristic parameters of the ellipse, generating the prolate spheroid (the inter focal distance d and the eccentricity ε), can directly be recovered from the expansion coefficients in the spherical wave function expansions [124]. Extension of this idea to conducting canonical shapes (cylinder and sphere) is carried out by Boerner and Das in [24] where they make use of the hypothesis that the Fourier coefficients contain all necessary and sufficient information to recover the electrical size ρ and the material surface impedance η of homogeneous scatterers. In particular they show that ρ and η can be recovered from a characteristic equation, which has identical analytic form for the circular cylindric and the spherical case, by iterative methods.

In a most recent publication Hill [52] considers the inverse scattering

from a perfectly conducting prolate spheroid in the quasi-static domain of a magnetic dipole. He shows that from one observation of the radial and transverse scattered magnetic fields, the parameters which identify the spheroid (inter-focal distance and eccentricity) can be uniquely recovered. The intermediate step requires the determination of the two magnetic polarizabilities. It is possible to choose the observation point anywhere, even coincident with the source field if desired. Similar results are obtained for the prolate spheroid by a transformation. Obviously, the approach is valid only for the geophysical problem since the case treated is quasi-static.

Finally, Weston [132] considers the inverse problem in which the coefficients of a partial differential equation are to be determined from the knowledge of the asymptotic behavior of solution. He makes use of the theory of hyperbolic differential equations to determine the solution of this time dependent inverse problem. He has applied the analysis to electromagnetic scattering from a slab of varying conductivity and permittivity. The uniqueness of the method is demonstrated in [142].

1.6 FORMULATION OF THE PROBLEM

It has already been mentioned in the literature review that the first attempt to resolve the inverse problem rigorously using inverse boundary condition was made by Weston, Bowman and Ar [139,140] where they used $\underline{E} \times \underline{E}^*$ to invert perfectly conducting closed smooth shapes. But the bodies encountered in practice are rarely, if ever, perfectly

conducting. Therefore if the target identification theory has to achieve any practical value, methods to invert conducting shapes have to be established. An attempt to determine the impedance of conducting shapes was made by Weston et al in [139], where they suggest the use of the monostatic bistatic theorem of Kell. But no proper methods have been suggested for inverting the profile of such bodies.

Inspection of the inverse condition $\underline{E} \times \underline{E}^*$ suggests a similar boundary condition $\underline{H} \times \underline{H}^*$ for perfectly conducting bodies. The two forms together helped Boerner [136] to arrive at the conclusion that there must be some combination of above two conditions which should be valid for the bodies with arbitrary surface impedance. Starting with the Leontovich impedance boundary condition, its affine form and their conjugated formulations, he established two vectors whose properties are discussed in detail in *chapter two*. This thesis commences with the aim of exploiting the properties of these two vectors for inversion of conducting shapes.

Chapter two briefly reviews the impedance boundary conditions and the restrictions which have to be satisfied by the body for their application. The detailed derivation of the vector triplet, whose properties result in the required inverse boundary conditions, is also presented.

Chapter three presents the formulation of a set of inverse scattering boundary conditions resulting from theorems of *chapter two*. The expressions for recovering the surface impedance and the surface locus

are derived and the question of uniqueness of the inverted profile is considered.

Chapter four analyses the two-dimensional cylindrical mono-and two-body problems. The direct scattering solution for two parallel circular cylinders with impedance boundary is obtained. Application of the inverse boundary conditions with the aid of two-dimensional analytic continuation methods is illustrated for these two-dimensional shapes.

Chapter five considers three-dimensional mono-and two-body spherical shapes and presents direct scattering solutions for the two-sphere problem with arbitrary radii and surface impedances and illuminated by an arbitrarily polarized wave making an angle α with the line of centers. Three-dimensional analytic continuation is introduced. The inverse boundary conditions are then applied to these three-dimensional shapes to recover the profile.

The analysis of the errors, arising due to truncating the series representing the electromagnetic fields to a finite number of terms, is presented in *chapter six* where a novel approach for determining the truncation order is suggested.

The ideas presented in this work are summarized in *chapter seven* which also lists the contributions resulting from the present study. New problems arising out of this work are pointed out and some suggestions are made for their possible solution.

Appendix A.1 presents the derivation of the orthogonal triplet $\underline{A}$, $\underline{B}$ and $\underline{D}$ and various other important relations.

The coefficients of the fifth degree equation, for the phase angle ψ of the surface impedance, η are listed in *Appendix* A.2.

Appendix A.3 defines the coefficients appearing in the three-dimensional vector wave function addition theorem. A three-term recursion formula to calculate these coefficient is listed. Finally, the coefficients of the addition theorem for the specialized case of translation along z-axis and then recursion formula are presented.

Appendix A-4 briefly reviews the truncation criteria of Cabayan et al.

chapter two

THE CONCEPT OF INVERSE BOUNDARY CONDITIONS

2.1 INTRODUCTION

In direct problems of scattering and diffraction the shape and the material constituents of the scatterer which are known *a priori* together with the pre-specified incident field, may be incorporated into the boundary conditions. On the other hand, in the inverse problem, in general, no information about the scatterer may be assumed. Therefore, in this case such boundary conditions must be sought which depend neither on the shape nor the material properties of the scattering body, but allow one to specify those characteristic parameters uniquely from the near field recovered from far field measurements. Since it was shown in Boerner and Vandenberghe [25] and in Boerner and Aboul-Atta [21] that the near field representation can be found to an accuracy dictated only by measurement, the question remains as to how many and which characteristic parameters must be defined to uniquely determine the shape, the size and the material constituents of the unknown scatterer. Disregarding the local depolarization effects, it was found sufficient to specify the following parameters expressed in terms of an orthogonal three-dimensional system x_1, x_2 and x_3 as

i) the proper surface locus $S(x_1, x_2, x_3)$

ii) a relative local surface impedance $\eta(x_1, x_2, x_3)$ which is a scalar quantity, or the interior propagation constant $k_{int}(x_1, x_2, x_3)$

Thus at least three independent characteristic equations expressed in terms of the diffracted near field $\underline{E} = \underline{E}_i + \underline{E}_s$ and $\underline{H} = \underline{H}_i + \underline{H}_s$ must be sought to determine the surface locus $S(x_1, x_2, x_3)$ and the modulus and phase of the surface impedance $\eta = |\eta|\exp(j\psi)$. If such a set of independent scalar and vector equations exists, which can be employed to uniquely determine $S(x_1, x_2, x_3)$ and $\eta(x_1, x_2, x_3)$, then one may argue that the inverse scattering boundary condition $|\underline{E}x\underline{E}^*| = 0$ does constitute the remaining part of such a set of independent equations for the degenerate case of $\eta = 0$. The derivation of such a set of boundary conditions was first attempted by Weston and Boerner in a recent report [136], where it was anticipated that the concept of an impedance boundary condition can be favorably employed to determine the shape of imperfectly conducting shapes. The aim of the present study is to show that the Leontovich or scalar boundary conditions do offer the desired formulation and the properties of the vectors $\underline{A} = \underline{E}x\underline{E}^* - \eta\eta^*\underline{H}x\underline{H}^*$ and $\underline{B} = \eta\underline{E}^*x\underline{H} - \eta^*\underline{E}x\underline{H}^*$ result in the required boundary conditions for recovering the profile and surface impedance of the scattering objects [23].

Since the derivation of these novel conditions requires the application of the Leontovich boundary condition and its complementary and conjugated formulations, its relevant properties need to be reviewed for the express purpose of deriving criterions of applicability as well as defining the notation. Section 2.4 , presents the derivation of the vectors $\underline{A}$ and $\underline{B}$. The properties of these vectors are summarized in Theorems 1 and 2 and in Theorem 3, their degenerate nature at the

specular point on a smooth and closed scatterer is analysed.

2.2 THE LEONTOVICH OR IMPEDANCE BOUNDARY CONDITIONS

The impedance boundary conditions, which are widely employed in diffraction problems in which it is desirable to take into account the material constituents and/or surface characteristics of the body, may be stated in its simplest form as [82]

$$\underline{K}_m = -\eta Z_0 \hat{n} \times \underline{K}_e \qquad (2.2.1)$$

Here the tangent fields at the surface S of the conductor have been expressed in terms of the effective electric and magnetic surface currents

$$\underline{K}_e = \hat{n} \times \underline{H} \qquad \text{and} \qquad \underline{K}_m = -\hat{n} \times \underline{E} \qquad (2.2.2)$$

where $\hat{n}$ is a unit outward normal to the surface and $\underline{E}$ and $\underline{H}$ represent the total electric and magnetic fields respectively, in the region surrounding the body. The quantity η is the relative impedance of the body, designated as Leontovich impedance and has been normalized with respect to Z_0, the intrinsic impedance of free space. For a body composed of a material of large refractive index, $\eta = |\eta| e^{j\psi}$ may be written as

$$\eta = \left[\frac{\mu_0}{\mu} \left(\frac{\varepsilon}{\varepsilon_0} + i \frac{\sigma}{\omega \varepsilon_0} \right) \right]^{-1/2} \qquad (2.2.3)$$

where μ_0 and μ represent the permeabilities and ε_0 and ε the

permittivities of free space and the body material, respectively. Parameter σ represents the conductivity of the body.

In the analysis of the flat boundary the fundamental assumption was [51, 106] that the refractive index of the body is much larger than that of free space i.e.

$$|N| \gg 1 \qquad (2.2.4)$$

The above condition is sufficient to ensure that within the medium, the field is varying slowly along the surface and behaves essentially as a plane wave propagating in the direction of the inward normal. For the case of a curved surface, with ρ, the smallest radius of curvature at the point in question, the restriction

$$|N|\, k\rho \gg 1 \qquad (2.2.5)$$

ensures that the field shall vary little within a wavelength along the surface.

The above restrictions were valid for semi-infinite (or open) bodies. For closed surfaces an additional restriction

$$\delta \ll \rho \qquad (2.2.6)$$

is imposed to ensure that no outward travelling field appears on the farther side of the surface. Here δ is the skin depth in the conductor and is defined by

$$\delta \simeq \left(\frac{\omega\mu\sigma}{2} \right)^{-1/2} \qquad (2.2.7)$$

in terms of which the wave impedance and the wave number are

$$\eta \simeq \frac{1}{2}(1-i)\,\omega\mu\delta \quad , \qquad k_c \simeq (1+i)/\delta \tag{2.2.8}$$

If $\sigma >> \omega\varepsilon'$, inequality (2.2.6) can be written as

$$\left(\frac{\mu}{\mu_0}\frac{\sigma}{2\omega\varepsilon_0}\right)^{1/2} k\rho >> 1 \tag{2.2.9}$$

which in turn reduces to the inequality (2.2.5) if the conduction current dominates. On the other hand, if the displacement current dominates the inequality (2.2.6) represents an additional restriction which is stronger than (2.2.5). It may be pointed out here that due to restriction (2.2.6), lossless objects such as dielectric slabs, cylinders and spheres have been shown to be untreatable by the impedance boundary condition, regardless of dimensions (Leontovich[66]), i.e. for a body to be treated by the impedance boundary condition its surface impedance must be complex and condition $\delta << \rho$ must be strictly satisfied.

As Mitzner [82] has pointed out, a modification to treat smaller radii of curvature is implicit in Rytov [103] and is given explicitly (but with an error of a factor of 2, which has been corrected by Mitzner) by Leontovich [66]. The corrected form of the boundary condition is

$$K_{m_u} = (1-p)\eta K_{e_v} \quad , \qquad K_{m_v} = -(1+p)\eta K_{e_u} \tag{2.2.10}$$

for homogeneous conductors. Here the parameter p is defined by

$$p = \frac{i}{2k_c}(\kappa_v - \kappa_u) = \frac{1}{4}(1+i)\delta(\kappa_v - \kappa_u) \qquad (2.2.11)$$

and u and v are principal curvature coordinates so oriented that

$$\hat{e}_u \times \hat{e}_v = \hat{n} \qquad (2.2.12)$$

and κ_u and κ_v are principal curvatures defined positive when $\hat{n}$ points outwards from the body.

Mitzner [82], formulates the scattering problem in terms of two coupled integral equations relating the effective electric and magnetic surface currents $\underline{K}_e$ and $\underline{K}_m$. Each of the two equations involves the constitutive parameters of only one medium and is especially suited to the case of a high conductivity scatterer. Mitzner's formulation is quite general, and under increasingly restrictive assumptions, can lead first to an explicit expression for $\underline{K}_m$ in terms of $\underline{K}_e$, then a curvature dependent boundary condition relating the two currents, and finally the usual Leontovich boundary condition.

Senior [106] shows that for the case of statistically uniformly inhomogeneous surfaces whose refractive index $N = \frac{\mu}{\mu_0 \eta}$ satisfies the restriction (2.2.4) and an additional restriction

$$\left|\frac{1}{k\eta} \nabla\eta\right| << 1 \qquad (2.2.13)$$

the impedance boundary condition of eq. (2.2.1) involves averaged values of fields and the surface impedance. It should be noted that

the average fields are determined by the average value of η and not by the average value of ε or σ. In (2.2.13) $\nabla\eta$ represents spatial variation of η.

The impedance boundary condition may also be derived for statistically rough surfaces, in which case it can be replaced by a generalized impedance condition applied at the neighboring mean surface [107]. The surface impedance is a tensor function of the direction at which the field is incident as well as the statistical properties of the irregularities, but simplifies in certain particular cases. Since the Taylor series about the mean surface is used, it is clear that the expansion will only be valid if the behavior of the field at the actual surface differs only slightly from the behavior on the mean surface. Therefore, large gradients or abrupt changes in gradients cannot be allowed since such perturbations may produce significant changes in the field in their vicinity [18].

Weston has also generalized the concept of impedance boundary conditions to the consideration of scattering from complex shapes [133,138]. He has postulated two theorems concerning the class of surfaces which are invariant under 90° rotation about some axis of the body. The practical aspects of designing absorber layers are also considered in his paper. It should be noted that the admissible case of a purely real surface impedance which is not zero or infinity, can be encountered for multiple layer coated perfectly conducting scatterers [133, 126] and under certain conditions for statistically rough perfectly conducting scatterers [107].

2.3 FORMULATION OF A SET OF CHARACTERISTIC EQUATIONS

Since the aim of this study is to obtain an inverse set of boundary conditions, the *a priori* knowledge of the surface locus $S = S(\underline{r})$ or its unit local normal $\hat{n} = \hat{n}(\underline{r})$, or its local impedance $\eta = \eta(\underline{r})$ cannot be assumed. Therefore, to resolve the two unknowns $S(\underline{r})$ and η in the impedance boundary condition (IMBC), additional formulations of IMBC are required which, however, must contain identical information so that the surface locus $S(\underline{r})$ and the impedance $\eta(\underline{r})$ can be found from the knowledge of total electric and magnetic fields.

The Leontovich or impedance boundary condition can be written as

$$\underline{E} - (\hat{n}\cdot\underline{E})\hat{n} = Z_0 \hat{n} \times \underline{H} \qquad (2.3.1)$$

in which all the quantities involved have been defined in Section 2.2 .

The first additional relation is found by applying a vector product operation of $\hat{n}$ into (2.3.1) yielding

$$\underline{H} - (\hat{n}\cdot\underline{H})\hat{n} = -\xi Y_0 \hat{n} \times \underline{E} \qquad (2.3.2)$$

Thus (2.3.2) corresponds to (2.3.1) under the transformation $\underline{E} \rightarrow \underline{H}$, $Z_0\underline{H} \rightarrow -Y_0\underline{E}$ and $\eta \rightarrow \xi$ where $\xi = 1/\eta$ denotes the relative averaged local admittance. Senior [108] has shown the affinities of this transformation with Babinet's principle and has proved the invariance of this transformation attributing η to the material constituents of the body.

In addition to (2.3.1) and (2.3.2), its conjugated formulations are required and introduced [136] as

$$\underline{E}^* - (\hat{n}\cdot\underline{E}^*)\hat{n} = \eta^* Z_0 \hat{n} \times \underline{H}^* \qquad (2.3.3)$$

$$\underline{H}^* - (\hat{n}\cdot\underline{H}^*)\hat{n} = -\xi^* Y_0 \hat{n} \times \underline{E}^* \qquad (2.3.4)$$

The validity of statements (2.3.3) and (2.3.4) must strictly assume that all implied field quantities $\underline{E}$ and $\underline{H}$, as well as the relative local surface impedance $\eta = \eta(\underline{r})$ are analytical functions, and $\hat{n} = \hat{n}(\underline{r})$ is piecewise continuous, satisfying the set of linear eqs. (2.3.1) and (2.3.2) which in turn satisfy Maxwell's equations. In essence the conjugation of (2.3.1) and (2.3.2) implies the reversal of the reactive character of all implied electromagnetic quantities; thus the pair (2.3.1) and (2.3.2) bears similar affinities as does the pair (2.3.3) and (2.3.4), for a surface of reversed reactive character.

Applying scalar and vector product operations to (2.3.1) and (2.3.4) on one another a complex set of interdependent scalar and vector equations results [136,23] which are tabulated in *Appendix* A.1.

2.4 THE ORTHOGONAL VECTOR TRIPLET $\underline{A}$, $\underline{B}$ AND $\underline{D}$

Employing properties of the derived set of scalar and vector equations as tabulated in *Appendix* A.1, the following three orthogonal vectors (shown in Fig. 2.1) can be defined [136,23].

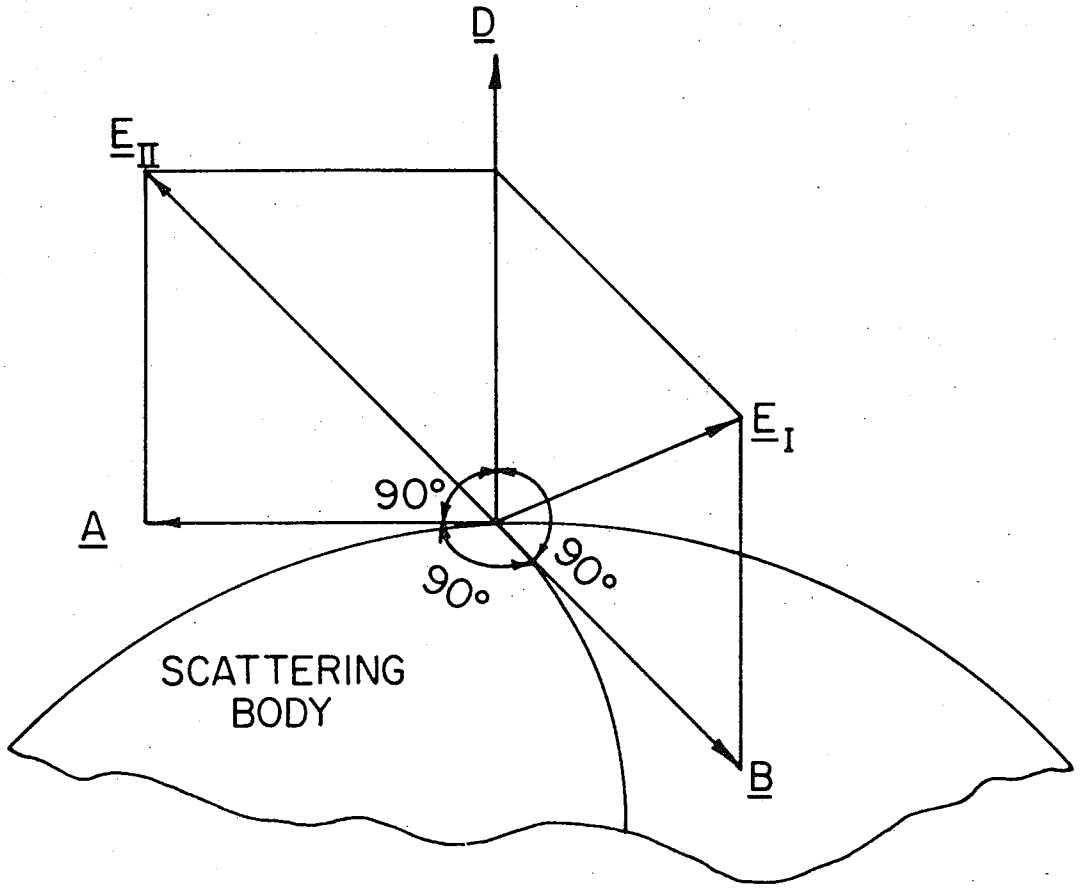

FIG. 2.1. Orthogonal Vector Triplet $\underline{A}, \underline{B}, \underline{D}$ and Additional Vectors $\underline{E}_I, \underline{E}_{II}$.

$$\hat{n}\cdot\underline{A} = 0 \tag{2.4.1}$$

$$\hat{n}\cdot\underline{B} = 0 \tag{2.4.2}$$

$$\underline{B} = \hat{n} \times \underline{A} \tag{2.4.3}$$

$$\underline{A} = \underline{B} \times \hat{n} \tag{2.4.4}$$

Thus it follows directly that

$$\underline{A}\cdot\underline{A} = (\underline{B}\times\hat{n})\cdot(\underline{B}\times\hat{n}) = \underline{B}\cdot\underline{B}-(\hat{n}\cdot\underline{B})^2 = \underline{B}\cdot\underline{B} = (\hat{n}\times\underline{A})\cdot\underline{B} = \hat{n}\cdot(\underline{A}\times\underline{B}) = \hat{n}\cdot\underline{D} \tag{2.4.5}$$

and

$$\underline{A}\cdot\underline{B} = (\hat{n}\times\underline{B})\cdot\underline{B} = \hat{n}\cdot(\underline{B}\times\underline{B}) = 0 \tag{2.4.6}$$

From inspection of (2.4.1) to (2.4.6) it follows that the two purely imaginary vector quantities $\underline{A}$ and $\underline{B}$ are perpendicular to one another and tangent to the local scattering surface. Therefore its cross product $\underline{D} = \underline{A} \times \underline{B}$, a purely negative real vector quantity, must be directed along the local outward normal $\hat{n} = \hat{n}(r)$ of the local scattering surface $S(\underline{r})$, where

$$\underline{D} = \underline{A} \times \underline{B} = [\hat{n}\cdot(\underline{A}\times\underline{B})]\hat{n} = (\underline{A}\cdot\underline{A})\hat{n} = (\underline{B}\cdot\underline{B})\hat{n} \tag{2.4.7}$$

Therefore, the local outward surface normal is defined as

$$\hat{n} = \frac{\underline{A}\times\underline{B}}{\hat{n}\cdot(\underline{A}\times\underline{B})} = \frac{\underline{A}\times\underline{B}}{\underline{A}\cdot\underline{A}} = \frac{\underline{A}\times\underline{B}}{\underline{B}\cdot\underline{B}} \tag{2.4.8}$$

These striking interrelations between $\underline{A}$, $\underline{B}$ and $\underline{D}$ are formulated in the following as Theorem 1, 2 and 3 , [136,23].

Theorem 1 - If the electromagnetic behavior in the vicinity of a scatterer satisfies the Leontovich or scalar impedance boundary condition

$$\underline{E} - (\hat{n}\cdot\underline{E})\hat{n} = \hat{n} \times \underline{H} \tag{2.4.9}$$

where $\underline{E} = \underline{E}_i + \underline{E}_s$ and $\underline{H} = Z_0(\underline{H}_i + \underline{H}_s)$ then the following purely reactive vector quantities

$$\underline{A} = \underline{E}x\underline{E}^* - \eta\eta^*\underline{H}x\underline{H}^* \tag{2.4.10}$$

$$\underline{B} = \eta(\underline{E}^* x\underline{H}) - \eta^*(\underline{E}x\underline{H}^*) \tag{2.4.11}$$

are orthogonal and are in the plane of the scatterer, and its vector product, a purely real vector quantity

$$\underline{D} = \underline{A}x\underline{B} = [\hat{n}\cdot(\underline{A}x\underline{B})]\hat{n} = (\underline{A}\cdot\underline{A})\hat{n} = (\underline{B}\cdot\underline{B})\hat{n} \tag{2.4.12}$$

is directed along the outward local normal of the scatterer which is given by

$$\hat{n} = \frac{\underline{A}x\underline{B}}{\underline{A}\cdot\underline{A}} = \frac{\underline{A}x\underline{B}}{\underline{B}\cdot\underline{B}} \tag{2.4.13}$$

Thus the three vector quantities

$$\underline{A} = \underline{B}x\hat{n} \qquad \underline{B} = \hat{n}x\underline{A} \qquad \underline{D} = \underline{A}x\underline{B} = [\hat{n}\cdot(\underline{A}x\underline{B})]\hat{n} \tag{2.4.14}$$

constitute a right-handed orthogonal vector triplet with identical magnitude

$$\underline{A}\cdot\underline{A} = \underline{B}\cdot\underline{B} = \hat{n}\cdot\underline{D} \tag{2.4.15}$$

Theorem 2 - If the electromagnetic behavior in the vicinity of a scatterer satisfies the Leontovich or impedance boundary condition, then the following two independent scalar equations

$$\underline{A}\cdot\underline{B} = [(\underline{E}\cdot\underline{E}^*) - \eta\eta^*(\underline{H}\cdot\underline{H}^*)][\eta(\underline{E}^*\cdot\underline{H}) + \eta(\underline{E}\cdot\underline{H}^*)] - \eta(\underline{E}\cdot\underline{H})[(\underline{E}^*\cdot\underline{E}^*) - \eta^{*2}(\underline{H}^*\cdot\underline{H}^*)]$$

$$-\eta^*(\underline{E}^*\cdot\underline{H}^*)[(\underline{E}\cdot\underline{E}) - \eta^2(\underline{H}\cdot\underline{H})] = 0 \tag{2.4.16}$$

$$\underline{A}\cdot\underline{A}-\underline{B}\cdot\underline{B} = [(\underline{E}\cdot\underline{E})-\eta^2(\underline{H}\cdot\underline{H})][(\underline{E}^*\cdot\underline{E}^*)-\eta^{*2}(\underline{H}^*\cdot\underline{H}^*)]-[(\underline{E}\cdot\underline{E}^*)-\eta\eta^*(\underline{H}\cdot\underline{H}^*)]^2$$

$$+[\eta(\underline{E}^*\cdot\underline{H})+\eta^*(\underline{E}\cdot\underline{H}^*)]^2-4\eta\eta^*(\underline{E}\cdot\underline{H})(\underline{E}^*\cdot\underline{H}^*) = 0 \qquad (2.4.17)$$

can be employed to specify the surface locus and the modulus and phase of the complex scalar impedance $\eta = |\eta|\exp j\psi$. The local surface $\hat{n}$ can be recovered from

$$n = \frac{2(\underline{A}x\underline{B})}{\underline{A}\cdot\underline{A}+\underline{B}\cdot\underline{B}} =$$

$$-\frac{2[(\underline{E}x\underline{E}^*)-\eta\eta^*(\underline{H}x\underline{H}^*)]\ x\ [\eta(\underline{E}^*x\underline{H})-\eta^*(\underline{E}x\underline{H}^*)]}{\{[(\underline{E}\cdot\underline{E})+\eta^2(\underline{H}\cdot\underline{H})][(\underline{E}^*\cdot\underline{E}^*)+\eta^{*2}(\underline{H}^*\cdot\underline{H}^*)]-[(\underline{E}\cdot\underline{E}^*)+\eta\eta^*(\underline{H}\cdot\underline{H}^*)]^2-[\eta(\underline{E}^*\cdot\underline{H})-\eta^*(\underline{E}\cdot\underline{H}^*)]^2\}}$$

(2.4.18)

It is to be noted that if both the surface locus $S(\underline{r})$ and the complex impedance $\eta = |\eta|\exp(j\psi)$ are *a priori* unknown, an additional independent characteristic equation would be required to uniquely determine the shape and the material surface properties of the scatterer in question. Such a third independent characteristic equation was, however, not found. Therefore, the degeneracy of the vectors $\underline{A}$ and $\underline{B}$ in the back scattering direction is exploited.

2.5 THE DEGENERATE BACKSCATTERING CASE

Although Theorems 1 and 2 are derived from the Leontovich boundary condition, and should hold in general, the properties of the basic vector quantities $\underline{A}$ and $\underline{B}$ must be further analysed for the case in which the incident wave is locally normal to a smooth imperfectly

conducting surface. Since the local region of a smooth scatterer may be considered to be a section of a planar surface of homogeneous surface impedance, the analysis of the degenerate properties of $\underline{A}$ and $\underline{B}$ is best facilitated by considering the case of normal plane wave incidence on an infinite planar and semi-transparent bounding surface. In this case, by Fresnel's laws of reflection, the reflected electric and magnetic field quantities must be along the same direction as the incident electric and magnetic field quantities, respectively. Therefore the total electric and total magnetic field vectors in the backscattering direction must be perpendicular to one another, i.e.

$$\underline{E}\cdot\underline{H} = 0$$

everywhere along the backscattering direction. Furthermore $\underline{E}^{*}\text{x}\underline{H}$ and $\underline{E}\text{x}\underline{H}^{*}$ in $\underline{B}$ are along the same direction and the modulus of their absolute values must be identical, i.e.

$$\underline{B} = \eta(\underline{E}^{*}\text{x}\underline{H})-\eta^{*}\underline{E}\text{x}\underline{H}^{*} = 0$$

in the backscattering direction, but since $\underline{A}\cdot\underline{A}-\underline{B}\cdot\underline{B} = 0$, we have

$$\underline{A} = (\underline{E}\text{x}\underline{E}^{*})-\eta\eta^{*}(\underline{H}\text{x}\underline{H}^{*}) = 0$$

in the backscattering direction.

Theorem 3 - If the electromagnetic behavior in the vicinity of a smooth, piecewise continuous scatterer satisfies the Leontovich or scalar impedance boundary conditions then the following three independent characteristic equations

$$\underline{E}\cdot\underline{H} = 0 \qquad (2.4.19)$$

$$\underline{B} = \eta(\underline{E}^{*}\text{x}\underline{H})-\eta^{*}(\underline{E}\text{x}\underline{H}^{*}) = 0 \qquad (2.4.20)$$

$$\underline{A} = (\underline{E}\text{x}\underline{E}^{*})-\eta\eta^{*}(\underline{H}\text{x}\underline{H}^{*}) = 0 \qquad (2.4.21)$$

are satisfied everywhere along the radiant vector in the back-scattering direction. In this particular degenerate case, i.e. for normal incidence on a locally planar scattering surface, the properties of Theorems 1 and 2 cannot be employed to recover the proper surface locus $S_0(\underline{r})$ and the associated relative surface impedance.

It should be noted that the degeneracy condition satisfies the tangentiality conditions $\hat{n} \cdot \underline{A} = 0$ and $\hat{n} \cdot \underline{B} = 0$ as $\hat{n}$ is synonymous with the unit vector in backscattering direction.

Therefore, for points lying on the proper surface $S_0(\underline{r})$ and in the neighborhood of the specular point for which the incident wave is normal to the local surface, the properties of Theorems 1 and 2 hold uniquely, whereas the degenerate condition of Theorem 3 should present a reasonable first order approximation. Therefore it should be possible to recover the proper surface locus $S_0(\underline{r})$ as well as the complex surface impedance for smooth and closed scatterers whose surface impedance is homogeneous i.e. $\eta(\underline{r}) = \eta = \text{const.}$, by employing the three theorems simultaneously as is shown in Sections (3.4).

2.6 INTERPRETATION OF ORTHOGONAL-VECTORS $\underline{A}$ and $\underline{B}$

The exact physical interpretation and the reason for the orthogonality of the vectors $\underline{A}$ and $\underline{B}$ are not yet clear. However, in a recent publication Musha [88] shows that the terms $\underline{E}x\underline{E}^*$ and $\underline{H}x\underline{H}^*$ represent torque density caused by the electric and the magnetic fields, respec-

tively. Vector $\underline{B}$ is the difference of a term proportional to the poynting's vector and its complex conjugate and is, therefore, proportional to the reactive energy in an electromagnetic wave.

The plots of $\underline{A}$ and $\underline{B}$ over the surface of a sphere of electrical radius $ka = 5.0$ and surface impedance $\eta = 0.5$ are presented in Figs. 2.2a and 2.2b. The directions of the vectors were computed at an interval of 5° in both θ - and ϕ - directions. The orthogonality of the two vectors is evident from the plots. In the back-scattering direction both vectors are identically zero and they exhibit singular nature near the nodal lines.

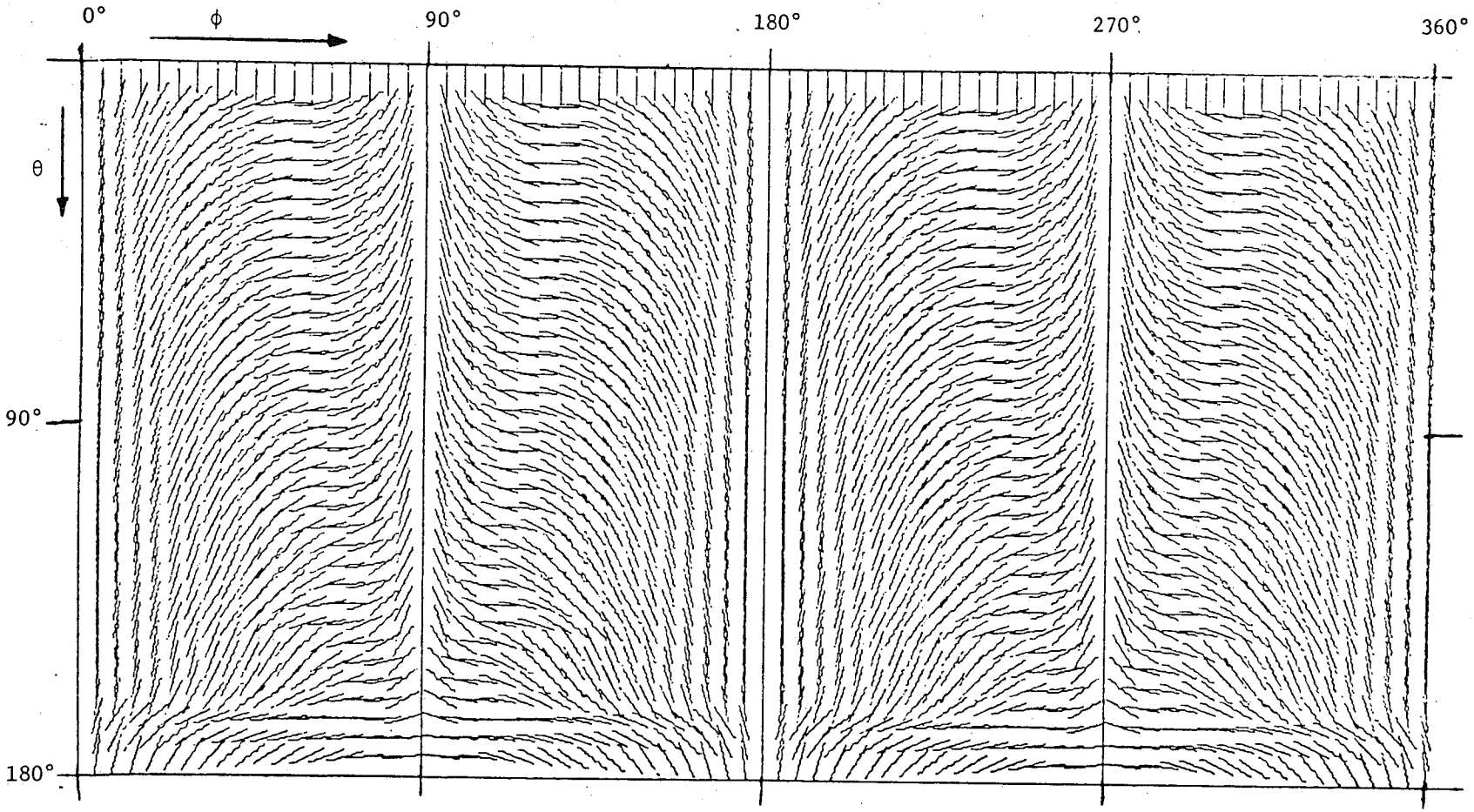

Fig.2.2a Vector $\underline{A} = \underline{E}\times\underline{E}^* - \eta\eta^*\underline{H}\times\underline{H}^*$ plotted on the surface of a sphere of ka = 5, $\eta = 0.5\ \underline{/0°}$

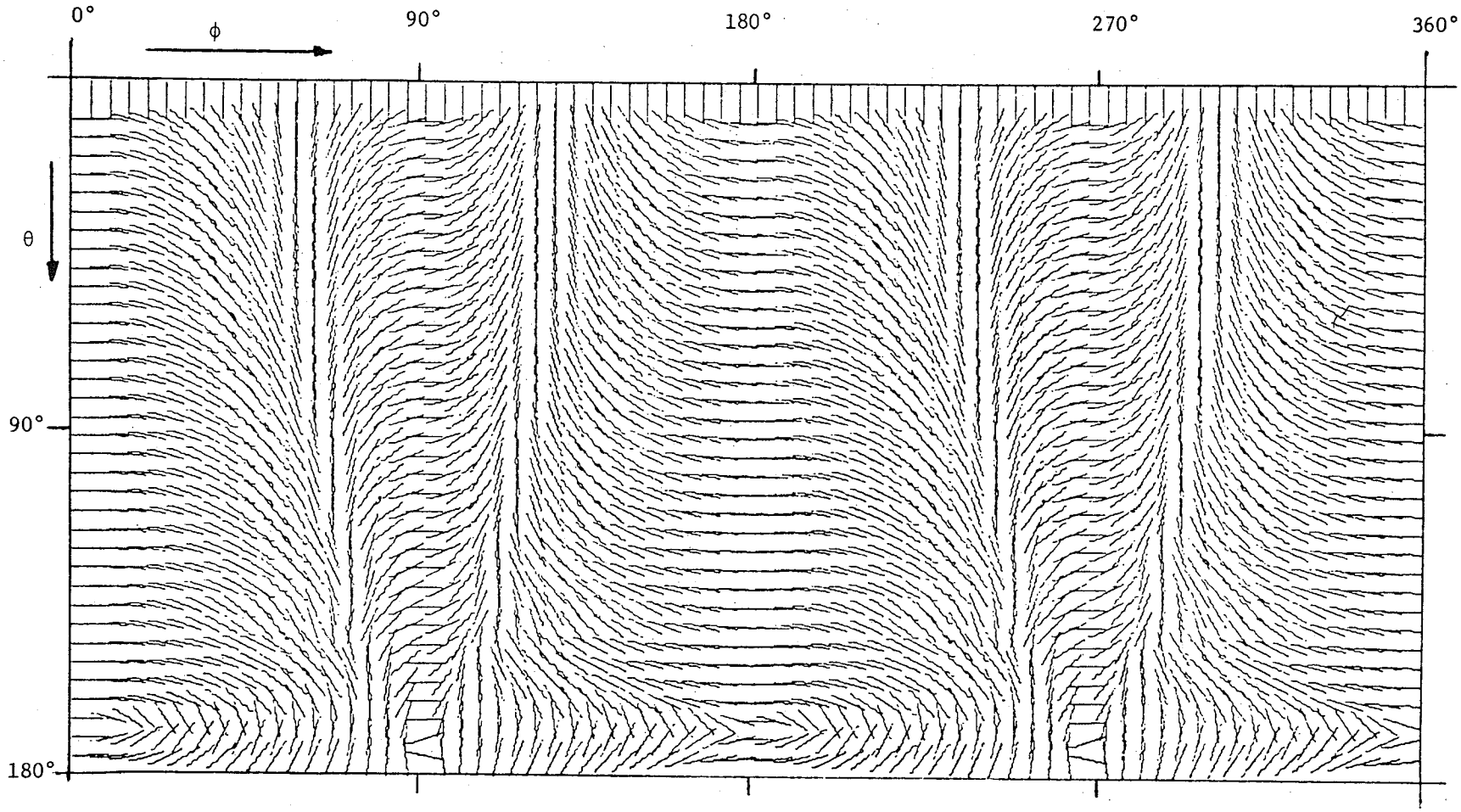

Fig.2.2b Vector $\underline{B} = \eta \underline{E}^* x \underline{H} - \eta^* \underline{E} x \underline{H}$ plotted on the surface of a sphere of ka = 5, $\eta = 0.5 \angle 0°$

chapter three

FORMULATION OF A SET OF INVERSE SCATTERING BOUNDARY CONDITIONS

3.1 INTRODUCTION

In applying the concept of inverse scattering boundary conditions, it is assumed that the expressions for the total electric and magnetic fields in the vicinity of the surface of a scattering body can be recovered from the measured far field data, as is analysed in Weston and Boerner [136] and in Boerner and Vandenberghe [25]. Thus, given the expressions for the total fields which can be computed in the vicinity of the surface of a scattering body, the next step is to employ techniques which will locate the surface of the body and will enable one to determine its associated averaged material surface properties. Since the electromagnetic fields can be continued into the regions inside the Wilcox circle/sphere by analytic continuation methods, the entire profile of convex or concave bodies can be recovered.

In establishing the required sets of inverse boundary conditions, it was found convenient to distinguish between the perfectly electric, perfectly magnetic and the imperfectly conducting cases. This order of presentation facilitates linking known results with the new concepts introduced. Furthermore, such a scheme was found necessary since for the degenerate perfectly conducting cases additional boundary conditions are being introduced which, though implicitly interlaced, do not hold in the imperfectly conducting case.

Obviously, the simplest case to start with is that of the perfectly conducting bodies, for which only the shape and size are to be recovered. Therefore, in this chapter we first list the inverse boundary conditions for perfectly conducting cases and discuss the questions of uniqueness of the recovered profile. The general inverse boundary conditions are discussed in detail, in Section 3.4 and it is shown that the inverse boundary conditions of Section 3.2 can be derived from the general case by letting η go to zero for a perfect electric conductor and η go to infinity for a perfect magnetic conductor. The expressions for the magnitude and phase of the surface impedance are derived in section 3.4.

3.2 INVERSE BOUNDARY CONDITIONS FOR PERFECTLY CONDUCTING BODIES

The inverse boundary conditions for this special case can easily be derived from the direct boundary conditions which, in simple words, state that the tangential component of the electric field and the normal component of the magnetic field vanish at the surface of an electrically perfectly conducting body. For a magnetically perfectly conducting body $\underline{E}$ and $\underline{H}$ interchange roles. Mathematically the above two conditions can be stated as $\hat{n} \times \underline{E} = 0$ and $\hat{n} \cdot \underline{H} = 0$.

An obvious consequence of these unique direct boundary conditions is that $\hat{n} \times \underline{E}^* = 0$ as well as $\hat{n} \cdot \underline{H}^* = 0$. Therefore necessary and sufficient conditions for a point to lie on the surface of a perfectly conducting body are that at that point the total electric ($\underline{E} = \underline{E}_i + \underline{E}_s$) and magnetic $\underline{H} = Z_0 (\underline{H}_i + \underline{H}_s)$ fields must satisfy

$$\underline{E} \cdot \underline{H} = 0 \qquad \textit{necessary and sufficient} \qquad (3.2.1)$$

or

$$\underline{E}^* \cdot \underline{H}^* = 0 \qquad \textit{necessary and sufficient} \qquad (3.2.2)$$

Exceptions of these conditions are the cases of local normal incidence on any scatterer, or normal plane wave incidence on a cylindrical structure for either purely parallel or normal polarization, in which case $\underline{E} \cdot \underline{H}$ vanishes identically. Another inverse condition, derived first by Weston [139], results from the fact that $\hat{n} \times \underline{E} = 0$ and $\hat{n} \times \underline{E}^* = 0$. Therefore, $\underline{E}\times\underline{E}^*=0$ holds on the surface of a perfect conductor. Physically this condition means that for the case of a perfectly conducting body, the $\underline{E}$ field has real direction.

Another approximate but important condition results from the physical optics current approximation which may be stated as $|\underline{E}_i| - |\underline{E}_s| = 0$. It must be noted that this condition though unique, only yields an approximate surface which approaches smooth, convex portions of the correct surface in the limit of high frequency scattering. The boundary condition stating that the tangential component of the electric field is zero has also been employed by some authors for the target identification of perfectly conducting shapes [54,55]. All these boundary conditions discussed above are summarized below

$$\underline{E}_{\text{tangential}} = 0 \qquad \textit{exact, necessary and sufficient} \qquad (3.2.3)$$

$$\{|\underline{E}_i| - |\underline{E}_s|\} = 0 \qquad \textit{approximate, necessary and sufficient} \qquad (3.2.4)$$

$$\underline{E} \cdot \underline{H} = 0 \qquad \textit{exact, necessary and sufficient} \qquad (3.2.5)$$

$$\underline{E} \times \underline{E}^{*} = 0 \qquad \textit{exact, necessary but not sufficient} \quad (3.2.6)$$

Similar boundary conditions, with $\underline{H}$ and $\underline{E}$ interchanged, apply to the perfectly magnetic conducting case and may be stated as

$$\underline{H}_{\text{tangential}} = 0 \qquad \textit{exact, necessary and sufficient} \quad (3.2.7)$$

$$\{|\underline{H}_i| - |\underline{H}_s|\} = 0 \qquad \textit{approximate, necessary and sufficient} \quad (3.2.8)$$

$$\underline{H} \cdot \underline{E} = 0 \qquad \textit{exact, necessary and sufficient} \quad (3.2.9)$$

$$\underline{H} \times \underline{H}^{*} = 0 \qquad \textit{exact, necessary but not sufficient} \quad (3.2.10)$$

3.2.1 QUESTIONS OF UNIQUENESS

Considering the fact that the total field expressions are formulated as the sums of the incident and the scattered fields, it is apparent that an interference-like pattern should result whenever a given total field expression is associated with a conjugated total field expression in terms of scalar or vector product operations. Consequently, if a surface $S_0(\underline{r})$ is found which satisfies (3.2.1) and/or (3.2.2), it must be the correct surface. Whereas, even if a surface $S_m(\underline{r})$ is found such that it satisfies one and/or all of the conditions (3.2.1) to (3.2.6), it would not necessarily be the correct surface $S_0(\underline{r})$, since these conditions are not unique and not independent.

Consider the scattered field due to a smooth, perfectly conducting, convex surface S, and assume that analytic expressions for both the

total electric and magnetic fields are known everywhere exterior to the equivalent source region which is enclosed by S. In seeking the surface S by looking for the surface on which the total electric and magnetic fields obey the required boundary conditions given in (3.2.1) to (3.2.6), it could be possible that more than one eligible surface may be found for a particular wave number k. Therefore, assume that two perfectly conducting surfaces S_0 and S_1, which surround the equivalent source region and are taken to be smooth, are found from any one of the above stated inverse conditions. Then, in the volume V between the two surfaces, within which the medium is assumed to be linear, homogeneous, isotropic and lossless, the total electric field satisfies the source free wave equation [137]

$$(\nabla^2 + k^2)\ \underline{E} = 0 \qquad (3.2.11)$$

and/or

$$(\nabla^2 + k^{*2})\ \underline{E}^* = 0 \qquad (3.2.12)$$

together with the equations

$$\nabla \cdot \underline{E} = 0 \qquad (3.2.13)$$

$$\nabla \cdot \underline{E}^* = 0 \qquad (3.2.14)$$

Similarly, the total magnetic field satisfies the source free wave equations

$$(\nabla^2 + k^2)\ \underline{H} = 0 \qquad (3.2.15)$$

and/or

$$(\nabla^2 + k^{*2})\ \underline{H}^* = 0 \qquad (3.2.16)$$

together with the equations

$$\nabla \cdot \underline{H} = 0 \qquad (3.2.17)$$

or

$$\nabla \cdot \underline{H}^* = 0 \qquad (3.2.18)$$

However, solutions of these equations in the simply connected cavity V such that

$$\hat{n} \times \underline{E} = 0 \quad \text{and/or} \quad \hat{n} \times \underline{E}^* = 0 \qquad (3.2.19)$$

and/or

$$\hat{n} \cdot \underline{H} = 0 \quad \text{and/or} \quad \hat{n} \cdot \underline{H}^* = 0 \qquad (3.2.20)$$

on the bounding surfaces, S_0 and S_1, exist only for a discrete set of eigenvalues. Thus, if k varies continuously, the shape of S_1 must change in order to satisfy the boundary conditions since, by definition, the scattering surface S_0 is independent of the wavelength of the incident field. The requirement that S_0 remains unchanged as the frequency is varied continuously, therefore, allows determination of the scattering surface uniquely, since the geometry of the additional surfaces depends on the frequency. Thus one method of discriminating the proper surface locus from the family of pseudo loci is to employ at least two frequencies. It is readily observed that the inverse conditions $\underline{E} \times \underline{E}^* = 0$, $\underline{E}^* \cdot \underline{H} = 0$, $\underline{E} \cdot \underline{H}^* = 0$, and $\underline{H} \times \underline{H}^* = 0$ are dependent on one another, i.e. the resulting discrete sets of eigenfrequencies for all of these four conditions must be identical. On the contrary, the inverse conditions $\underline{E} \cdot \underline{H} = 0$ and $\underline{E}^* \cdot \underline{H}^* = 0$ are unique, since if there could exist a second surface S_1 on which $\hat{n} \times \underline{E} = 0$ and $\hat{n} \cdot \underline{H} = 0$ or $\hat{n} \times \underline{E}^* = 0$ and $\hat{n} \cdot \underline{H}^* = 0$, respectively,

the surface S_1 must be an existing, perfectly conducting surface because the two unique direct boundary conditions $\hat{n} \times \underline{E} = 0$ and $\hat{n} \cdot \underline{H} = 0$, or their conjugated forms , are being satisfied simultaneously. Therefore, the conditions $\underline{E} \cdot \underline{H} = 0$ and $\underline{E}^* \cdot \underline{H}^* = 0$ are unique and will yield only one zero which defines the proper surface locus S_0. The obvious cases for which these conditions are violated are those for which $\underline{E}$ and $\underline{H}$ are always perpendicular, for example, in the case of local normal incidence and for normal plane wave incidence on cylindrical structures for either parallel or normal polarization.

Although the inverse conditions $\underline{E} \times \underline{E}^* = 0$, $\underline{E}^* \cdot \underline{H} = 0$, $\underline{E} \cdot \underline{H}^* = 0$ and $\underline{H} \times \underline{H}^* = 0$ are necessary but not sufficient conditions and, furthermore, depend on one another, it should still be possible to discriminate the proper surface locus of a closed and smooth scatterer from the 'interior caustic generated' and the 'exterior' pseudo loci, since these pseudo loci are not closed. The application of the boundary conditions to the total fields results in interference like patterns. Therefore, no pseudo loci can exist in the shadow region of the scatterer and the generated pseudo loci are open surfaces. In this sense,the inverse boundary condition (3.2.6) is not *locally* but *globally* sufficient when the scattering body is closed and smooth.

The question of uniqueness for perfectly conducting bodies has been discussed in more detail by Weston in [134],where he suggests the use of a different incident wave but of the same frequency to eliminate the pseudo loci. He eliminates those surfaces which do not enclose (or are not

enclosed by) the proper surface S_0 by using the fact that in this case they would not contain any singularities of the em field. In order to determine the set of measurements required to eliminate pseudo locus S_1 as a candidate for the surface of the obstacle, he considers the properties of eigenfunctions given by

$$\underline{E}(y) = 2 \int_S \underline{\mu} \times \nabla\phi \, d\sigma_x \tag{3.2.21}$$

in detail. Here ϕ and $\underline{\mu}$ are defined by the following relations

$$\phi = \frac{\exp(jkR)}{4\pi R} \qquad R = |x-y| \tag{3.2.22}$$

where y is any point in volume V enclosed by the surface and x is the variable of integration over the surfaces $S = S_0 + S_1$ and

$$\underline{\mu} = \frac{1}{2} \hat{n} \times (\underline{H}^- - \underline{H}^+) \tag{3.2.23}$$

where $\hat{n}$ is the unit outward normal to the surfaces, and $\underline{H}^-$ and $\underline{H}^+$ are the respective values of magnetic field on the interior and exterior of the surfaces.

The necessary and sufficient conditions for $\underline{E}(y)$ to represent the modes is that $\underline{\mu}$ must satisfy the following integral equations

$$\underline{\mu} + \int_S \hat{n}(y) \times (\underline{\mu} \times \nabla\phi) \, d\sigma_x = 0 \qquad y \in S_0 \tag{3.2.24}$$

$$\underline{\mu} + \int_S \hat{n}(y) \times (\underline{\mu} \times \nabla\phi) \, d\sigma_x = 0 \qquad y \in S_1 \tag{3.2.25}$$

There is only a finite number N of independent eigenfunctions $(\underline{E}_m, \underline{H}_m)$ [155]. Weston also argues that an upper-bound N for the pseudo

surfaces can be obtained and he proves that only a finite set of measurements (in practice only a few) at one frequency but different incidence will eliminate the pseudo loci.

3.3 THE IMPERFECTLY CONDUCTING CASE $\eta \neq 0$ or ∞

Having discussed the inverse boundary conditions for the idealized situation of electrically perfectly conducting bodies, we now attempt the derivation of these conditions for the more practical case of imperfectly conducting shapes. First of all, the fact must be reconsidered that the Leontovich condition which, though not entirely unique, may be considered most practical for treating the scattering problems of electromagnetic waves by imperfectly conducting bodies of regular and smooth shape. Obviously, the physical importance of this condition has not been fully exhausted and, as stated in Theorem 1, it is vital to note that two purely reactive vector quanitiies $\underline{A}$ and $\underline{B}$ exist which lie in the local plane of the scattering body ($\hat{n} \cdot \underline{A} = \hat{n} \cdot \underline{B} = 0$), are orthogonal ($\underline{A} \cdot \underline{B} = 0$) and are of equal magnitude ($\underline{A} \cdot \underline{A} = \underline{B} \cdot \underline{B}$). These basic properties are now exploited to establish novel inverse boundary conditions.

In contrast to the perfectly conducting case for which only the proper surface locus is to be determined; for the imperfectly conducting case, in addition, both modulus and phase of the averaged surface impedance $\eta = |\eta| \exp j\psi$ must be recovered. However since modulus and phase of η are involved in all the independent relations derived in Section 2.4 ,

those must be "prespecified" in a first step and then the proper surface locus must be discriminated re-employing the expressions of the appropriate complex local surface impedance. Furthermore, it is logical to treat three different cases for which it is assumed that (i) $\eta \neq 0$ or ∞ known and $S(\underline{r})$ is to be determined, (ii) $\eta = |\eta|$ and $S(\underline{r})$ are to be determined and (iii), $\eta(\underline{r})$ and $S(\underline{r})$ are to be determined from the expressions of the total electric and magnetic fields given in the vicinity of the bounding surface. An additional case in which the shape of the body is known but its surface impedance and the electrical size is to be determined is also considered.

3.4.1 $\eta \neq 0$ or ∞ KNOWN AND $S(\underline{r})$ IS TO BE DETERMINED

Assuming that the relative surface impedance is known *a priori* or can be recovered by other means, as e.g. described in Weston, Bowman and Ar [139], and that the total electric and magnetic fields can be computed in the vicinity of the scattering surface, then the two independent conditions $\underline{A} \cdot \underline{B} = 0$ and $\underline{A} \cdot \underline{A} = \underline{B} \cdot \underline{B}$ of Theorem 2 can be employed to uniquely determine the proper surface locus $S(\underline{r})$. Any one of these conditions, by itself, is necessary but not *locally* sufficient, producing in addition to the proper surface locus an infinity of pseudo loci. However, since

$$\underline{A}\cdot\underline{B} = [(\underline{E}\cdot\underline{E}^*)-\eta\eta^*(\underline{H}\cdot\underline{H}^*)][\eta(\underline{E}^*\cdot\underline{H}) + \eta^*(\underline{E}\cdot\underline{H}^*)]-\eta(\underline{E}\cdot\underline{H})[(\underline{E}^*\cdot\underline{E}^*) -\eta^{*2}(\underline{H}^*\cdot\underline{H}^*)]-\eta^*(\underline{E}^*\cdot\underline{H}^*)[(\underline{E}\cdot\underline{E})-\eta^2(\underline{H}\cdot\underline{H})] \equiv 0 \qquad (3.4.1)$$

and

$$\underline{A}\cdot\underline{A}-\underline{B}\cdot\underline{B} = [(\underline{E}\cdot\underline{E})-\eta^2(\underline{H}\cdot\underline{H})][(\underline{E}^*\cdot\underline{E}^*)-\eta^{*2}(\underline{H}^*\cdot\underline{H}^*)]-[(\underline{E}\cdot\underline{E}^*)-\eta\eta^*(\underline{H}\cdot\underline{H}^*)]^2$$

$$+ [\eta(\underline{E}^*\cdot\underline{H})+\eta^*(\underline{E}\cdot\underline{H}^*)]^2-4\eta\eta^*(\underline{E}\cdot\underline{H})(\underline{E}^*\cdot\underline{H}^*) \equiv 0 \qquad (3.4.2)$$

are independent conditions, only the resulting proper surface loci will be identical, whereas the independent sets of additional loci do not coincide. Therefore, if η is given, the proper surface locus can be determined from the total field expressions given in the vicinity of the bounding surface for one single frequency only.

For the case in which $\eta = 0$, the second characteristic equation (3.4.2) reduces to

$$(\underline{E}\times\underline{E}^*)\cdot(\underline{E}\times\underline{E}^*) = (\underline{E}\cdot\underline{E})(\underline{E}^*\cdot\underline{E}^*)-(\underline{E}\cdot\underline{E}^*)^2 = 0 \qquad \eta = 0 \qquad (3.4.2a)$$

and similarly for $\xi = 1/\eta = 0$ the same equation becomes

$$(\underline{H}\times\underline{H}^*)\cdot(\underline{H}\times\underline{H}^*) = (\underline{H}\cdot\underline{H})(\underline{H}^*\cdot\underline{H}^*) - (\underline{H}\cdot\underline{H}^*)^2 = 0 \quad \xi = 1/\eta = 0 \quad (3.4.2b)$$

In both of these special cases, it is not possible to determine the outward local normal from (3.4.2).

3.4.1a PROOF OF UNIQUENESS (IMPERFECTLY CONDUCTING CASES)

Consider the scattered field due to a smooth surface $S(\underline{r})$ on which the Leontovich boundary condition is satisfied and the relative impedance η is known. Let us assume that analytic expressions for the total field $\underline{E}$ and $\underline{H}$ are known everywhere exterior to the equivalent source region which resides in $S(\underline{r})$. In seeking the surface $S(\underline{r})$ by

looking for the surface on which either $\underline{A}\cdot\underline{B} = 0$ or $\underline{A}\cdot\underline{A} = \underline{B}\cdot\underline{B}$, it is possible that more than one eligible surface may be found for a particular wavenumber k.

Let us assume, therefore, that two surfaces $S_0(\underline{r})$ and $S_1(\underline{r})$ have been found on which either $\underline{A}\cdot\underline{B} = 0$ or $\underline{A}\cdot\underline{A} = \underline{B}\cdot\underline{B}$. Both these surfaces surround the equivalent source region and are taken to be smooth. In the volume V between the two surfaces the total electric and magnetic fields satisfy the source-free wave equations

$$(\nabla^2+k^2)\underline{E} = 0 \qquad (\nabla^2+k^2)\underline{H} = 0 \tag{3.4.3}$$

together with the equations

$$\nabla\cdot\underline{E} = 0 \qquad \nabla\cdot\underline{H} = 0 \tag{3.4.4}$$

However, solutions of these equations in the simply connected cavity V such that

$$\underline{E} - (\hat{n}\cdot\underline{E})\hat{n} = \eta\hat{n} \times \underline{H} \tag{3.4.5}$$

on the bounding surfaces $S_0(\underline{r})$ and $S_1(\underline{r})$ exist only for a discrete set of real or complex eigen-frequencies depending on whether η is real or complex, respectively. Thus, if k varies continuously, only the shape $S_1(\underline{r})$ must change in order to satisfy the boundary condition since, by definition, $S_0(\underline{r})$ is independent of wavelength.

The requirement that $S_0(\underline{r})$ remain unchanged as the frequency is varied continuously, therefore, allows determination of the scattering surface uniquely.

If η is known, the proper surface locus can be discriminated from the additional sets of pseudo-loci by computing the two independent characteristic equations (3.4.1) and (3.4.2) along radiant vectors for various aspect angles. Since these equations represent independent properties of the vectors $\underline{A}$ and $\underline{B}$, and $S_0(\underline{r})$ in both cases remains constant, the additional pseudo loci can easily be discriminated because they do not overlap for the two conditions. Furthermore, since the total field expressions are being defined as the vector sums of the incident and the scattered fields, plots of the orthogonality and the normality conditions display interference-like patterns. Therefore, the psuedo loci cannot be closed in the shadow region of the object while the locus representing the finite, closed and smooth scatterer is closed. This additional property leads to unique determination of the proper surface locus by employing either the orthogonality or the normality condition at one and the same operating frequency, assuming that both the electric as well as magnetic near field expressions are given over the entire unit sphere of directions. Therefore, this property makes each of the *locally* insufficient orthogonality and normality conditions *globally* sufficient.

3.4.2 η REAL OR IMAGINARY AND $S_0(\underline{r})$ ARE TO BE DETERMINED

For the case in which $\eta = |\eta|$ is not known *a priori*, the two independent characteristic equations (3.4.1) and (3.4.2) are first employed to determine the modulus of the relative surface impedance η. For $\eta = |\eta|$ the orthogonality condition $\underline{A} \cdot \underline{B} = 0$ simplifies to

$$\underline{A}\cdot\underline{B} = |\eta|[(\underline{E}\times\underline{E}^*)-|\eta|^2(\underline{H}\times\underline{H}^*)]\cdot[(\underline{E}^*\times\underline{H})-(\underline{E}\times\underline{H}^*)] = 0 \qquad (3.4.6)$$

and therefore the square modulus becomes

$$|\eta|_0^2 = \frac{(\underline{E}\times\underline{E}^*)\cdot[(\underline{E}^*\times\underline{H})-(\underline{E}\times\underline{H}^*)]}{(\underline{H}\times\underline{H}^*)\cdot[(\underline{E}^*\times\underline{H})-(\underline{E}\times\underline{H}^*)]} \qquad (3.4.7)$$

Similarly, the normality condition $\underline{A}\cdot\underline{A}-\underline{B}\cdot\underline{B} = 0$ can be simplified, resulting in a quadratic equation for the square modulus,

$$|\eta|^4|\underline{H}\times\underline{H}^*|^2-2|\eta|^2\{[(\underline{E}\times\underline{E}^*)\cdot(\underline{H}\times\underline{H}^*)-(\underline{E}^*\times\underline{H})\cdot(\underline{E}\times\underline{H}^*)]$$

$$+\frac{1}{2}[|\underline{E}^*\times\underline{H}|^2+|\underline{E}\times\underline{H}^*|^2]\} + |\underline{E}\times\underline{E}^*|^2 = 0 \qquad (3.4.8)$$

and therefore, another two-fold solution for the square modulus is found, where

$$|\eta|_{1,2}^2 = \frac{\{(\underline{E}\times\underline{E}^*)\cdot(\underline{H}\times\underline{H}^*)-(\underline{E}^*\times\underline{H})\cdot(\underline{E}\times\underline{H}^*)+\frac{1}{2}[|\underline{E}^*\times\underline{H}|^2+|\underline{E}\times\underline{H}^*|^2]\}}{(\underline{H}\times\underline{H}^*)\cdot(\underline{H}\times\underline{H}^*)}$$

$$\pm\frac{1}{(\underline{H}\times\underline{H}^*)\cdot(\underline{H}\times\underline{H}^*)}\{\{[(\underline{E}\times\underline{E}^*)\cdot(\underline{H}\times\underline{H}^*)-(\underline{E}^*\times\underline{H})\cdot(\underline{E}\times\underline{H}^*)]$$

$$+\frac{1}{2}[|\underline{E}^*\times\underline{H}|^2+|\underline{E}\times\underline{H}^*|^2]\}^2-|\underline{E}\times\underline{E}^*|^2|\underline{H}\times\underline{H}^*|^2\} \qquad (3.4.9)$$

Since the orthogonality (3.4.1) and the normality (3.4.2) conditions are independent of each other, it should be possible to discriminate the proper value of the surface impedance by simultaneous computation

of (3.4.7) and (3.4.9). For a point lying on the surface, only one of the solutions of (3.4.9) provides the proper value of $|\eta|^2$ which must be identical to that obtained, at that point from the single value provided by (3.4.7). The value of η_0 calculated from (3.4.7) at each point along a radiant vector is substituted into equations (3.4.1) and (3.4.2) to calculate the orthogonality and the normality conditions at those points. The point at which equations (3.4.1) and (3.4.2) have a coincident minimum, in addition to the values of one of the roots of (3.4.9) being identical with the root of (3.4.7), is the proper point on the surface. Another point for which the above two conditions are satisfied simultaneously cannot exist because (3.4.1) and (3.4.2) are independent relations. Furthermore, the resulting values of the square modulus must vary continuously and uniformly since the expressions for the total field vectors $\underline{E}$ and $\underline{H}$ are assumed to be analytic. Thus both the modulus $|\eta|$ and the point on the proper surface can be directly and uniquely specified from simultaneous computation of (3.4.7), (3.4.9), (3.4.1) and (3.4.2). For the purpose of increasing the resolution, the method outlined in (i) may be repeated using the correct value of the surface impedance calculated above. It is to be noted that for the case in which $\eta = 1 \exp j\psi$, both ψ and $S_0(\underline{r})$ can be uniquely determined by applying a procedure identical to that outlined above.

3.4.3 $\eta = |\eta| \exp j\psi$ and $S_0(\underline{r})$ ARE TO BE DETERMINED

For this general case, in which neither the modulus nor the phase of $\eta = \eta(r,w)$ are assumed to be known *a priori*, the two necessary but not

sufficient (though independent) conditions $\underline{A}\cdot\underline{B} = 0$ and $\underline{A}\cdot\underline{A} = \underline{B}\cdot\underline{B}$ must again provide all the required information, since no additional unique condition has been found in Section 2.4 . However, if it is known that η is homogeneous, the degeneracy condition can be employed in the neighborhood of the back-scattering direction to recover the correct value of the surface impedance η.

Defining $\underline{E}x\underline{E}^* = j\underline{a}$, $\underline{H}x\underline{H}^* = j\underline{b}$, $\underline{E}^*x\underline{H} = \underline{c}+j\underline{d}$ and $\eta = |\eta|(\cos\psi+j\sin\psi)$, the basic vector quantities $\underline{A}$ and $\underline{B}$ become

$$\underline{A} = j[\underline{a} - |\eta|^2\,\underline{b}] \tag{3.4.10}$$

$$\underline{B} = 2|\eta|\; j\;[\underline{c}\,\sin\psi + \underline{d}\,\cos\psi] \tag{3.4.11}$$

and from $\underline{A}\cdot\underline{B} = 0$ it follows that

$$|\eta|^2 = \frac{\underline{a}\cdot\underline{c}\,\sin\psi + \underline{a}\cdot\underline{d}\,\cos\psi}{\underline{b}\cdot\underline{c}\,\sin\psi + \underline{b}\cdot\underline{d}\,\cos\psi} \tag{3.4.12}$$

and similarly $\underline{A}\cdot\underline{A} - \underline{B}\cdot\underline{B} = 0$ becomes

$$\underline{a}\cdot\underline{a}-2|\eta|^2\underline{a}\cdot\underline{b}+|\eta|^4\underline{b}\cdot\underline{b} = 4|\eta|^2[\underline{c}\cdot\underline{c}\sin^2\psi+2\underline{c}\cdot\underline{d}\sin\psi\cos\psi+\underline{d}\cdot\underline{d}\cos^2\psi] \tag{3.4.13}$$

Substituting (3.4.12) into (3.4.13) results in a fourth order equation in $\tan\psi$

$$e_1\tan^4\psi+e_2\tan^3\psi+e_3\tan^2\psi+e_4\tan\psi+e_5 = 0 \tag{3.4.14}$$

where the coefficients e_r are given in *Appendix* A.2.

From equation (3.4.14), it follows that, in general, a four-fold

solution for the phase ψ of η results, and with (3.4.12) we obtain a four-fold solution for $\eta = |\eta|\exp(j\psi)$. But only one of these four resulting roots can be the correct value of η. It is to be noted that this four-fold solution was to be expected since the four complementry sets of the Leontovich equation had been employed to derive the unique relationships summarized in Theorem 1 and 2. In order to discriminate the proper value of η uniquely, at least another independent basic vector would be required so that additional independent and necessary conditions could be obtained. Therefore, for a general case, it is not yet possible to uniquely determine an arbitrary unknown $\eta = \eta(r,\omega)$.

However, if it is known that $\eta = |\eta|\exp j\psi$ is homogeneous and that the scatterer is closed and smooth, the degeneracy conditions as summarized in Theorem 3 can be favorably employed to uniquely specify the proper surface locus as well as $\eta = |\eta|\exp j\psi$ from the given set of total near field data computed in the vicinity of the scattering surface. In accordance with Theorem 3, the procedure is to determine first the backscattering point for which $\underline{E}\cdot\underline{H} = 0$, $\underline{A} = 0$ and $\underline{B} = 0$ and then to apply the degeneracy condition $\underline{A} \simeq 0$ and $\underline{B} \simeq 0$ at neighboring points, in addition to computing ψ and $|\eta|$ from (3.4.14) and (3.4.12) respectively. Although the degeneracy condition can be strictly applied only at the specular point as defined in Theorem 3, it is a sufficient first-order approximation if the curvature of the scattering surface in the neighborhood of that point is varying continuously and slowly.

Thus to discriminate the proper values of η from the resulting four roots of (3.4.14) and (3.4.12), modulus and phase of η are computed as first order approximations from $\underline{A} \simeq 0$, $\underline{B} \simeq 0$, where

$$|\eta|^2 \simeq \frac{\underline{E}x\underline{E}^*}{(\underline{H}x\underline{H}^*)} \qquad (3.4.15)$$

and

$$\exp j2\psi \simeq \frac{\underline{E}x\underline{H}^*}{\underline{E}^* x\underline{H}} \qquad (3.4.16)$$

Thus, once sufficient confidence in having discriminated the proper value of η is attained by repeated computation of (3.4.14), (3.4.15) along radiant vectors for different neighboring aspect angles, the discriminated proper η is directly substituted into the orthogonality and normality conditions, $\underline{A}\cdot\underline{B} = 0$ and $\underline{A}\cdot\underline{A} = \underline{B}\cdot\underline{B}$ respectively. Simultaneous computation along the radiant vectors thus should allow local discrimination of the exact point on the proper surface $S_0(\underline{r})$ as has been explained in Subsection 3.4.2 .

If the scatterer is known to be inhomogeneous but nondispersive, double frequency checking techniques may be employed. In this technique, values of the phase ψ and the magnitude $|\eta|$ of the surface impedance are calculated from equations (3.4.14) and (3.4.12) for two or more frequencies. The correct value of surface impedance will be found to be stationary along the radiant vector at the point which lies on the surface, while all other values will shift with change of frequency.

It is important to mention here that equations (3.4.15) and (3.4.16) are the special cases of the more general equations resulting from the orthogonality of the vectors $\underline{A}$, $\underline{B}$ and $\hat{n}$ which yields

$$\hat{n}\cdot\underline{A} = \hat{n}\cdot(\underline{E}\times\underline{E}^{*} - |\eta|^{2}\,\underline{H}\times\underline{H}^{*}) \equiv 0 \qquad (3.4.17)$$

$$\hat{n}\cdot\underline{B} = \hat{n}\cdot(\eta\underline{E}^{*}\times\underline{H} - \eta^{*}\underline{E}\times\underline{H}^{*}) \equiv 0 \qquad (3.4.18)$$

Therefore, the general expressions for $|\eta|$ and ψ are given by

$$|\eta|^{2} = \frac{\hat{n}\cdot(\underline{E}\times\underline{E}^{*})}{\hat{n}\cdot(\underline{H}\times\underline{H}^{*})} \qquad (3.4.19)$$

$$\exp(j2\psi) = \frac{\hat{n}\cdot(\underline{E}\times\underline{H}^{*})}{\hat{n}\cdot(\underline{E}^{*}\times\underline{H})} \qquad (3.4.20)$$

But, unfortunately the unit normal vector $\hat{n}$ cannot be determined independently of $\underline{A}$ and $\underline{B}$ and the equation of the surface of the scatterer. But, if the shape of the body is known (i.e. $\hat{n}$ is known) and only the unknown η of the scatterer and its electrical size are to be determined, equations (3.4.19) and (3.4.20) can be successfully employed.

chapter four

APPLICATION OF INVERSE BOUNDARY CONDITIONS TO TWO-DIMENSIONAL BODIES

4.1 INTRODUCTION

In order to demonstrate the validity of Theorems 1 to 3, as postulated in Section 2.4 and the applicability of the established sets of inverse boundary conditions as derived in Sections 3.2 - 3.4, the identification procedure for two-dimensional mono-body and two-body shapes is presented in this Chapter. The model targets chosen are circular cylinders of arbitrary radii and arbitrary, though homogeneous, material surface properties. This choice was dictated by the fact that sufficiently accurate information on the direct scattering solutions is available for cylindrical scatterers for which the electric and magnetic fields in the vicinity of the scattering surface satisfy the Leontovich or scalar impedance boundary condition. Since sufficiently accurate data for the cylindrical scattering case with inhomogeneous relative surface impedance $\eta(\underline{r})$ was not found in the literature [28], only the homogeneous cases are considered here.

The formulation of the electromagnetic fields, to which the inverse boundary conditions are applied, is based on the approach of Boerner et al [25] where the far scattered transverse field components are related to the Fourier coefficients of a properly truncated expansion in terms of circular cylindrical wave functions [49] via the scattered field matrix.

The *a priori* unknown expansion coefficients are recovered via a matrix inversion procedure to a degree of accuracy dictated only by measurement of both the amplitude and phase of the bistatic transverse scattered electric field components according to the theorems on optimal measurement aspect allocation [25 ,26]. Since the main objective of this thesis is to demonstrate the validity of the derived inverse boundary conditions,the results presented in [25] are readily applied and thus it is assumed that a sufficient number of Fourier coefficients has been recovered to the required degree of accuracy.

The direct scattering solution for a single circular cylinder with arbitrary surface impedance will be employed for obtaining the required Fourier coefficients. Since the direct scattering solution for two parallel circular cylinders with arbitrary radii and arbitrary surface impedances is not available in the literature, Olaofe's approach [92] for dielectric cylinders has been extended to this more general case in Section 4.2.2. In order to calculate the electromagnetic fields within the minimum circle enclosing the body, analytic continuation methods have been employed and a brief review of this technique is given in Section 4.3. Finally Section 4.4 presents the numerical verification of inverse boundary conditions.

4.2.1 THE MONOBODY CIRCULAR CYLINDRICAL CASE

Consider a plane electromagnetic wave, arbitrarily polarized, travelling along and in the direction of the negative x-axis and normally incident

on a circular cylindrical scatterer of electrical radius ka and surface impedance η as illustrated in Fig. 4.1. The incident field can be resolved in two components [41], the parallel polarized ($\underline{E}_{\parallel}$) and the normal polarized ($\underline{E}_{\perp}$) components with respect to the curvilinear circular cylindric coordinate surface [102,84], i.e.

$$\underline{E}_{inc} = (E_{\perp}\hat{a}_{\phi} + E_{\parallel}\,\hat{a}_{Z})\,\exp\,(-jkx) \qquad (4.2.1)$$

where the time dependence $\exp(-j\omega t)$ has been suppressed and k represents the free space wavenumber.

Without presenting elaborate detail, the parallel component of the incident field and the Z-component of the scattered field at point P' (Fig.4.1) can be expressed as

$$E_Z^i(r,\phi) = \sum_{n=-\infty}^{\infty}(-j)^n\, J_n(kr)\exp(jn\phi) \qquad (4.2.2)$$

$$E_Z^s(r,\phi) = E \sum_{n=-\infty}^{\infty}(-j)^n\, A_n H_n^{(1)}(kr)\exp(jn\phi) \qquad (4.2.3)$$

and

$$H_Z^s(r,\phi) = (E/Z_0) \sum_{n=-\infty}^{\infty}(-j)^n B_n H_n^{(1)}(kr)\exp(jn\phi) \qquad (4.2.4)$$

where $H_n^{(1)}(kr)$ designates the cylindrical Hankel function of the first kind and of order n and argument kr, and the remaining field components result from direct application of Maxwell's equations.

The TM and the TE Fourier coefficients A_n and B_n, respectively, are functions only of the radius a and the averaged relative surface

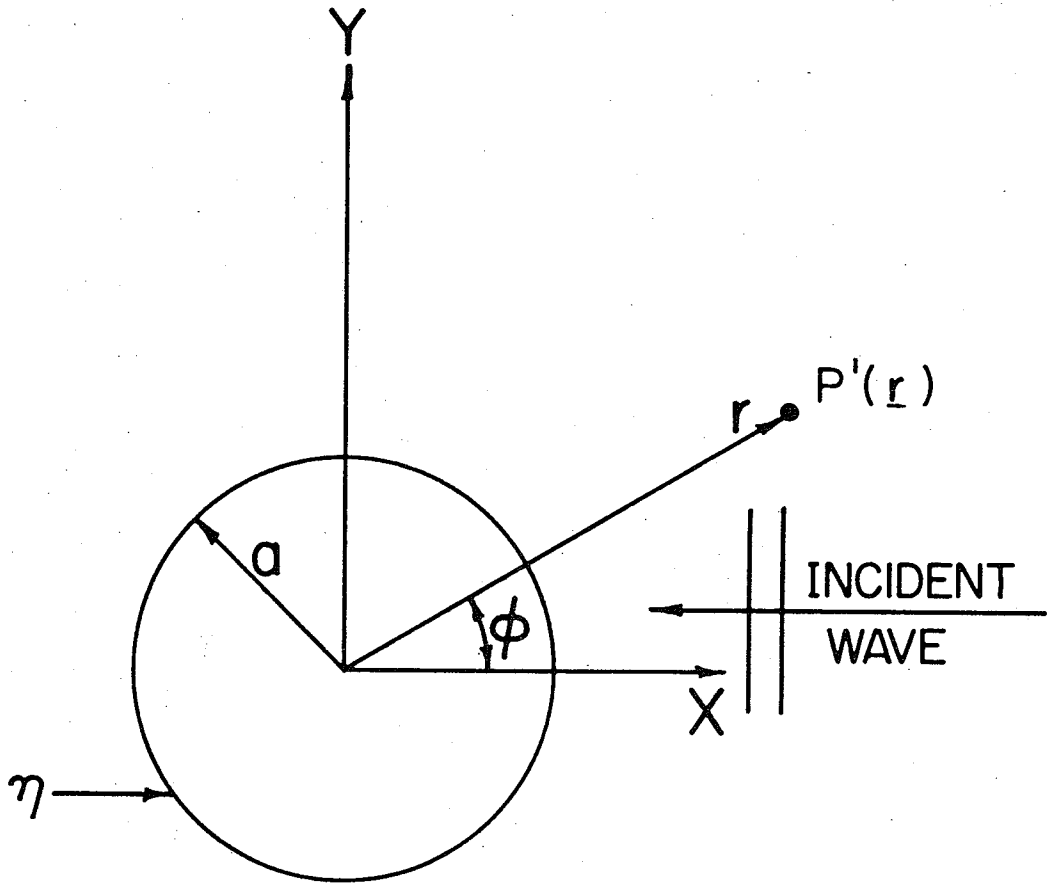

FIG. 4.1. A PLANE WAVE INCIDENT UPON A CYLINDER OF RADIUS a AND SURFACE IMPEDANCE η

impedance η, given for the considered case by

$$A_n = - \frac{J_n(ka) - j\eta J_n'(ka)}{H_n^{(1)}(ka) - j\eta H_n^{(1)'}(ka)} \qquad (4.2.5)$$

and

$$B_n = - \frac{\eta J_n(ka) - j\, J_n'(ka)}{\eta H_n^{(1)}(ka) - j\, H_n^{(1)'}(ka)}$$

where $J_n(ka)$ represents the Bessel function of order n and argument ka and the primed expressions denote differentiation with respect to $kr(=ka)$.

It should be noted that the superposition of existent $TM(A_n)$ and $TE(B_n)$ fields [2] are strictly required in the cylindrical case of normal plane wave incidence for the valid applicability of the inverse boundary conditions derived in Section 3.4 [23].

4.2.2 THE TWO-BODY CIRCULAR CYLINDRICAL CASE

The method of solution presented in this subsection follows that of van der Hulst [125] and Olaofe [92] in which the fields are expressed in terms of the Debye transverse magnetic and electric scalar potential functions, and well established methods of coordinate origin transformation [115 , 54 ,147 , 78 ,136] are employed..

Consider two infinite, non-overlapping, parallel circular cylindric

scatterers of arbitrary radii a_1 and a_2, and homogeneous relative surface impedances η_1 and η_2 illuminated by a mixed-polarized plane wave, normally incident at an angle β with respect to the geodesic of length $d > (a_1+a_2)$, connecting the centers 0_1 and 0_2 of the two scatterers, as illustrated in Fig. 4.2. The total field is represented in terms of two scalar potential functions, namely the TM($E_{inc} = E_Z = \psi^{TM}$) and the TE($H_{inc} = H_Z = \psi^{TE}$) modes [125], where the potentials of the incident field are given by

$$\psi_i^{TM}(r_i,\phi_i) = \varepsilon_i \sum_{n=-\infty}^{\infty} (-j)^n J_n(kr_i)\exp(jn\phi_i) \qquad (4.2.7)$$

and

$$\psi_i^{TE}(r_i,\phi_i) = \varepsilon_i \sum_{n=-\infty}^{\infty} (-j)^n J_n(kr_i)\exp(jn\phi_i) \qquad (4.2.8)$$

where

$$\varepsilon_i = \exp[jkd(2-i)\cos\beta] \qquad (4.2.9)$$

and $i = 1$ or 2 designates the cylinder of radius a_1 or a_2 and of surface impedance η_1 or η_2, respectively.

The scattered field potentials U_i^{TM} and V_i^{TE} for the TM and TE components are respectively given [92] by

$$U_i^{TM}(r_i,\phi_i) = \sum_{n=-\infty}^{\infty} {}_i a_n (-j)^n H_n^{(1)}(kr_i)\exp(jn\phi_i) \qquad (4.2.10)$$

and

$$V_i^{TE}(r_i,\phi_i) = \sum_{n=-\infty}^{\infty} {}_i b_n (-j)^n H_n^{(1)}(kr_i)\exp(jn\phi_i) \qquad (4.2.11)$$

where ${}_i a_n$ and ${}_i b_n$ are the scattering coefficients of cylinder $i(=1 \text{ or } 2)$ in the presence of cylinder $i'(=2,1) \neq i(1,2)$.

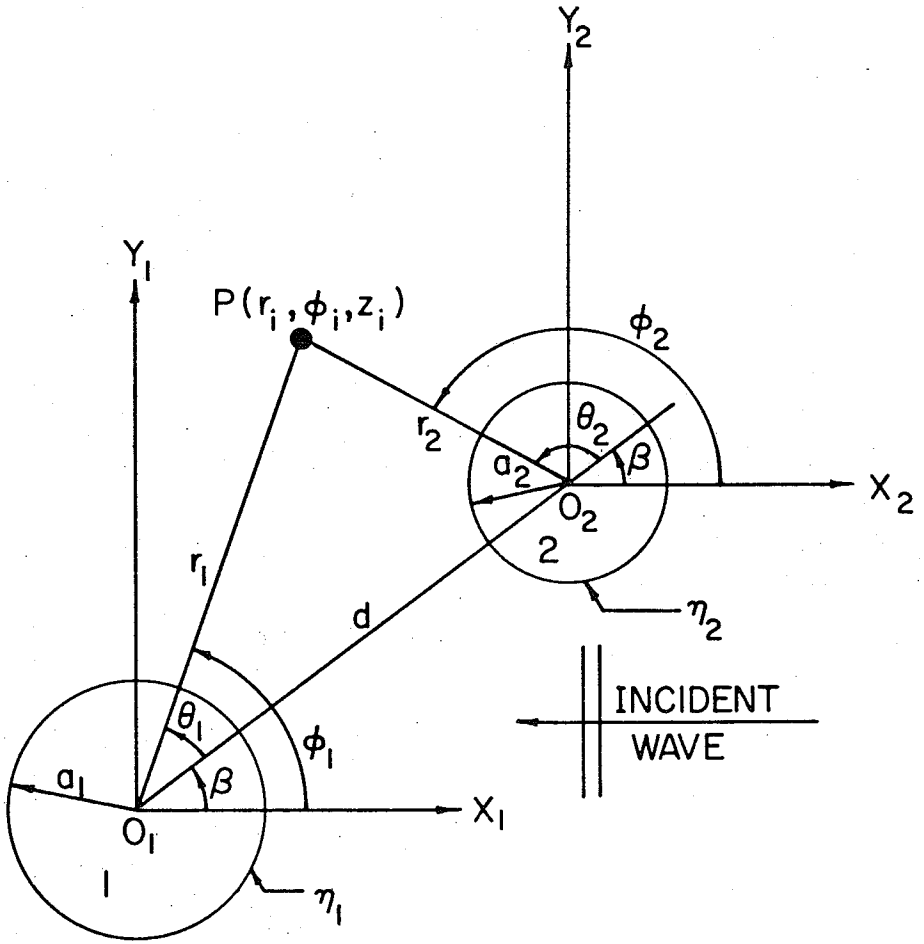

FIG. 4.2. SCATTERING BY TWO CYLINDERS OF RADII a_1 AND a_2 AND SURFACE IMPEDANCES η_1 AND η_2

In order to apply the boundary conditions on cylinder $i(=1,2)$, the fields of cylinder $i'(=2,1)$ have to represented in the coordinate system of cylinder $i(1,2)$. Employing Watson's scalar addition theorems [133] in accordance with the definition of Fig. 4.2, i.e.

$$\exp(jn\theta_2)H_n^{(1)}(kr_2)=(-1)^n\sum_{\ell=-\infty}^{\infty}H_{n+\ell}^{(1)}(kd)J_\ell(kr_1)\exp(-j\ell\theta_1) \quad (4.2.12)$$

and

$$\exp(jn\theta_1)H_n^{(1)}(kr_1)=\sum_{\ell=-\infty}^{\infty}(-1)^\ell H_{n+\ell}^{(1)}(kd)J_\ell(kr_2)\exp(-j\ell\theta_2) \quad (4.2.13)$$

the total field U_i^{tot} outside the ith cylinder for the TM case is given by

$$U_i^{tot}(r_i,\phi_i)=\sum_{n=-\infty}^{\infty}(-j)^n\{[\varepsilon_i J_n(kr_i)+{}_ia_nH_n^{(1)}(kr_i)]\exp(jn\phi_i)$$

$$+{}_ia_n\exp(jn\beta)\sum_{\ell=-\infty}^{\infty}(-1)^{n(2-i)+\ell(i-1)}H_{n+\ell}^{(1)}(kd)J_\ell(kr_i)\exp(-j\ell\theta_i)\} \quad (4.2.14)$$

It is now convenient to introduce the following abbreviation

$${}_{i'i}A_n=\sum_{\ell=-\infty}^{\infty}(-j)^\ell(-1)^{\ell(2-i)+n(i-1)}{}_{i'}a_\ell H_{n+\ell}^{(1)}(kd)\exp(j\ell\beta) \quad (4.2.15)$$

so that (2.2.8) reduces to

$$U_i^{tot}(r_i,\phi_i)=\sum_{n=-\infty}^{\infty}\{(-j)^n[\varepsilon_i J_n(kr_i)+{}_ia_nH_n^{(1)}(kr_i)]$$

$$+{}_{i'i}A_{-n}J_{-n}(kr_i)\exp(-jn\beta)\exp(jn\phi_i)\} \quad (4.2.16)$$

Application of the scalar impedance boundary condition (2.3.1) onto

(4.2.16) at $r_i = a_i$ results in

$$U_i^{tot}(r_i,\phi_i) = \frac{j\eta}{k}\frac{\partial}{\partial r}\left[U_i^{tot}(r_i,\phi_i)\right] \tag{4.2.17}$$

so that

$${}_i a_n = A_n^i\left[\varepsilon_i+(-j)^n {}_{i'i}A_{-n}\exp(-jn\beta)\right] \tag{4.2.18}$$

where A_n^i denotes the TM coefficients as defined in equation (4.2.5) for independent mono-body scattering from a circular cylinder of radius a_i and surface impedance η_i. The corresponding results for the TE case can be obtained by following a similar approach. In this case the total magnetic potential is given by

$$V_i^{tot}(r_i,\phi_i) = \sum_{n=-\infty}^{\infty}\{(-j)^n[\varepsilon_i J_n(kr_i)+{}_i b_n H_n^{(1)}(kr_i)]$$

$$+{}_{i'i}B_{-n}J_{-n}(kr_i)\exp(-jn\beta)\}\exp(jn\phi_i) \tag{4.2.19}$$

with

$${}_i b_n = B_n^i\left[\varepsilon_i+(-j)^n {}_{i'i}B_{-n}\exp(-jn\beta)\right] \tag{4.2.20}$$

and

$${}_{i'i}B_n = \sum_{\ell=-\infty}^{\infty}(-j)^{\ell(2-i)+n(1-i)}\,{}_{i'}b_\ell H_{n+\ell}^{(1)}(kd)\exp(j\ell\beta) \tag{4.2.21}$$

and B_n^i denotes the TE coefficients as defined in (4.2.6) for independent mono-body scattering from a circular cylinder of radius a_i and surface impedance η_i.

Equations (4.2.18) and (4.2.20), each of which consists of two coupled equations, can be solved either by a matrix inversion or by an iteration method where for convenience the latter method has been employed. It should be noted that the rate of convergence becomes very rapid as the electrical distance between the axes increases i.e. $kd \geq 4ka_m$ where a_m denotes the layer of the two radii of the scatterers [92]. Furthermore, observe that for the end-fire ($\beta = 0$) case ${}_ia_n = {}_ia_{-n}$ and ${}_ib_n = {}_ib_{-n}$, whereas for broad-side illumination ${}_ia_n = {}_{i'}a_{-n}$ and ${}_ib_n = {}_{i'}b_{-n}$ with $i \neq i'$ $(=1,2)$.

4.3 TWO-DIMENSIONAL ANALYTIC CONTINUATION

In order to determine the shape and the material surface constituents over all surface regions enclosing the target, near field expressions for the total fields are required everywhere in the vicinity of the target. Since the field expansions of (4.2.15) and (4.2.16) are convergent only outside the minimum circle enclosing the equivalent sources [85,146], the field must be continued analytically. By changing the origin of the coordinate system one would obtain an expansion outside a different minimum circle. Thus, by repeatedly changing the coordinate system and with simultaneous reformulation of the associated field expansions, one can obtain convergent expressions for the near scattered field everywhere outside the minimum convex shape enclosing the equivalent sources as has been shown in Weston, Bowman and Ar [140]. This method, further analysed in [136], has been employed by Imbriale and Mittra [54] for the profile characteristics

inversion of two-dimensional perfectly conducting shapes, using the fact that the tangential component of the electric field vanishes on a perfectly conducting body. The scattered field expansion, valid outside the circle of minimum radius r_a enclosing the equivalent sources, as defined in Fig. 4.3, is

$$U(r,\phi) = \sum_{n=-\infty}^{\infty} a_n (-j)^n H_n^{(1)}(kr)\exp(jn\phi) \tag{4.3.1}$$

Note that for $r < r_a$ this series representation diverges, so it is possible to determine the radius $r = r_a$ from numerical behavior of the series for $r < r_a$. With respect to a new circular cylindric coordinate system centered at 0' with all three axes parallel to that of the initial system centered at 0, as shown in Fig. 4.3, the field can be represented outside the circle of minimum radius r_a' as

$$U'(r',\phi') = \sum_{m=-\infty}^{\infty} a_m' (-j)^m H_m^{(1)}(kr')\exp(jm\phi') \tag{4.3.2}$$

The coefficients a_m', can be expressed in terms of the a_n by the use of scalar addition theorem [115]

$$H_n^{(1)}(kr)\exp(jn\phi) = \sum_{m=-\infty}^{\infty} \begin{Bmatrix} H_{n-m}^{(1)}(kr_0) \\ J_{n-m}(kr_0) \end{Bmatrix} \exp j(n-m)\phi_0 \begin{Bmatrix} J_m(kr') \\ H_m^{(1)}(kr') \end{Bmatrix} \exp(jm\phi') \quad \text{for} \begin{cases} r_0 > r' \\ r_0 < r' \end{cases} \tag{4.3.3}$$

Substitution of (4.3.3) into (4.3.2) and a change of summation index results in the following expression for a_m' [147]

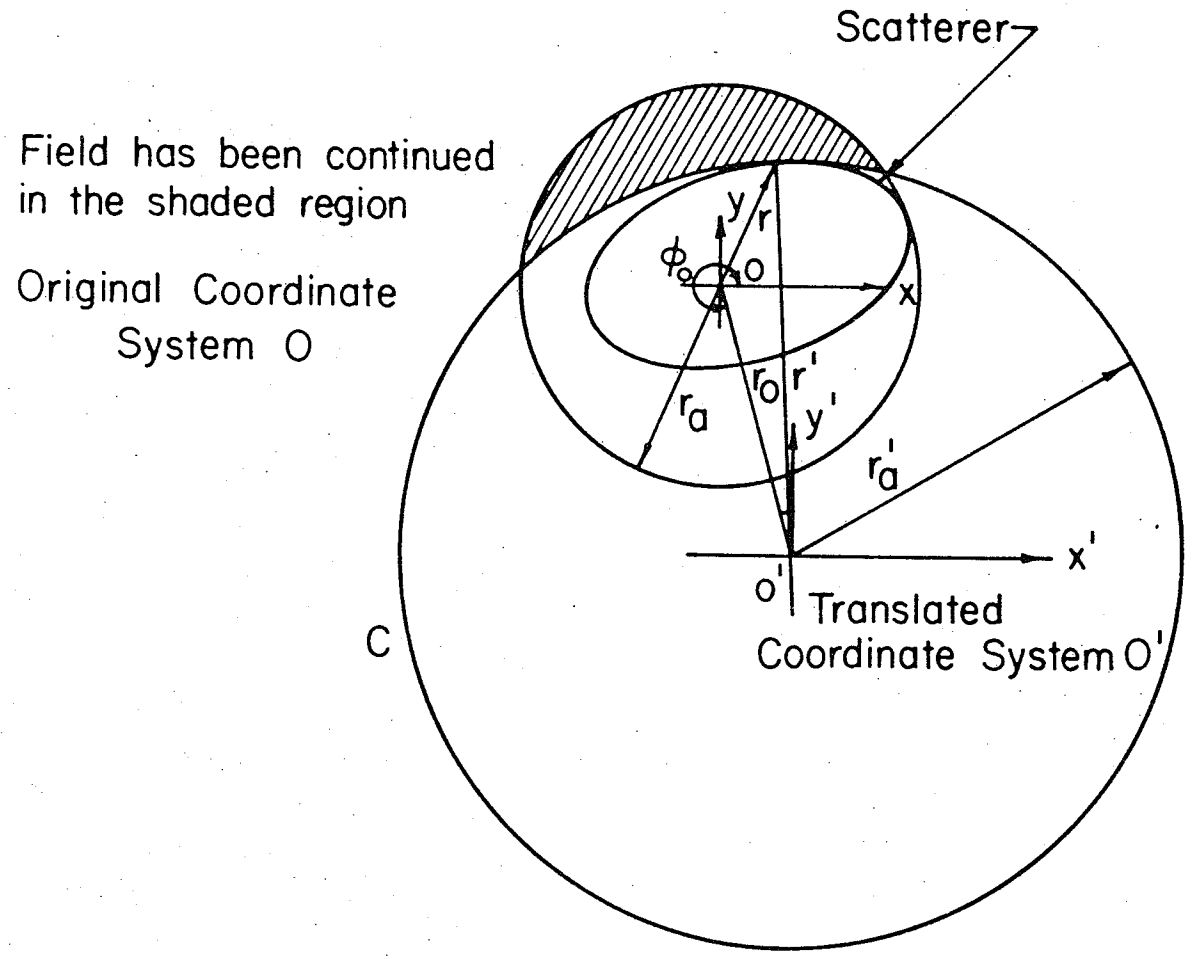

FIG.4.3. ANALYTIC CONTINUATION OF THE ELECTRO-MAGNETIC FIELD USING OUTSIDE EXPANSION

$$a'_m = \sum_{n=-\infty}^{\infty} a_n j^{n-m} J_{m-n}(kr_0)\exp[j(n-m)\phi_0] \qquad (4.3.4)$$

where kr_0 ($<kr'$) denotes the electrical translation distance and ϕ_0 designates the transformation angle as defined in Fig.4.3.

Using the above expansions the field can be continued everywhere in the vicinity of a smooth convex scatterer [75 -78]. But for bodies of arbitrary convex/concave shape the fields must be expanded in terms of cylindrical wave functions which are valid within the largest circle of radius r_0 which excludes the body [78]. Within this circle defined in Fig. 4.4, the field can be expressed as

$$U'(r',\phi') = \sum_{\ell=-\infty}^{\infty} a'_\ell (-j)^\ell J_\ell(kr')\exp(j\ell\phi') \qquad (4.3.5)$$

where a'_ℓ , the scattering coefficients in the new coordinate system can be expressed in terms of the coefficients a_n associated with the initial frame, (4.3.1) by using the addition theorem of equation (4.3.3), noting that $kr_{ab} > kr_b$. These coefficients are given, as is also shown in [147], by

$$a'_\ell = \sum_{n=-\infty}^{\infty} a_n j^{n-\ell} H^{(1)}_{\ell-n}(kr_{ab})\exp[j(n-\ell)\phi_0] \qquad (4.3.6)$$

The expansions represented by equations (4.3.1) to (4.3.6) will be exact if summation is performed over the complete range $-\infty \leq n \leq \infty$. But, in practice, one has to truncate the series to a finite number of terms and the question, at which bound one should truncate the series is of paramount importance for numerical computation and will be discussed in *chapter six*.

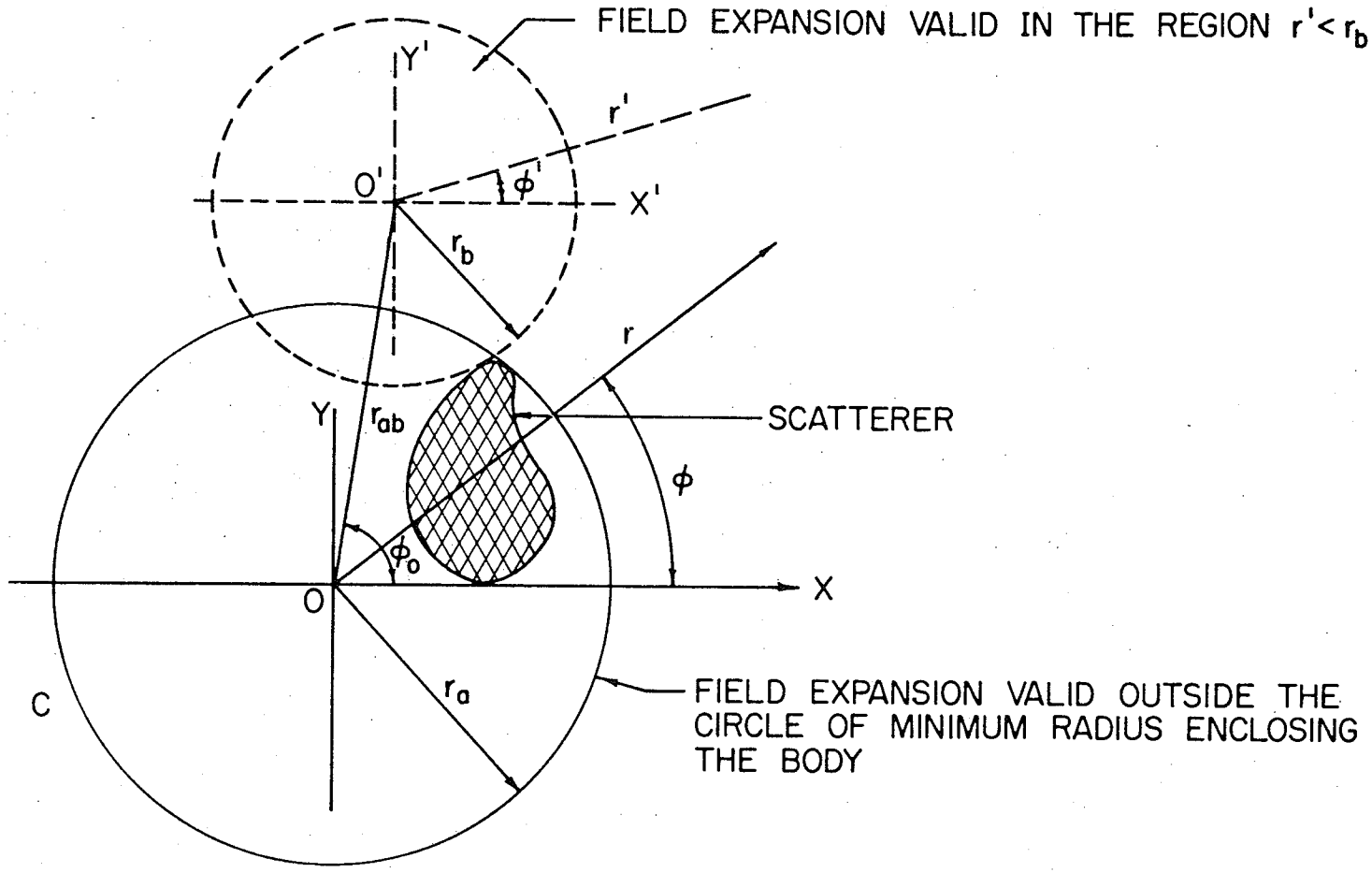

FIG.4.4. ANALYTIC CONTINUATION OF ELECTROMAGNETIC FIELD USING INSIDE EXPANSION

4.4 NUMERIC COMPUTATIONAL VERIFICATION (2-DIM.)

In order to invert the profile of the scattering bodies accurately and optimally, efficient computational techniques based on maximum use of recursive and iterative techniques must be used. All the programs were written in Fortran IV language, using double precision arithmetic for special functions and single precision for all other routines. The special functions, the expansion coefficients, A_n and B_n for the single cylinder, and ${}_i a_n$, ${}_i b_n$ for two cylinders and the program for two-dimensional analytic continuation were generated as subroutines which are called by the main program when required.

For the purpose of demonstrating the applicability of the various sets of inverse boundary conditions efficiently, the numerical verification has been divided into two parts. The perfectly conducting cases are treated first to introduce the identification procedure resulting from the simultaneous application of the relevant inverse boundary conditions (3.2.3) to (3.2.10) and numerical methods are introduced for this case in detail. The techniques so established are then applied to the imperfectly conducting cases employing the various sets of inverse boundary conditions derived in Subsection 3.3.

4.4.1a PERFECTLY CONDUCTING MONOBODY CASE

The total electric and magnetic field expressions in this case are readily obtained from the definitions of (4.2.2) to (4.2.4). The

series representation of these equations are truncated according to the criterion developed in *chapter six*. For the perfectly electric conducting target of electrical radius ka = 5, selected here, the order of truncation N of both of TM and TE field expansions employed here was chosen to be N = 8, thus lying within the lower bound N_ℓ = 5 and the upper bound N_u = 16. The inverse conditions Q_1 = Min $\{[\underline{E}x\underline{E}^*)\cdot(\underline{E}x\underline{E}^*)\}$, Q_2 = Min$\{\underline{E}\cdot\underline{H}\}$ and Q_3 = Min$\{|\underline{E}_{inc}|-|\underline{E}_{scat}|\}$, resulting from (3.2.6), (3.2.5) and (3.2.4) respectively are then applied to the computed fields. The plots of Q_1, Q_2 and Q_3 resulting from computation along the arbitrarily chosen radiant vector defined by ϕ = 22.5° vs. the radial distance kr are shown in Fig. 4.5a. It is evident from this figure that the conditions Q_2 and Q_3 produce only one minimum, whereas Q_1 produces an infinite set of pseudo minima in addition to the highly pronounced minimum specifying the proper point on the exact surface $S_0(\underline{r})$. This behavior of these three inverse conditions proves that Q_1 is a necessary but not *locally* sufficient condition but Q_2 and Q_3 are both necessary and *locally* sufficient conditions. The proper minimum of Q_1 can be discriminated with the aid of conditions Q_3 and Q_2. It is evident from Fig. 4.5a that the conditions Q_1 and Q_2 specify the exact point on the proper surface locus $S_0(\underline{r})$ to a higher of accuracy as compared to the physical optics condition Q_3. This statement is more strongly valid for those portions of the scattering surface which lie in the umbra region, as has also been shown in Weston and Boerner [137] where they demonstrate that for the low frequency case, the physical optics boundary condition becomes rather inadequate.

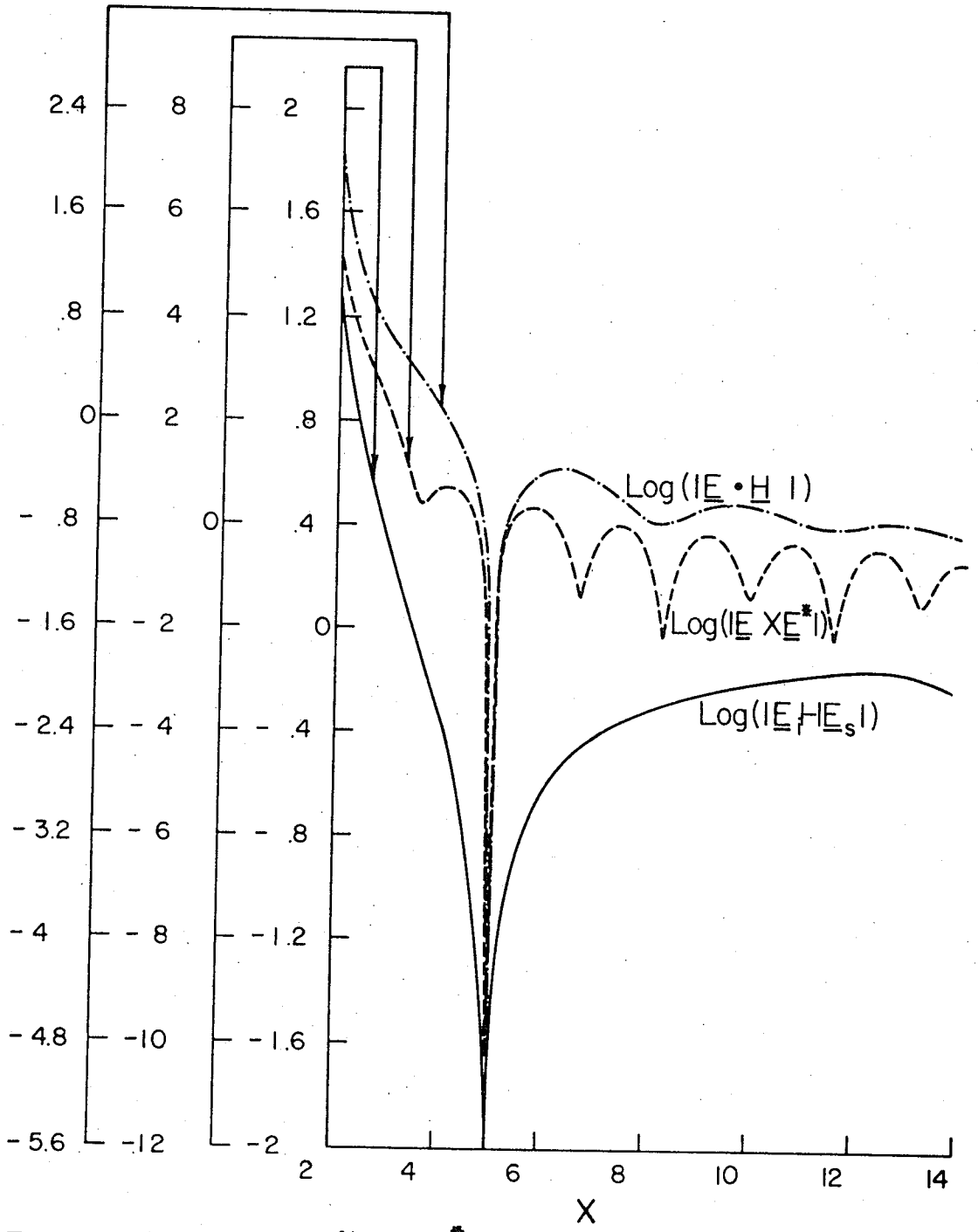

Fig. 4.5a. Plot of Log $\{|\underline{E} \times \underline{E}^* |^2\}$, Log$\{|\underline{E}_i|-|\underline{E}_s|\}$, Log$\{|\underline{E}\cdot\underline{H}|\}$ Versus Radiant Vector $X = kR$ for a Cylindrical Target of $ka = 5.0$, $\eta = 0$ for a Ray $\phi = 22.5°$

The various loci resulting from the simultaneous application of Q_1, Q_2 and Q_3 are plotted in Fig. 4.5b demonstrating that Q_1 and Q_2 specify the proper surface locus to a high degree of accuracy. Furthermore, it should be observed that the additional pseudo loci are not closed in the umbra region for the closed circular cylindrical shape selected here. This reflects the interference behavior of the total field expressions and thus makes the exact, necessary but not *locally* sufficient condition $|\underline{E}x\underline{E}^*| = 0$, *globally* sufficient for those cases in which the scatterer is of closed shape [2]. Therefore, it is concluded that from the simultaneous application of the three inverse boundary conditions $Q_1 = \text{Min}\{(\underline{E}x\underline{E}^*)\cdot(\underline{E}x\underline{E}^*)\}$, $Q_2 = \text{Min}\{\underline{E}\cdot\underline{H}\}$ and $Q_3 = \text{Min}\{|\underline{E}_{inc}|-|\underline{E}_{scat}|\}$, it should be possible to uniquely and exactly recover the proper shape of a closed scatterer, given field data everywhere in the vicinity and closer neighborhood of a scatterer for only one operating frequency. However, it should be noted that for the valid application of the inverse conditions $\underline{E}\cdot\underline{H} = 0$, and $\underline{E}^*\cdot\underline{H} = 0$ or $\underline{E}\cdot\underline{H}^* = 0$ (which are not being employed here, since they display the same characteristics as does the condition $\underline{E}x\underline{E}^* = 0$ [23]) the incident wave must contain both parallel and normal polarized components since otherwise $\underline{E}\cdot\underline{H} = \underline{E}^*\cdot\underline{H} = \underline{E}\cdot\underline{H}^* \equiv 0$ everywhere [23].

4.4.1b PERFECTLY CONDUCTING TWO-BODY CASE

In order to show that the inverse boundary conditions applied above, and also employed in [23] to the monobody spherical cases, also hold

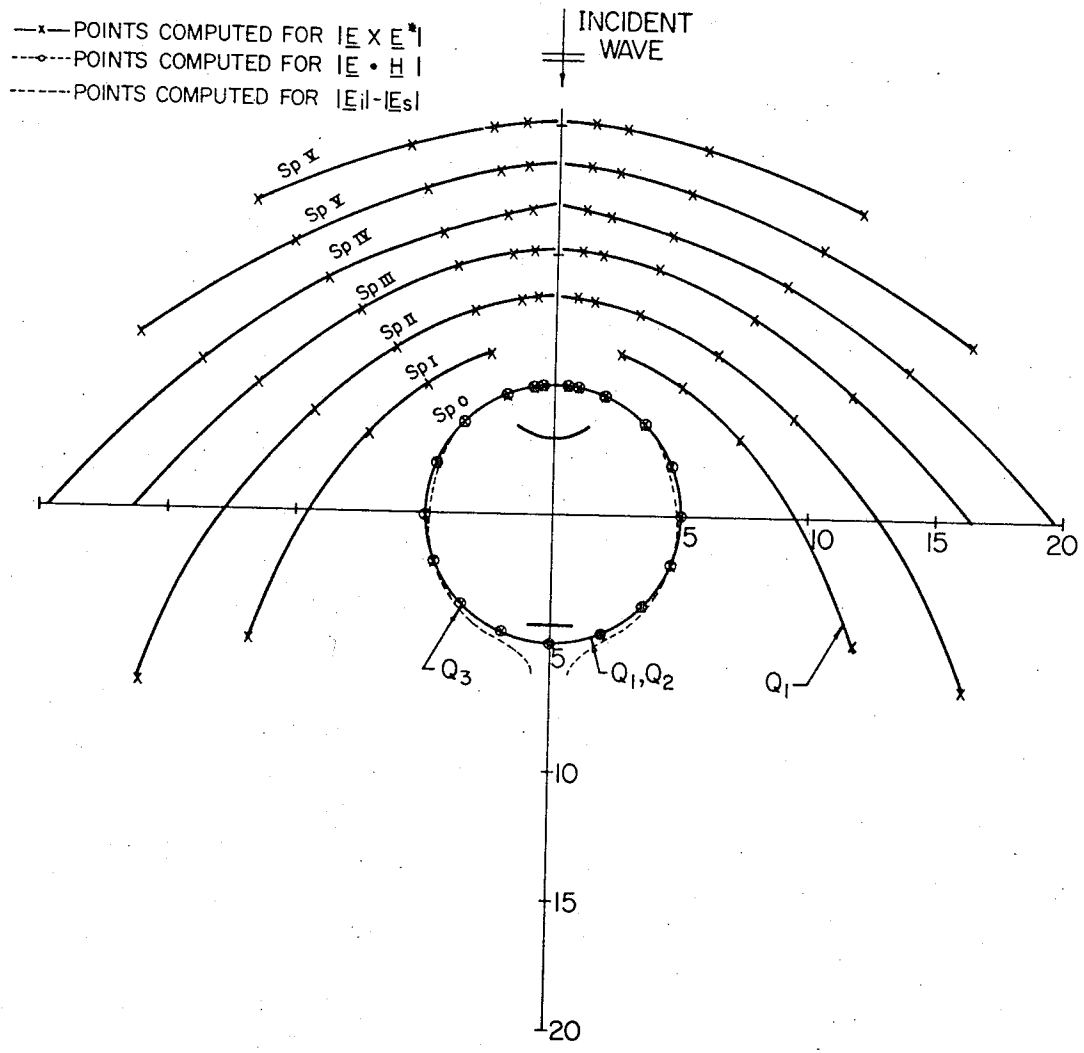

Fig. 4.5 b. LOCI OF SUCCESSIVE MINIMA OF $\underline{E} \times \underline{E}^*$ FOR A PERFECTLY CONDUCTING CYLINDER OF ELEC. RADIUS 5.0

for more complicated smooth and closed shapes, a two-dimensional configuration of two non-overlapping electrically perfectly conducting circular cylinders as defined in Fig. 4.2, has been selected. The selection of this configuration results from the fact that it represents the curves and contours of a general body and exact direct scattering solutions for this configuration are available (Subsection 4.2.2 and [92]). The single precision expansion coefficients $_{i}a_{n}$ and $_{i}b_{n}$ for the two-body configuration of Fig. 4.2 are calculated according to (4.2.18) and (4.2.20) for $\eta = 0$ and great care has been taken in applying valid order of truncation bounds as is analysed in *chapter six*. The test cases selected for illustration consist of two parallel electrically perfectly conducting circular cylinders of equal electrical radii $ka_1 = ka_2 = 1.0$ with their centers separated by an electrical distance $kd = 4.0$. Mixed polarized, normal plane wave incidence at an angle β with respect to the line joining the centers 0_1 and 0_2 of the two cylinders as shown in Fig.4.2 is assumed.

Since the main objective of this work is to verify the validity of the inverse boundary conditions, rather than to establish a perfected computational discrimination procedure, a grid of computational rays passing through the centers of the cylinders was selected over the entire plane. In order to demonstrate the interference of the individual patterns of the pseudo loci effectively, more computational lines have been employed in the vicinity of the line of incidence passing through the center of the configuration. However, it should be mentioned here that a discrimination procedure applicable in those practical cases for which no *a priori* information

on the nature of the scattering geometry can be assumed, could easily be established employing the minimax method of Rosenbrock [100], as has also been proposed in [54].

Thus, in the presented analysis, the origins of the translated coordinates have been chosen to lie on each of these rays. The scattering coefficients for each of the cylinders in the presence of the other, as given by (4.2.18) and (4.2.20) for $\eta = 0$, are transformed to the new coordinate system defined in Fig. 4.4 using (4.3.5) and (4.3.6) for the inside analytic continuation. Due to the linearity of the fields, the sums C_n and d_n of the translated coefficients associated with the two electrically perfectly conducting cylinders, ${}_1a'_n$, ${}_2a'_n$ and ${}_1b'_n$, ${}_2b'_n$ for $\eta = 0$ respectively, provide the scattering coefficients for the two-body configuration with respect to the translated coordinate system. A similar approach was employed to discriminate points lying on the minimum circle enclosing the two scatterers where use was made of (4.3.2) and (4.3.4) for outside analytic continuation.

Figs. 4.6a to 4.6d display the plots of the families of loci resulting from the application of the inverse boundary condition $Q_1 = \text{Min}\{(\underline{E}x\underline{E}^*)\cdot(\underline{E}x\underline{E}^*)\}$ on a selected grid of rays for different values of the relative angle of incidence $\beta(90°,75°,45°,0°)$. It is observed that the pseudo loci Sp_n result from the superposition of the family of loci displayed by individual cylinders in Fig. 4.5b. In the vicinity of that line of incidence which passes through the center of the con-

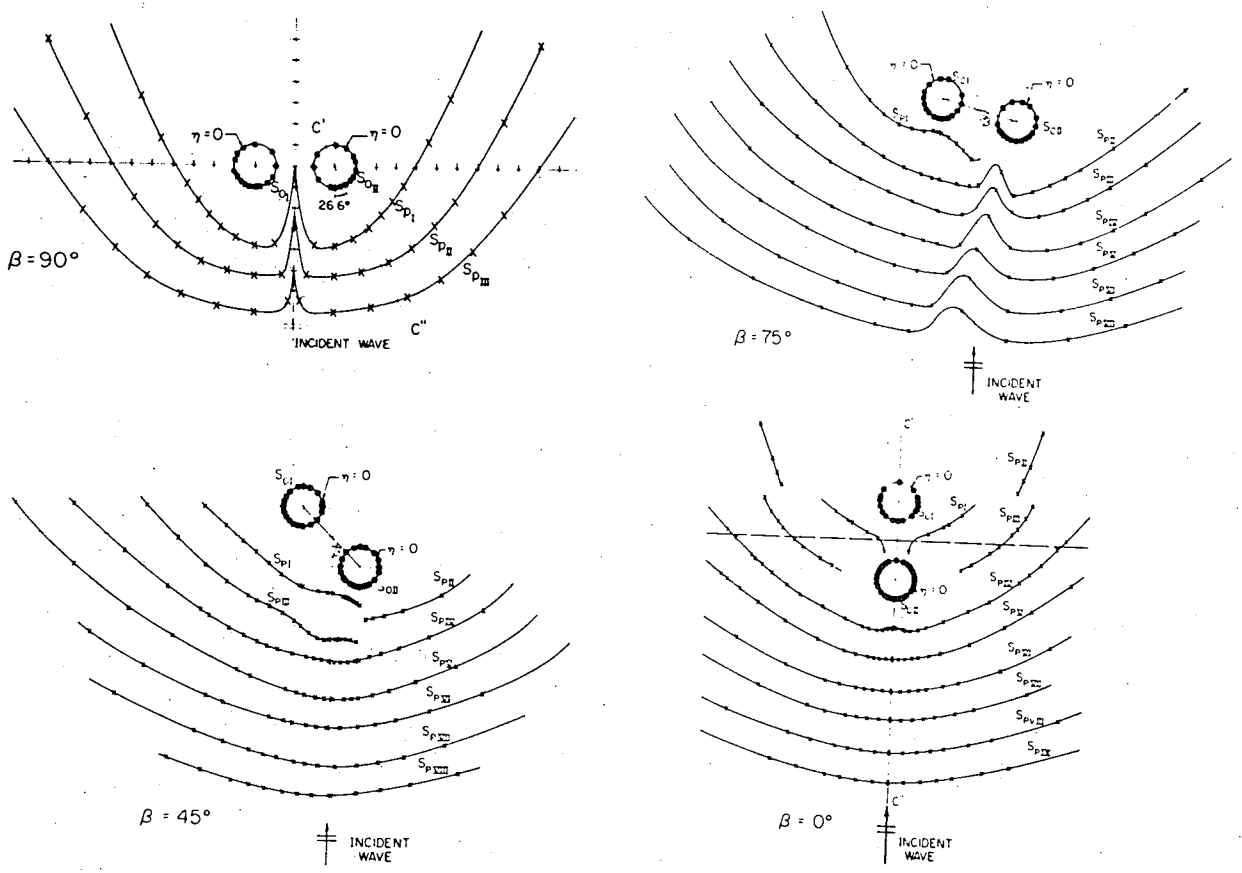

Fig. 4.6. Loci of Successive Minima of $\underline{E} \times \underline{E}^*$ for Two Perfectly Conducting Cylinders of Elec. Radii $ka_1 = ka_2 = 1.0$ and Separation between Centers $kd = 4$

—x— Points Computed for $|\underline{E} \times \underline{E}^*|$

—o— Points Computed for $|\underline{E} \cdot \underline{H}|$

figuration the pseudo loci are depressed inward and the depression decreases with decreasing relative angle of incidence β as would be expected. Similar to the case of the single cylinder, the additional pseudo loci Sp_n are not closed in the umbra region, whereas the exact locus $S_0(\underline{r})$ is closed, thus confirming the property that $\underline{E}x\underline{E}^* = 0$ is a globally sufficient condition. Again, as has been shown in the monobody case, the inverse condition Q_1 specifies the proper surface locus to a high degree of accuracy. Therefore, the approximate, though necessary and sufficient condition $Q_3 = \text{Min}\{|\underline{E}_{inc}|-|\underline{E}_{scat}|\}$ is not required except that Q_2 and Q_3 do aid in the discrimination of the proper surface locus. In Fig. 4.7a the curves resulting for the three inverse conditions Q_1, Q_2 and Q_3 are plotted along a selected computational line C'-C" for the case of broad-side incidence illustrated in Fig. 4.6a whereas in Fig. 4.7b the results are presented for the endfire case of Fig. 4.6d, thus verifying the accuracy of the discrimination criteria established above.

The fact that even the entire configuration of Figs.4.6d and 4.7b can be identified so accurately, very strongly proves the soundness of the introduced inversion technique. These conditions have also been successfully tested for a variety of combinations of two cylinders of non-identical radii and for arbitrary relative angle of incidence β.

Since the method of profile inversion of magnetically perfectly conducting shapes follows identical procedures [23] no further results are presented here.

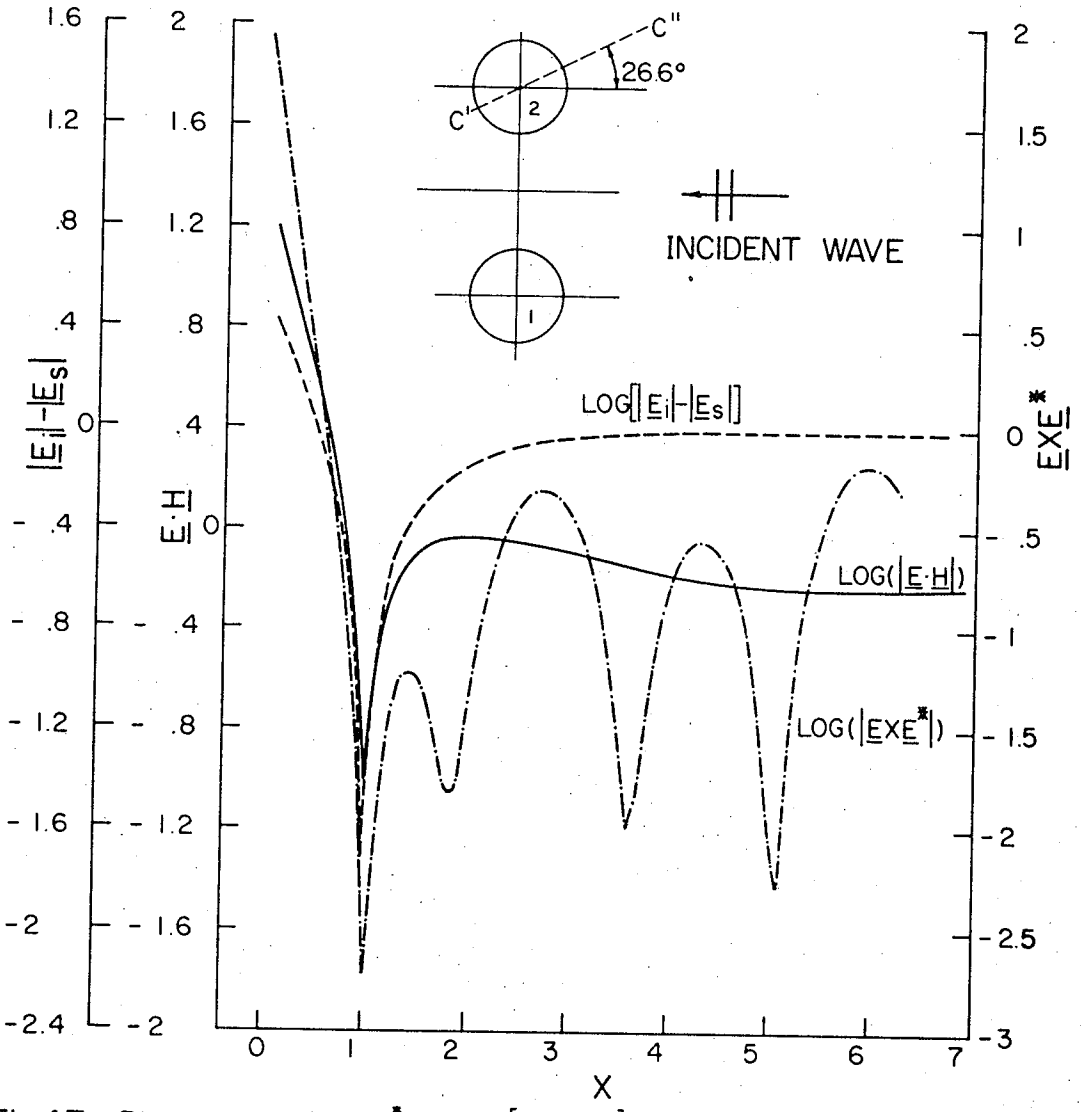

Fig.4.7a. Plots of Log($|\underline{E}\underline{X}\underline{E}^*|$), Log$[|\underline{E}_i|-|\underline{E}_s|]$ and Log($|\underline{E}\cdot\underline{H}|$) for Two Perfectly Conducting Cylinders of Elec. Radii $ka_1 = ka_2 = 1$ Separation between Centers $kd = 4$ along the Ray C'C'' of Fig. 6a

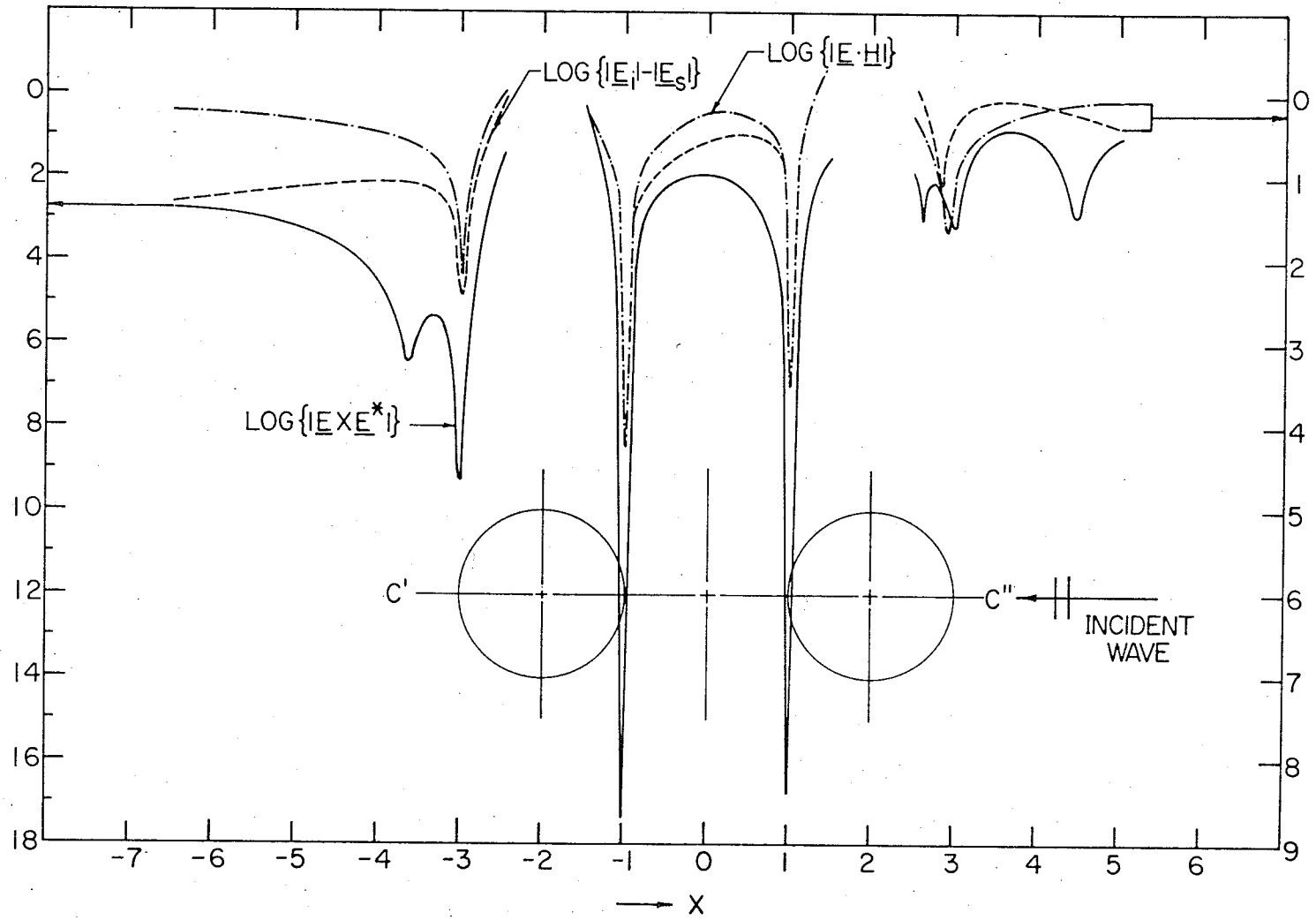

Fig.4.7b. End Fire Incidence

4.4.2 IMPERFECTLY CONDUCTING CASES

Similar to the perfectly conducting cases, the test targets chosen are single circular cylinders of different radii and surface impedances, and two non-overlapping cylinders of arbitrary radii a_1 and a_2 and surface impedances η_1 and η_2 with separation distance d between the centers. Since the numerical formulation of the total field expressions is identical to that employed for the perfectly conducting cases except that $\eta \neq 0$ or ∞, major emphasis will be laid on the novel conceptual approaches of discriminating the exact surface locus $S_0(\underline{r})$ from the infinity of additional pseudo loci $Sp_n(\underline{r})$ as well as of extracting the proper impedance value η_0 from the four-fold solution which pertains to the general case of *a priori* unknown η. It is assumed that a mixed polarized incident wave is travelling perpendicular to the axes of the cylinders at an angle β with respect to the line joining their centers as defined in Fig. 4.2. For the sake of clarity of presentation the imperfectly conducting case has been divided into three distinct classes.

(i) $\eta \neq 0$ known and $S(\underline{r})$ is to be determined

(ii) $\eta = |\eta|$ and $S(\underline{r})$ are to be determined

(iii) η and $S(\underline{r})$ are to be determined.

4.4.2a $\eta \neq 0$ KNOWN AND $S(\underline{r})$ IS TO BE DETERMINED

In this case it is assumed that η is either known *a priori* or that

η has been recovered by other methods of electromagnetic remote sensing as e.g. described in [139]. The total electric and magnetic fields to which the orthogonality and normality conditions of (3.4.1) and (3.4.2) are to be applied are calculated along a selected grid of rays using properly truncated series expansions of equations (4.2.14) and (4.2.19). The scalars $y_1 = \text{Min}\{\underline{A}\cdot\underline{B}\}$ and $y_2 = \text{Min}\{A^2-B^2\}$ have been plotted in Fig. 4.8a along a radiant vector ($\phi = 45°$) for a single conducting cylinder of electrical radius $ka = 2.0$ and of surface impedance $\eta = 0.5$. A similar plot for two conducting cylinders of electrical radii $ka_1 = ka_2 = 1.0$, surface impedances $\eta_1 = \eta_2 = 5.0 \exp(j45°)$, electrical separation $kd = 3.0$ and relative angle of incidence $\beta = 75°$, is presented along the computational line C-C' in Fig. 4.9a. An examination of these and many other similar plots for different parameters reveals that only one pair of minima out of the infinity of minima resulting from y_1 and y_2 is coincident, and this single minimum defines the correct point on the proper surface locus $S_0(\underline{r})$. This property makes both the orthogonality and the normality conditions necessary but locally insufficient. The descending parts of y_1 and y_2 of this common minimum always displayed greatest slope and this minimum in general is much sharper and deeper than the rest of the pseudo minima. Both conditions are seen to be applicable for all values of $\eta(\neq 0, \infty)$, be it purely real, purely imaginary or complex. The infinity of loci Sp_n and Sq_n resulting from the application of (3.4.1) and (3.4.2) respectively, are plotted in Fig. 4.8b for the mono-body case and in Fig. 4.9b for the two-body case, on a plane

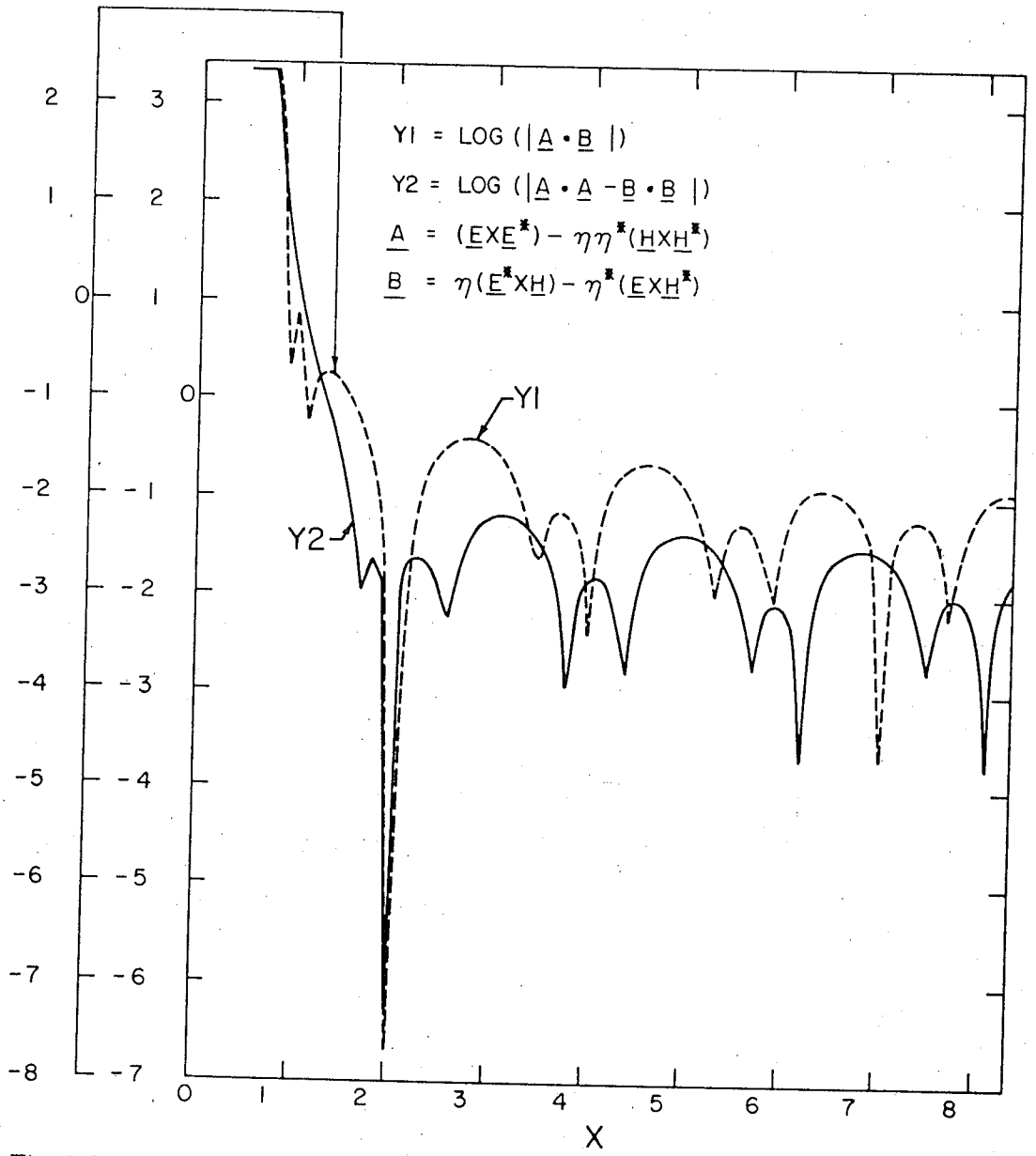

Fig.4.8a. Plot of Y1 and Y2 vs Radiant Vector X for a Cylindrical Target of ka = 2 and $\eta = 0.5\angle 0°$ along the Ray $\phi = 45°$

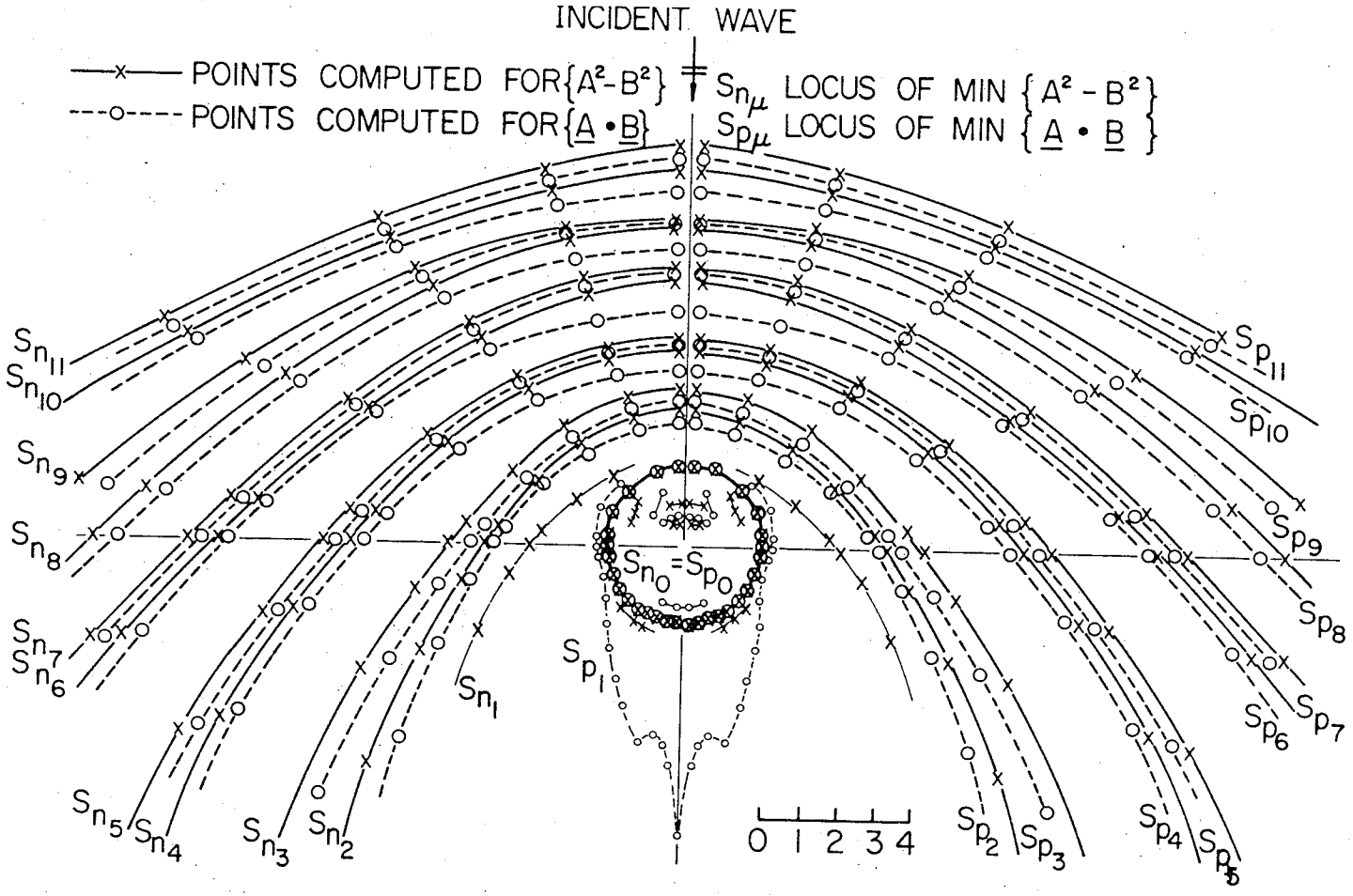

Fig. 4.8b. Plot of the Loci $S_{n\mu}$ and $S_{p\mu}$ of Successive Minima of $A^2 - B^2$ and $\underline{A} \cdot \underline{B}$ for a Cylindrical Target of Electrical Radius ka = 2 and Surface Impedance $\eta = 0.5$

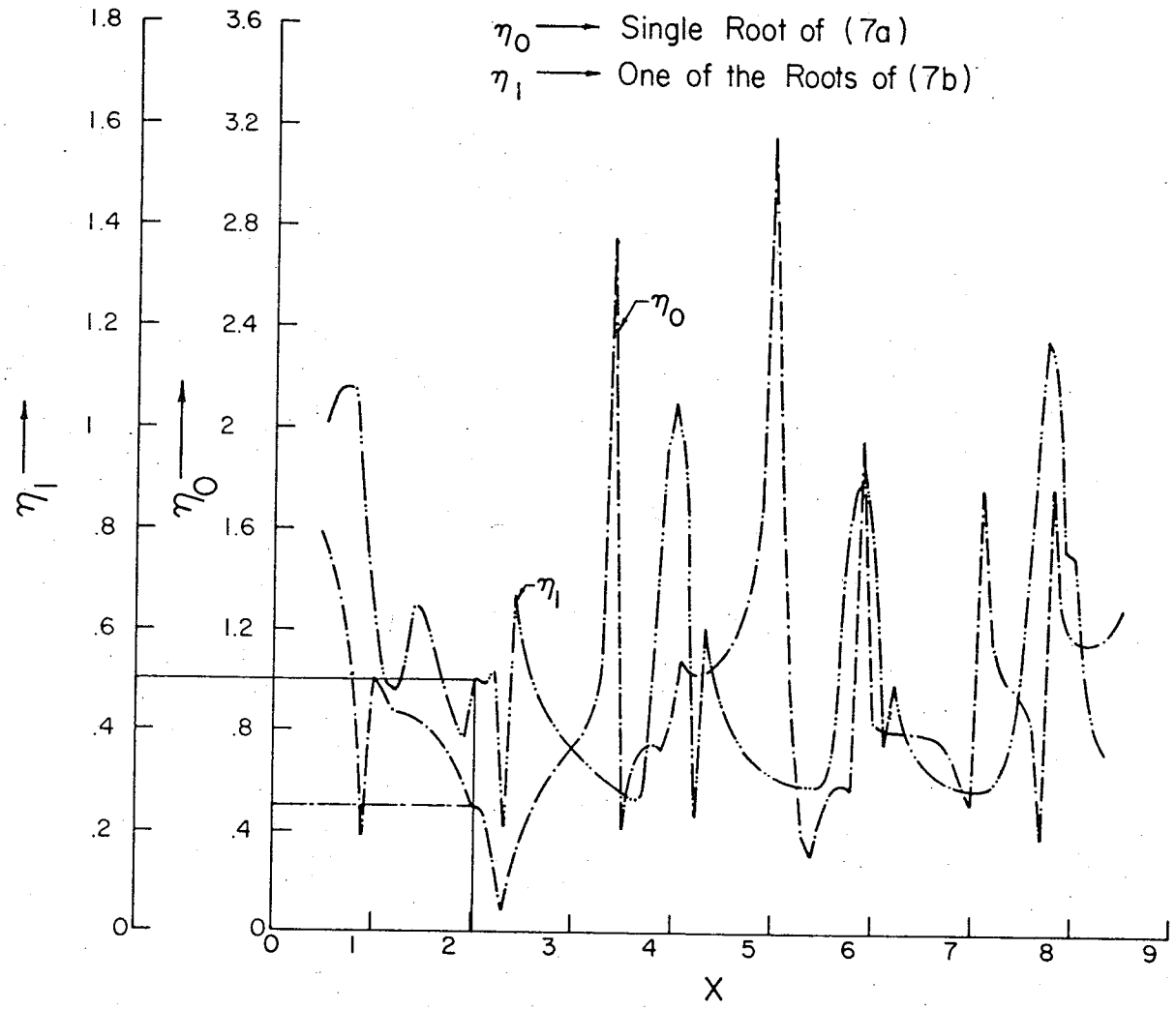

Fig.4.8c. Plot of η_0 and η_1 versus Radiant Vector X along a Ray ($\phi = 45°$) for a Cylindrical Target of ka = 2 and $\eta = .5\angle 0°$

normal to the invariant Z-axis. Inspection of Fig. 4.8b shows that for the monobody case each of the two conditions generates a series of non-coincident parabolic pseudo loci in addition to the proper coincident locus $S_0(\underline{r})$. The plots of Fig. 4.9b confirm the above observation for the two-body case. The pseudo loci in this case are the superposition of the infinite families of discrete loci resulting for the constituent cylinders. It should also be observed that in both the monobody and two-body cases the pseudo interior caustics and the exterior pseudo loci are not closed in the shadow region and only the proper surface locus $S_0(\underline{r})$ is closed. Therefore, it is concluded that each of the conditions by itself should be sufficient to discriminate the proper locus of a system of closed conducting scatterers, given measurement data for one frequency only. This observation makes the necessary but *locally* insufficient orthogonality and normality conditions necessary and *globally* sufficient. The simultaneous application of both conditions should make the proposed inversion technique unique also in those cases for which the given field data are not very accurate.

4.4.2b $|\eta|$ and $S_0(\underline{r})$ ARE TO BE DETERMINED

In those cases for which η is known to be purely real i.e. $\eta = \eta^*$ or purely imaginary ($\eta = -\eta^*$), the roots of (3.4.7) and (3.4.9) have to be calculated along a grid of rays. The values so calculated are plotted in Fig. 4.8c along the ray $\phi = 45°$ for the mono-body case illustrated in Figs. 4.8a and 4.8b. The plots for the two-body case are not given because the resulting curves for any individual constituent

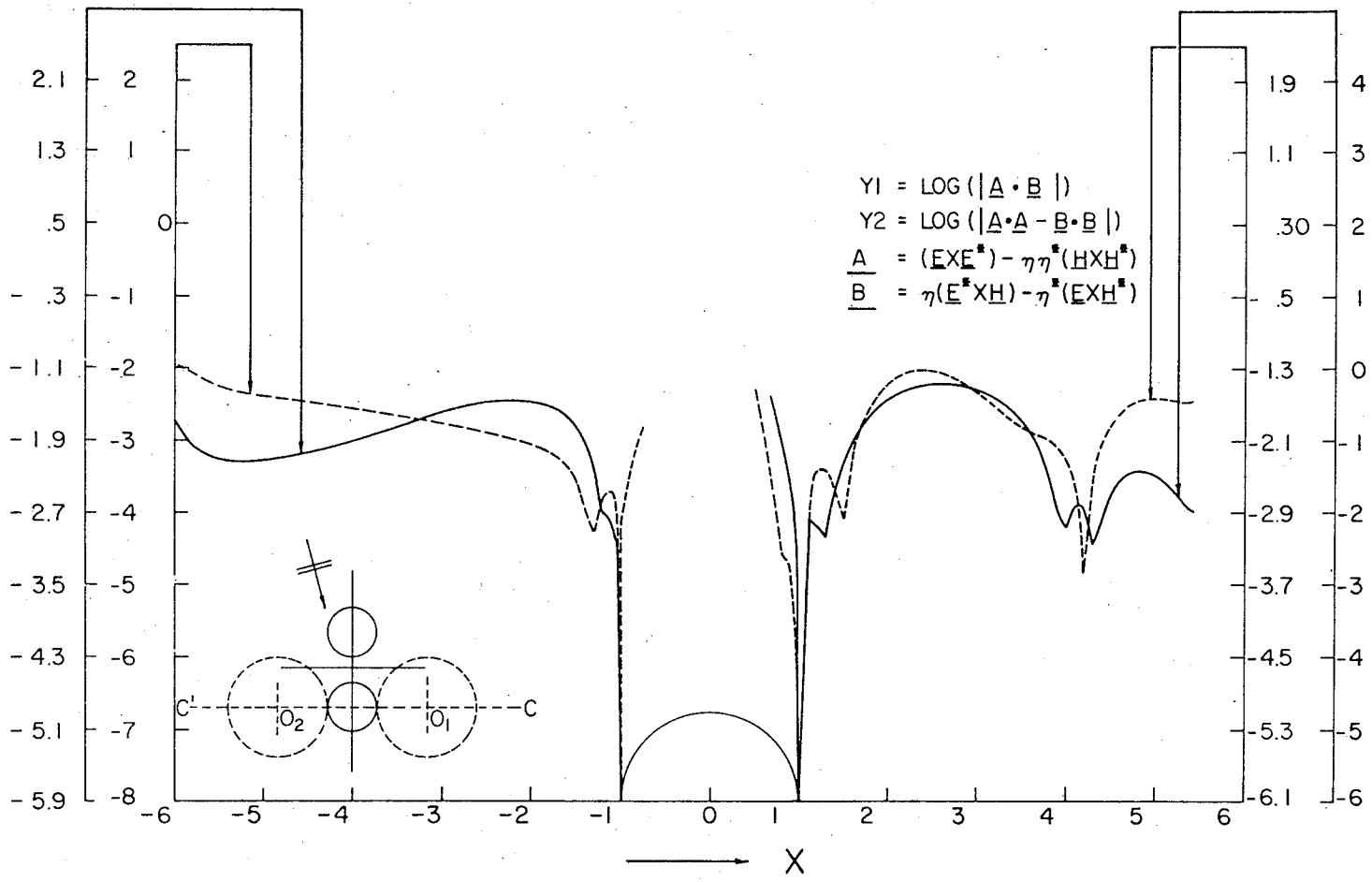

Fig.4.9a. Plot of Y1 and Y2 vs Radiant Vector X for Two Cylinders of Elec. Radii $ka_1 = 1$, $ka_2 = 1$ and Separation Between Centers $kd = 3$ and the Surface Impedances $\eta_1 = \eta_2 = 50\angle 45°$ along the Ray CC'.

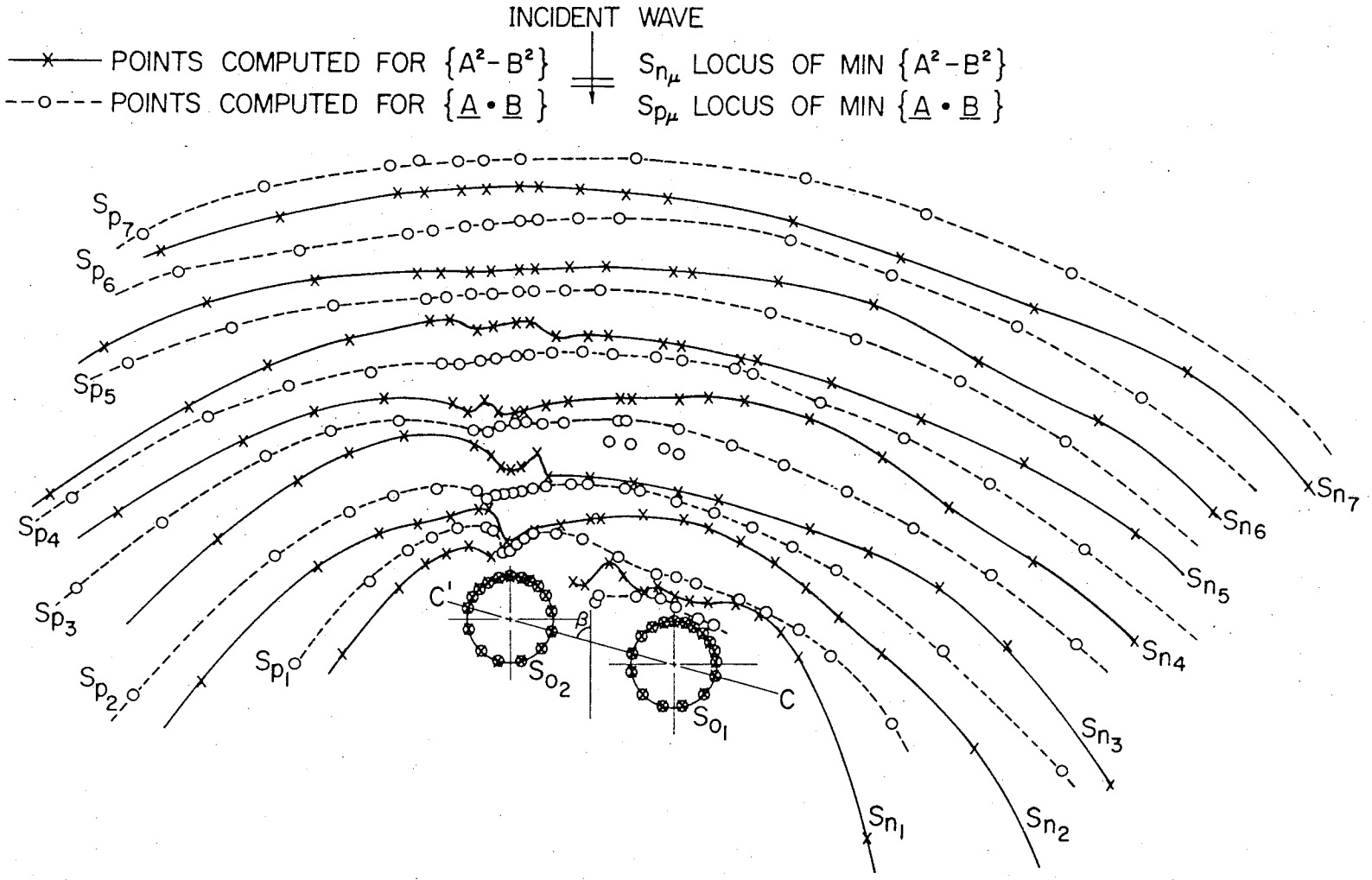

Fig. 4.9b. Plot of the Loci S_{n_μ} and S_{p_μ} of Successive Minima of $A^2 - B^2$ $\underline{A} \cdot \underline{B}$ for the Target of Fig. 7a

cylinder are alike. In Fig. 4.8c, η_0 represents the single root of (3.4.7) and η_1 is one of the roots of (3.4.9). The plot for the other root η_2 of (3.4.9) has been omitted in Fig. 4.8c since it was found to differ from η_0 for all points along the computational line considered. At each point along the ray the calculated value of η_0 is used in y_2 and that of η_1 in y_1 (as defined in (3.4.1) and (3.4.2), respectively), resulting in plots similar to those given in Figs. 4.8a and 4.9a. The single common minimum of y_1 and y_2 was found to be identical only at that point for which $\eta_0 = \eta_1$, defining the proper point on the proper locus $S_0(\underline{r})$. The proposed single frequency discrimination procedure would have to be repeated over a grid of rays spanning the total cross-sectional plane (Z = const.) if $\eta = \eta^*$ (or $\eta = -\eta^*$) is inhomogeneous, whereas for the homogeneous case the discrimination procedure presented in Subsection (4.3.5a) can be used after sufficient confidence in the accuracy of the recovered η has been established. Employing proper truncation bounds defined in *chapter six*, it was found that the accuracy to which $\eta = \eta^*$ and $S_0(\underline{r})$ can be recovered is better than 99% for all computations performed.

4.4.2c $\eta = |\eta|\exp(j\psi)$ and $S_0(\underline{r})$ ARE TO BE DETERMINED

If both modulus and phase of η are *a priori* unknown, then η must be assumed to be either homogeneous or nondispersive. The homogeneity requirement is sufficient whenever the scattering geometry defines a single convex-shaped scatterer so that the degeneracy conditions of (3.4.15) and (3.4.16) can be applied with (3.4.12) and (3.4.14) for the

discrimination of ψ and $|\eta|$. The degeneracy condition, however, does not hold for the general multibody case except for end-fire incidence on an on-line collection of purely convex-shaped scatterers. Therefore, the double-frequency discrimination method must be applied which requires that η to be nondispersive but may be inhomogeneous.

For the case of a single cylinder of electrical radius $ka = 2.0$ and $\eta = \text{const.} = 0.5$ the method outlined in Subsection 3.4.3 is applied. The results so calculated are presented in Table 4.1, in which the single root ψ_0 of (3.4.16) and the four roots $\psi_\nu (\nu = 1,2,3 \text{ and } 4)$ of (3.4.14) resulting from computation along a ray $\phi = 1.0°$ i.e. in the immediate neighborhood of back-scattering direction are tabulated. The correct value of phase ψ of η is found for that particular value of ψ_0 which is identical to one or more roots ψ_ν of (3.4.14), occuring for the presented case at $X = 2.0$ with $\psi_0 = \psi_2 = \psi_4 = 0$. The value of ψ so calculated is substituted into (3.4.12) to obtain $|\eta|$ resulting in 0.5, as is also shown in Table 4.1. To guarantee proper discrimination of the point lying on $S_0(\underline{r})$, the orthogonality scalar Y_1, and the normality scalar Y_2, have been recalculated along the same computational line. The entries Y_1' and Y_2' of Table 4.1 have been calculated using the impedance value η_0 resulting at each point of computation along the selected ray while the entries Y_1 and Y_2 correspond to computation for which $\eta(x = 2.0) = 0.5$ was used for all points along the ray. To recover the entire surface locus $S_0(\underline{r})$ from field data given everywhere for one single frequency only, it must be assumed that η is homogeneous in which case the identification

TABLE 4.1

Retrieval of ψ and $|\eta|$

for the Single Cylinder of Fig. 4.8A

X=kr	ψ_o	ψ_1	ψ_2	ψ_3	ψ_4	$\lvert\eta\rvert$	Y_1'	$Y_2' \times 10^8$	Y_1	$Y_2 \times 10^2$
1.7	28.02	26.00	29.37	-	-	0.19	0.029	0.102	0.195	1.34
1.8	18.45	-	-	-	-	0.46	0.068	0.178	0.082	0.212
1.9	8.93	9.30	-	-	8.57	0.50	0.019	0.250	0.019	0.011
2.0	*0.00*	-	*0.00*	-	*0.00*	*0.50*	0.032×10^{-7}	0.568×10^{-5}	0.061×10^{-7}	0.157×10^{-7}
2.1	- 7.88	8.24	-	-	7.55	0.47	0.014	0.210	0.016	0.067
2.2	-14.45	-	-	-	-	0.43	0.041	0.668	0.055	0.295
2.3	-19.63	-	-	-	-	0.38	0.063	0.293	0.107	0.639

procedure reduces to that for *a priori* known η as was analysed in Subsection 4.3.5a .

For the general two-body configuration considered, it must be assumed that η is nondispersive so that the double-frequency checking procedure can be applied. The test configuration chosen consists of two parallel circular cylinders of $ka_1 = 2.0$, $\eta_1 = 0.1 \exp(j30°)$ and $ka_2 = 1.0$, $\eta_2 = 0.25 \exp(j60°)$ with the centers an electrical distance $kd = 5.0$ apart. The incident wave is a mixed polarized plane wave normally incident at an angle $\beta = 75°$ with respect to the line joining the centers 0_1 and 0_2 as shown in Fig.4.10. The four roots of (3.4.14) for cylinder 1, calculated along the line of centers with translated origin located at 0' such that $k(0'-0_1) = 3.0$ and $k(0'-0_2) = 2.0$, are presented in Table 4.2 for two different frequencies $f_1 = f$ and $f_2 = 1.5f$. For the purpose of specifying the proper value ψ at the point on $S_0(\underline{r})$, a matching pair of values ψ resulting from computation at the two different frequencies along the chosen computational line (0_1-0_2) were sought first. The procedure was then repeated for increasingly finer computational increments $\Delta\chi$, resulting in an averaged value $\overline{\psi} = 30.1°$ at $\chi/k = 1.0$. Substituting the discriminated value $\overline{\psi}$ into (3.4.12), $|\eta|$ is calculated along the same ray 0_1-0_2 for both frequencies. The computed results are presented in Table 4.2a where the averaged value of the magnitude of the surface impedance is $|\overline{\eta}| = 0.1$ at $x/k = 1.0$. Repeating this recovery procedure for other adjacent computational lines, it was concluded that $\overline{\eta}_1 = 0.1 \exp(j30.1°)$. The same procedure was adopted for

TABLE 4.2

Retrieval of ψ and $|\eta|$ Using Double Frequency Technique for Two Cylinder Configuration of Fig. 4.10

A. Computed Values for Cylinder I

At Frequency f						At Frequency 1.5 f				
X/k	ψ_1	ψ_2	ψ_3	ψ_4	$\|\eta\|$	ψ_1'	ψ_2'	ψ_3'	ψ_4'	$\|\eta'\|$
0.7	-	-	20.44	7.06	0.74	28.73	-	-	0.22	0.71
0.8	-	-	23.20	0.00	0.70	28.26	-	-	7.91	0.65
0.9	51.21	65.02	34.02	25.07	0.65	28.59	-	-	11.86	0.64
1.0	-	-	*30.22*	22.65	*0.10*	-	-	30.65	*29.99*	*0.10*
1.1	-	-	28.54	8.39	0.60	-	-	22.02	10.04	0.56
1.2	-	-	26.67	26.46	0.44	-	-	8.83	7.61	0.63
1.3	-	-	28.96	23.77	0.33	-	-	7.33	4.11	0.69

B. Computed Values for Cylinder II

At Frequency f						At Frequency 1.5 f				
X/k	ψ_1	ψ_2	ψ_3	ψ_4	$\|\eta\|$	ψ_1'	ψ_2'	ψ_3'	ψ_4'	$\|\eta'\|$
0.7	-	-	39.84	30.13	1.28	45.74	16.75	-	-	1.83
0.8	-	-	45.85	33.00	0.70	-	-	-	-	2.40
0.9	52.75	-	-	34.27	0.35	-	-	-	-	0.72
1.0	*59.46*	-	-	33.88	*0.25*	47.46	*61.33*	-	-	*0.24*
1.1	-	-	26.91	12.66	0.43	-	-	9.82	8.56	0.53
1.2	-	-	15.67	10.25	0.55	-	-	3.39	1.51	0.61
1.3	-	-	4.16	3.92	0.63	-	-	1.19	1.17	0.64

cylinder 2 and the corresponding values so computed are presented in Table 4.2b where η_2 has been identified as $\bar{\eta}_2 = 0.5 \exp(j60.4°)$, the average of the values at x/k = 1.0 for the two different frequencies. It should be noted, that the double-frequency discrimination procedure should be applicable to specify the local $\bar{\eta}$ and $S_0(\underline{r})$ for all portions of the scattering configuration within an error of less than 1% as has been clearly verified by computation for a number of different two-body configurations. However, if it is known that η is homogeneous, in addition to being nondispersive, the discrimination procedure analysed in Subsection 4.3.5a may readily be applied. The results for such a case are presented in Fig.4.10 which corresponds to the configuration analysed above. Finally, it should be mentioned that the values computed were in general found to be very sensitive to variations in the radial distance χ and, therefore, the computational increment $\Delta\chi$ had to be considerably reduced in the final search loop of the identification routine.

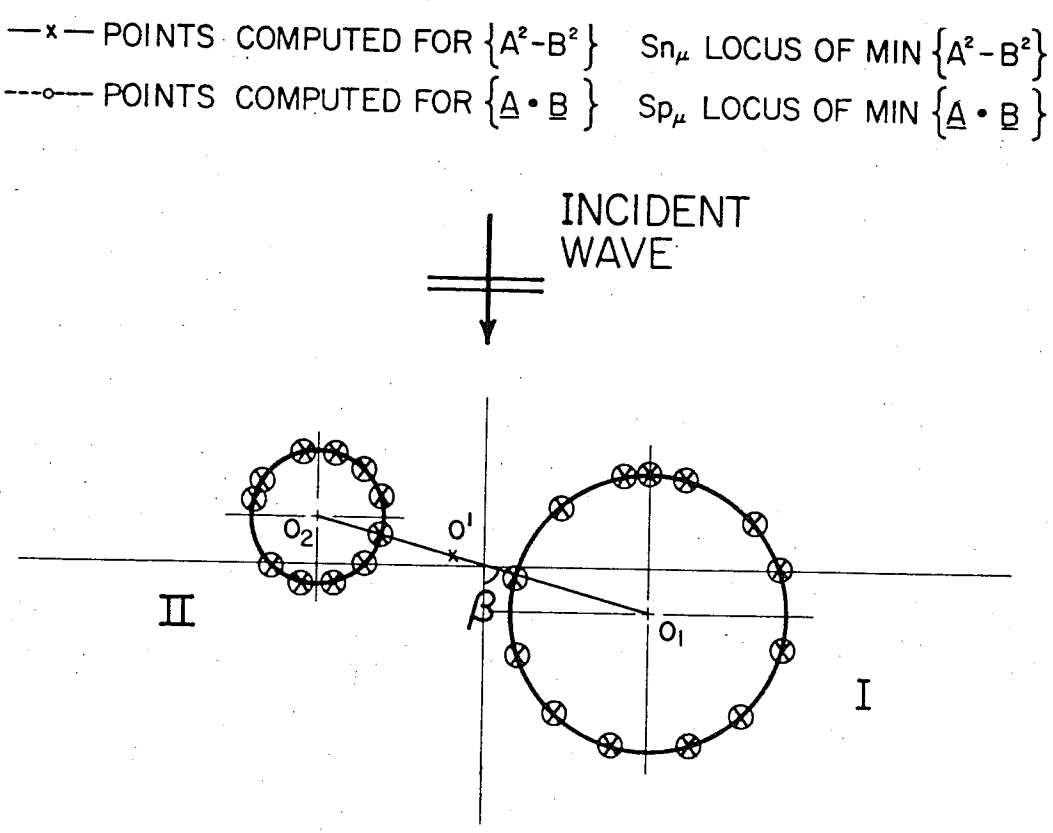

Fig. 4.10. Identification of Two Cylinders of Elec. Radii $ka_1 = 2$, $ka_2 = 1$; Surface Impedances $\eta_1 = 0.1\angle 30°$, $\eta_2 = 0.25\angle 60°$, Elec. Distance between the Centers $kd = 5$, $\beta = 75°$

chapter five

APPLICATION OF INVERSE BOUNDARY CONDITIONS TO THREE-DIMENSIONAL BODIES

5.1 INTRODUCTION

In *chapter four*, the inverse boundary conditions established in Sections 3.2 and 3.3 were applied to the target identification of two-dimensional bodies. It was demonstrated that it is possible to invert perfectly conducting mono-body and two-body configurations very accurately. For the case of imperfectly conducting shapes with known surface impedance, each of the conditions was found to be sufficient to discriminate the proper locus of a system of closed conducting scatterers, given measurement data for only one frequency. If both the locus $S_0(\underline{r})$ and the surface impedance $\eta = |\eta|\exp(j\psi)$ are *a priori* unknown, certain restrictions had to be placed on the nature of the target. For a smooth convex target η has to be either homogeneous or nondispersive, where the degeneracy condition may be employed for the former case and the two frequency technique for the latter. To invert the general two-body configuration, it must be assumed that η is nondispersive so that the double-frequency checking procedure may be applied. In order to recover the profile characteristics of those portions of the scatterer which lie within the minimum circle enclosing the scatterers, it was found necessary to analytically continue the em fields.

In the present analysis, the application of inverse boundary conditions to profile characteristics inversion of perfectly and imperfectly conducting spherical mono-body and two-body scatterers is considered. As in the two-dimensional case, the choice for three-dimensional bodies was dictated by the fact that sufficiently accurate information on the direct scattering solutions is available only for spherical scatterers satisfying the impedance boundary conditions [141,127].

A brief review of the formulation of the scattered field and direct scattering by single sphere is presented in Section 5.2. The solution for direct scattering by two spheres [30] has been extended in Section 5.3 to the case of imperfectly conducting spheres satisfying impedance boundary conditions. For the purposes of recovering the profile of those portions of the scatterer which lie within the Wilcox sphere, methods of interior and exterior analytic continuation in three-dimensions are introduced in Section 5.4. The numerical results for three-dimensional bodies are presented in Section 5.5 where it is confirmed that the IBCs are also valid for three-dimensional scatterers.

5.2 FORMULATION OF THE SCATTERED FIELD IN SPHERICAL COORDINATES

For the three-dimensional bodies, the far field is expressed in terms of a properly truncated expansion in vector spherical wave functions. The near field representation of the scattered electric and magnetic fields is obtained by recovering the associated expansion coefficients from the measured far field employing a matrix inversion technique

developed by Weston and Boerner [136] and presented in more detail in Boerner and Vandenberghe [25] and in Boerner and Aboul-Atta [21]. The matrix inversion technique imposes severe restrictions on the distribution of the computed aspect angle due to the instability inherent in the associated inversion. The instabilities which in this case are caused by the particular properties of the Hansen vector wave expansion, can be effectively studied from the properties of the determinant associated with the scattered field matrix [25, 122].

5.2.1 MONO-BODY SCATTERING

Consider a plane, homogeneous electromagnetic wave travelling along and in the direction of the negative z-axis, polarized in the positive x direction, and incident on a scatterer of arbitrary closed and smooth shape with arbitrary homogeneous material surface properties. Let the center of the body coincide with the origin of a spherical coordinate system as defined in Fig. 5.1. The incident electric and magnetic field vectors, after suppressing the time dependence $\exp(-j\omega t)$ may be written as

$$E_i = \hat{a}_x E_0 \exp[j(\alpha_t - kz)] = E_0 \{\sin\theta\cos\phi\hat{a}_R + \cos\theta\cos\phi\hat{a}_\theta - \sin\phi\hat{a}_\phi]$$

$$\exp[j(\alpha_t - kR\cos\theta] \qquad (5.2.1)$$

$$H_i = -\hat{a}_y Z_0^{-1} E_0 \exp[j(\alpha_t - kz)] = -H_0 \{\sin\phi\hat{a}_R + \cos\theta\sin\phi\hat{a}_\theta + \cos\phi\hat{a}_\phi\}$$

$$\exp[j(\alpha_t - kR\cos\theta)] \qquad (5.2.2)$$

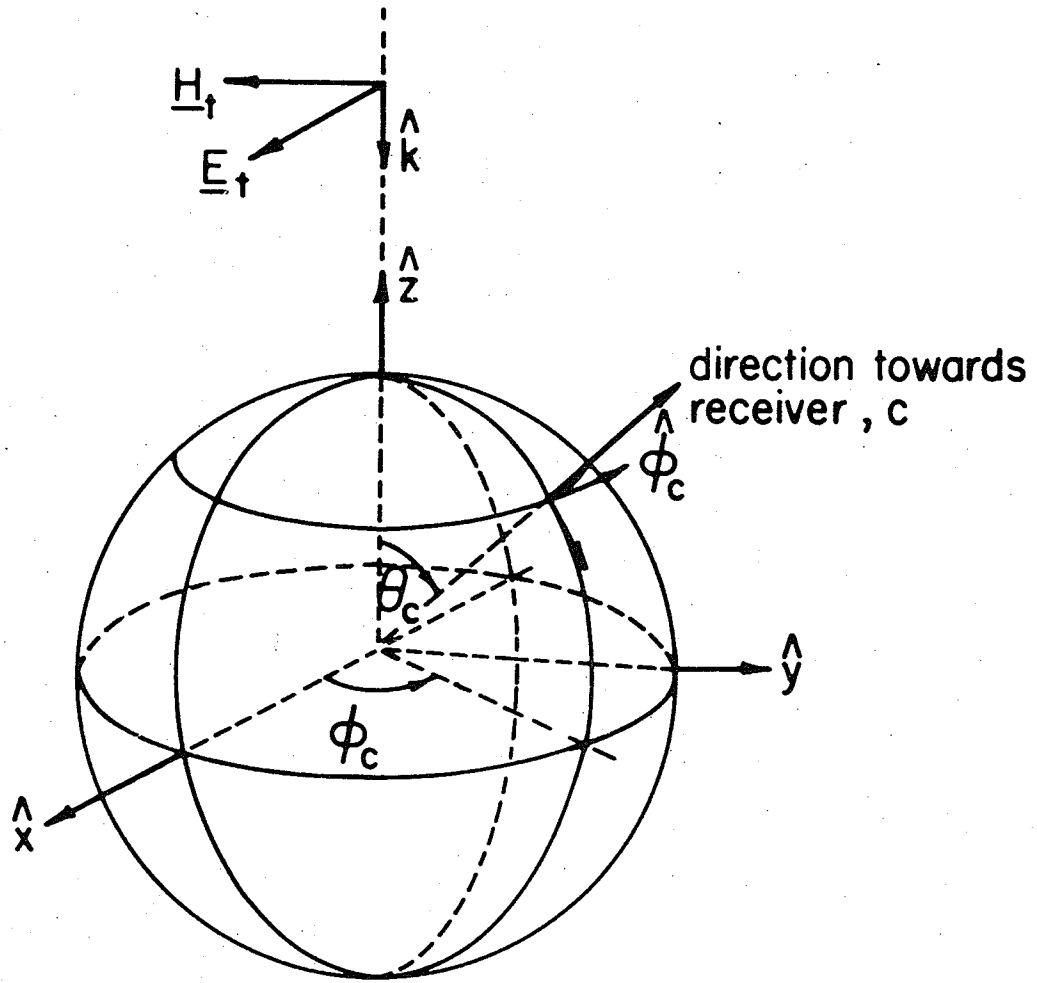

FIG.5.1. SPHERICAL GEOMETRY

where $k = \omega(\mu_0 \varepsilon_0)^{1/2}$ and $Z_0 = (\mu_0/\varepsilon_0)^{1/2}$. For $E_0 = 1$ and $\alpha_t = 0$, the scattered fields at (R, θ, ϕ) can be expressed in terms of a series expansion in vector spherical wave functions [25] as

$$\underline{E}_s(R,\theta,\phi) = \sum_{n=1}^{\infty} \sum_{m=0}^{n} [j^{n+1} a_{e_{0mn}} \underline{M}_{e_{0mn}}(R,\theta,\phi) + j^n b_{e_{0mn}} \underline{N}_{e_{0mn}}(R,\theta,\phi)] \quad (5.2.3)$$

$$\underline{H}_s(R,\theta,\phi) = -j[\frac{\varepsilon_0}{\mu_0}]^{1/2} \sum_{n=1}^{\infty} \sum_{m=0}^{n} [j^{n+1} a_{e_{0mn}} \underline{N}_{e_{0mn}}(R,\theta,\phi) + j^n b_{e_{0mn}} \underline{M}_{e_{0mn}}(R,\theta,\phi)] \quad (5.2.4)$$

According to Müller [85] and Wilcox [146], for a fixed origin of coordinate system the above expansion is convergent down to at least the minimum sphere enclosing the equivalent sources of the body. Hansen's spherical vector wave functions as derived from the Mie Series are defined by [115]

$$\underline{M}_{e_{0mn}}(R,\theta,\phi) = \pm\{h_n^{(1)}(kR) S_n^m(\theta) \begin{matrix}\sin\\\cos\end{matrix}(m\phi)\}\hat{a}_\theta - \{h_n^{(1)}(kR) R_n^m(\theta) \begin{matrix}\cos\\\sin\end{matrix}(m\phi)\}\hat{a}_\phi \quad (5.2.5a)$$

$$\underline{N}_{e_{0mn}}(R,\theta,\phi) = \{\frac{n(n+1)}{kR} h_n^{(1)}(kR) P_n^m(\cos\theta) \begin{matrix}\cos\\\sin\end{matrix}(m\phi)\}\hat{a}_R + \{k_n^{(1)}(kR) R_n^m(\theta) \begin{matrix}\cos\\\sin\end{matrix}(m\phi)\}\hat{a}_\theta$$

$$\pm\{k_n^{(1)}(kR) S_n^m(\theta) \begin{matrix}\sin\\\cos\end{matrix}(m\phi)\}\hat{a}_\phi \quad (5.2.5b)$$

where $P_n^m(\cos\theta)$ is the associated Legendre's function of the first kind, degree m and order n, defined in [25], by

$$P_n^m(x = \cos\theta) = \frac{m!}{2^n} \binom{n+m}{m} (1-x^2) \sum_{\nu=0}^{(n-m)/2} (-1)^\nu \binom{n}{\nu} \binom{2n-2\nu}{n+m} x^{n-m-2\nu}$$

with

$$S_n^m(\cos\theta) = \frac{m}{\sin\theta} P_n^m(\cos\theta) \qquad R_n^m(\cos\theta) = \frac{\partial P_n^m(\cos\theta)}{\partial\theta} \tag{5.2.6}$$

and $k_n^{(1)}(kr)$ denotes the derivative of the spherical Hankel function of the first kind and order n given in terms of the cylindrical Hankel function

$$h_n^{(1)}(kR) = \left(\frac{\pi}{2\pi R}\right)^{1/2} H_{n+1/2}^{(1)}(kR)$$

by

$$k_n^{(1)}(kR) = \frac{1}{kR}\frac{d}{dR}\{Rh_n^{(1)}(kR)\}$$

For a sphere of relative surface impedance η, only the coefficients a_{01n} and b_{e1n} need to be retained for the assumed incident polarization case. These coefficients are explicitly derived in Weston and Hemenger [141] and with a slight modification are rewritten for the above employed formulation as

$$a_{01n} = -j(-1)^{n+1}\frac{2n+1}{n(n+1)} A_n \tag{5.2.7a}$$

$$b_{e1n} = -j(-1)^{n}\frac{2n+1}{n(n+1)} B_n \tag{5.2.7b}$$

with

$$A_n = \frac{\eta[k_a j_n(ka)]'+j[k_a j_n(ka)]}{\eta[k_a h_n^{(1)}(ka)]'+j[k_a h_n^{(1)}(ka)]} \tag{5.2.8a}$$

$$B_n = \frac{[k_a j_n(ka)]'+j\eta[k_a j_n(ka)]}{[k_a h_n^{(1)}(ka)]'+j\eta[k_a h_n^{(1)}(ka)]} \tag{5.2.8b}$$

where $j_n(ka)$ and $h_n^{(1)}$ denote spherical Bessel and Hankel functions of the first kind, respectively, and the primed expressions define first order partial derivatives with respect to ka.

The first step in the inversion procedure is to recover the coefficients $a_{\substack{e\\0}mn}$ and $b_{\substack{e\\0}mn}$ from the scattered field data commonly measured in the Fraunhofer region. This is accomplished by considering only the transverse electric field components of the scattered field which after employing the asymptotic approximations of the spherical Hankel functions can be written as

$$E^s_{\theta_c}(\theta_c,\phi_c) \simeq \sum_{n=1}^{M}\sum_{m=0}^{n}\{a_{\substack{e\\0}mn} S_{\substack{e\\0}mn}(\theta_c,\phi_c)+b_{\substack{e\\0}mn} R_{\substack{e\\0}mn}(\theta_c,\phi_c)\}\frac{\exp(ikR)}{(kR)} \quad (5.2.9a)$$

$$E^s_{\phi_c}(\theta_c,\phi_c) \simeq \sum_{n=1}^{m}\sum_{m=0}^{n}\{-a_{\substack{e\\0}mn} R_{\substack{e\\0}mn}(\theta_c,\phi_c)+b_{\substack{e\\0}mn} S_{\substack{e\\0}mn}(\theta_c,\phi_c)\}\frac{\exp(ikR)}{(kR)} \quad (5.2.9b)$$

where the spherical vector surface harmonics $S_{\substack{e\\0}mn}(\theta,\phi)$ and $R_{\substack{e\\0}mn}(\theta,\phi)$ are defined by

$$S_{\substack{e\\0}mn}(\theta,\phi) = S_n^m(\cos\theta_c)\begin{matrix}\sin\\\cos\end{matrix}(m\phi_c) \quad (5.2.10a)$$

$$R_{\substack{e\\0}mn}(\theta,\phi) = R_n^m(\cos\theta_c)\begin{matrix}\cos\\\sin\end{matrix}(m\phi_c) \quad (5.2.10b)$$

The method of recovering these *a priori* unknown expansion coefficients is presented in detail in Boerner and Vandenberghe [25] for the purely spherical symmetric case and further analytical results for the general

non-symmetrical case are presented in Boerner and Aboul-Atta [21]. There it is shown that the near field expansion can be recovered to an accuracy dictated only by any suitable measurement technique which enables simultaneous recording of both the modulus and phase of the transverse electric field quantities.

Since the primary incentive of this presentation is to establish unique inverse boundary conditions and verify them numerically, the expansion coefficients of equations (5.2.8a) and (5.2.8b) will be used in the verification.

5.3 DIRECT SCATTERING BY TWO SPHERES WITH ARBITRARY SURFACE IMPEDANCE

The direct scattering solution for two perfectly conducting spheres has been attempted by various authors [119, 32 , 149, 118]. Liang and Lo[69] and Crane [36] reformulated the two-sphere problem using a newly derived form of the addition theorem given by Stein [112] and Cruzan [38]. The solution of Liang and Lo [69] has been extended to the case of dielectric spheres of arbitrary radii by Bruning [30]. Employing the approach of Bruning and Lo [31], the solution to the two-sphere problem is extended to the case where the spheres have arbitrary surface impedance and satisfy the Leontovich impedance boundary condition.

Let an arbitrarily polarized plane wave be incident at an angle α

with the z-axis, on two spheres of arbitrary radii a and b and surface impedances η_a and η_b as shown in Fig. 5.2. The multipole expansion of the incident field is given by

$$\underline{E}_{inc} = \sum_{n=1}^{\infty} \sum_{m=-n}^{n} [p(m,n)\underline{N}_{mn}^{(1)} + q(m,n)\underline{M}_{mn}^{(1)}] \qquad (5.3.1)$$

where the multipole coefficients of the incident plane wave can be determined by using the orthogonality properties of the vector spherical wave functions and the trigonometric functions resulting into

$$p(m,n) = j^{n+1} \frac{2n+1}{n(n+1)} \frac{(n-m)!}{(n+m)!} [R_n^m(\cos\alpha)\cos\gamma + jS_n^m(\cos\alpha)\sin\gamma] \qquad (5.3.2a)$$

$$q(m,n) = j^{n+1} \frac{2n+1}{n(n+1)} \frac{(n-m)!}{(n+m)!} [S_n^m(\cos\alpha)\cos\gamma + jR_n^m(\cos\alpha)\sin\gamma] \qquad (5.3.2b)$$

with $S_n^m(\cos\alpha)$ and $R_n^m(\cos\alpha)$ given by equations (5.2.6).

Similarly, the scattered field for sphere $\sigma(1,2)$ in the presence of sphere $\sigma'(2,1)$ with respect to its own coordinate system can be expressed as

$$\underline{E}_s^{\sigma} = \sum_{n=1}^{\infty} \sum_{m=-n}^{n} [A_{\sigma}(m,n)\underline{M}_{mn}^{(3)} + B_{\sigma}(m,n)\underline{N}_{mn}^{(3)}] \qquad (5.2.3)$$

$$\underline{H}_s^{\sigma} = -\frac{ik}{w\mu} \sum_{n=1}^{\infty} \sum_{m=-n}^{n} [A_{\sigma}(m,n)\underline{N}_{mn}^{(3)} + B_{\sigma}(m,n)\underline{M}_{mn}^{(3)}] \qquad (5.2.4)$$

where the A_{σ}, B_{σ} for $\sigma = 1,2$ are the magnetic and electric type scattering coefficients for sphere σ in the presence of σ'. Here the vector spherical wave functions $\underline{M}_{mn}^{(i)}$ and $\underline{N}_{mn}^{(i)}$ involve the exponential

variation with respect to the angle ϕ, i.e. $\exp(im\phi)$ is to be used in equations (5.2.5a) and (5.2.5b). The superscripts $i = 1,2,3$ and 4 denote the appropriate radial dependence involving the spherical Bessel functions j_n, n_n, $h_n^{(1)}$ or $h_n^{(2)}$, respectively.

In order to satisfy the impedance boundary conditions on each sphere in the presence of the other, the multipole fields about 0 have to be expressed with respect to 0' and vice versa. The translational addition theorems to be used for this case of translation along z-axis are the specialized form of the generalized theorems by Stein [112] and Cruzan [38] which can be written as

$$\underline{M}_{mn}^{(3)} = \sum_{\nu=(1,m)}^{\infty} (A_{m\nu}^{mn} \underline{M}_{m\nu}^{(1)'} + B_{m\nu}^{mn} \underline{N}_{m\nu}^{(1)'}) \qquad (5.3.5a)$$

$$\underline{N}_{mn}^{(3)} = \sum_{\nu=(1,m)}^{\infty} (A_{m\nu}^{mn} \underline{N}_{m\nu}^{(1)'} + B_{m\nu}^{mn} \underline{M}_{m\nu}^{(1)'}) \qquad (5.3.5b)$$

where the wave functions on the left-hand side of (5.3.5a) and (5.3.5b) refer to the original set of coordinates 0, while those on the right hand side refer to the translated coordinates 0', and (1,m) symbolizes the larger of 1 or m (as m can also be negative). For the reverse translation, i.e. translation from 0' to 0, the corresponding theorem is given by

$$\underline{M}_{mn}^{(3)'} = \sum_{\nu=(1,m)}^{\infty} (-1)^{n+\nu} [A_{m\nu}^{mn} \underline{M}_{m\nu}^{(1)} - B_{m\nu}^{mn} \underline{N}_{m\nu}^{(1)}] \qquad (5.3.6a)$$

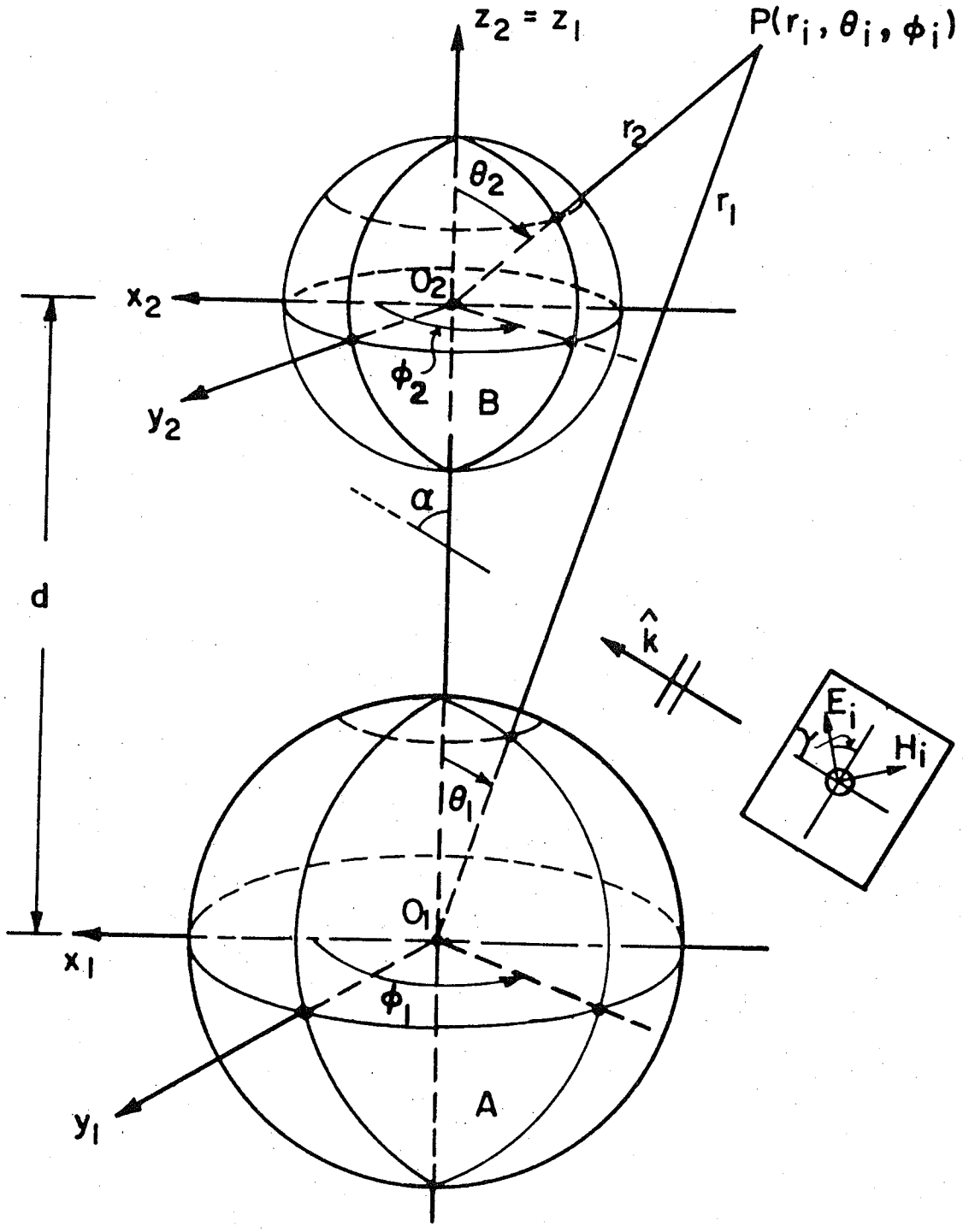

Fig. 5.2. SPHERICAL TWO-BODY SCATTERING

$$\underline{N}_{mn}^{(3)'} = \sum_{\nu=(1,m)}^{\infty} (-1)^{n+\nu} [A_{m\nu}^{mn} \underline{N}_{m\nu}^{(1)} - B_{m\nu}^{mn} \underline{M}_{m\nu}^{(1)}] \qquad (5.3.6b)$$

5.3.1 EXPANSION OF THE TOTAL FIELD AND APPLICATION OF IMPEDANCE BOUNDARY CONDITION

The scattered fields of spheres A and B with respect to their own centers 0_1 and 0_2 and in the presence of each other are given by

$$\underline{E}_s^A = \sum_{n=1}^{\infty} \sum_{m=-n}^{n} A_1(m,n)\, \underline{M}_{mn}^{(3)} + B_1(m,n)\, \underline{N}_{mn}^{(3)} \qquad r \geq a \qquad (5.3.7a)$$

$$\underline{E}_s^{B'} = \sum_{n=1}^{\infty} \sum_{m=-n}^{n} A_2(m,n)\, \underline{M}_{mn}^{(3)'} + B_2(m,n)\, \underline{N}_{mn}^{(3)'} \qquad r' \geq b \qquad (5.3.7b)$$

The total field about 0_1 can be written as

$$\underline{E}_T = \sum_{n=1}^{\infty} \sum_{m=-n}^{n} [p(m,n)\underline{N}_{mn}^{(1)} + q(m,n)\underline{M}_{mn}^{(1)} + A_1(m,n)\underline{M}_{mn}^{(3)} + B_1(m,n)\underline{N}_{mn}^{(3)}$$

$$+ A_2(m,n) \sum_{\nu=1}^{\infty} (-1)^{n+\nu} (A_{m\nu}^{mn} \underline{M}_{m\nu}^{(1)} - B_{m\nu}^{mn} \underline{N}_{m\nu}^{(1)})$$

$$+ B_2(m,n) \sum_{\nu=1}^{\infty} (-1)^{n+\nu} (A_{m\nu}^{mn} \underline{N}_{m\nu}^{(1)} - B_{m\nu}^{mn} \underline{M}_{m\nu}^{(1)})] \qquad (5.3.8)$$

Similarly the total field about 0_2 is

$$\underline{E}_T' = \sum_{n=1}^{\infty} \sum_{m=-n}^{n} [p'(m,n)\underline{N}_{mn}^{(1)'} + q'(m,n)\underline{M}_{mn}^{(1)'} + A_2(m,n)\underline{M}_{mn}^{(3)'} + B_2(m,n)\underline{N}_{mn}^{(3)'}$$

$$+ A_1(m,n) \sum_{\nu=1}^{\infty} (A_{m\nu mn}\underline{M}_{m\nu mn}^{(1)'} + B_{m\nu mn}\underline{N}_{m\nu mn}^{(1)'})$$

$$+ B_1(m,n) \sum_{\nu=1}^{\infty} (A_{m\nu mn}\underline{N}_{m\nu mn}^{(1)} - B_{m\nu mn}\underline{M}_{m\nu mn}^{(1)})] \qquad (5.3.9)$$

The magnetic fields are obtained by interchanging the $\underline{M}_{mn}$'s and $\underline{N}_{mn}$'s and multiplying the result by $-ik/\omega\mu$.

The impedance boundary conditions

$$E_\theta = -\eta Z_0 H_\phi$$

$$E_\phi = \eta Z_0 H_\theta$$

may now be applied to the total fields. After using the orthogonality relations for Legendre's functions, the following set of four coupled, linear, simultaneous equations in unknown multipole coefficients is obtained

$$A_1(m,n) = a_{1_n}(k_1 a)\{q_1(m,n) + \sum_{\nu} (-1)^{n+\nu}[A_{mn}^{m\nu} A_2(m,\nu) - B_{mn}^{m\nu} B_2(m,\nu)]\} \qquad (5.3.10a)$$

$$B_1(m,n) = b_{1_n}(k_1 a)\{p_1(m,n) + \sum_{\nu} (-1)^{n+\nu}[A_{mn}^{m\nu} B_2(m,\nu) - B_{mn}^{m\nu} A_2(m,\nu)]\} \qquad (5.3.10b)$$

$$A_2(m,n) = a_{2_n}(k_2 b)\{q_2(m,n) + \sum_{\nu} [A_{mn}^{m\nu} A_1(m,\nu) + B_{mn}^{m\nu} B_1(m,\nu)]\} \qquad (5.3.10c)$$

$$B_2(m,n) = b_{2_n}(k_2 b)\{p_2(m,n) + \sum_{\nu} [A_{mn}^{m\nu} B_1(m,\nu) + B_{mn}^{m\nu} A_1(m,\nu)]\} \qquad (5.3.10d)$$

where the incident field coefficients p_2 and q_2 differ from p_1 and q_1 only by a multiplicative phase factor $\exp(jkd\cos\alpha)$ with p_1 and q_1 defined in (5.3.2a) and (5.3.2b), respectively. The expansion coefficients a_{σ_n} and b_{σ_n} of the external fields of the spheres 1 and 2 in isolation are given by equations (5.2.8a) and (5.2.8b), respectively. The transformation coefficients $A_{mn}^{m\nu}$ and $B_{mn}^{m\nu}$ are given in *Appendix* A.3.

The set of equations (5.3.10) can be solved by iterative methods or by matrix inversion techniques. Since the iterative methods were not found to yield accurate values for the expansion coefficients, equations (5.3.10) were solved by matrix inversion.

5.4 THREE-DIMENSIONAL ANALYTIC CONTINUATION

The incident and the scattered fields are expanded in terms of well established spherical vector wave functions, where the electric and magnetic fields are given by

$$\underline{E}^{(i,s)} = \sum_{m,n} [A(m,n)\, \underline{M}_{mn}^{(r)} + B(m,n)\, \underline{N}_{mn}^{(r)}] \qquad (5.4.1)$$

$$\underline{H}^{(i,s)} = \frac{jk}{\omega\mu} \sum_{m,n} [A(m,n)\underline{N}_{mn}^{(r)} + B(m,n)\, \underline{M}_{mn}^{(r)}] \qquad (5.4.2)$$

with the superscripts i,s specifying incident or scattered fields, A(m,n) and B(m,n) are the expansion coefficients and $M_{mn}^{(r)}$ and $N_{mn}^{(r)}$ denote the spherical vector wave functions.

Since the field expansions are valid only outside the Wilcox sphere, fields must be continued analytically for general scattering shapes so that the inverse boundary conditions can be applied. Both interior and exterior analytic continuations are required. The interior expansion valid inside the sphere S' of Fig. 5.3 can be expressed as

$$\underline{E}' = \sum_{m,n} [\alpha_i(m,n)\, \underline{M}_{mn}^{(1)'} + \beta_i(m,n)\, \underline{N}_{mn}^{(1)'}] \qquad (5.4.3)$$

In order to determine the new expansion coefficients $\alpha(m,n)$ and $\beta(m,n)$, the spherical vector wave functions of (5.4.1) must be translated into the new coordinate system 0' using the following addition theorem [38 , 112]

$$\underline{M}_{mn}^{r}(R,\theta,\phi) = \sum_{\nu=1}^{\infty} \sum_{\mu=-\nu}^{\nu} [A_{\mu\nu}^{mn} \underline{M}_{\mu\nu}^{(r')'}(R',\theta',\phi') + B_{\mu\nu}^{mn} \underline{N}_{\mu\nu}^{(r')'}(R',\theta',\phi')] \qquad (5.4.4a)$$

$$\underline{N}_{mn}^{r}(R,\theta,\phi) = \sum_{\nu=1}^{\infty} \sum_{\mu=-\nu}^{\nu} [A_{\mu\nu}^{mn} \underline{N}_{\mu\nu}^{(r')'}(R',\theta',\phi') + B_{\mu\nu}^{mn} \underline{M}_{\mu\nu}^{(r')'}(R',\theta',\phi')] \qquad (5.4.4b)$$

where r' = 1 for interior expansion and r' = 3 for exterior expansion. The translation coefficients $A_{\mu\nu}^{mn}$ and $B_{\mu\nu}^{mn}$ are derived in Stein [112] and Cruzan [38] and for computational purposes the following

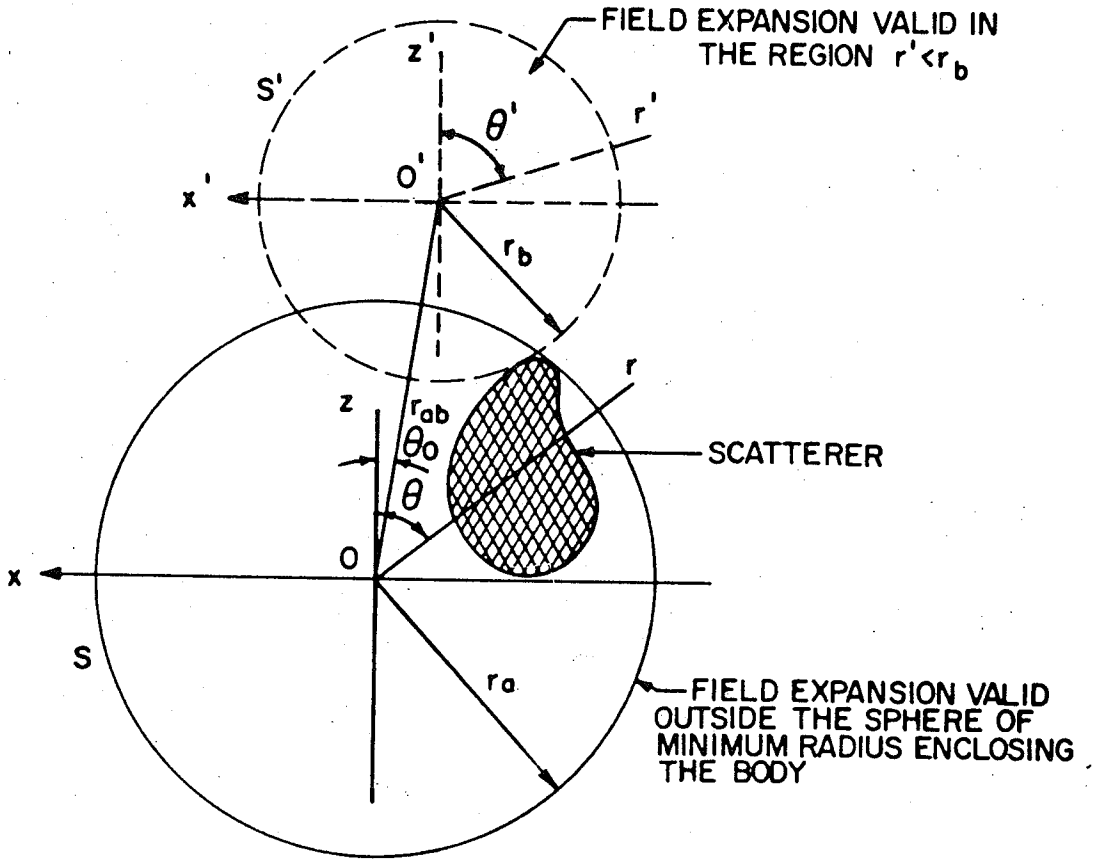

Fig.5.3. ANALYTIC CONTINUATION OF ELECTROMAGNETIC FIELD USING INSIDE EXPANSION ($\phi = 0° / \phi = 180°$ PLANE)

forms were found convenient

$$A_{\mu\nu}^{mn} = (-1)^{\mu} j^{\nu-n} \frac{2\nu+1}{2\nu(\nu+1)} \sum_{p} j^{p[n(n+1)+\nu(\nu+1)-p(p+1)]}$$

$$a(m,n,-\mu,\nu,p) Z_p^{(r)}(kd) P_p^{m-\mu}(\cos\theta_0) \exp[j(m-\mu)\phi_0] \qquad (5.4.5a)$$

and

$$B_{\mu\nu}^{mn} = \frac{jkR_0 \cos\theta_0}{\nu(\nu+1)} \mu\alpha_{\mu,\nu}^{mn} - \frac{jkR_0 \sin\theta_0 \exp(-j\phi_0)}{2\nu(\nu+1)} \alpha_{\mu-1,\nu}^{mn}$$

$$- \frac{jkR_0 \sin\theta_0 \exp(j\phi_0)}{2\nu(\nu+1)} (\nu+\mu+1)(\nu-\mu) \alpha_{\mu+1,\nu}^{mn} \qquad (5.4.5b)$$

In the above expression, the expansion coefficient $\alpha_{\mu\nu}^{mn}$, relating to the scalar addition theorem, is given by [112].

$$\alpha_{\mu\nu}^{mn} = (-1)^{\mu} j^{\nu-n} (2\nu+1) \sum_{p} j^{p} a(m,n,-\mu,\nu,p) Z_p^{(r)}(kd)$$

$$P_p^{m-\mu}(\cos\theta_0) \exp[j(m-\mu)\phi_0] \qquad (5.4.5c)$$

and is taken to vanish whenever $|\mu| > \nu$; and p in (5.4.5a) and (5.4.5b) extends from $|n-\nu|$ to $|n+\nu|$ with integer steps of 2.

Transforming the scattered electric field $\underline{E}^s$ of equation (5.4.1) (with r = 3) to system 0' of Fig. 5.3, we obtain

$$\underline{E}' = \sum_{m,n} \sum_{\mu,\nu} A(m,n)\{A_{\mu\nu-\mu\nu}^{mn} \underline{M}_{(1)}' + B_{\mu\nu-\mu\nu}^{mn} \underline{N}_{(1)}'\} + B(m,n)\{A_{\mu\nu-\mu\nu}^{mn} \underline{N}_{(1)}' + B_{\mu\nu-\mu\nu}^{mn} \underline{M}_{(1)}'\} \qquad (5.4.6)$$

where the translational addition theorems given by equations (5.4.5) have been employed.

Comparison of (5.4.6), after a simple interchange of indices, with (5.4.3) results in the following expressions for the transformed expansion coefficients for interior expansion valid inside the circle of maximum radius r_b as shown in Fig. 5.3.

$$\alpha_i(m,n) = \sum_{\mu,\nu} [A(\mu,\nu)\ A_{mn}^{\mu\nu} + B(\mu,\nu)\ B_{mn}^{\mu\nu}] \qquad (5.4.7a)$$

$$\beta_i(m,n) = \sum_{\mu,\nu} [A(\mu,\nu)\ B_{mn}^{\mu\nu} + B(\mu,\nu)\ A_{mn}^{\mu\nu}] \qquad (5.4.7b)$$

where $A_{mn}^{\mu\nu}$ and $B_{mn}^{\mu\nu}$, defined by equations (5.4.5), involve Hankel functions $h_n^{(1)}(kr)$.

The expressions for the exterior analytic continuation valid outside the circle of minimum radius r_a' can be obtained by a similar approach (Fig. 5.4). For this case the scattered field in the translated coordinate $0'$ may be written as

$$\underline{E}' = \sum_{m,n} [\alpha_e(m,n)\underline{M}_{mn}^{(3)'} + \beta_e(m,n)\ \underline{N}_{mn}^{(3)'}] \qquad (5.4.8)$$

Translating equation (5.4.1) with $r = 3$, to the coordinate system $0'$ for exterior expansion, we obtain

$$\underline{E}' = \sum_{m,n} \sum_{\mu,\nu} [A(m,n)\{A_{\mu\nu-\mu\nu}^{mn}\underline{M}_{\mu\nu-\mu\nu}^{(3)'} + B_{\mu\nu-\mu\nu}^{mn}\underline{N}_{\mu\nu-\mu\nu}^{(3)'}\} + B(m,n)\{A_{\mu\nu-\mu\nu}^{mn}\underline{N}_{\mu\nu-\mu\nu}^{(3)'} + B_{\mu\nu-\mu\nu}^{mn}\underline{M}_{\mu\nu-\mu\nu}^{(3)'}\}] \qquad (5.4.9)$$

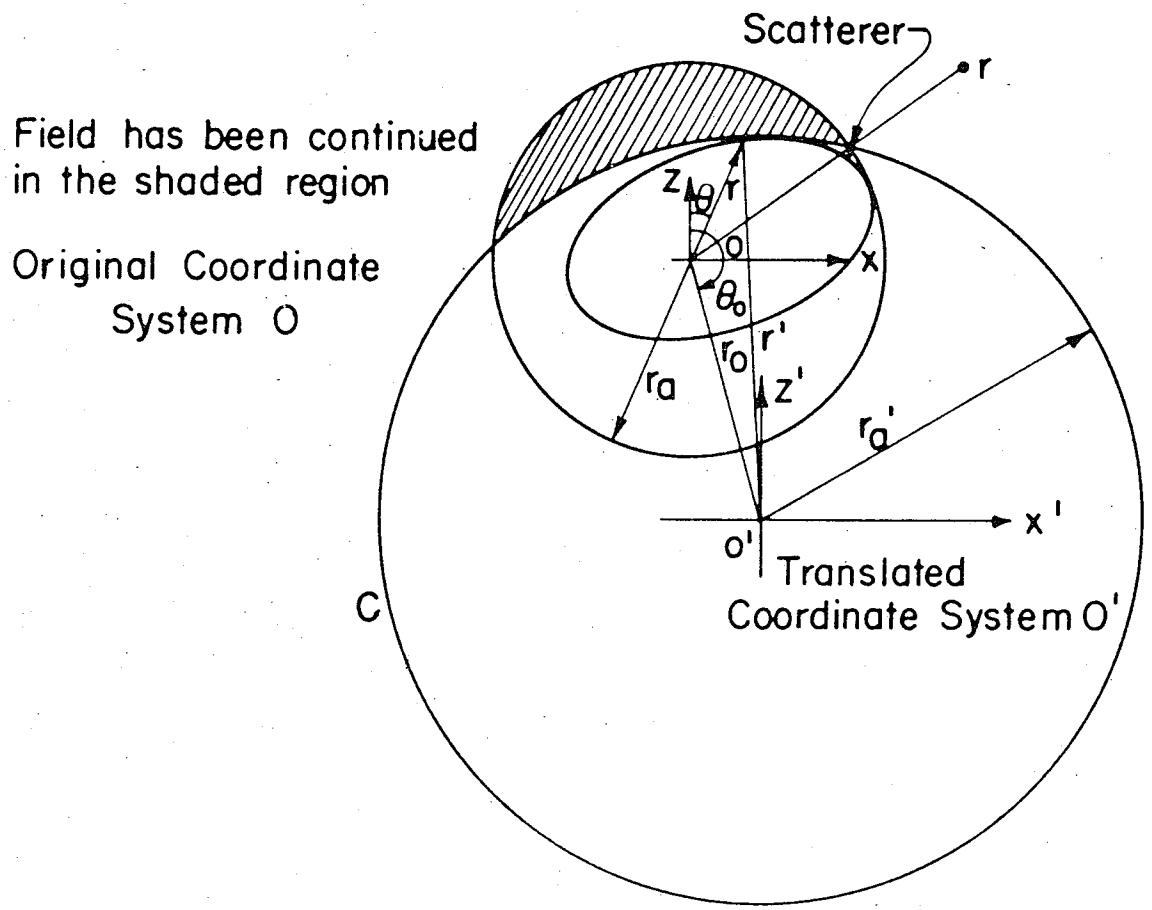

Fig.5.4. 3-D Analytic Continuation of the Electro - magnetic Field on a ϕ = Constant Plane using Outside Expansion.

Interchanging the indices m and n with μ and ν, respectively in (5.4.9) and comparing the result with (5.4.8), the exterior expansion coefficients are found to be

$$\alpha_e(m,n) = \sum (A(\mu,\nu)\ A_{mn}^{\mu\nu} + B(\mu,\nu)\ B_{mn}^{\mu\nu}) \qquad (5.4.10a)$$

$$\beta_e(m,n) = \sum (A(\mu,\nu) B_{mn}^{\mu\nu} + B(\mu,\nu)\ A_{mn}^{\mu\nu}) \qquad (5.4.10b)$$

where $A_{mn}^{\mu\nu}$ and $B_{mn}^{\mu\nu}$, defined by equations (5.4.5), involve Bessel's functions $j_n(kr)$.

5.5 NUMERIC COMPUTATIONAL VERIFICATION (3-DIM.)

The numerical verification for the three-dimensional case involves the use of a variety of special functions, e.g. Bessel's functions, Legendre's functions, Wigner symbols, etc. Therefore, in order to achieve accurate inversion, maximum use of recursive and iterative techniques has to be made.

All the special functions, the scattering coefficients A_n and B_n for the single sphere (5.2.8) and the three-dimensional analytic continuation routines were generated as subroutines which are called by the main program when required. The spherical Bessel functions are generated using a program developed by Shafai [110], in which he uses backward recursion to minimize the disastrous accumulation of errors. The Legendre's functions may be calculated using well known recursion

formulas for $P_n^m(x)$ in order and degree, in either direction, without worrying about error accumulation. Backward recursion in order was used for the presented computations.

Calculation of the translation coefficients of (5.4.5a) and (5.4.5b) presents the most challenging problem. The special case of (5.4.5a) and (5.4.5b) for which translation is along z-axis has been treated in detail by Bruning [30] and his recursion relations, summarized in *Appendix* A.3, have been employed for the calculation of the scattering coefficients given by (5.3.10) for the two-sphere problem. A three term recursion formula for the general three-dimensional translation has been derived using Bruning's approach [30] and is presented in *Appendix* A.3. For those particular cases in which the recursion relation (A3.4) of *Appendix* A.3 fails to yield the value of the translation coefficient, the original definition of these coefficients, given in *Appendix* A.3 by (A3.2) was employed.

As in the two-dimensional case, the numerical verification of the inverse boundary conditions has been divided into two distinct categories. In the first category, the numerical verification of the IBCs for perfectly conducting cases is considered. The second category comprises of those targets whose surface impedance $\eta \neq 0$ or ∞ satisfies Leontovich boundary conditions. The perfectly conducting case has been subdivided into the perfectly electric ($\eta = 0$) and perfectly magnetic ($\eta = \infty$) conducting cases. Under imperfectly conducting scatterers the following four cases have been treated i) η known and $S_0(\underline{r})$ to be re-

covered, ii) $|\eta|$ and $S_0(\underline{r})$ to be recovered, iii) $\eta = |\eta|\exp(j\psi)$ and $S_0(\underline{r})$ to be recovered and iv) $\hat{n}(\underline{r})$ known and η, $S_0(\underline{r})$ to be determined.

In each case the total electric and magnetic fields are computed at different discrete points along various radiant vectors which for the three-dimensional case are defined by the bistatic angles (θ,ϕ) with θ and ϕ being parametric constants and $x = kR$ being the variable with arbitrarily chosen finite increments $\Delta x = k\Delta R$. The fields calculated using spherical vector wave function expansions are then substituted into the appropriate boundary conditions applicable in the respective cases as established in *chapter three*. Unless otherwise specified, the fields employed in the boundary conditions are calculated using the center of the body as origin of the coordinate system.

5.5.1 PERFECTLY CONDUCTING CASE

5.5.1.1 PERFECTLY ELECTRIC CONDUCTING BODIES

5.5.1.1a MONO-BODY CASE

For the case of perfectly electric conducting spheres the boundary conditions $Q_1 = \text{Min}\{|\underline{E}\times\underline{E}^*|^2\}$, $Q_2 = \text{Min}\{|\underline{E}_i|-|\underline{E}_s|\}$, $Q_3 = \text{Min}\{\underline{E}\cdot\underline{H}\}$ and $Q_4 = \text{Min}\{\underline{E}\cdot\underline{H}^*\}$ were used and the resulting curves are plotted in Fig. 5.5a. As is evident from Fig. 5.5a the conditions Q_2 and Q_3 produce only one distinct minimum, whereas Q_1 and Q_4 produce an

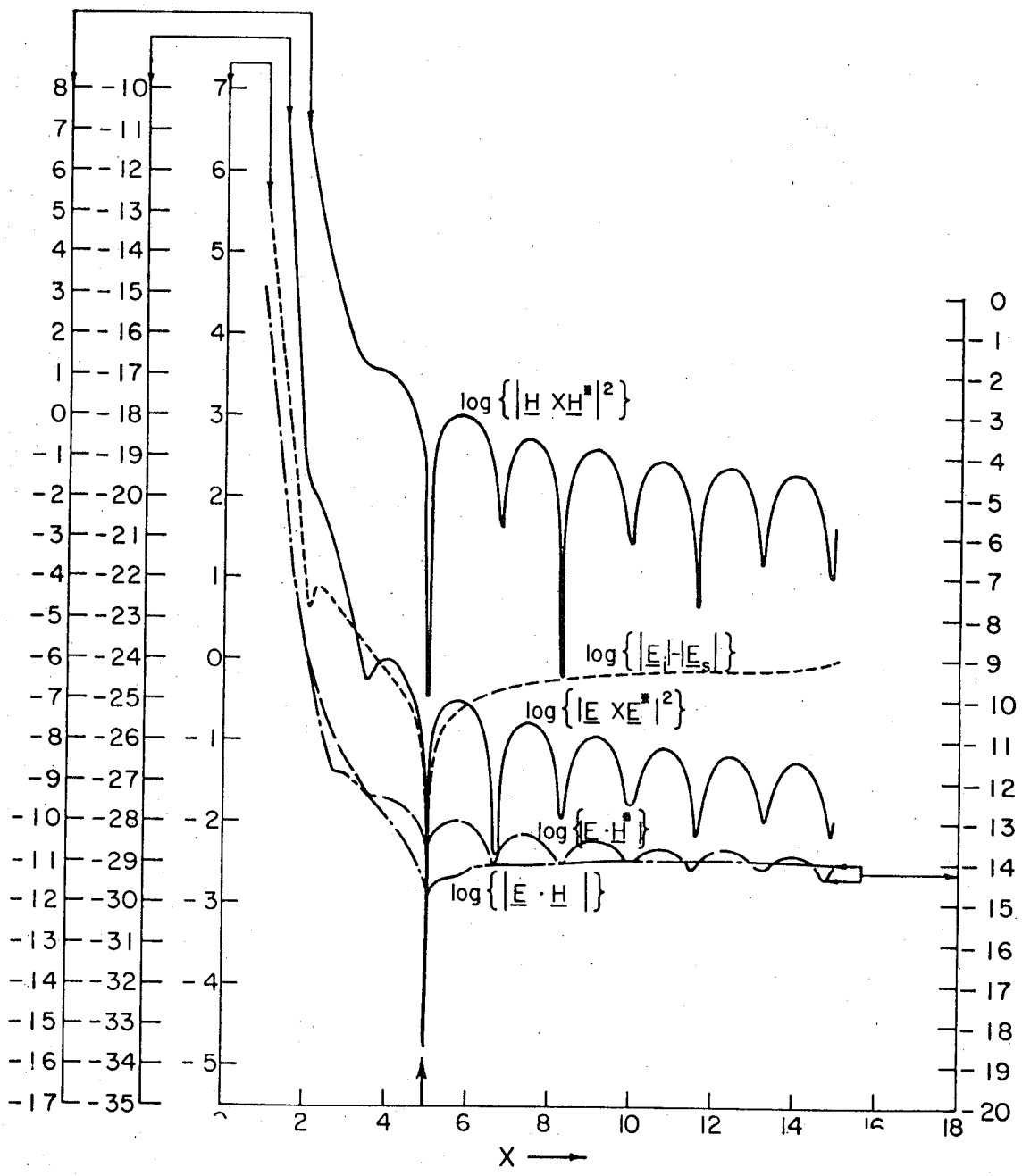

Fig. 5.5a. Plot of $\text{Log}\{|\underline{E} X \underline{E}^*|^2\}$, $\text{Log}|\underline{E}_i - \underline{E}_s|$, $\text{Log}\{|\underline{E} \cdot \underline{H}|\}$, $\text{Log}|\underline{E} \cdot \underline{H}^*|$, $\text{Log}\{|\underline{H} X \underline{H}^*|^2\}$ versus Radiant Vector $X = kR$ for the Sperical Test Case $ka = 5, \eta = 0, \theta = 22.5°$

infinite set of *identical* minima. Therefore, the physical optics condition Q_2 and the condition Q_3 can determine the proper surface locus unambiguously. However, it is evident from Fig. 5.5b that the physical optics condition holds with sufficient accuracy only in the illuminated region, whereas, the condition $\underline{E}\cdot\underline{H} = 0$ is necessary and sufficient and holds also in the shadow region. All the four IBC's are plotted on a plane defined by $\phi = -90°, 90°$ in Fig. 5.5b The minima of Q_2 and Q_3 define only the proper surface of the body whereas, Q_1 generates an infinite number of pseudo loci in addition to the locus defining the true surface of the scatterer. Similar to the two-dimensional case, for a smooth and closed, perfectly electric conducting scatterer the proper locus is closed, but the additional pseudo loci cannot be closed in the shadow region of the scatterer. This property results from the fact that the total field expressions implicitly describe an interference pattern. Therefore, if it is known *a priori* that the scattering surface is closed, IBC Q_1 can be employed to uniquely specify the proper surface locus from the total near field data given for only one operating frequency. This again confirms that the *locally* insufficient condition Q_1 is *globally* sufficient.

5.5.1.1b TWO-BODY CONFIGURATION

In order to test the applicability of the IBCs Q_1, Q_2 and Q_3 to the general three-dimensional case, a two-body configuration was selected.

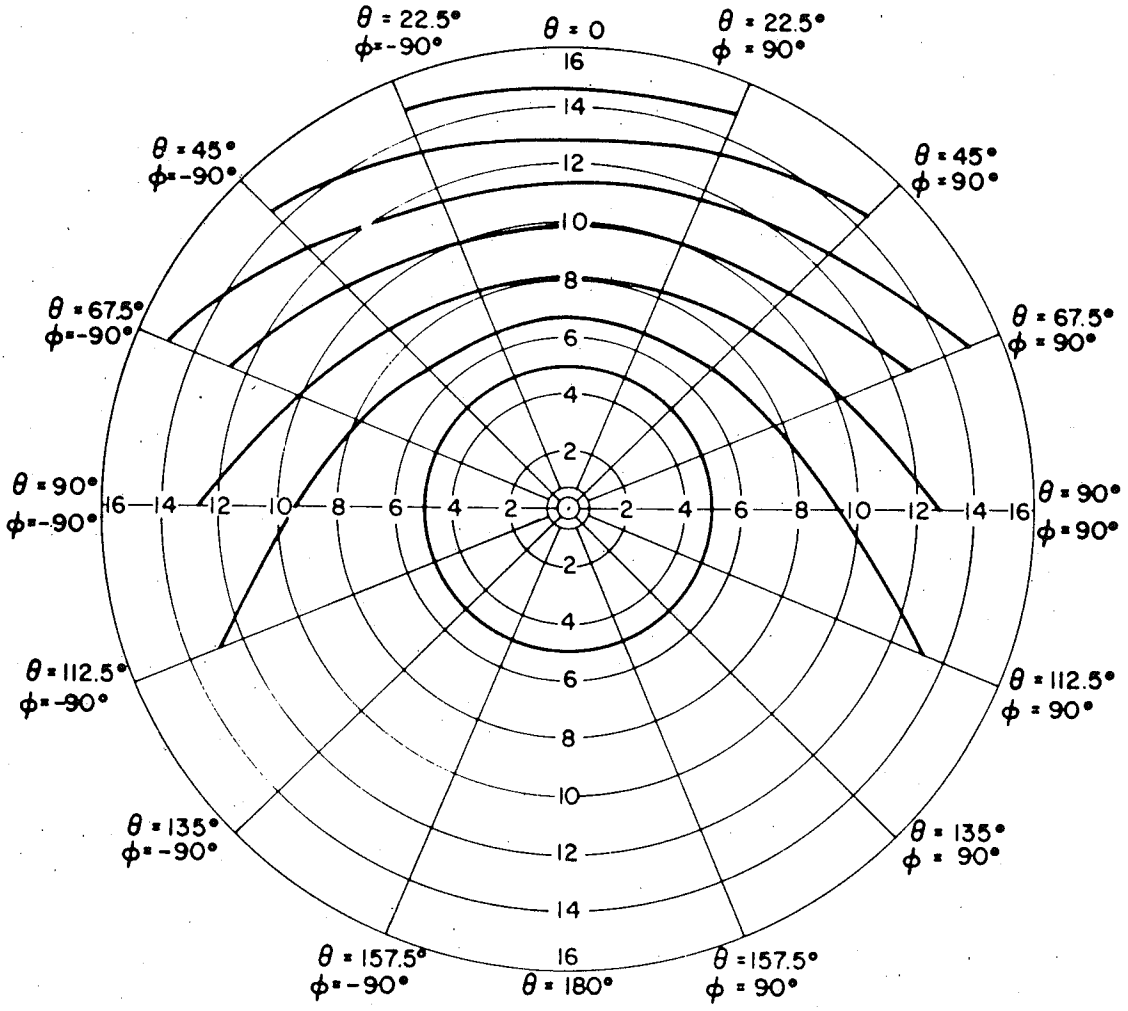

Fig. 5.5b. Surface Loci of Successive Minima of $\underline{E} \times \underline{E}^*$ for a Spherical Test case $\eta = 0$, $ka = 5.0$

The test case selected for presentation consists of two perfectly conducting spheres of equal electrical radii $ka_1 = ka_2 = 0.4$ with their centers separated by an electrical distance $kd = 1.2$. The electrical dimensions of the target were chosen to be small to improve the rate of convergence of the total field expressions and hence to reduce the required computer time. The incident wave is polarized normal to the z-axis and makes an angle $\alpha = 90°$ with the line joining the centers as shown in Fig. 5.2. The scattering coefficients for each of the spheres in the presence of the other, given by (5.3.10a) to (5.3.10d), are transformed to the new coordinate system $0'$ of Fig. 5.3 using the interior continuation of (5.4.3) and (5.4.7). Due to the linearity of the fields, the sums $C(m,n)$ and $D(m,n)$ of the translated coefficients $\alpha_1(m,n)$, $\alpha_2(m,n)$ and $\beta_1(m,n)$, $\beta_2(m,n)$, respectively, provide the scattering coefficients for the two-body configuration with respect to the translated coordinate system $0'$. A similar approach was employed to discriminate points lying on the minimum circle enclosing the two scatterers where use was made of the exterior analytic continuation of (5.4.8) and (5.5.10) as shown in Fig. 5.4, [3].

The values computed for Q_1, Q_2 and Q_3 are plotted in Fig. 5.6a along a ray $\theta = 0, 180°$, $\phi = 180°$ and the loci resulting from computation of the three IBCs along a selected grid of rays on a plane $\phi = 180°$ are shown in Fig. 5.6b. The origins of the translated coefficients were selected to lie on each of these rays and the pseudo loci were computed using exterior expansion of the em fields. Figs.

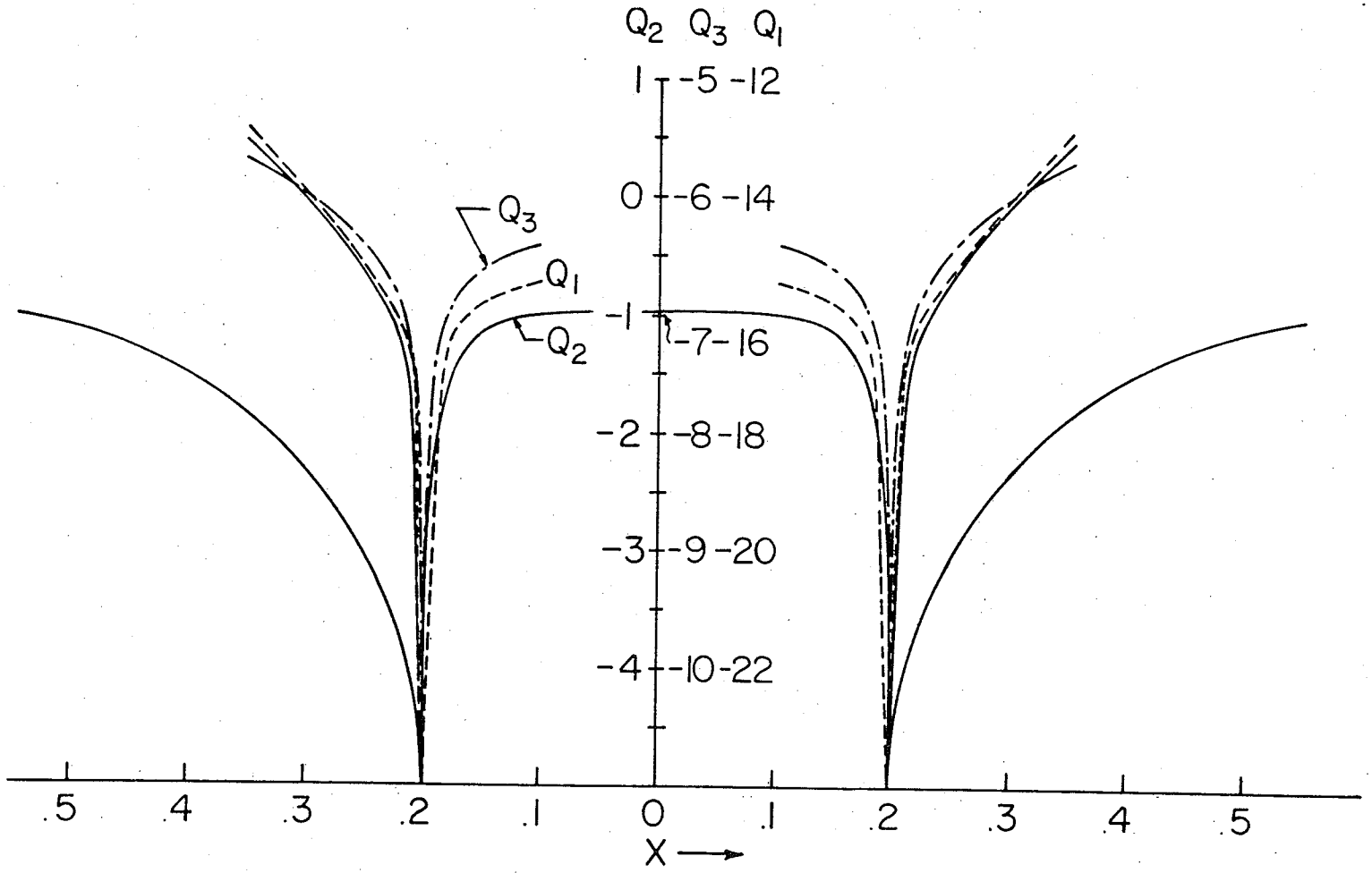

Fig. 5.6a. Plots of $Q_1 = \text{Log}|\underline{E} \times \underline{E}^*|^2$, $Q_2 = \text{Log}[|\underline{E}_i| - |\underline{E}_s|]$ and $Q_3 = \text{Log}[|\underline{E} \cdot \underline{H}|]$ vs Radiant Vector X for Perfectly Conducting Two-Sphere Configuration $ka_1 = ka_2 = 0.4$, $kd = 1.2$, $\alpha = 90°$ along the Ray $\theta = 0, 180°$ and $\phi = 180°$

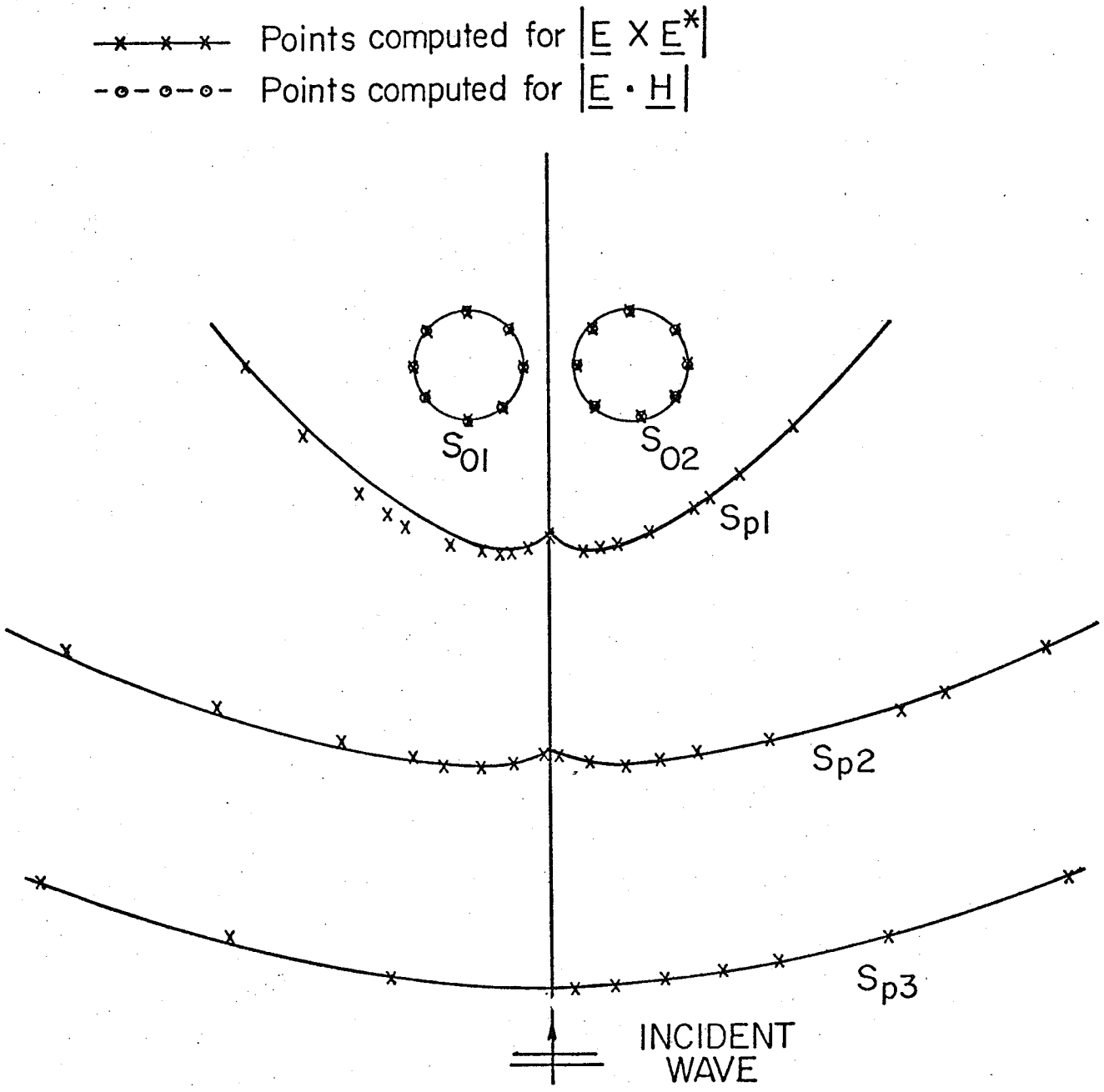

Fig. 5.6 b. Loci of Successive Minima of $\underline{E} \times \underline{E}^*$ and $\underline{E} \cdot \underline{H}$ for Two Pefectly Conducting Spheres of Elec. Radii $ka_1 = ka_2 = 0.4$ and Separation between the Centers $kd = 1.2$, $\alpha = 90°$

5.6a and 5.6b confirm the properties of the IBCs Q_1, Q_2 and Q_3 stated for the single spherical scatterer. It should be observed that similar to the two-dimensional case, discussed in Subsection 4.4.2 the pattern of pseudo loci resulting for the two-body case is the superposition of the patterns of pseudo loci for the individual spheres. Therefore, it is concluded that by the simultaneous application of the three IBCs, it is possible to recover the proper surface locus of a closed scatterer uniquely and accurately from the knowledge of the total em fields given everywhere in the vicinity of the scatterer for only one frequency.

5.5.1.2 PERFECT MAGNETIC CONDUCTING CASE

The proper surface of a perfectly magnetic conducting smooth and closed scatterer can be determined using the boundary conditions complementary to the set mentioned for perfect electric conductors as derived in Section 3.2 i.e. $QH_1 = \text{Min}\{|\underline{H}\times\underline{H}^*|^2\}$, $QH_2 = \text{Min}\{|\underline{H}_i|-|\underline{H}_s|\}$ and $QH_3 = \text{Min}\{\underline{E}\cdot\underline{H}\}$. The corresponding plots resulting from the computation of the respective boundary conditions along a ray defined by ($\theta = 22.5°$, $\phi = 80°$) are shown in Fig. 5.7a and the corresponding loci in Fig. 5.7b. As expected the IBCs QH_1, QH_2 and QH_3 for the perfectly magnetic conducting case possess the same characteristics as do their counterparts Q_1, Q_2 and Q_3, respectively, for the perfectly electric conducting case. Namely, QH_2 and QH_3 can again be seen to be necessary and sufficient conditions and QH_1 is necessary, *locally* insufficient but *globally* sufficient condition. Therefore, it is concluded that in both the

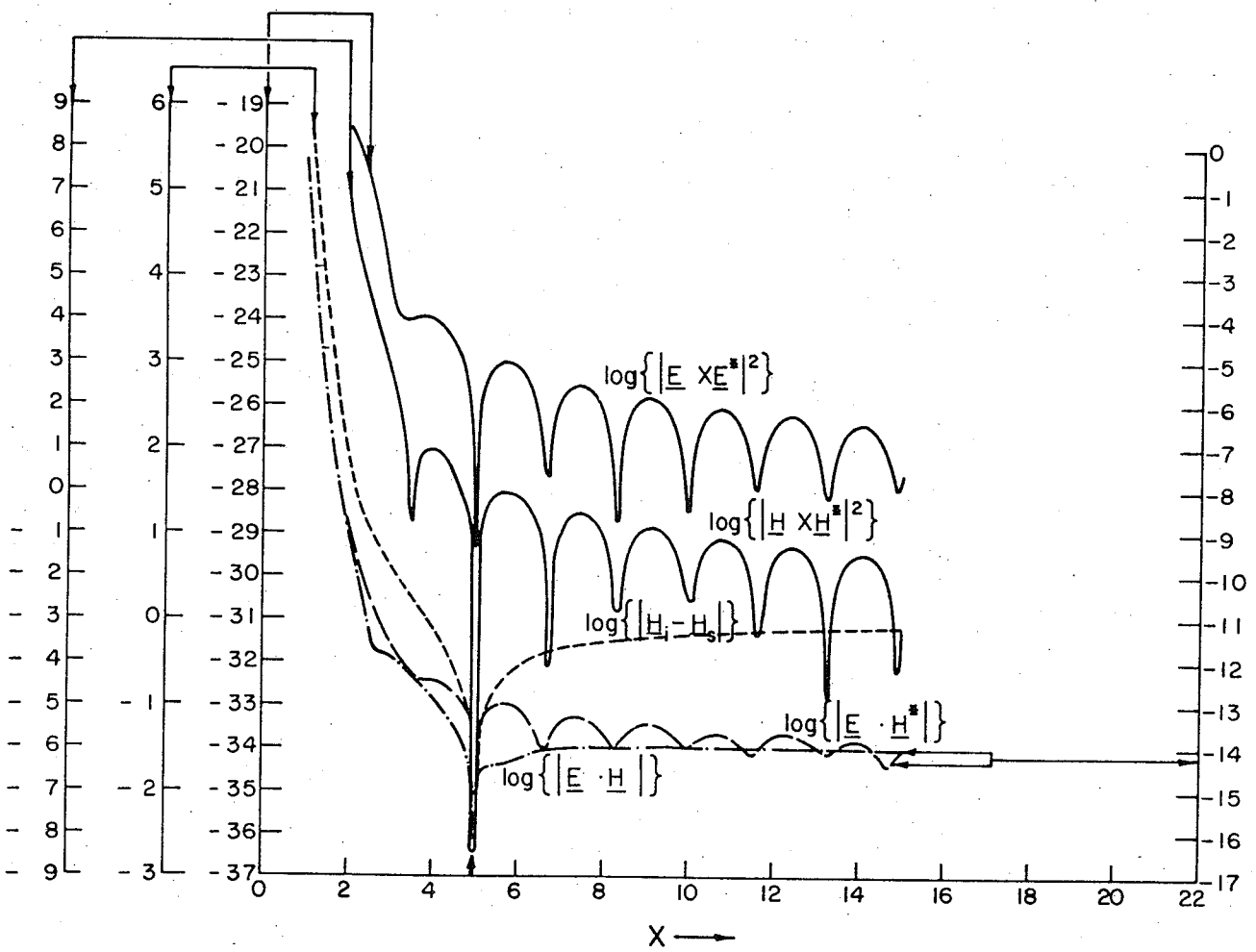

Fig. 5.7a. Plot of Log $\{|\underline{H}_T X \underline{H}_T^*|^2\}$, Log $|\underline{H}_i - \underline{H}_s|$, Log$(|\underline{E}_T \cdot \underline{H}_T|)$, Log$(|\underline{E}_T \cdot \underline{H}_T^*|)$, Log $\{|\underline{E} X \underline{E}^*|^2\}$, versus Radiant Vector X=kR for the Spherical Case ka=5.0, $\eta=\infty$, $\theta=22.5$ and $\phi=-90°$

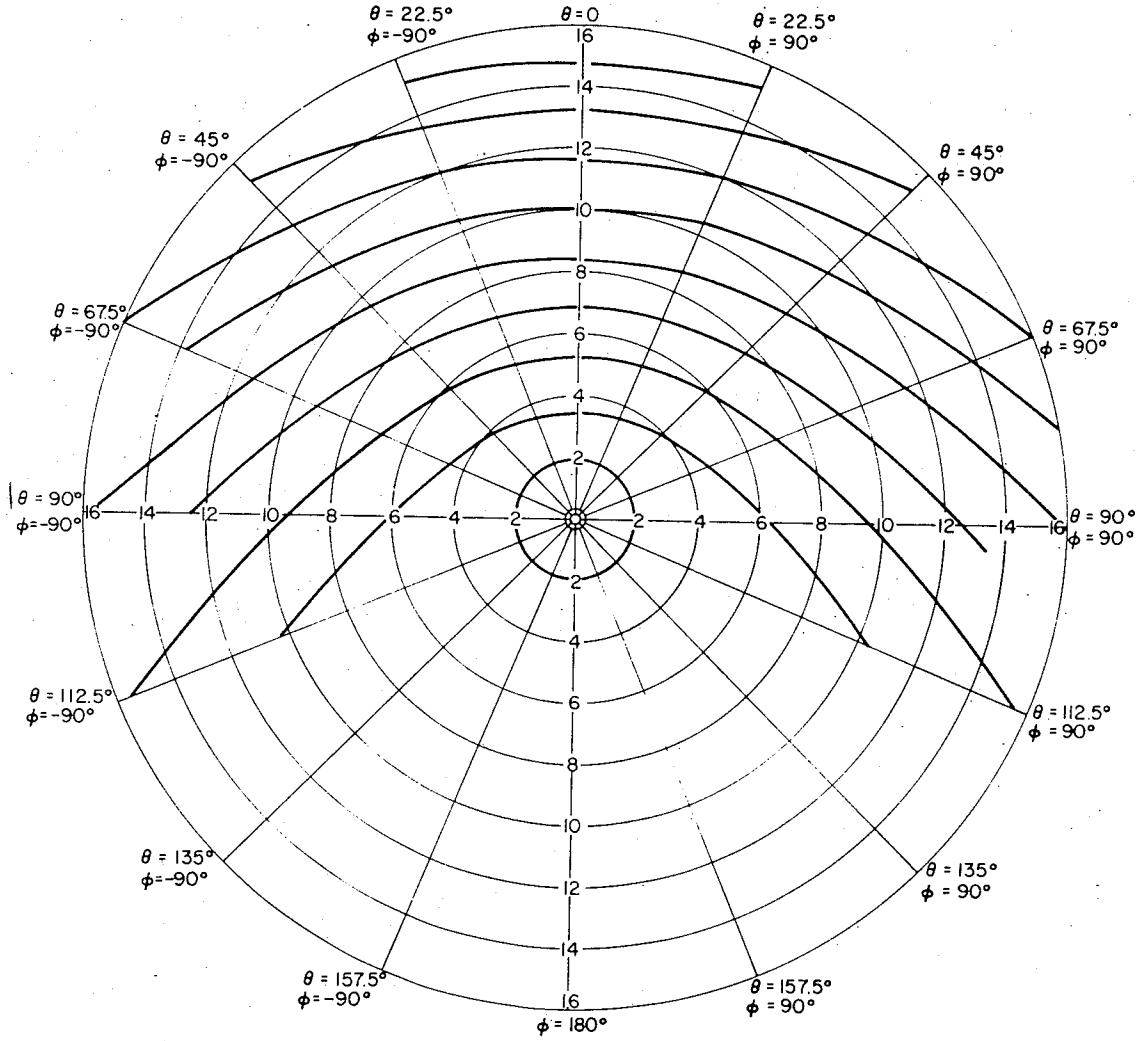

Fig. 5.7 b. Loci of the Successive Minima of $H X H^{*}$ for $\eta = \infty$

perfectly electric as well as magnetic conducting cases the proper surface locus can be uniquely determined using measurements compiled for a single operating frequency.

5.5.2 THE IMPERFECTLY CONDUCTING CASE

The test targets selected for verifying the IBCs for this case consist of mono- and two-body configurations. The formulation of the em fields is identical to that of the perfectly conducting case except that the appropriate value of η is substituted into (5.2.8)

5.5.2a η KNOWN AND $S_0(r)$ TO BE DETERMINED

The procedure is first verified for a single sphere centered at 0 (Fig. 5.3) using field expansions with respect to 0, and then by displacing the origin to 0' (Fig. 5.3) using analytic continuation.

The orthogonality condition $Y_1 = \text{Min}\{\underline{A}\cdot\underline{B}\}$ and the normality condition $Y_2 = \text{Min}\{A^2-B^2\}$ are computed along a radiant vector ($\theta = 22.5°$, $\phi = 90°$) for three different values of surface impedance, i.e. a) purely real, b) purely imaginary, and c) complex, for a sphere of electrical radius $ka = 5$ and the computed results are presented in Figs. 5.8a, 5.8b and 5.8c. From inspection of these plots, it is observed that the minima defining the proper point on the surface are much sharper than those resulting for the additional pseudo loci. The slope of the descending part of the curves Y_1 and Y_2 for the

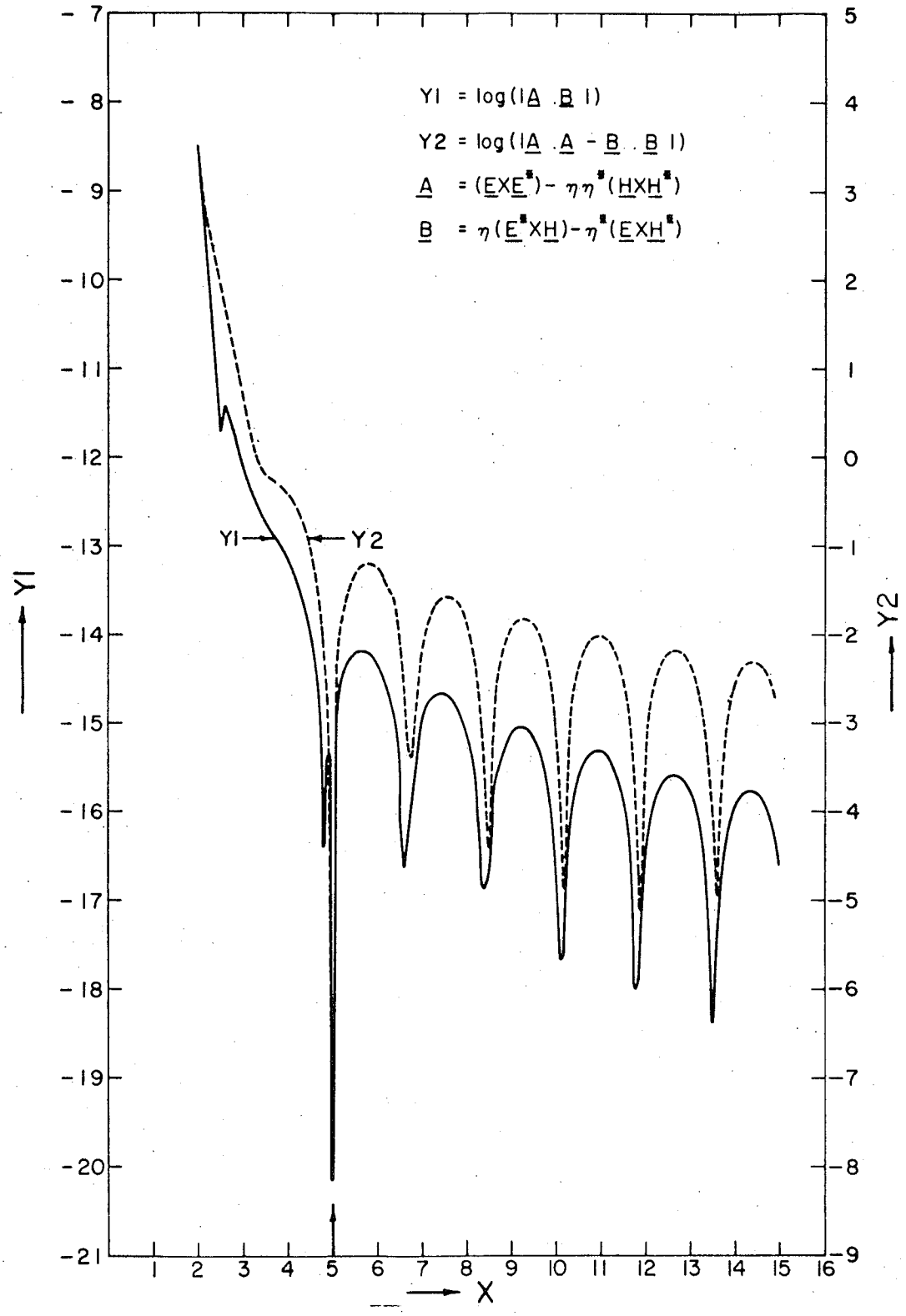

Fig. 5.8a. Plot of Y1 and Y2 vs Radiant Vector X for a Spherical Target of ka = 5.0 and $\eta = 0.5$ for $\theta = 30.00$, $\phi = 90°$

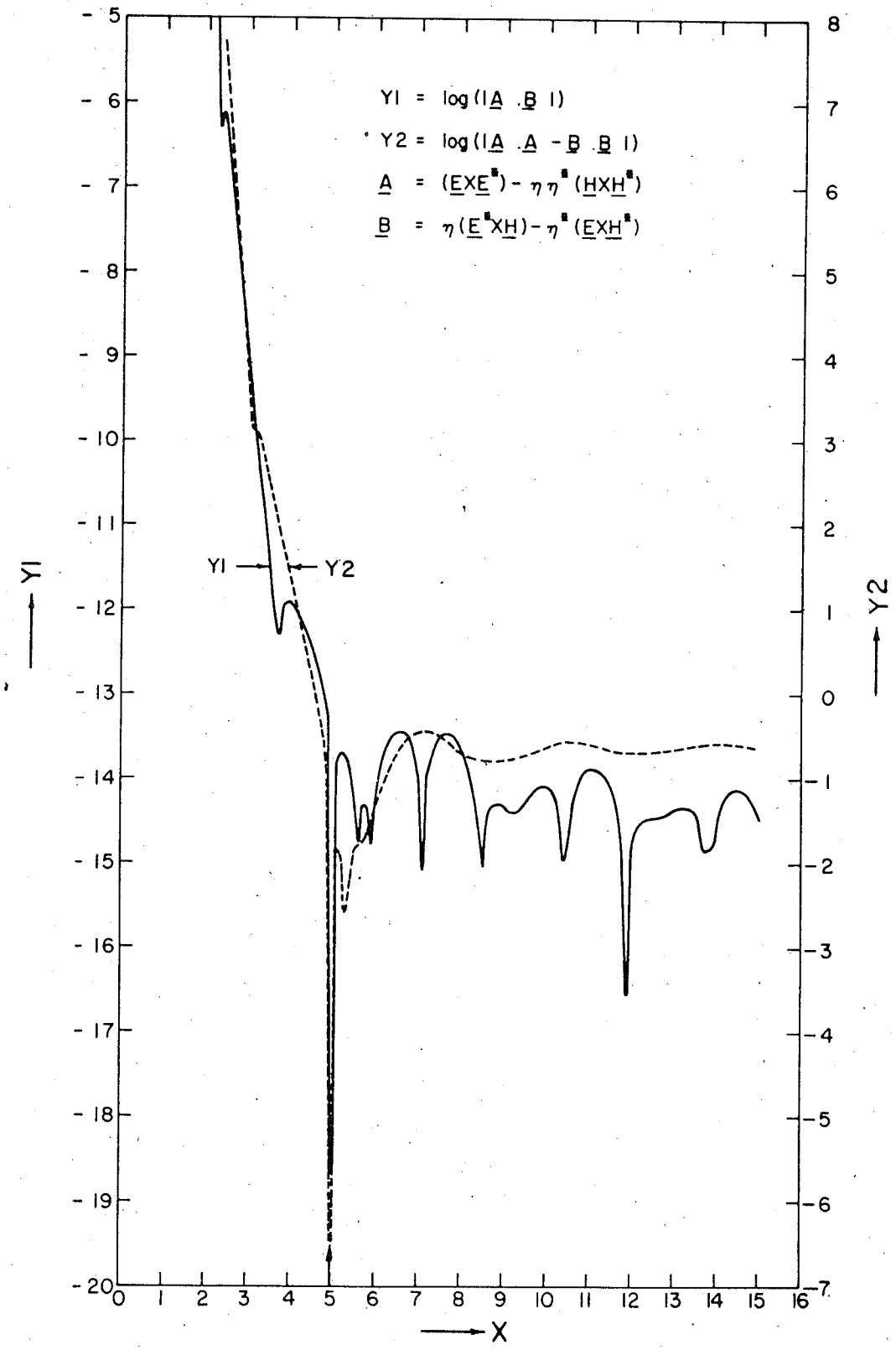

Fig. 5.8b. Plot of Y1 and Y2 vs Radiant Vector X for a Spherical Target of ka = 5.0, $\eta = j(0.5)$ for $\theta = 30°$, $\phi = 90°$

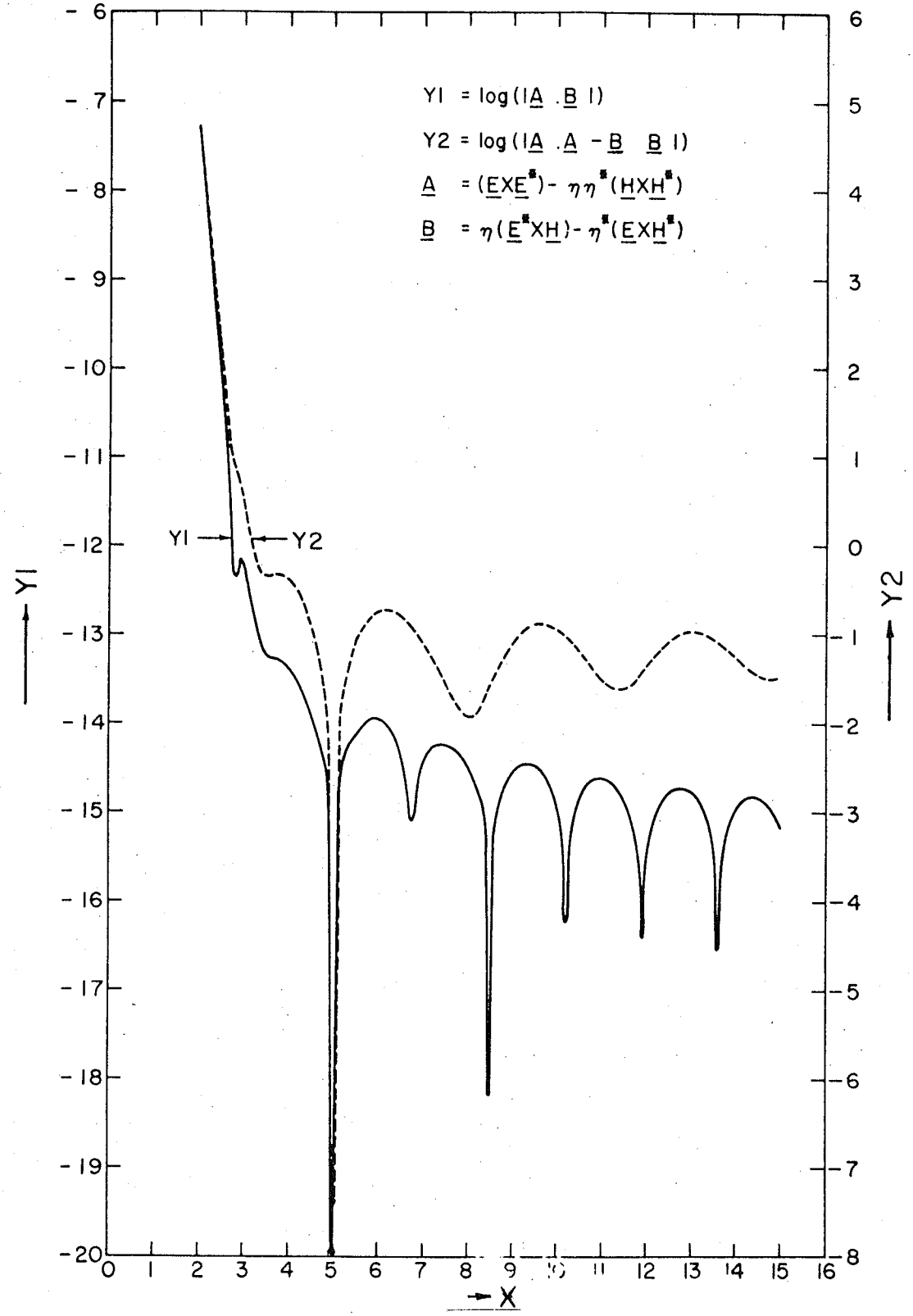

Fig. 5.8 c. Plot of Y1 and Y2 vs Radiant Vector X for a Spherical Target of ka=5.0, η= 0.433+j.25 for θ=30°, ϕ = 90°

proper minima are steeper than for the other minima. Both conditions are seen to work for all values of surface impedance ($\eta \neq 0$ or ∞) be it real, imaginary or complex, though the additional minima are found to flatten out as the surface impedance becomes more and more reactive. Though the simultaneous application of the two conditions is sufficient to uniquely discriminate the proper surface locus given computed near field expressions for only one frequency, the double-frequency checking technique can help to discriminate the proper minimum from some other accidently coincident minima, provided $\eta \neq \eta(\omega)$ i.e. the material of the body is nondispersive. Figs. 5.9a and 5.9b show the plots of Y_1 and Y_2 versus the geometrical distance resulting from computation using near field expressions for two different frequencies. It can be seen, as expected, that only the minima at $R = 5$ (which was chosen to be the radius of the unknown sphere) coincide and all other minima are shifted . The loci resulting from the use of the orthogonality condition are shown in Fig. 5.10 on a plane $\phi = -90, 90°$. The interference-like pattern generated by Y_1 possesses the properties displayed by the IBC $\underline{E} \times \underline{E}^* = 0$ and $\underline{H} \times \underline{H}^* = 0$ for the degenerate perfectly conducting cases (Fig. 5.6b). Similar behavior is also displayed by the normality condition as is clear from Fig. 5.8 . Namely, the IBCs Y_1 and Y_2 are both necessary, *locally* insufficient but *globally* sufficient.

Fig. 5.11 presents the plots of Y_1 and Y_2 along a ray $\theta = 45°$, $\phi = 130°$ for a spherical scatterer of electrical radius $ka = 0.5$ and surface impedance $\eta = 0.25$. Here the scalars Y_1' and Y_2' have

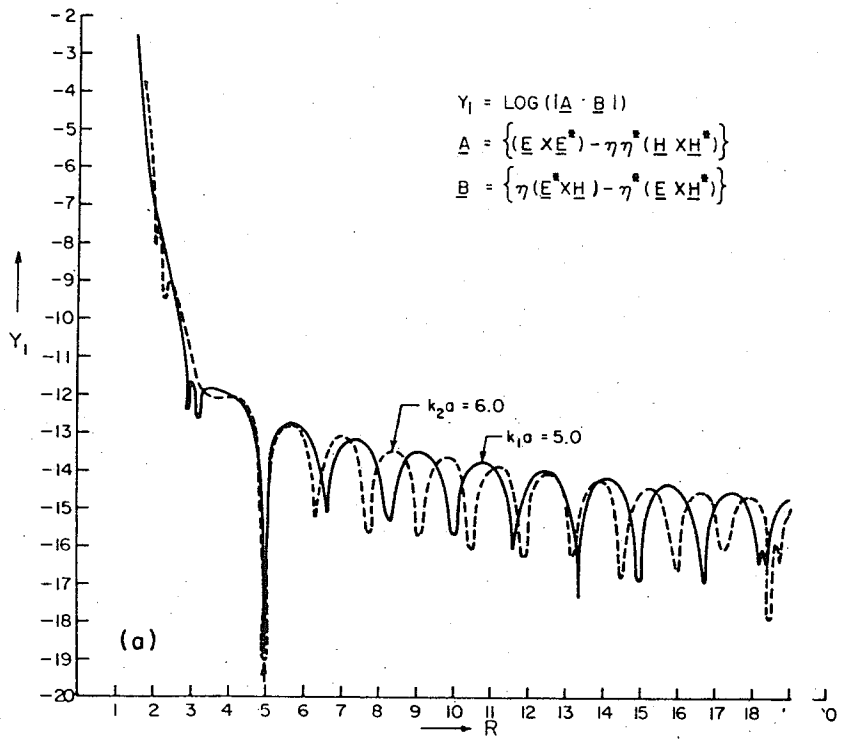

Fig.5.9a. Plot of Y1 vs Geometrical Distance R at Two Frequencies for a Sperical Test Case such that $k_1a = 5.0$ and $k_2a = 6.0$ for $\eta = 2.0$, $\theta = 22.5°$ and $\phi = 90°$

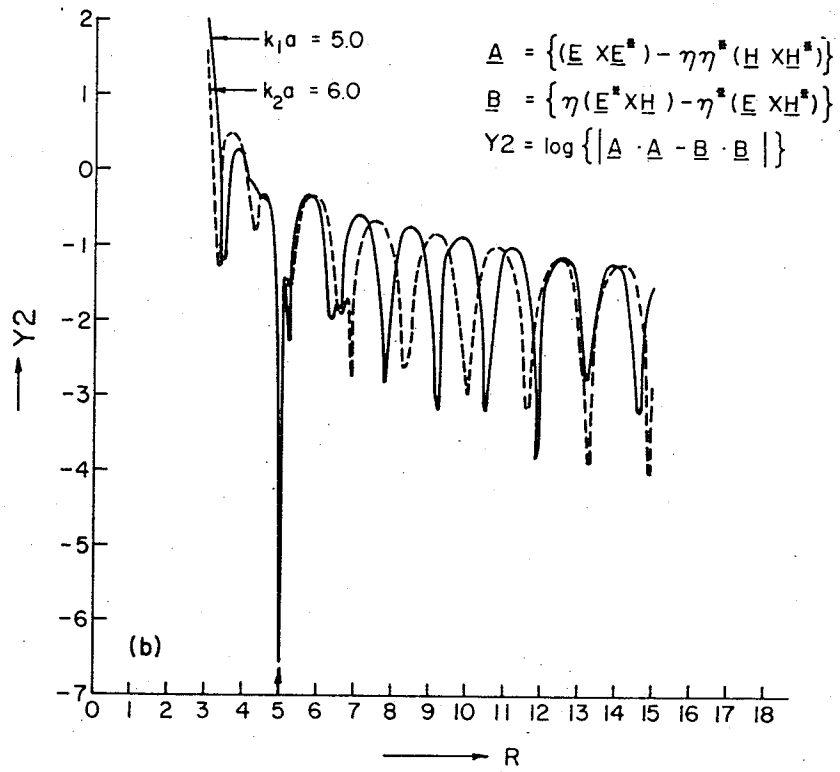

Fig. 5.9b. Plot of Y2 vs Geometrical Distance R along a Ray ($\theta = 22.5, \phi = 90°$) for a Spherical Test Case with Known $\eta = 2.0$ and $a = 5.0$ at Two Frequencie such that $k\,a_1 = 5.0$ and $k_2 = 6.0$

$$\underline{A} = (\underline{E} \times \underline{E}^*) - \eta\eta^*(\underline{H} \times \underline{H}^*)$$
$$\underline{B} = \eta(\underline{E}^* \times \underline{H}) - \eta^*(\underline{E} \times \underline{H}^*)$$

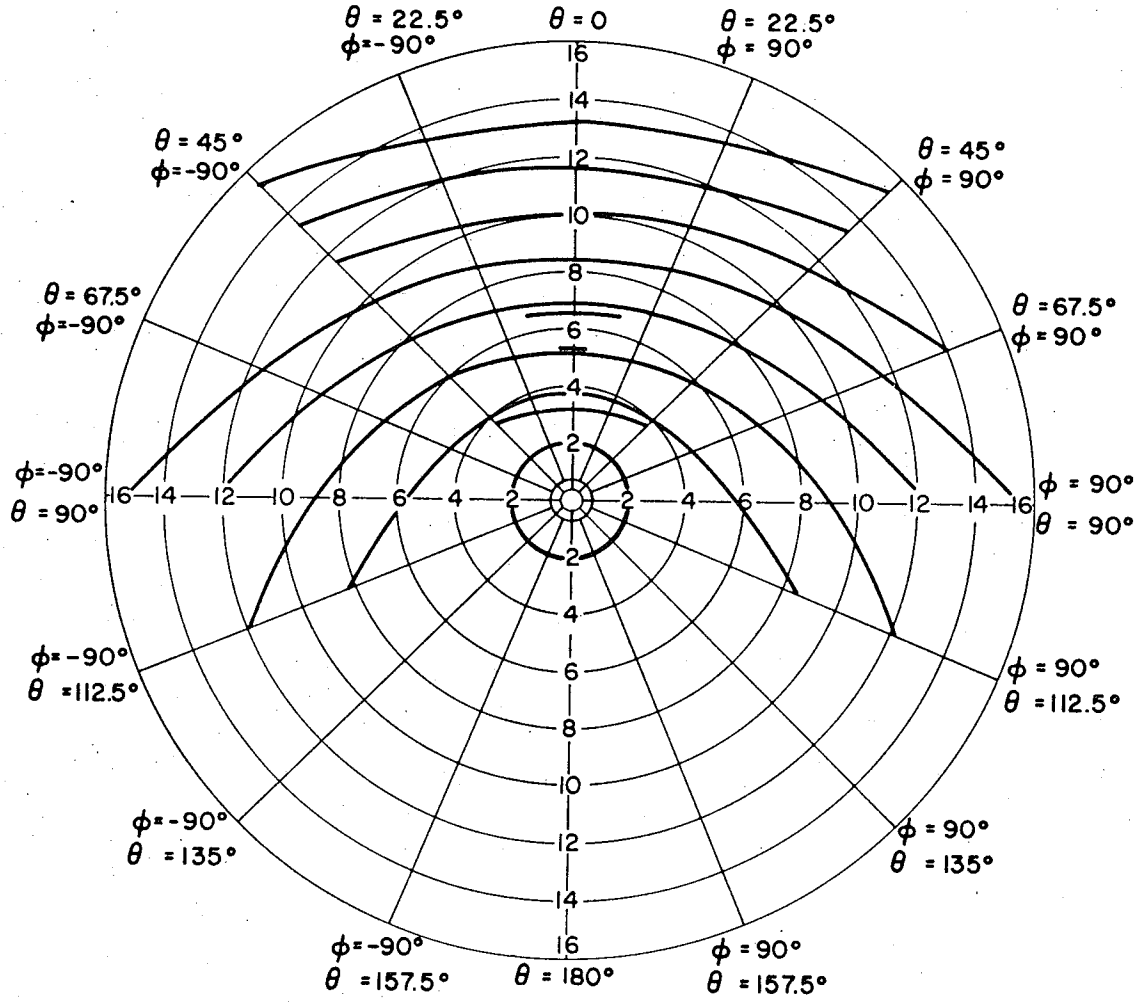

Fig.5.10. Loci of the Successive Minima of $\underline{A} \cdot \underline{B}$ for ka=2, η=0.25

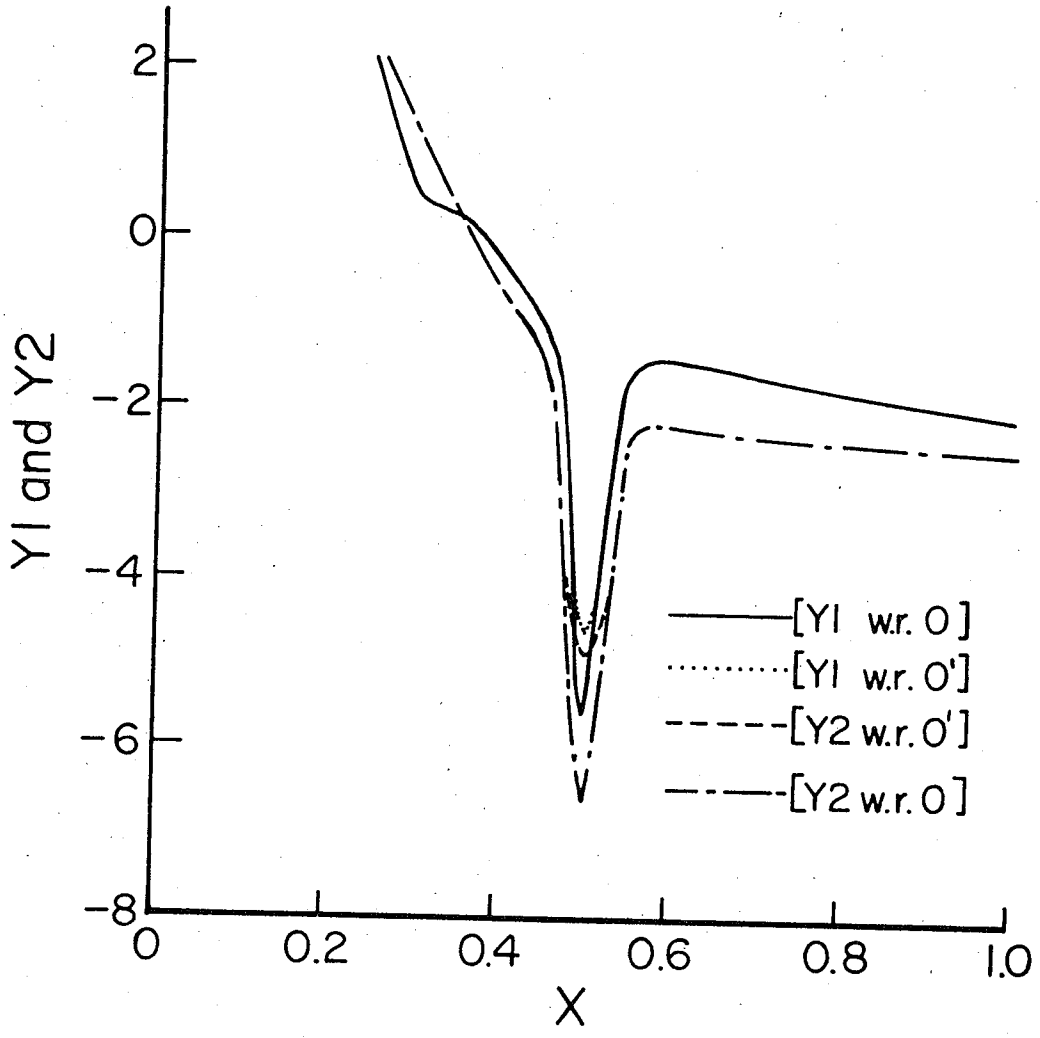

Fig. 5.11. Plots Y1 and Y2 along a Ray $\theta = 45°$ and $\phi = 130°$ for a Spherical Scatterer of Elec. Radius ka=0.5 and $\eta = 0.25 \angle 0°$

been computed using field expansion with respect to the origin 0 which coincides with the center of the sphere (Fig. 5.3) and Y''_1 and Y''_2 with respect to a translated origin 0' with $\theta_0 = 45°$, $\phi_0 = 130°$ and kd = .75°. Since the fields calculated using analytic continuation are not as accurate as those calculated with respect to the center 0, the minima of Y''_1 and Y''_2 are not as sharp as those of Y'_1 and Y'_2 but still occur at the same points along the ray.

The loci generated by Y_1 and Y_2 for the two-body case are presented in Fig. 5.12. The same properties, as for the mono-body case, are exhibited by the interference pattern of Fig. 5.12, where the pseudo loci are the superposition of the families of discrete loci resulting for the constituent spheres. Therefore, it is concluded that each of the IBCs Y_1 or Y_2 is sufficient to uniquely discriminate the proper locus of smooth, closed scatterers with known surface impedance η, (be it homogeneous or inhomogeneous, dispersive or nondispersive), given the total em fields everywhere in the vicinity of the scatterers for only one frequency. The simultaneous application of both conditions makes the proposed inversion technique more reliable.

5.5.2b $|\eta|$ and $S_0(\underline{r})$ TO BE DETERMINED

For this particular case, the real impedance is calculated using (3.4.7) and (3.4.9) where the former equation results in one root for η (say η_0) and the later results in two independent roots for η, (say η_1 and η_2). The values of η_0, η_1 and η_2 are then calculated along

—×—×— Points computed for Y1= A · B
—⊙—⊙— Points computed for Y2= $A^2 - B^2$

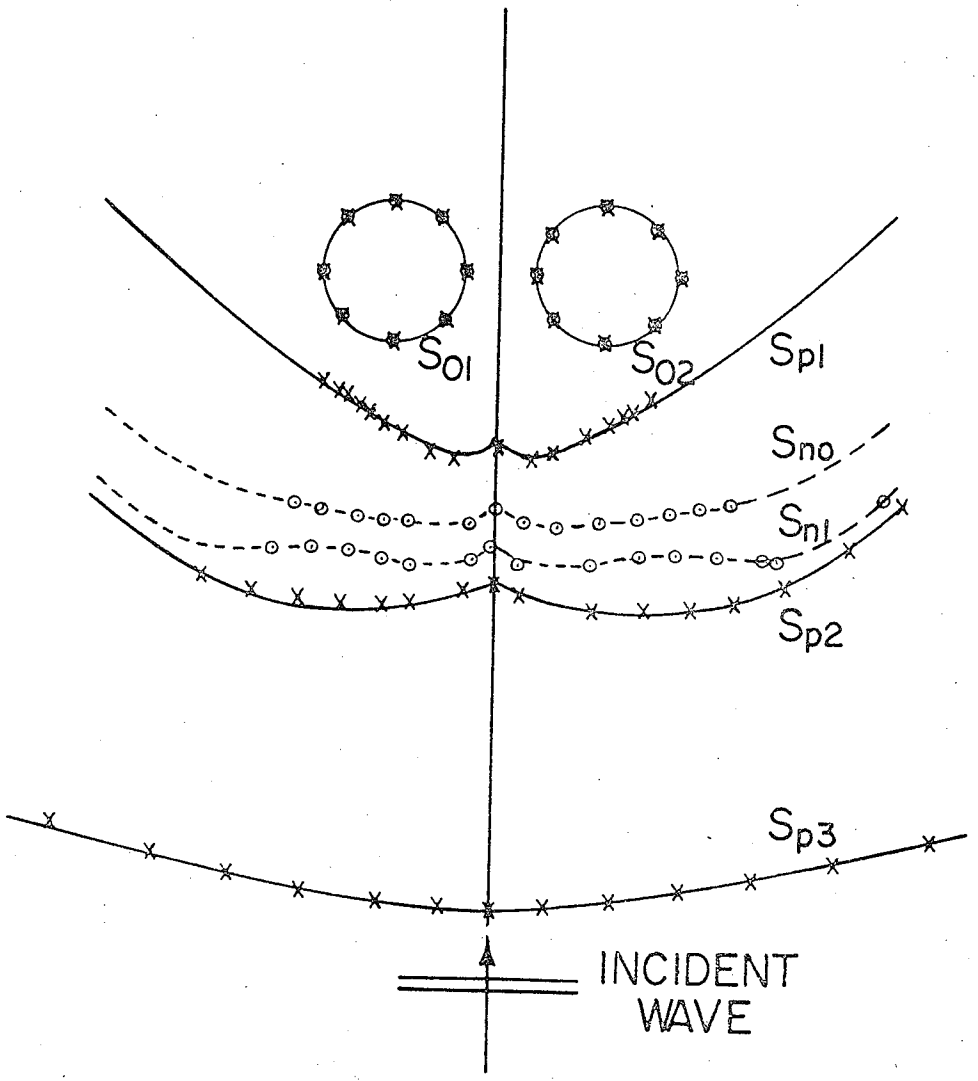

Fig. 5.12. Loci of Successive Minima of Y1 and Y2 for Two Conducting Spheres of Elec. Radii $ka_1 = ka_2 = 0.4$ and Separation between Centers $kd = 1.2$, $\alpha = 90°$

radiant vectors (excluding the backscattering direction). Now, the value of η_0 is substituted into the normality condition Y_2, whereas η_1 and η_2 into the orthogonality condition Y_1 and the $\text{Min}\{A^2-B^2, \eta_0\}$, $\text{Min}\{\underline{A}\cdot\underline{B}, \eta_1\}$ and $\text{Min}\{\underline{A}\cdot\underline{B}, \eta_2\}$ are then calculated for the above chosen computational points along the same radiant vectors. In Fig. 5.13a the curves resulting for $\eta_0(R)$, $\eta_1(R)$, $\text{Min}\{A^2-B^2, \eta_0(R)\}$ and $\text{Min}\{A\cdot B, \eta_1(R)\}$ are plotted versus the radiant vector R for $\theta = 45°$, $\phi = 60°$, where the curves corresponding to the values $\eta_2 = (R)$ have been omitted for the sake of clarity since there exists no value of $\eta_2(R)$ which is identical to $\eta_0(R)$. From inspection of Fig. 5.13a, it is seen that $\eta_0(R)$ and $\eta_1(R)$ can be identical at more than one point along a ray. However, with the aid of $\text{Min}\{A^2-B^2, \eta_0(R)\}$ and $\text{Min}\{\underline{A}\cdot\underline{B}, \eta_1(R)\}$ the correct point on the proper surface along that ray can easily be discriminated since only at that point do the two minima coincide. Another unique recovery criterion is to employ (3.4.16) which specifies the phase ψ of η in the backscattering direction. Since it is known that $\eta = |\eta|$, the point for which $\psi = 0$ can be employed along with the orthogonality and normality conditions to discriminate the proper surface locus and the correct value of η. In order to make the inversion technique more reliable for cases in which η is known to be homogeneous, the above procedure may be repeated for another frequency as is shown in Fig. 5.13b. Comparing Figs. 5.13 and 5.13b, it is evident that except for those minima defining the proper point on the surface, all other minima and all other identical values of η_0 and η_1 are shifted along the ray.

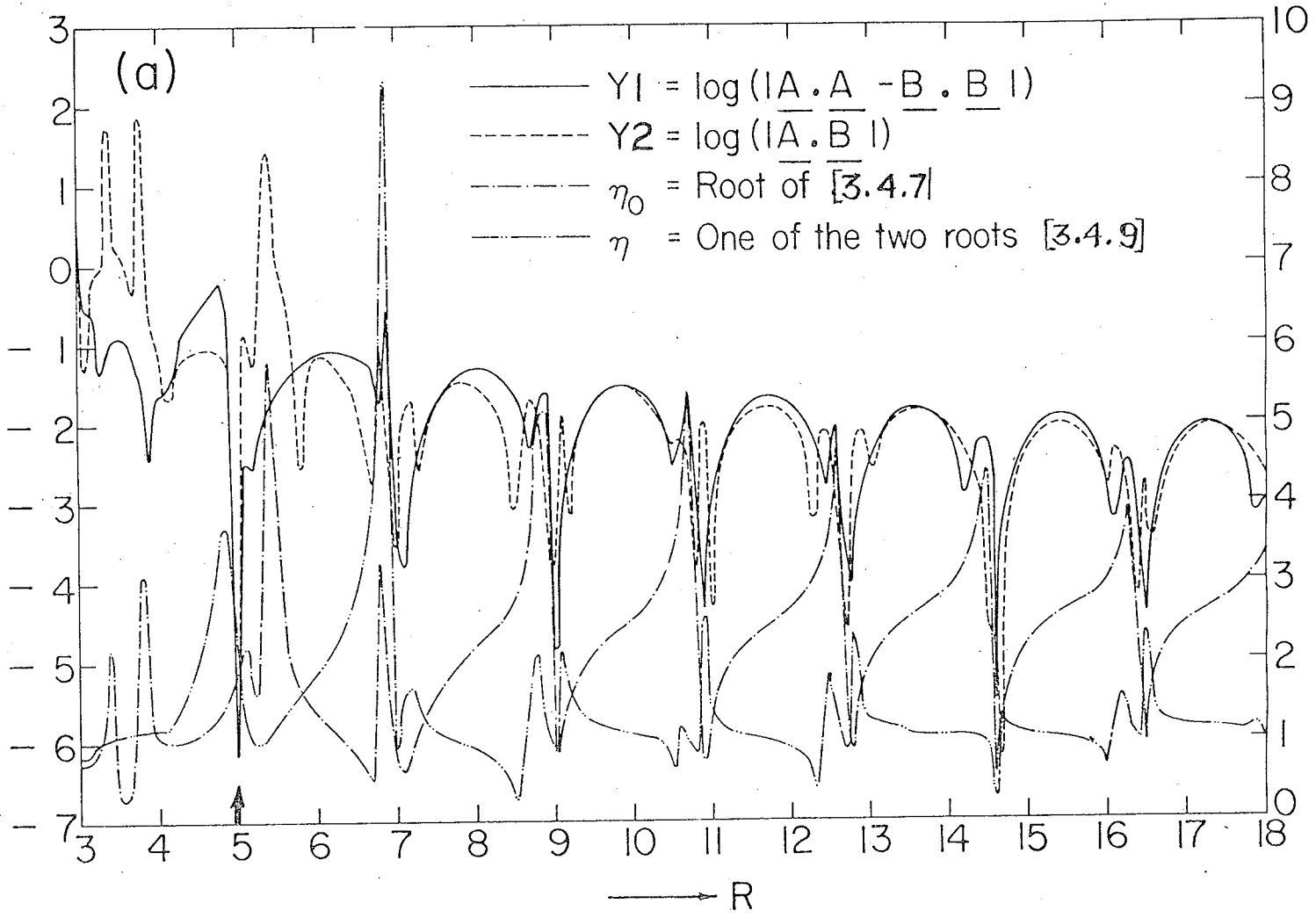

Fig. 5.13a. Plot of Y1, Y2, η_0 and η_1 vs Geometrical Distance R along a Ray (θ=45°, ϕ= 60°) for a Spherical Target of a=5.0, ka=5.0 and η=2.0

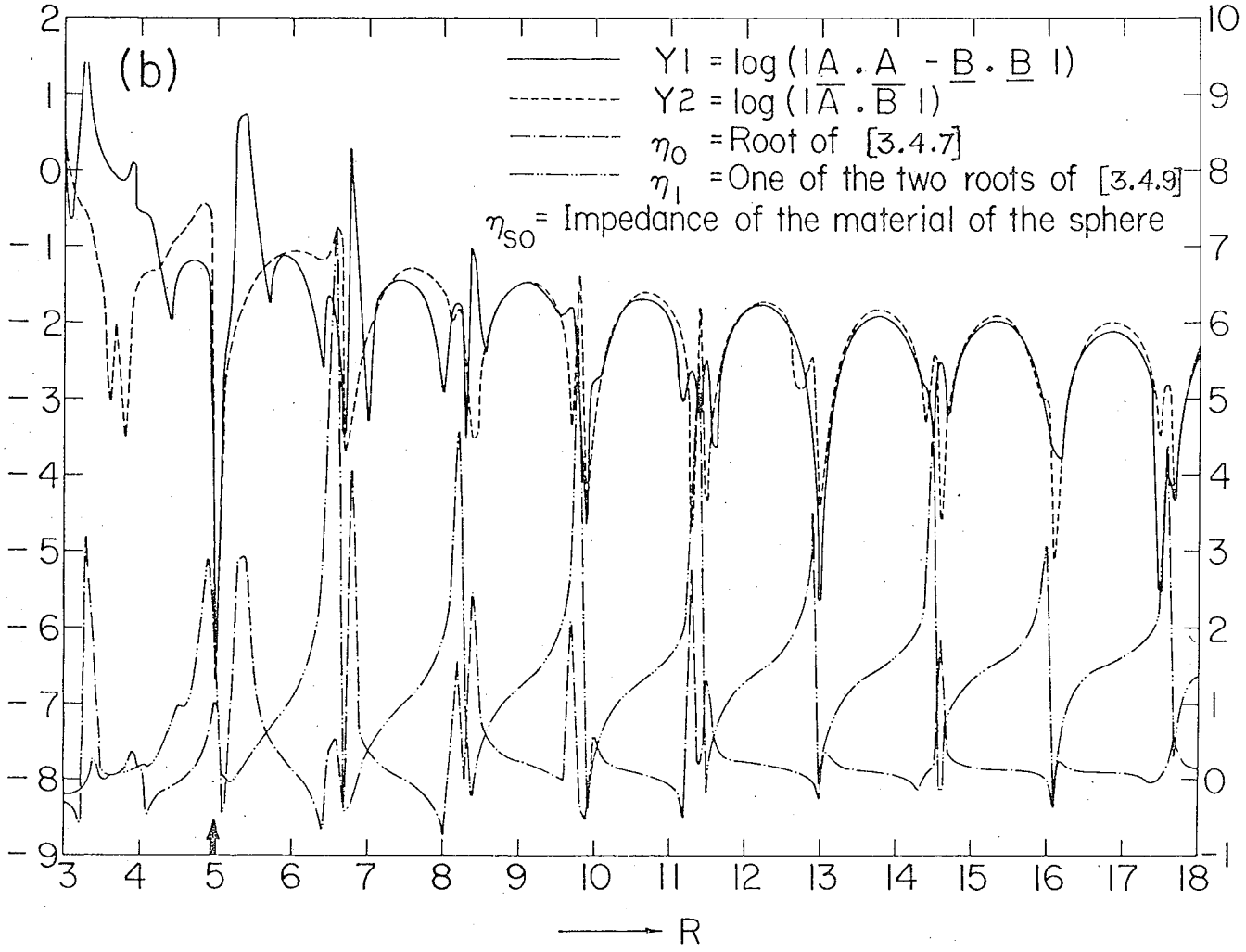

Fig. 5.13 b Plot of Y1, Y2, η_0 and η_1 vs Geometrical Distance R along a Ray (θ=45°, ϕ=60°) for a Spherical Target of a=5.0, ka=8.0 and η=2.0

After repeated calculations for various aspect angles belonging to the same cross-section ϕ = const., an interference-like pattern for the family of pseudo loci similar to that illustrated in Fig. 5.10 is obtained. It should be observed that the impedance curves $\eta_0(R)$ and $\eta_1(R)$ of Figs. 5.13a and 5.13b display the character of a decaying standing wave similar to that known from transmission line theory [65], i.e. $\eta = \eta(R)$ represents a tangent-like interference curve.

The value of the surface impedance η_{s_0} in the case of a smooth, closed and homogeneous scatterer can be determined from computation at a single frequency and along a single ray. This computed value of $\eta = \eta_{s_0}$ = const. may then be used as outlined in Subsection 5.5.2a to determine the proper surface $S_0(\underline{r})$. The proposed single-frequency discrimination procedure will have to be repeated over a grid of rays spanning the total sphere if $|\eta|$ is inhomogeneous.

5.5.2.c $\eta = |\eta| \exp(j\psi)$ and $S_0(\underline{r})$ TO BE DETERMINED

In this most general case the properties of Theorems 1, 2 and 3 of Section 2.4 need to be employed. Since the degeneracy condition is involved, only that case can be uniquely resolved for which the *a priori* unknown surface impedance is homogeneous i.e. $\eta \neq \eta(\theta,\phi)$.

The recovery procedure adopted is comprehensively analysed for a spherical model scatterer of radius a. In Table 5.1 computational

results are presented for a complex impedance $\eta = 2\exp(j\pi/12)$ for $a = 5$, $ka = 5$ and $ka = 8$ and in Table 5.2 for $\eta = 0.25\exp(j0)$ with $a = 2$, $ka = 2$ and $ka = 3.2$ respectively. Thus two sets of values with identical column arrangement, as defined in the heading, are presented in each table. Although computations were carried out for many different rays and for computational intervals $1.0 \leq R(\Delta R = 0.1) \leq 20.0$, it was found sufficient to present values within the range $4.5 \leq R (\Delta R = 0.1) \leq 5.5$ for one ray only. From the inspection of Table 5.1 it can be seen that the correct values of ψ and $|\eta|$ occur for computation with $ka = 5$ and $ka = 8$ at $R = a = 5$ which defines the proper surface locus, whereas the identical values occuring for $ka = 5$ at $R = 4.5$ for ψ_0, ψ_3 and ψ_4 are no longer identical for $ka = 8$ at $R = 4.5$. It is to be noted that a 'dash' under the values of ψ_1 to ψ_4 indicates that the respective root of term ψ_ν was complex and therefore, is of no physical significance. The values given in the last two columns result from the application of the normality and orthogonality conditions, respectively, into which the proper value of η, resulting for $R = a = 5$, had been substituted, and coincidence of the two very pronounced minima at $R = 5$ is evident from inspection. Similar results are obtained for a model scatterer of radius $a = 2$ and impedance $\eta = 0.25$ as is shown in Table 5.2. It should be noted that when a computational increment of $\Delta R = 0.001$ was used, the correct minima are still found to coincide with the exact value of $R = a = 2$ of the employed model scatterer, provided a sufficient number of expansion coefficients, accurate up to the 7th digit are used as is illustrated in Table 5.3 which is self-explanatory. Finally, Table

TABLE 5.1

RECOVERY OF PHASE ψ_{so}, MODULUS $|\eta_{so}|$, AND SURFACE LOCUS $S_o(R=a)$ FOR A SCATTER HAVING AN *A PRIORI* UNKNOWN HOMOGENEOUS, COMPLEX SURFACE IMPEDANCE $\eta_{so}=|\eta_{so}|\exp(j\psi_{so})$

Selected Model Scatterer: Sphere of radius $a = 5.0$ and impedance $\eta_{so} = 2.0 \exp(j15°)$. Values, computed along the ray $(\theta = 1°, \phi = 30°)$ within $4.5 \leq R(\Delta R = 0.1) \leq 5.5$ are: ψ_o: root of (3.4.16); ψ_1, ψ_2, ψ_3 and ψ_4: roots of(3.4.14); $|\eta|$: root of(3.4.12) using $\psi_{so} = \psi_o$; $Y_1 = \log\{|\underline{A} \cdot \underline{A} - \underline{B} \cdot \underline{B}|, \eta = \eta_{so}\}$; $Y_2 = \log\{|\underline{A} \cdot \underline{B}|, \eta = \eta_{so}\}$

	R	ψ_o	$\lvert\eta\rvert$	$\pm\psi_1$	$\pm\psi_2$	$\pm\psi_3$	$\pm\psi_4$	Y_1	Y_2
ka = 5.0	4.5	-34.597	1.972	10.824	18.306	34.608	34.575	0.335	- 3.305
	4.6	-24.836	2.161	4.959	14.035	24.862	24.801	0.130	- 3.591
a = 5.0	4.7	-14.096	2.268	0.568	8.857	14.124	14.066	-0.144	- 3.990
	4.8	- 3.275	2.267	4.496	5.808	3.259	3.286	-0.531	- 4.692
	4.9	6.643	2.165	10.442	63.079	---	---	-1.180	- 5.121
	5.0	14.994	2.003	13.308	24.556	14.983	14.933	-9.235	-10.536
	5.1	21.559	1.809	14.415	24.048	---	---	-1.311	- 4.597
	5.2	26.420	1.619	15.701	28.979	---	---	-0.793	- 4.269
	5.3	29.775	1.443	16.311	35.090	29.694	29.850	-0.541	- 4.123
	5.4	31.825	1.286	16.353	42.070	31.865	31.782	-0.409	- 4.072
	5.5	32.727	1.149	15.903	49.568	---	---	-0.353	- 3.987
ka = 8.0	4.5	42.868	0.455	---	---	---	47.132	0.624	- 2.971
	4.6	-40.292	1.574	---	---	---	---	0.488	- 3.152
a = 5.0	4.7	-29.696	1.905	---	---	---	29.692	0.263	- 3.433
	4.8	-15.354	2.154	---	---	---	---	-0.096	- 3.880
	4.9	0.714	2.189	---	---	---	0.713	-0.735	- 4.786
	5.0	14.994	2.001	---	---	---	14.988	-8.968	- 9.800
	5.1	25.317	1.710	---	---	---	---	-0.905	- 4.435
	5.2	31.587	1.424	---	---	---	31.585	-0.441	- 4.109
	5.3	34.456	1.179	---	---	---	34.416	-0.274	- 4.045
	5.4	34.445	0.981	---	---	---	34.448	-0.270	- 4.182
	5.5	31.772	0.825	---	---	---	---	-0.417	- 4.769

TABLE 5.2

RECOVERY OF PHASE ψ_{so}, MODULUS $|\eta_{so}|$, AND SURFACE LOCUS $S_o(R=a)$ FOR A SCATTERER HAVING AN *A PRIORI*, UNKNOWN, HOMOGENEOUS COMPLEX SURFACE IMPEDANCE $\eta_{so} = \eta_{so} \exp(j\psi_{so})$

Selected Model Scatterer: Sphere of radius $a = 2.0$ and impedance $\eta_{so} = 0.25$.
Values, computed along the ray ($\theta = 0.5°$, $\phi = 30°$) within $1.5 \leq R(\Delta R = 0.1) \leq 2.5$, are:
ψ_o: root of (3.4.16); ψ_1, ψ_2, ψ_3 and ψ_4: roots of (3.4.14); $|\eta|$: roots of (3.4.12) using
$\psi_{so} = \psi_o$; $Y_1 = \log\{|\underline{A} \cdot \underline{A} - \underline{B} \cdot \underline{B}|, \eta = \eta_{so}\}$ $Y_2 = \log\{|\underline{A} \cdot \underline{B}|, \eta = \eta_{so}\}$

	R	ψ_o	$\lvert\eta\rvert$	$\pm\psi_1$	$\pm\psi_2$	$\pm\psi_3$	$\pm\psi_4$	Y_1	Y_2
ka = 2.0	1.5	7.883	---	6.078	22.271	82.283	81.959	- 0.700	- 4.918
	1.6	- 5.551	0.496	11.305	23.012	---	---	- 0.954	- 5.360
a = 2.0	1.7	-22.195	0.326	15.030	21.941	---	---	- 1.268	- 5.950
	1.8	-43.579	0.241	46.304	46.538	17.358	16.988	- 1.689	- 7.400
	1.9	21.934	0.227	14.134	17.039	22.097	21.766	- 2.362	- 6.644
	2.0	0.011	0.250	13.287	49.910	0.005	0.000	-10.927	-11.967
	2.1	-15.890	0.300	2.669	21.241	16.017	15.865	- 2.516	- 6.432
	2.2	-26.448	0.365	20.263	67.646	---	---	- 1.997	- 6.139
	2.3	-33.320	0.441	19.131	68.386	---	---	- 1.734	- 6.006
	2.4	-37.719	0.525	17.968	59.295	---	---	- 1.579	- 5.934
	2.5	-40.373	0.618	16.317	55.656	---	---	- 1.488	- 5.923
ka = 3.2	1.5	10.666	---	---	---	16.805	16.516	- 0.524	- 4.535
	1.6	- 0.047	---	---	---	19.107	8.775	- 0.673	- 4.819
a = 2.0	1.7	-11.222	1.006	---	---	21.296	1.513	- 0.919	- 5.190
	1.8	-27.028	0.492	3.543	21.206	---	---	- 1.297	- 5.698
	1.9	36.142	0.257	---	---	12.523	6.239	- 1.949	- 6.669
	2.0	0.004	0.250	3.663	48.089	0.003	0.000	-11.602	-12.944
	2.1	-26.018	0.330	19.773	80.849	---	---	- 2.116	- 6.314
	2.2	-39.014	0.458	19.920	31.007	39.059	38.957	- 1.632	- 5.981
	2.3	-44.850	0.614	16.823	28.839	---	---	- 1.424	- 5.878
	2.4	43.384	1.800	12.880	27.050	46.637	46.595	- 1.348	- 5.909
	2.5	44.556	1.985	9.025	25.258	---	---	- 1.366	- 6.050

TABLE 5.3

QUANTITIES OF TABLE 5.2 CALCULATED WITH A FINER

INTERVAL $1.99 \leq R\ (\Delta R = .001) \leq 2.005$

	R	ψ_o	$\lvert\eta\rvert$	$\pm\psi_1$	$\pm\psi_2$	$\pm\psi_3$	$\pm\psi_4$	Y_1	Y_2
ka = 2.0	1.995	0.971	0.248	13.680	49.161	0.965	0.962	- 5.024	- 7.785
	1.996	0.778	0.249	13.628	49.993	0.772	0.768	- 5.216	- 7.886
a = 2	1.997	0.585	0.249	13.502	49.218	0.575	0.579	- 5.462	- 8.010
	1.998	0.393	0.249	13.473	49.030	0.383	0.387	- 5.806	- 8.189
	1.999	0.202	0.250	13.444	45.802	0.191	0.196	- 6.383	- 8.485
	2.000	0.011	0.250	13.339	45.785	0.005	0.000	-10.536	-11.714
	2.001	-0.179	0.251	13.283	43.515	0.185	0.190	- 6.499	- 8.483
	2.002	-0.369	0.251	13.214	42.520	0.375	0.380	- 5.866	- 8.181
	2.003	-0.557	0.251	13.158	42.206	0.563	0.569	- 5.504	- 8.007
	2.004	-0.746	0.252	13.045	40.391	0.758	0.752	- 5.250	- 7.878
	2.005	-0.933	0.252	13.015	37.260	0.946	0.939	- 5.054	- 7.773
ka = 3.2	1.995	1.708	0.248	4.127	15.414	---	---	- 4.618	- 7.915
	1.996	1.364	0.248	4.037	18.018	---	---	- 4.812	- 8.008
a = 2	1.997	1.022	0.249	3.947	23.821	---	---	- 5.062	- 8.122
	1.998	0.682	0.249	3.858	26.399	0.681	0.679	- 5.413	- 8.300
	1.999	0.342	0.250	3.776	40.490	0.342	0.338	- 6.011	- 8.588
	2.000	0.004	0.250	3.663	48.089	0.003	0.000	-11.602	-12.944
	2.001	-0.333	0.251	3.571	65.517	0.337	0.334	- 6.032	- 8.580
	2.002	-0.669	0.251	3.472	76.669	0.673	0.669	- 5.426	- 8.265
	2.003	-1.003	0.251	3.352	58.147	1.008	1.004	- 5.073	- 8.080
	2.004	-1.336	0.252	3.252	55.355	1.341	1.337	- 4.823	- 7.958
	2.005	-1.667	0.252	3.151	45.431	1.672	1.669	- 4.630	- 7.857

TABLE 5.4

Retrieval of ψ and $|\eta|$ by Double-Frequency Technique for a Single Sphere Using Interior Analytic Continuation

Target: Sphere of elec. radius ka = 0.5 and surface impedance η = 0.25 exp jo, Fields Computed w.r. 0' ($\theta_o = 45^o$, $\phi = 130^o$, kd = 1.0)

A. Computed Values At Frequency $f_1 = f$

R	ψ_1	ψ_2	ψ_3	ψ_4	$\|\eta\|$	Y_1	Y_2
.35	-	-	-	-	.2980	.02197886	.001517956
.40	-	-	-	-	.2799	.0257287	.00164368
.45	-	-	-	-	.2591	.02443074	$.9319349X10^{-3}$
.50	-	*.01*	-	-	*.2476*	$.8177150X10^{-3}$	$.5070390X10^{-3}$
.55	15.837	72.776	-	-	.2597	.1112544	.00496126
.60	83.707	-	-	24.359	.3022	.5756167	.07459009
.65	32.007	-	-	79.055	.3701	2.493501	.5519352

B. Computed Values At Frequency $f_2 = .8\ f$

R	ψ_1	ψ_2	ψ_3	ψ_4	$\|\eta\|$	Y_1	Y_2
.35	-	-	-	-	.1348	.02881918	.005033627
.40	-	-	-	-	.1101	.03240844	.005457051
.45	-	-	-	-	.1897	.02915064	.005376853
.50	-	*.002*	-	-	*.2453*	$.7013585X10^{-3}$	$.9597663X10^{-3}$
.55	78.897	-	-	23.10	.3061	.1138315	.02918787
.60	31.468	78.500	-	-	.3821	.5221265	.1967003
.65	73.221	-	-	37.658	.4739	1.940373	1.075720

5.4 presents the four roots ψ_ν of (3.4.14) and root $|\eta|$ of (3.4.12) for a target of elec. radius ka = 0.5 and surface impedance η = 0.25 exp j0. The em fields for this case were analytically continued with respect to a translated origin (θ_0 = 45°, ϕ = 130°, kd = 1.0). The averaged surface impedance η can be seen to be $|\overline{\eta}|$ = .2465 $\overline{\psi}$ = .006.

5.5.2d $\hat{n}(r)$ KNOWN, $S_0(\underline{r})$ and $\eta(\underline{r})$ TO BE DETERMINED

In cases, where the shape of a scatterer is known *a priori*, but the electrical dimensions and the complex surface impedance have to be determined, the simultaneous computation of (3.4.12), (3.4.14), (3.4.19) and (3.4.20) can resolve all of these parameters accurately and uniquely. The method is verified in Table 5.5 for a spherical target of ka = 0.5, η = 0.25exp(j 0) for fields expanded about the center 0 of Fig. 5.3. The entries Y_1' and Y_2' have been computed using the impedance value of η resulting at each point of computation, and the entries Y_1 and Y_2 correspond to computation for which $\eta(X=0.5)$ = .25 exp(j0) was used for all points along the ray. The presented results clearly indicate that $\eta(\underline{r})$ and $S_0(\underline{r})$ can be recovered very accurately.

If an expression for $\hat{n}(\underline{r})$ can be obtained independently of the conditions (3.4.1) and (3.4.2), methods of Subsections 5.5.2c and 5.5.2d could be combined to resolve the problem uniquely, given the total em fields everywhere in the vicinity of a scatterer for only one frequency.

TABLE 5.5

Recovery of Phase ψ_{s_o}, Modulus $|\eta_{s_o}|$ and Surface Locus S_o (R=a) for a Scatterer Having an *A Priori* Known Shape

Selected Model Scatterer: Sphere of radius ka = 0.5 and impedance η_{s_o} = 0.25 exp jo

Values computed along the ray ($\theta = 45^o$, $\phi = 130^o$) are:

ψ_{s_o} root of (3.4.20), η_{s_o} root of (3.4.19)

X	Y1'	Y2'	ψ_{s_o}	η_{s_o}	Y1	Y2
.35	1.36112	-15.6535	39.752	3.096	.299005	.264397
.40	.475426	-15.6272	-43.198	0.962	-.254754	-.565107
.45	.405271	-16.8577	-21.603	0.477	-.922403	-1.42820
.50	*-5.91584*	*-16.8577*	*.0002*	*0.250*	*-5.57363*	*-6.64025*
.55	-1.22534	--	7.1513	.1902	-1.53615	-2.27987
.60	1.20405	--	9.3261	.2451	-1.48931	-2.26450
.65	1.35926	2.91474	9.8747	.3239	-1.54030	-2.29835

chapter six

TRUNCATION ERROR ANALYSIS

6.1 INTRODUCTION

In verifying the inverse boundary conditions of *chapter three*, direct scattering solutions for conducting cylindrical and spherical shapes, in terms of cylindrical and spherical vector wave functions respectively, were employed. In a practical situation, the near field is to be reconstructed from a known incident field and the measured far field distribution. It is assumed that the associated sets of expansion coefficients explicitly contain all the necessary and sufficient information about the unique near field expansion. These coefficients, representing the unknowns, must first be recovered from the finite set of measured scattered field data as is discussed in Boerner and Vandenberghe [25] and in more detail in Boerner and Aboul-Atta [21] where matrix inversion procedures are proposed for recovering these coefficients. Furthermore, employing a novel optimization procedure for the encountered generalized Vandermonde determinants, it is shown in Vandenberghe and Boerner [25] that the retrieval of the unknown expansion coefficients, theoretically, depends only on the employed measurement technique.

However, since only matrices of finite and relatively low order (2N) can be inverted with the required degree of accuracy, a lower bound on the order N of truncation of a_{mn} and b_{mn} must be taken into consideration.

In addition, since both amplitude and phase of the scattered transverse field components must be measured, in practice, a lower bound M on the degree of accuracy of the recovered expansion coefficients is also inflicted.

In this chapter, the bounds at which the series representation of the em fields should be truncated are discussed. The criteria for establishing the lower and the upper truncation bounds for two-dimensional bodies are presented in Section 6.2. An outline of the extension of the approach used for two-dimensional bodies to three-dimensional cases is given in Section 6.3. Subsection 6.4.1 describes a novel truncation approach based on the concept of inverse boundary conditions. The proposed procedure has been verified numerically in Subsection 6.4.2. Finally, a brief numerical study of the rate of convergence of the analytically continued fields is presented in Section 6.5.

6.2 LOWER AND UPPER TRUNCATION BOUNDS FOR TWO-DIMENSIONAL CASES

For a two-dimensional scattering geometry, the scattered field valid for $r \geq r_a$ in Fig. 4.3, may be expressed as

$$u(r,\phi) = \sum_{n=-\infty}^{\infty} a_n j^{-n} H_n^{(1)}(kr)\exp(jn\phi) \qquad (6.2.1)$$

where $H_n^{(1)}$ is the Hankel function of first kind. The associated far field will behave as

$$u(r,\phi) \simeq \exp(-jkr)(2j/\pi kr)^{1/2} g(\phi) \qquad (6.2.2)$$

where $g(\phi)$ is called the pattern function defined by

$$g(\phi) = \sum_{n=-\infty}^{\infty} a_n \exp(jn\phi) \qquad (6.2.3)$$

The coefficients of this pattern function are subsequently used in the reconstruction of the near field. In practice there exists a lower bound N_ℓ and an upper bound N_u for the number of these coefficients. The lower bound is dependent on the fact that the space acts as a filter for the higher harmonics and only those cylindrical modes which are not cut off are of importance [48]. This means that the summation, in (6.2.1) should at least extend to $|n| \simeq kr_a$ with r_a denoting the largest dimension of the scatterer. This approximate estimate for $|n|$ ensures the inclusion of the dominant terms of the Fourier spectrum [78 ,81]. The upper bound N_u depends on r_a and the error level $\overline{\varepsilon^2}$ due to measurement and quadrature errors [33 ,120].

Twomey [120] discusses the inherent limitations and difficulties which attend the inference of the function $f(x)$ from $g(y)$ when the kernel $k(x,y)$ is a smooth function of x. He also establishes criteria for determining the upper bound on the number of terms in a series representation of a function $f(x)$.

Any inverse problem may be represented in the form

$$g(y) = \int_a^b k(x,y) f(x) dx \qquad (6.2.4)$$

where $g(y)$ is the measured pattern, $k(x,y)$ represents the data

kernel and $f(x)$ is the function to be recovered. In operator notation, (6.2.4) may be written as

$$g = Tf \tag{6.2.5}$$

where g and f represent $g(y)$ and $f(x)$ respectively. In matrix notation (6.2.5) becomes

$$Ax = y + \varepsilon \tag{6.2.6}$$

where A, x and y are the discrete form of the operators T, f and g, respectively and ε represents the total equivalent error vector. Twomey [120] proves that the N equations contained in the matrix equation (6.2.6) are fully independent in the presence of errors only if the inequality

$$c\lambda_n >> \sum_i \varepsilon_i^2 \tag{6.2.7}$$

is satisfied by all the eigenvalues λ_n of A^*A, where c is a fixed known positive number and A^* denotes the adjoint of A.

The error vector ε includes both the quadrature errors and the observational errors. The observational errors are often more serious than the quadrature errors, which for reasonably large N and smooth integrands can be considerably smaller than 1% - an accuracy not readily achieved in many physical measurements [120]. In addition to measurement errors, in many cases an approximation is involved in reducing a problem to a linear one, e.g. approximations involved in the derivation of Leontovich conditions.

It may be added here that in (6.2.6) the larger N is, the higher the frequencies being introduced in the solution and the greater the instability of the solution. Therefore, increasing the number of data points worsens, rather than improves, the discrepancies between the solution and the expectation.

Cabayan et al [33] determine the eigen-values λ_n of the matrix equation associated with the two-dimensional inverse scattering problem. Starting with Helmholtz's equation, they obtain the following expression for the eigen-values λ_n, as is outlined in *Appendix* A4.

$$\lambda n = \frac{|H_n^{(1)}(kr_1)|^2}{|H_n^{(1)}(kr_a)|^2} \qquad (6.2.8)$$

The stability criterion (6.2.7) sets a strict limit on choosing the largest dimension of the projection space. The smallest eigenvalue defined by (6.2.8) must be greater than the error level

$$\overline{\varepsilon}^2 = \sum \varepsilon_i^2 \qquad (6.2.9)$$

For the specialized case in which $r_1 \to \infty$, the eigenvalues may be written as

$$\lambda n = \frac{1}{|H_n^{(1)}(kr_a)|^2} \qquad (6.2.10)$$

The three regions of numerical behavior of the reconstructed em field are shown in Fig. 6.1 which has been taken from Cabayan et al [33]. They explain these regions in connection with the stability criteria

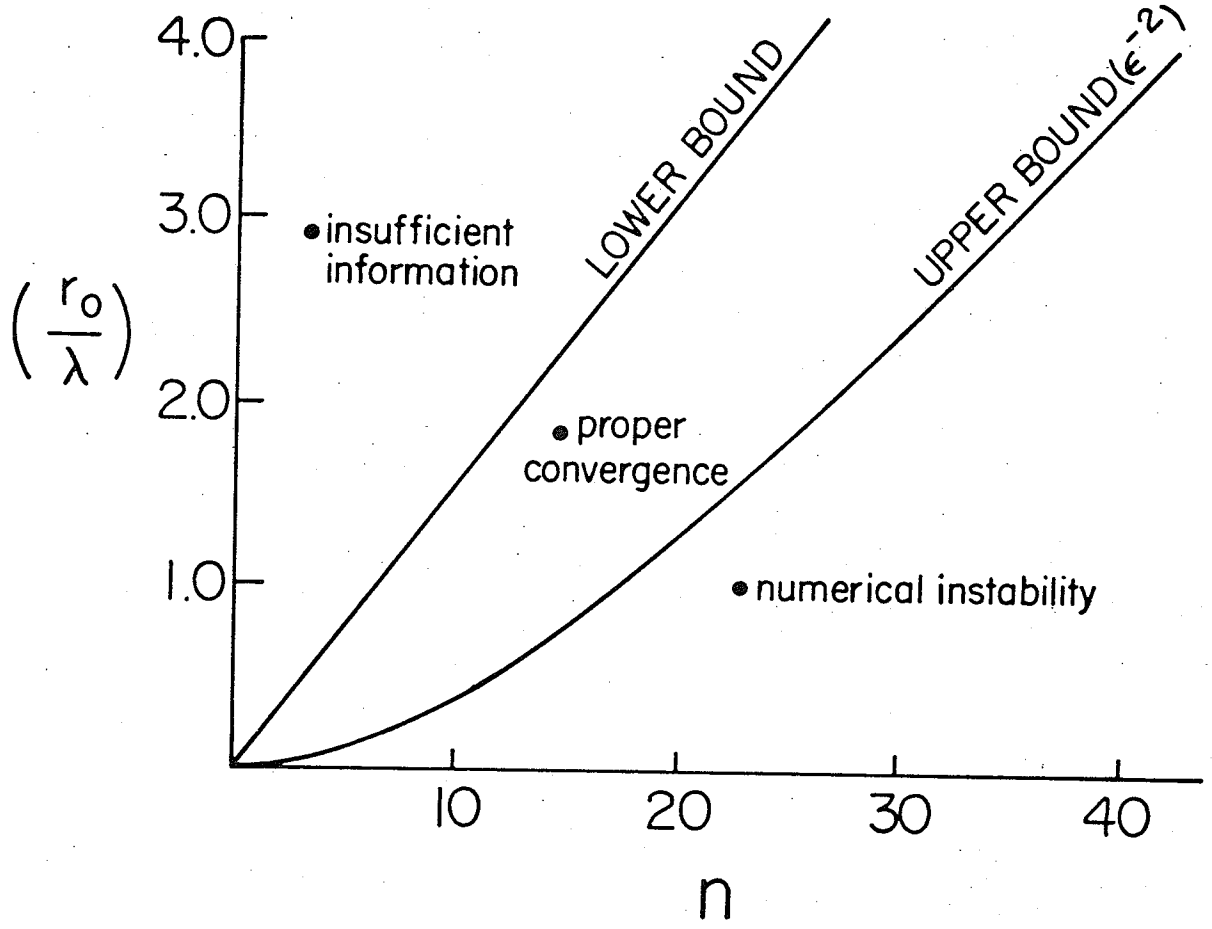

Fig. 6.1. Regions of Numerical Behavior of the Reconstructed em Field.

developed above. Assuming that the expansion coefficients are accurate up to 5 to 6 digits, we can estimate the numerical error as one part in 10^5, i.e. $\varepsilon = 10^{-5}$. Therefore, λ_n, the cutoff eigen-value, is related to $\overline{\varepsilon}^2 = 10^{-10}$. Similar diagrams for less accurate data will have the curve representing the upper bound nearer to the one representing the lower bound.

In order to apply the above criteria on the truncation level N to an off-axis cylinder, the parameter of importance for exterior continuation of Fig. 4.3 will be r_a', the minimum radius enclosing the cylinder. The trend of the number of significant coefficient $n_{r_a'}$ for the translated system versus $r_{a'}/\lambda$ gives a convergence region similar to and contained within, the convergence region shown in Fig. 6.1 [33, 87]. As regards the order of truncation $|n| = N$ in (4.3.4), Wilton [147] states that for $N > kr_a$ the coefficients a_n decay exponentially faster than the exponential growth of the Hankel functions for $r > r_a$ so that the scattered field representation converges. The validity of this statement has most recently been confirmed by Millar [78]. The numerical results presented in Section 4.4 are also in agreement, where M in (4.3.3) was chosen to be slightly larger than the sum of kr_o and kr_a [148].

6.3 LOWER AND UPPER TRUNCATION BOUNDS FOR THREE-DIMENSIONAL PROBLEMS

The incident and the scattered fields for three-dimensional problems are

expanded in terms of spherical vector wave functions. There are many tests such as power conservation [154], statistical and numerical checks [153] which may be used for checking the accuracy of the obtained results. Ludwig [70] describes a sensitive technique in which the basic idea is to obtain two different spherical-wave expansions of the same electromagnetic field. The two expansions may then be evaluated on a common surface and compared. Ludwig argues that an agreement between the two results strongly indicates that both expansions are valid because it is extremely unlikely that numerical errors would affect both expansions in the same way. The two expansions may be obtained by selecting different coordinate origins for each expansion. To make the test highly sensitive, the common surface should be chosen as close as possible to the source. Obviously the method may also be used for two-dimensional problems.

The lower empirical bound for three-dimensional problems is also determined by the radius r_a of the minimum sphere enclosing the body and is $|n| = kr_a$. An empirical formula for the truncation point for an error of less than .01% in the radar cross-section for a sphere of electrical radius ka is [109]

$$N \simeq [1 + ka + 3(ka)^{1/3}] \qquad (6.3.1)$$

The upper bound form numerical stability point of view may be determined by evaluating the eigen-values of the matrix equation associated with the three-dimensional problem. An approach similar to the one

used by Cabayan et al [33] for the two-dimensional case may be used for the three-dimensional problem. The details for this case are much more complicated because the Green's function for this case involves dyadic operators. Therefore, only an outline of the method is presented below.

Application of Helmholtz's theorem [57] to the source-free region outside the minimum sphere enclosing the body gives

$$\underline{g}(\theta,\phi) = kr_o \int_0^{2\pi}\int_0^{\pi} \underline{f}(\theta,\phi) \cdot \frac{\partial \underline{\underline{G}}}{\partial(kr)} \sin\theta \, d\theta \, d\phi \qquad (6.3.2)$$

where $\underline{g}(\theta,\phi)$ represents the far field pattern and $\underline{f}(\theta,\phi)$ is the near field to be recovered. Here $\underline{\underline{G}}$ is the dyadic Green's function of the first kind and is given by [116],

$$\underline{\underline{G}}_{1s}(\underline{R}/\underline{R}') = \frac{ik}{4\pi} \sum_{n=1}^{\infty} \sum_{m=0}^{n} (2-\delta_0) \frac{2n+1}{n(n+1)} \frac{(n-m)!}{(n+m)!}$$

$$[a_{e_{0mn}} \underline{M}^{(1)}_{o_{mn}} \underline{M}'^{(1)}_{e_{0mn}} + b_{e_{0mn}} \underline{N}^{(1)}_{e_{0mn}} \underline{N}'^{(1)}_{o_{mn}}] \qquad (6.3.4)$$

where the coefficients $a_{e_{0mn}}$ and $b_{e_{0mn}}$ may be determined by applying the Dirichlet boundary condition to the entire function $\underline{\underline{G}}_1$ which may be written as

$$\underline{\underline{G}}_1(\underline{R}/\underline{R}') = \underline{\underline{G}}_0(\underline{R}/\underline{R}') + \underline{\underline{G}}_{1s}(\underline{R}/\underline{R}') \qquad (6.3.5)$$

Here $\underline{\underline{G}}_0(\underline{R}/\underline{R}')$, the free space dyadic Green's function, is given by

$$\underline{\underline{G}}_0(\underline{R}/\underline{R}') = \frac{ik}{4\pi} \sum_{n=1}^{\infty} \sum_{m=0}^{n} (2-\delta_0) \frac{2n+1}{n(n+1)} \frac{(n-m)!}{(n+m)!}$$

$$[\underline{M}_{e_{0mn}} \underline{M}'^{(1)}_{e_{0mn}} + \underline{N}_{e_{0mn}} \underline{N}'_{e_{0mn}}] \quad , \quad \underline{R} < \underline{R}' \qquad (6.3.6)$$

In (6.3.4) and (6.3.6) $\delta_0 = 1$ for $m = 0$ and $\delta_0 = 0$ for $m \neq 0$.

The expansion coefficients $a_{e_{0mn}}$ and $b_{e_{0mn}}$ in (6.3.4) are

$$a_{e_{0mn}} = -j_n(ka)/h_n^{(1)}(ka) \qquad (6.3.7)$$

$$b_{e_{0mn}} = -\frac{d}{d\rho}[\rho\, j_n(\rho)] \,/\, \frac{d}{d\rho}[\rho\, h_n^{(1)}(\rho)] \qquad (6.3.8)$$

The normal derivative of $\partial \underline{\underline{G}}_{1s}/\partial(kr)$ at $r = r_a$ is substituted into (6.3.2) to obtain $\underline{g}(\theta,\phi)$ in the form of a Fourier series. The expression for $\underline{g}(\theta,\phi)$ defines the operator $\underline{\underline{T}}$ in the following equation in operator notation

$$\underline{g} = \underline{\underline{T}} \cdot \underline{f} \qquad (6.3.9)$$

The eigen-values of the associated matrix equation may then be determined using an approach similar to that of Cabayan et al [33].

6.4.1 NOVEL TRUNCATION APPROACH BASED ON INVERSE BOUNDARY CONDITIONS

The inverse scattering approach employed in this work assumes that complete information about the scattering geometry is contained in the expansion coefficients of the measured far field. Therefore, the recovered parameters of the body depend on the accuracy of these expansion

coefficients (M digits) and the order of truncation N of the series representing the field. The estimates on these lower bounds N and M may then be defined from the application of the inverse boundary conditions by properly truncating the order as well as the number of the first significant digits of the expansion coefficients. As relates to the truncation of significant digits in the expansion coefficients, criteria on convergence and the measurement accuracy should be distinguished. Only convergence aspects are considered in the present study, i.e. truncation in the first significant figures of any expansion coefficient irrespective of the exponential power factor.

The lower bounds N and M are defined by the desired accuracy to which the parameters of the body must be recovered. To illustrate how estimates of the bounds on the order of truncation can be established, the target identification procedure for that model case is chosen in which the phase ψ of η is assumed to be known, but the modulus $|\eta|$ and the proper surface locus $S_0(\underline{r})$ need to be recovered as outlined in Subsections (3.4.2), (4.3.5c) and (5.5.2b). Disregarding second-order effects on truncation estimates (i.e. the dependance on local incidence, polarization, aspect angle, etc.), the first-order estimates on N and M may then be specified by analyzing the obtained degree of accuracy in determining $|\eta|$, according to (3.4.12), and the point on the proper surface locus, by computing the orthogonality and the normality conditions along any ray not coinciding with the backscattering direction. For each of the various different sets of ka and η chosen, the recovery procedure is repeated by increasing the order

N of series truncation, and also the order $M(=3,5,7$ and $14)$ of the truncation in significant figures of the expansion coefficients.

6.4.2 NUMERICAL VERIFICATION

The influence of the series truncation on the accuracy of the orthogonality condition is illustrated in Fig. 6.2 for the case $ka = 5$, $\eta = 2.0$ employing single precision format for the expansion coefficients and double precision format for the calculation of the field components. From inspection of Fig. 6.2 it is found that there exists a lower bound $N_\ell = 10$, for which the proper minimum can still be distinguished accurately, as well as an upper bound $N_u = 16$ after which the effect of additional series terms is negligible. It should be noticed that as the order N of truncation is increased, the proper minimum becomes more and more pronounced, whereas the curves for $x(=kR) \geq ka(=5)$ coalesce.

To analyse the specification of truncation bounds further, numerical values of $Y_1 = \log\{|\underline{A}\cdot\underline{B}|, \eta = \eta_{s_0}\}$, $Y_2 = \log\{|\underline{A}\cdot\underline{A}-\underline{B}\cdot\underline{B}|, \eta = \eta_{s_0}\}$, and $|\eta|$ are presented in Tables 6.1 and 6.2 for various different values of η and for $ka = 2$ and $ka = 5$, respectively. Single precision format was employed for the expansion coefficients. Careful inspection of these tables indicates that it is useful to introduce three different error bounds on the order of series truncation, i.e. N_5, $N_{0.5}$ and $N_{0.1}$ for which $|\eta|$ can be recovered with an error of less than 5%, 0.5% and 0.1%, respectively, so that the proper minimum in all of these cases can still be discriminated uniquely. The additional effect of the truncation of the first M significant figures of the expansion coefficients

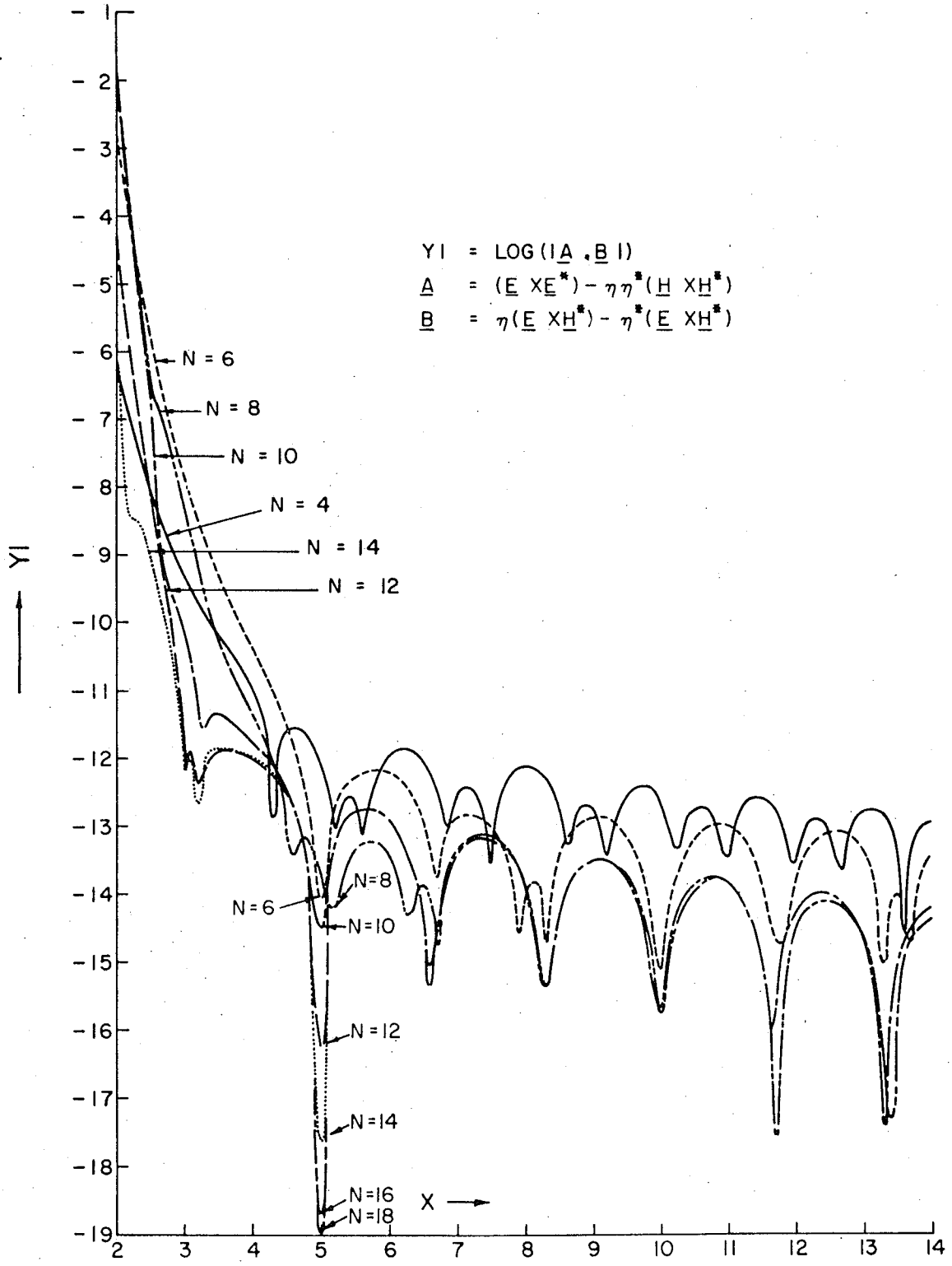

Fig. 6.2. Plot of YI vs Radiant Vector X = kR for the Spherical Test Case ka=5 for an increasing Number N of Expansion Terms θ=22.5°, ϕ=90°, η= 2.0

TABLE 6.1

'ORDER OF TRUNCATION' ANALYSIS FOR A SPHERICAL SCATTERER OF ELECTRICAL RADIUS ka = 2.0 AND THREE DIFFERENT VALUES OF IMPEDANCES η

Quantities, computed along the ray ($\theta = 30°$, $\phi = 60°$) within $1.9 \leq R(\Delta R = 0.1) \leq 2.1$, are: $|\eta|$: root of (3.4.12) where ψ is assumed to be known, $Y_1 = \log\{|\underline{A} \cdot \underline{A} - \underline{B} \cdot \underline{B}|$, $Y_2 = \log\{|\underline{A} \cdot \underline{B}|$, $\eta = \eta_{So}\}$

N: Order of series truncation

	R	Target I: $\lvert\eta_s\rvert = 0.99$, $\psi_s = 0°$			Target II: $\lvert\eta_s\rvert = 0.25$, $\psi_s = 45°$			Target III: $\lvert\eta_s\rvert = 4.0$, $\psi_s = 60°$		
		Y_1	Y_2	$\lvert\eta\rvert$	Y_1	Y_2	$\lvert\eta\rvert$	Y_1	Y_2	$\lvert\eta\rvert$
N = 4	1.9	0.6674	1.3242	0.3049	-1.8536	-3.5207	0.2365	1.1507	0.5744	2.4909
	2.0	-0.3906	0.9037	0.3915	-3.2718	-3.7760	0.2406	0.3587	0.0369	3.0342
	2.1	-0.6771	0.5326	0.4642	-2.1598	-2.8454	0.0981	0.9798	-0.3886	5.4156
N = 6	1.9	-2.2690	-2.3150	$0.9044^{\cdot 5}$	1.9936	-2.4810	0.3556	1.2233	0.2609	2.7320
	2.0	-3.2363	-3.3086	$0.9757^{\cdot 5}$	-4.1664	-4.6114	$0.2515^{\cdot 5}$	-1.5970	-1.4411	$4.0769^{\cdot 5}$
	2.1	-2.6985	-2.7140	1.0910	-2.1248	-2.8381	---	0.8832	-0.0818	---
N = 8	1.9	-2.3069	-2.3465	0.9081	-1.9260	-2.5035	0.3539	1.2286	0.2762	2.6913
	2.0	-5.1636	-5.2302	$0.9902^{\cdot 5}$	-5.3537	-5.8663	$0.2499^{\cdot 1}$	-2.7202	-2.8413	$4.0030^{\cdot 5}$
	2.1	-2.5939	-2.6174	1.1220	-2.1177	-2.8267	---	0.8847	-0.0842	---
N = 10	1.9	-2.3065	-2.3462	0.9081	-1.9263	-2.5031	0.3540	1.2286	0.2769	2.6904
	2.0	$-\infty$	$-\infty$	$0.9900^{\cdot 1}$	-7.5837	-7.8476	0.2500	-4.9067	-4.6056	$4.0000^{\cdot 1}$
	2.1	-2.5950	-2.6184	1.1216	-2.1180	-2.8271	---	0.8846	-0.0846	---
N = 14	1.9	-2.3065	-2.3462	0.9081	-1.9263	-2.5031	0.3540	1.2286	0.2769	2.6904
	2.0	-7.5258	-7.6507	0.9900	-7.8268	-8.3777	0.2500	-5.0664	-4.9792	4.0000
	2.1	-2.5950	-2.6184	1.1216	-2.1180	-2.8271	---	0.8846	-0.0846	---
N = 16	1.9	-2.3065	-2.3462	0.9081	-1.9263	-2.5031	0.3540	1.2286	0.2769	2.6904
	2.0	-7.5258	-7.6507	0.9900	-7.8368	-8.3777	0.2500	-5.5435	-4.9792	4.0000
	2.1	-2.5950	-2.6184	1.216	-2.1180	-2.8271	---	0.88461	-0.0846	---

Superscripts $^{\cdot 5}$, $^{\cdot 5}$, $^{\cdot 1}$ indicate that $|\eta|$ is recovered with an error of less than 5%, 0.5%, and 0.1%, respectively

TABLE 6.2

'ORDER OF TRUNCATION' ANALYSIS FOR A SPHERICAL SCATTERER OF ELECTRICAL RADIUS ka = 5.0 AND THREE DIFFERENT VALUES OF IMPEDANCES η

Quantities, computed along the ray $(\theta = 30°, \phi = 30°)$ within $4.9 \leq R(\Delta R = 0.1) \leq 5.1$, are: $|\eta|$ root of (3.4.12) where ψ is assumed to be known, $Y_1 = \log\{|\underline{A} \cdot \underline{A} - \underline{B} \cdot \underline{B}|, \eta = \eta_{So}\}$, $Y_2 = \log\{|\underline{A} \cdot \underline{B}|, \eta = \eta_{So}\}$

N: order of series truncation.

		Target I: $\lvert\eta_s\rvert = 0.01$, $\psi_s = 30°$			Target II: $\lvert\eta_s\rvert = 0.5$, $\psi_s = 60°$			Target III: $\lvert\eta_s\rvert = 2.0$, $\psi_s = 0$		
	R	Y_1	Y_2	$\lvert\eta\rvert$	Y_1	Y_2	$\lvert\eta\rvert$	Y_1	Y_2	$\lvert\eta\rvert$
N = 6	4.9	-1.6550	- 2.8455	0.8457	-1.1793	-1.3276	0.7267	-1.2212	-1.6728	2.5527
	5.0	-1.5950	- 3.0035	0.8033	-2.5774	-1.5946	0.6454	-1.5693	-2.2011	8.6745
	5.1	-1.2438	- 3.2793	0.6858	-1.2078	-1.9952	0.5701	-1.4848	-1.3736	---
N = 8	4.9	-1.5452	- 4.1566	0.2584	-1.2924	-2.0257	0.5694	-1.0757	-3.1429	1.9482
	5.0	-3.0603	- 4.1701	---	-2.8102	-2.5618	$0.4740^{.5}$	-2.1483	-3.2311	$2.0561^{.5}$
	5.1	-2.0173	- 3.8194	0.5546	-1.2893	-1.9726	0.3592	-1.9741	-1.9552	1.1004
N = 10	4.9	-1.6667	- 3.8703	0.4121	-1.2565	-1.8363	0.6125	-1.1764	-2.1303	2.4664
	5.0	-4.9774	- 5.1526	---	-3.7908	-3.9809	0.5010	-4.0417	-4.5535	$1.9974^{.5}$
	5.1	-1.8747	- 3.9460	0.4603	-1.2884	-2.0277	0.3749	-1.9862	-1.6879	---
N = 12	4.9	-1.6728	- 3.8405	0.4247	-1.2551	-1.8475	0.6103	-1.1799	-2.1553	2.4317
	5.0	-5.5450	- 6.0533	0.1230	-4.3903	-4.1572	$0.4993^{.5}$	-4.4288	-4.6333	1.9978
	5.1	-1.8720	- 3.9676	0.4535	-1.2890	-2.0241	0.3742	-1.9669	-1.6871	---
N = 14	4.9	-1.6714	- 3.8440	0.4228	-1.2551	-1.8446	0.6110	-1.1785	-2.1543	2.4345
	5.0	-7.0553	- 7.6268	0.1228	-5.6015	-5.5503	$0.5000^{.1}$	-5.8606	-6.0322	$2.0000^{.1}$
	5.1	-1.8730	- 3.9654	0.4544	-1.2895	-2.0267	0.3749	-1.9702	-1.6886	---
N = 16	4.9	-1.6714	- 3.8439	0.4228	-1.2551	-1.8447	0.6109	-1.1786	-2.1543	2.4344
	5.0	-7.8485	- 9.2808	$0.0095^{.5}$	-6.1455	-6.9517	0.5000	-6.7567	-6.7493	2.0000
	5.1	-1.8729	- 3.9654	0.4544	-1.2895	-2.0266	0.3749	-1.9700	-1.6886	---
N = 18	4.9	-1.6714	- 3.8439	$0.4228^{.1}$	-1.2551	-1.8447	0.6109	-1.1786	-2.1543	2.4344
	5.0	-7.8499	-10.3600	$0.0100^{.1}$	-6.1108	-6.9375	0.5000	-6.7128	-6.7556	2.0000
	5.1	-1.8729	- 3.9654	0.4544	-1.2895	02.0266	0.3749	-1.9700	-1.6886	---

Superscripts ^{s}, $^{.5}$, $^{.1}$ indicate that $|\eta|$ is recovered with an error of less than 5%, 0.5% and 0.1%, respectively

on N_5, $N_{0.5}$ and $N_{0.1}$ is illustrated for $M = 3$, 5 and 7 in Table 6.3, employing spherical model scatterers of various electrical sizes (ka = 1 and 2, 4, 6,....14, 16) and a set of values for $|\eta|$, symmetrically chosen about $|\eta| = 1$ within the range $\eta = 0.02$ and $\eta = 50$. First of all, it is observed that, as expected, N_5, $N_{0.5}$ and $N_{0.1}$ increase with increasing ka. Furthermore, the least number N of expansion coefficients, for any ka, is required for values of η close, but not equal, to unity and N_5, $N_{0.5}$ and $N_{0.1}$ increase as the standing wave ratio

$$S = \frac{1 + |\Gamma|}{1 - |\Gamma|} \qquad |\Gamma| = \left| \frac{\eta - 1}{\eta + 1} \right|$$

increases. As can be seen from Tables 6.1, 6.2 and 6.3, it is possible to accurately recover $|\eta|$ and to uniquely discriminate the proper locus for values of η almost equal to unity, zero or infinity. It was noted that the bounds obtained with double-precision expansion coefficients (M = 14) were identical to those obtained with single-precision expansion coefficients (M = 7). Therefore, only values for M = 3, 5 and 7 are presented in Table 6.3. This observation was found to hold also for those cases in which the standing wave ratio S approaches infinity. In addition, it was found that the order of magnitude of individual expansion coefficients evaluated for different values of η within the range $0 \leq \eta \leq \infty$, for one and the same electrical radius ka is independent of η.

In conclusion it can be said that as long as $S \leq 5$ and $ka \leq 4$, $M = 3$ is sufficient to accurately recover $|\eta|$ and the exact point on the

TABLE 6.3
Truncation Analysis of $\underline{N}$ and $\underline{M}$

Analyzed quantities, computed along the ray ($\theta=30°, \phi=60°$), are: $|\eta|$ root of (3.4.12) where ψ is assumed to be known, $Y_1=\log\{|\underline{A}\cdot\underline{A}-\underline{B}\cdot\underline{B}|, \eta=\eta_{S_0}\}$, $Y_2=\log\{|\underline{A}\cdot\underline{B}, \eta=\eta_{S_0}\}$. Bounds on order of series truncation: N_5($|\eta|$ recovered with an error of less than 5%), $N_{0.5}$($|\eta|$ recovered with an error of less than 0.5%), $N_{0.1}$($|\eta|$ recovered with an error less than 0.1%). Order of truncation in significant digits of a_{0in} and b_{0in}: M(3,5,and 7{14}). Dashes indicate that the required accuracy had not been obtained, ka: electrical radius of the spherical model scatterer analyzed

Targets		η=0.02 expj 45°			η=0.05 expj 30°			η=0.25 expj -40°			η=0.5 expj 10°			η=0.99 expj 0°			η=2.0 expj 30°			η=4.0 expj 40°			η=20 expj -30°			η=50 expj -45°		
ka	M	N_5	$N_{0.5}$	$N_{0.1}$	N_5	$N_{0.5}$	$N_{0.1}$	N_5	$N_{0.5}$	$N_{0.1}$	N_5	$N_{0.5}$	$N_{0.1}$	N_5	$N_{0.5}$	$N_{0.1}$	N_5	$N_{0.5}$	$N_{0.1}$	N_5	$N_{0.5}$	$N_{0.1}$	N_5	$N_{0.5}$	$N_{0.1}$	N_5	$N_{0.5}$	$N_{0.1}$
1.0	3	10	12	-	8	8	-	6	8	10	4	6	6	4	6	8	6	8	8	6	8	9	8	10	-	10	-	-
	5	8	10	12	8	8	10	6	8	8	4	6	6	4	6	6	6	8	8	6	8	8	8	8	10	8	10	12
	7	8	10	12	8	8	10	6	8	8	4	6	6	4	6	6	6	8	8	6	8	8	8	8	10	8	10	12
2.0	3	10	-	-	8	11	-	8	8	10	6	8	10	6	8	10	8	10	10	8	8	-	8	12	-	10	-	-
	5	9	10	12	8	10	10	7	8	10	6	8	10	6	8	10	7	8	10	7	8	10	8	10	12	10	12	-
	7	10	10	12	8	10	10	7	8	10	6	8	10	6	8	10	7	8	10	7	8	10	8	10	12	10	12	14
4.0	3	-	-	-	16	-	-	10	12	-	10	12	14	8	12	16	9	12	14	10	12	-	14	-	-	-	-	-
	5	16	-	-	14	16	-	10	12	14	10	12	14	8	10	14	10	12	14	10	12	14	14	16	-	16	18	-
	7	16	18	18	14	16	18	10	12	14	10	12	14	8	10	14	10	12	14	10	12	14	14	14	16	16	18	18
6.0	3	-	-	-	-	-	-	10	-	-	14	14	-	12	14	-	12	14	-	14	-	-	-	-	-	-	-	-
	5	16	-	-	16	16	-	10	14	16	14	14	16	12	14	16	12	14	16	13	14	16	16	18	-	18	-	-
	7	16	16	20	14	16	16	10	14	16	10	14	16	12	14	16	12	14	16	13	14	16	16	16	18	16	18	20
8.0	3	-	-	-	-	-	-	14	-	-	14	16	-	14	15	-	13	14	-	14	-	-	-	-	-	-	-	-
	5	20	-	-	18	20	-	14	16	18	12	16	18	12	14	16	14	16	18	15	16	20	20	20	-	20	-	-
	7	20	22	-	16	18	20	14	18	18	12	14	18	12	14	16	14	16	18	15	16	20	18	20	22	20	22	-
10	3	-	-	-	-	-	-	16	20	-	16	-	-	15	16	-	16	18	-	16	18	-	-	-	-	-	-	-
	5	24	22	-	20	22	24	16	20	22	14	18	22	15	16	22	16	18	22	16	20	22	22	24	-	24	-	-
	7	22	22	-	20	22	24	16	20	22	14	16	20	15	16	22	16	18	22	16	20	22	21	22	24	22	28	-
12	3	-	-	-	-	-	-	18	22	-	18	20	-	16	-	-	16	18	-	20	22	-	-	-	-	-	-	-
	5	26	-	-	22	26	-	19	20	22	16	20	24	16	20	22	16	18	22	20	22	24	24	26	-	26	-	-
	7	24	28	-	22	26	30	19	20	22	16	20	22	16	20	22	16	18	20	20	22	24	24	26	30	28	32	-
14	3	-	-	-	-	-	-	22	-	-	20	-	-	20	24	-	22	24	-	22	-	-	-	-	-	-	-	-
	5	30	-	-	28	-	-	22	22	26	18	22	24	20	22	26	22	22	26	22	24	26	28	28	-	28	-	-
	7	30	-	-	26	28	32	22	22	26	18	22	24	20	22	24	22	22	26	22	24	26	26	28	30	28	-	-
16	3	-	-	-	-	-	-	22	-	-	22	30	-	22	-	-	22	24	-	26	-	-	-	-	-	-	-	-
	5	-	-	-	28	30	-	22	26	28	22	24	26	22	26	28	22	24	28	24	26	28	28	-	-	-	-	-
	7	32	-	-	28	32	34	22	26	28	22	24	26	22	26	28	22	24	26	24	26	28	28	30	32	30	-	-

proper surface, whereas for $5 \leq S \leq 10$, $ka \leq 20$ and $10 \leq S \leq \infty$ the values $M = 5$ and $M = 7$, respectively, are sufficient. The presented truncation error analysis indicates that the accuracy required in recovering the expansion coefficients could be within the realm of presently available measurement techniques employing a matrix inversion procedure [25 , 21].

6.5 RATE OF CONVERGENCE OF ANALYTICALLY CONTINUED FIELDS

To study the rate of convergence of the analytically continued fields, the total electric and magnetic fields are calculated using multipole expansions which are given by (5.4.1) and (5.4.2), respectively. The targets employed for this study consist of spheres of electrical radius $ka = 0.5$, $\eta = 0$, .25, .5 and .9 centered at 0 of Fig. 5.2. The fields are first calculated with respect to the center 0 along the arbitrary ray $0 - 0'$ ($\theta = 45°$, $\phi = 130°$) and then with respect to the translated origin 0' ($kd = 1.0$, $\theta_0 = 45°$ and $\phi_0 = 130°$) of Fig.5.2 along the same ray $0 - 0'$ using analytic continuation given by (5.4.3). The results are presented in Table 6.4, where the values of magnitude and phase of E_r - component of the scattered electric field are tabulated in column 1 with respect to the expansion about 0, and in the next three columns with respect to the translated origin 0' for different orders of truncation $N = 6$, 10, 14 of n in (5.4.3). The series expansion of (5.4.7a) and (5.4.7b) for the spheres of electrical radius $ka = 0.5$ and $\eta = 0$, .25, .5 and .9 were truncated at $\nu = 6$

because the higher order expansion coefficients $A(\mu,\nu)$ and $B(\mu,\nu)$ were negligible. Similar calculations for different translation parameters kd, θ_0 and ϕ_0 revealed that many more translation coefficients $\alpha(m,n)$ and $\beta(m,n)$ are required to express the em fields accurately as the computational point approaches the true surface of the scatterer as is evident from inspection of Table 6.4. In particular, it was found that the rate of convergence of the analytically continued fields deteriorates as the maximum radius of the sphere of convergence centered at 0' increases and the more η deviates from 1. Therefore, in applying the IBCs, it was found useful to successively reduce the translation distance 0 - 0' in order to reduce the radius of the maximum sphere of convergence and hence to improve the accuracy of the continued fields. Obviously, the rate of convergence will slow down further if analytic continuation is applied to field expressions for multi-body scattering as the rate of convergence of the associated total field expressions is very slow. In particular, the number of expansion coefficients $A(\mu,\nu)$ and $B(\mu,\nu)$ in (5.4.7a) and (5.4.7b) depends on the parameters of the configuration, especially the electrical radius of the minimum sphere enclosing the scatterers. It should be noted that it seems possible to obtain more efficient formulations of vector translation theorems (5.4.4a) and (5.4.4b) which possess a faster rate of convergence, and further studies in finding such formulations are required to reduce the extensive computer time for computing the translation coefficients.

TABLE 6.4

TRUNCATION ERROR ANALYSIS FOR INTERIOR ANALYTIC CONTINUATION

Model Target: Sphere of Elec. Radius ka=0.5 and η=0, .25, .5, .75

(X/k measured along 0-0' of Fig.5.3 w.r.o.)

η=0

	kd = 0		kd = 0.75						kd = 1.0					
X	N = 6		N = 6		N = 9		N = 12		N = 6		N = 9		N = 12	
	$\lvert E_r^s \rvert$	$\lvert \theta_x^s \rvert$	$\lvert E_r^s \rvert$	$\lvert \theta_r^s \rvert$	$\lvert E_r^s \rvert$	$\lvert \theta_r^s \rvert$	$\lvert E_r^s \rvert$	$\lvert \theta_r^s \rvert$	$\lvert E_r^s \rvert$	$\lvert \theta_r^s \rvert$	$\lvert E_r^s \rvert$	$\lvert \theta_r^s \rvert$	$\lvert E_r^s \rvert$	$\lvert \theta_r^s \rvert$
.35	3.532472	-6.809245	2.870047	4.484735	3.351082	-5.947093	3.488847	-6.533195	2.065625	-2.079577	2.844227	-4.205718	3.242183	5.457619
.40	2.396197	-4.744843	2.155439	-3.495327	2.351331	-4.415823	2.388937	-4.672917	1.673540	-1.456521	2.123665	-3.220344	2.304769	-4.095883
.45	1.708829	-2.974434	1.629051	-2.372978	1.699368	-2.871242	1.707879	-2.960153	1.355211	-.7359093	1.604339	-2.1293576	1.681608	-2.689832
.50	*1.267561*	*-1.380547*	*1.244720*	*-1.134799*	*1.265994*	*-1.355771*	*1.267488*	*-1.378538*	*1.098583*	*0.9156387*	*1.229538*	*-.9450865*	*1.260081*	*-1.2687858*
.55	.9706246	.1113633	.9656089	.1898159	.9704403	.1154301	.9706216	.1115502	.8930589	1.032310	.9577562	.3157007	.9687682	.1497705
.60	.7629707	1.550317	.7621531	1.567222	.7629607	-1.550705	.7629730	1.550347	.7294068	2.088330	.7590259	1.635531	.7621019	1.5615570
.65	.6130580	2.969513	.6129959	2.971315	.6130599	2.969603	.6130602	2.969540	.5996797	3.256105	.6119986	3.0011534	.6129879	2.972220

η = 0.25 |o°

.35	3.353642	5.010784	2.735261	7.453129	3.186117	5.919106	3.313819	5.301821	1.975954	9.957418	2.711998	7.745438	3.085142	6.433741
.40	2.281740	7.175203	2.056700	8.481240	2.240280	7.519727	2.275115	7.250478	1.601822	10.59828	2.027341	8.768217	2.197112	7.854488
.45	1.631086	9.017606	1.556453	9.643219	1.622342	9.125023	1.630221	9.032406	1.297960	11.33803	1.533465	9.896462	1.605881	9.313926
.50	*1.212229*	*10.66580*	*1.190852*	*10.92014*	*1.210784*	*10.69133*	*1.212166*	*10.66772*	*1.052897*	*12.18574*	*1.176688*	*11.11656*	*1.205305*	*10.78148*
.55	.9297367	12.19987	.924852	12.28082	.9295662	12.20411	.9297338	12.20011	0.8565472	13.14742	0.9177029	0.9233665	0.9280171	12.23955
.60	.7318059	13.67289	.731040	13.69032	.7317966	13.67336	.7318080	13.67299	.7001198	14.22459	.7281161	13.76049	.7314357	13.68451
.65	.5886824	15.12018	.588624	15.12210	.5886842	15.12030	.5886845	15.12029	.5760481	15.41315	.5876914	15.15158	.5886175	15.12303

η=0.50 |o°

.35	3.137938	16.07132	2.568995	18.64479	2.985488	17.03093	3.10439	16.37897	1.862607	21.25989	1.917731	30.27646	1.838037	38.66957
.40	2.141258	18.34653	1.933957	19.71564	2.103515	18.70833	2.135307	18.42552	1.510786	21.92030	1.554552	28.08096	1.509027	32.66623
.45	1.534228	20.26877	1.465423	20.92137	1.526268	20.38084	1.533453	20.28407	1.224949	22.68105	1.257320	26.69086	1.235418	29.06213
.50	1.142393	21.97713	1.122676	22.24109	1.141079	22.00345	1.142338	21.97890	.9943352	23.55092	1.016414	26.00528	1.007196	27.15320
.55	.8775356	23.55794	.8730292	23.64163	.8773807	23.56230	.8775333	23.55815	.8094800	24.53557	.8232530	25.92458	0.8198388	26.43503
.60	.6916149	25.06871	.6909084	25.08664	.6916066	25.06917	.6916170	25.06879	.6621377	25.63593	.6699106	26.34651	.6688084	26.54973
.65	.5569637	26.54709	.5569104	26.54903	.5569657	26.54718	.5569659	26.54716	.5452066	26.84729	.5491094	27.16588	.5488064	27.23586

η=.75 |o°

.35	2.910384	26.16809	2.391247	28.88347	2.772797	27.18336	2.878488	26.49399	1.739724	31.61859	2.373158	29.20671	2.689185	27.75626
.40	1.991513	28.56273	1.802149	30.00009	1.957440	28.94322	1.986216	28.64575	1.411862	32.29979	1.778032	30.31512	1.921721	29.31245
.45	1.430083	30.57077	1.367186	31.25272	1.422896	30.68796	1.429394	30.58667	1.145407	33.08287	1.348042	31.52855	1.409286	30.89438
.50	1.066762	32.34322	1.048714	32.61830	1.065559	32.37102	1.066696	32.34546	.9303520	33.97635	1.036850	32.83055	1.061033	32.46867
.55	.8206290	33.97485	.8165073	34.06157	.8204896	33.97935	.8206274	33.97507	.7578981	34.98541	.8105015	34.20074	.8192111	34.01743
.60	.6475585	35.52615	.6469126	35.54463	.6475516	35.52660	0.6475610	35.52620	.6203766	36.11044	.6444530	35.61928	.6472540	35.53848
.65	.5220264	37.03787	.5219780	37.03983	.5220286	37.03793	.5220288	37.03792	.5111820	37.34607	.5211928	37.07097	.5219736	37.04082

chapter seven

CONCLUSIONS

7.1 SUMMARY AND DISCUSSIONS

The inverse problem of electromagnetic scattering has been resolved, in principle, using the concept of inverse boundary conditions. A variety of methods of target portrayal, based on scattering center concepts [4], comparison of monostatic-bistatic scattering cross-sections, target signature comparison [122], the physical optics approximation [19,67], the geometric optics approximation [63 ,130], etc. are treated in the literature. But all these methods involve some basic approximations in their formulation and provide a sufficiently accurate solution to the profile inversion of only perfectly conducting shapes in the limit of high-frequency scattering. Therefore, in order to invert the profile characteristics of perfectly and imperfectly conducting shapes, given the total fields everywhere for a single operating frequency anywhere within the entire frequency spectrum, additional inverse boundary conditions were required.

A first attempt in this direction was made by Weston, Bowman and Ar [139] where it was shown that the inverse condition $\underline{E}x\underline{E}^*$ is an exact, necessary condition but is not sufficient because it generates an infinite set of pseudo loci, in addition to the proper surface locus $S_0(\underline{r})$ of the perfectly conducting scatterer. Since this condition, in general, requires additional inverse boundary conditions so that

the proper surface locus can uniquely be discriminated without the aid of the physical optics condition, other necessary and sufficient inverse boundary conditions were sought. This search resulted in the straightforward cognizance that $\underline{E}\cdot\underline{H} = 0$, $\underline{E}^*\cdot\underline{H} = 0$ and $\underline{E}\cdot\underline{H}^* = 0$ [23]. The boundary condition $\underline{E}\cdot\underline{H} = 0$ is an exact necessary and sufficient condition for a point to lie on a perfectly electric or magnetic conducting surface except in those cases for which $\underline{E}$ and $\underline{H}$ are intrinsically perpendicular to one another. The conditions $\underline{E}^*\cdot\underline{H} = 0$ and $\underline{E}\cdot\underline{H}^* = 0$ are exact, necessary but not sufficient because they generate an infinite set of pseudo loci in addition to the proper surface locus $S_0(\underline{r})$ and they are not independent of $\underline{E}\times\underline{E}^* = 0$ for the perfectly electric conducting case and of $\underline{H}\times\underline{H}^*=0$ for the perfectly magnetic conducting case [23], respectively.

The next step was to search for inverse boundary conditions which can be applied to specify the relative, averaged, local surface material properties, i.e. η, in addition to simultaneously specifying the size and the exact surface locus of curvilinear scatterers of finite radii of curvature. It was anticipated that at least three independent characteristic equations are required to uniquely specify the size, the shape, and the modulus and phase of the relative surface impedance η, which, however, need not independently be sufficient by themselves [136]. In fact, global physical laws and concepts, as e.g. Heisenberg's uncertainty principle[50,58]inherently implied, contradict the explicit uniqueness of the inverse problems of electromagnetic scattering. Namely, nature reveals in real time occurences that whenever decisions

of uniqueness in remote object specification are to be performed, global laws of discrimination are implied. The problem of non-uniqueness is also high-lighted in a most recent publication by Sleeman [111] where he discusses the three-dimensional inverse scattering problem for the Helmholtz equation. According to Müller [85] and Wilcox [146], given a radiation pattern $g(\theta,\phi)$, the sources which generate the field u must lie within a closed sphere of radius r_c where r_c is uniquely determined by $g(\theta,\phi)$. For axi-symmetric fields Cotton [34] has recently given more precise information concerning the location of these sources by using entire function theory and function theoretic methods in the theory of partial differential equations. Similar problems have been considered by Millar [77] and Weston, Bowman and Ar [140]. However, in both these papers some *a priori* knowledge is assumed. Sleeman's main theorems [111] state that the scattered field may be thought of as produced by a set of equivalent sources located on or within the surface of the scattering body. At points outside the geometrical surface of the body, the field produced by these fictitious sources is identical to the scattered field of the body. These fictitious sources are not, in general, unique, although, they are confined to some finite region of space. This non-uniqueness suggests that, in general, the solution to the inverse scattering problem is non-unique. But, the hypothesis has been proposed in[136] that the inverse boundary conditions, required to uniquely resolve the inverse problem of electromagnetic scattering, may consist of a set of independent, exact, necessary though not sufficient conditions. However, simultaneous application of these conditions provides a unique

solution to the problem of target characteristics inversion, given the total near field expansions everywhere for one single operating frequency only [23].

A logical approach in the search for such inverse boundary conditions was to critically review the properties of the Leontovich or scalar impedance boundary conditions [82], since these conditions though approximate, are hitherto, the simplest relations known to resolve scattering from general imperfectly conducting shapes. The intuitive attempt to invert these direct boundary conditions, resulted in the astounding finding [136] that two basic vector quantities, $\underline{A} = \underline{E}x\underline{E}^* - \eta\eta^*\underline{H}x\underline{H}^*$ and $\underline{B} = \eta\underline{E}^*x\underline{H} - \eta^*\underline{E}x\underline{H}^*$, exist which are orthogonal, $\underline{A}\cdot\underline{B} = 0$, lie in the local scattering plane of a smooth curvilinear scatterer of finite radii of curvature, $\hat{n}\cdot\underline{A} = \hat{n}\cdot\underline{B} = 0$, and are of identical magnitude $A^2 = B^2$. Obviously, both the total electric and the total magnetic field expressions are required which was to be expected from the basic definition of an intrinsic impedance.

To verify the validity of the sets of inverse boundary conditions of Sections 3.2 and 3.3, a variety of targets comprised of mono- and two-body circular cylindrical and spherical shapes have been tested numerically. For the cylindrical bodies, well established techniques of coordinate transformation and analytic continuation have been employed to continue the em fields in the region within the minimum circle enclosing the body. Three-dimensional analytic continuation has been introduced to treat non-canonical shapes in spherical coordinates.

The perfectly electric conducting cases have been analysed first to eliminate the inadequacies resulting from the continual application of the approximate physical optics condition and to provide the numerical fundament for treating the more sophisticated imperfectly conducting bodies. To demonstrate the uniqueness of the novel discrimination procedure clearly, the imperfectly conducting case for known η was treated first. In treating the case of partially complete *a priori* given information, i.e. $\eta = \eta^*$ or $\eta = -\eta^*$, it was demonstrated that this case can uniquely be resolved for the inhomogeneous and dispersive bodies, given field data everywhere for one single operating frequency only. For the general case of *a priori* unknown η, the mono-body case for homogeneous η was treated first proving that η = const. and $S_0(\underline{r})$ can uniquely be recovered, given data everywhere for one single operating frequency only. The degeneracy condition was employed to resolve this case. However, for the two-body case or for the case in which the scattering surface about monostatic direction is concave, the double-frequency checking procedure must be applied in which case η must be assumed to be nondispersive, though, it could, in general, be inhomogeneous. In essence, it has been demonstrated that the concept of inverse boundary conditions can effectively be applied to the inversion of conducting shapes, though for resolving the most general cases an additional independent condition is required.

It is important to mention here that the tangentiality condition, i.e. $\hat{n}\cdot\underline{A} = \hat{n}\cdot\underline{B} = 0$, has not yet resulted in an independent relation. It might be possible to combine the ideas of Weyl [144] with the tangentiality

condition to obtain another independent unique relationship for convex surfaces. Namely, in Weyl's problem [144,91], one is given positive definite quadratic form ds^2 defined at every point of the unit sphere and the existence of a closed convex surface which may be mapped one to one onto the sphere,so that its fundamental form in terms of the parameters on the sphere is ds^2, is to be proved. The tangentiality condition provides the tangent plane at each point of the quadratic surface to help achieve uniqueness. Similarly in Minkowski's problem [79,114] which is also applicable only to convex surfaces, one is given a positive function $K(\hat{n})$ defined on the unit sphere (here $\hat{n}$ represents the inner unit normal to the sphere), and the existence of a closed convex surface having $K(\hat{n})$ as its Gaussian curvature at the point on the surface where the inner normal is $\hat{n}$, is to be investigated. The function $K(\hat{n})$ is assumed to satisfy the condition, which holds for any regular closed convex surface,

$$\int K(\hat{n})\hat{n}\, d\omega(\hat{n}) = 0$$

where the integration is carried over the unit sphere with $d\omega$ representing the element of area on the sphere. For this case the vector $\underline{D} = \underline{A}x\underline{B}$ defines the direction of the normal which could be integrated based on Minkowski's idea to obtain possibly another unique relation.

As has been demonstrated in Sections 4.4 and 5.5, the proposed boundary conditions are found to provide parameters of the scatterers whose surface impedance is purely real or purely imaginary or complex. This observation gives rise to the hypothesis that the intuitively established

inverse boundary conditions could represent the degenerate subset of a more generalized set of basic unique electromagnetic vector quantities implicitly prescribed in the definition of Maxwell's equations [117]. In particular, it is anticipated that $\underline{A}$ and $\underline{B}$ bear close affinities to a more generalized complex-conjugated formulation of Maxwell's electrodynamic stress tensor [17] when applied across a bounding curvilinear surface of finite radii of curvature. The third unique basic vector quantity, say $\underline{N}$, defined along the outward local normal, was not found to result from the inversion of the Leontovich conditions [136,23]. This additional basic vector quantity, which intuitively should exist, may result from the more general formulation resulting from the Maxwell's stress-tensor approach.

7.2 CONTRIBUTIONS TO THE FIELD OF ELECTROMAGNETIC THEORY

The proposed inversion technique should be of great importance to the basic problem of target identification. At present radar detection is the only means to detect remote bodies. In spite of all the sophistications introduced after the second world war, nobody has yet been able to determine the material properties and exact profile of remote objects. We do not mean to suggest here that at the present stage of development the proposed technique will resolve the problem. But with advancement in technology the following set up is suggested to achieve the required goal.

A high-powered transmitter illuminates the target, and the total field

is detected by the receiving stations, set up at locations whose angular bearings are optimized according to Boerner and Aboul Atta's [21] optimization procedure. The received data (the magnitude and phase of the scattered field) goes to the central processing unit where the scattering coefficients for the target are calculated for the appropriate expansion of the fields using matrix inversion [25]. Now, the inverse boundary conditions can be applied to the total fields to recover the surface impedance and the profile of the scatterer, which can be appropriately integrated into the proper shape to be displayed on the radar screen.

Using the same procedure, bodies of interest to the radio-astronomers can be identified. Regarding the immediate contribution to the field of em theory, Theorems 1 to 3 presented in Section 2.4 can be employed even for direct scattering problems, since all the em fields have to satisfy the orthogonality and normality conditions of the vectors $\underline{A}$ and $\underline{B}$, where vector $\underline{B}$ represents the reactive energy in a wave. Moreover, since the proposed technique is based on rigorous Maxwell's equations, it provides a method for checking any future approximate methods, e.g. those based on the physical or the geometrical optics approximations.

The results analysed in Section 6.4 reveal that a new dimension has been added to the error analysis; the lower and upper truncation bounds N_ℓ and N_u, respectively, depend upon the standing wave ratio among other relevant parameters. The estimates on the lower and the upper

truncation bounds may be obtained by the application of inverse boundary conditions. The minimum number of terms, which results in the required degree of accuracy for the calculated surface impedance and the profile, defines the lower bound N. The upper bound is defined by the number of terms beyond which no significant improvement in the solution is obtained. In fact, beyond a certain number N_{max}, the accuracy of the solution will deteriorate because of stability criteria as analysed in Section 6.2.

The proposed inversion technique can be employed in the design of tomographic apparatus and eventual supplementation of the x-ray techniques by microwave techniques [22 , 16]. As a by-product, solutions for multibody scattering for the case of cylinders and spheres with arbitrary surface impedances have been obtained. Similar solutions for perfectly conducting cases and dielectric materials are found in the literature [92 , 31], but the case of arbitrary surface impedance has never been treated before, though, the extension is simple.

7.3 NEW RESEARCH TOPICS ARISING FROM THE PRESENT WORK

The present research has raised a number of questions which have to be answered for further development of the proposed inversion technique.

More detailed physical insight into the nature of the vectors $\underline{A} = \underline{E}x\underline{E}^*-\eta\eta^*\underline{H}x\underline{H}^*$ and $\underline{B} = \eta\underline{E}^*x\underline{H}-\eta^*\underline{E}x\underline{H}^*$ is needed to interpret the reasons for their orthogonality, equality and tangentiality to the surface of

the scatterer at all the points. The possibility of their use in the direct scattering problems is to be investigated.

The concept of inverse boundary conditions has been applied to the canonical shapes of cylinders and spheres and certain non-canonical shapes like multiple cylindrical and spherical bodies. But they have still to be tested for many other non-canonical shapes, though, there does not seem to be any doubt in their success in achieving the inversion.

In addition to the intrinsic problem of defining a third unique vector quantity, the problem of establishing a general mini-max searching routine which can be applied in practice, still remains an open question. The search for such a unique mini-max discrimination technique, as proposed in Rosenbrock [100], however, was not the subject of this study.

The implementation of the novel concept of inverse boundary conditions still requires the resolution of the complicated problem of recovering bistatic amplitude and phase information for the measured scattered transverse field quantities to an accuracy required here. But taking into consideration the rapid progress on how Fourier-optical, holographic and interferometric techniques are entering the field of measurement data recording, storage and retrieval, the answer to this vexed question does not seem to be far-fetched.

The practical significance of the results presented in this work would be greatly increased if the ideas of Weston and Boerner and those ideas,

suggested in this work, could be combined with those of Jull [59,60] who had success operating on data obtained from actual measurement on aerials [14].

In order to approach the problem of recovering the phase, one of the useful approaches would be to exploit the ideas of Refs. [12,97,93, 128]. In [128,93], Adriaan Walther proves that phase reconstruction is possible and is unique if the aperture of the lens is finite. In [12,13], Bates shows that the unavoidable incompleteness and imperfections of a practical hologram do not prevent an approximate reconstruction of the unknown source, although errors are inevitably introduced. Examples of source reconstruction are given in the companion paper [13].

The extension of the proposed methods of profile inversion to the case of moving objects is to be carried out. An immediate effect of allowing the body to have an arbitrary linear motion is that TM or TE wave normally incident in the 0 coordinate frame, in which the source and the observer are stationary, results in a super-position of TM and TE waves obliquely incident in the 0' coordinate frame in which the body is stationary [53,98].

To conclude, extensive research is still needed in the field of inverse scattering if the target identification of the general configurations with arbitrary surface impedance is to become a reality. By introducing the concept of inverse boundary conditions for the profile

characteristics inversion of conducting shapes, a new dimension has been added to the solution of this intricate problem. It is, therefore, hoped that the modest contribution made by the present work will open up new avenues which will help in the eventual solution of this vexed problem.

REFERENCES

1. Z.S. Agranovich and V.A. Marchenko, 'The Inverse Problem of Scattering Theory', Translated by B.D. Seckler, Gordon and Breach Science Publishers, New York and London, 1963.

2. H.P.S. Ahluwalia and W.M. Boerner, "Application of a set of inverse boundary conditions to the profile characteristics inversion of conducting circular cylindrical shapes", IEEE Trans. on Ant. and Propag. AP-21, (5), 1973,

3. H.P.S. Ahluwalia and W.M. Boerner, "Application of electromagnetic inverse boundary conditions to profile characteristics inversion of conducting spherical shapes", Radio Science, submitted.

4. J.L. Altman, R.H.T. Bates and E.N. Fowle, 'Introductory notes relating to em inverse scattering', The Mitre Corporation, Bedford, Massachusetts, Rep. SR-121, 1964.

5. G. Backus and F. Gilbert, "Numerical applications of a formalism for geophysical inverse problems", Geophys. J. Roy. Astr. Soc. 13, 1967, 247-276.

6. G. Backus and F. Gilbert, "The resolving power of gross earth data", Geophys. J. Roy. Soc. 16, 1968, 169-205.

7. G. Backus and F. Gilbert, "Uniqueness in the inversion of inaccurate gross earth data", Phil. Trans. R. Soc. A266, 1970, 123-192.

8. R.C. Bailey, "Inversion of the geomagnetic induction problem", Proc. R. Soc. 315, 1970, 185-194.

9. R.J. Banks, "Geomagnetic variations and the electrical conductivity of the upper mantle", Geophys. J. Roy. Astr. Soc. 17, 1969, 457-487.

10. R.B. Barrar and C.L. Dolph, "On a three-dimensional problem of em theory", J. Rational Mech. and Anal. 3, (6), 1954, 725-743.

11. D.K. Barton, "Sputnik II as observed by C-band radar", IRE National Convention Record, 7, Part 5, 1959, 67-73.

12. R.H.T. Bates, "Holographic approach to radiation pattern measurement - I, General Theory", Inst. J. Eng. Sci. 9, 1971, 1107-1121.

13. R.H.T. Bates, "Holographic approach to radiation pattern measurement - II, Experimental Verification", Inst. J. Eng. Sci. 9, 1971, 1193-1208.

14. R.H.T. Bates, "Inverse scattering for totally reflecting objects", Arch. Rat. Mech. and Anal. 38, (2), 1970, 123-130.

15. R.H.T. Bates, "Towards estimating the shapes of radar targets", The Institution of Engineers, Australia, Elec. Eng. Trans., Sept. 1969, 290-294.

16. R.H.T. Bates, "Towards improvements in tomography", New Zealand J. of Science, 14, (4), Dec. 1971, 883-896.

17. R. Becker and F. Sauter, 'Electromagnetic Fields and Interactions, Vol. I'(Electromagnetic Theory and Relativity, Translation of 'Theorie der Elektrizität' by Abraham and Becker, Teubner Verlag, Germany, 1940), Blaisdell Publ. Co., New York, 1964.

18. P. Beckmann and A. Spizzichino, 'The Scattering of Electromagnetic Waves from Rough Surfaces', Intern. Series of Monographs on Electromagnetic Waves, Vol. 4, The McMillan Company, New York, 1963.

19. N.N. Bojarski, ' Three-Dimensional Electromagnetic Short Pulse Inverse Scattering', Syracuse Univ. Res. Corp., Syracuse, N.Y., Feb. 1967.

20. N.N. Bojarski, "Electromagnetic inverse scattering", in Ref. 89, 6.34 - 6.47.

21. W.M. Boerner and O.A. Aboul-Atta, "General properties of the scattered field matrix in spherical coordinates", Utilitas Mathematica, 3, 1973, 163-237.

22. W.M. Boerner and H.P.S. Ahluwalia, "Application of em inverse scattering techniques to 3-dim. image reconstruction", Intern. Confer. on Med. & Biol. Engineering, Session 6, Dresden,G.D.R., August 1973.

23. W.M. Boerner and H.P.S. Ahluwalia, "On a set of continuous wave em inverse scattering boundary conditions", Can. J. Phys. 50, (23), 1972, 3023-3061.

24. W.M. Boerner and Y. Das, "On a classical approach to profile characteristics inversion of conducting canonical shapes", Can. J. Phys. 51, 1973.

25. W.M. Boerner and V.H. Vandenberghe, "Determination of the elect. radius of a spherical scatterer from the scattered field", Can. J. Phys. 49, (11), 1971, 1507-1535.

26. W.M. Boerner, F.H. Vandenberghe and M.A.K. Hamid, "Determination of the elec. radius ka of a circular cyl. scatterer from the scatt. field", Can. J. Phys. 49, (7), 1971, 804-819.

27. M. Born and E. Wolf, 'Principles of Optics', Pergamon Press, New York, Second Edition, 1964.

28. J.J. Bowman, T.B.A. Senior and P.L.E. Uslenghi, 'Electromagnetic and Acoustic Scattering by Simple Shapes', North Holland Publ. Co., Amsterdam, Netherlands, 1969.

29. C. Brindley, "Target recognition", Space/Aeronautics, 43, (6), June 1965, 62-88.

30. J.H. Bruning, 'Multiple scattering by spheres', Ph.D. Thesis, Univ. of Illinois, Urbana, Illinois, 1969.

31. J.H. Bruning and Y.T. Lo, "Multiple scattering of em waves by spheres, Part I - Multipole expansion and ray-optical solutions", IEEE Trans. Ant. and Propag. AP-19, (3), 1971, 378-390.

32. J.E. Burke and V. Twersky, "On scattering of waves by many bodies", Radio Science, 68D, 1964, 500.

33. H.S. Cabayan, R.C. Murphy and T.J.F. Pavlasek, "Numerical stability and near field reconstruction", IEEE Trans. Ant. and Propag. AP-21, (3), 1973, 346-351.

34. D. Cotton, "On the inverse scattering problem for axially symmetric solutions of the Helmholtz equation", Quart. J. Math., Oxford Ser. 22, 1971, 125-130.

35. R.K. Crane, "Atmospheric radar sounding", in Ref. 89, 2.13-2.22.

36. R.K. Crane, 'Cooperative scattering by dielectric spheres', Technical Note 1967-31, Lincoln Lab., M.I.T., Lexington, Massachusetts, 1967.

37. J.W. Crispin, Jr. and K.M. Siegel, 'Methods of Radar Cross-Section Analysis', Academic Press, New York, 1968.

38. O.R. Cruzan, "Translation addition theorems for spherical vector wave functions", Quart. Applied Math. 20, 1962, 33.

39. G.A. Deschamps, "Ray techniques in electromagnetics", Proc. IEEE, 60, (9), 1972, 1022-1035.

40. A.R. Edmonds, 'Angular Momentum in Quantum Mechanics', (Princeton Univ. Press, Princeton, N.J.), 1957.

41. O. Einarsson, R.E. Kleinman, P. Laurin and P.L.E. Uslenghi, 'Studies in radar cross-sections, L-diffraction and scattering by regular bodies IV: "The circular cylinder', Univ. of Michigan Radiation Laboratory, Rept. No. 7133-3-T, 1966.

42. L.D. Faddeyev, "The inverse problem in the quantum theory of scattering", J. Math. Physics, 4, (1), Jan. 1963, 72-104.

43. A. Fedotowsky, G. Boivin and R. Tremblay, "Inversion of microwave scattering pattern", Can. J. Phys. 49, 1971, 3082-3094.

44. A. Freedman, "The portrayal of body shape of a sonar or radar system", The British Institute of Radio Engineers, 25, 1963, 51-64.

45. M.S. Gazzaniga, "One brain - two minds?", American Scientist, 60, (3), 1972, 311-317.

46. B. Gopinath and M.M. Sondhi, "Inverse of the telegraph equations and synthesis of non uniform lines", Proc. IEEE, 59, 1971, 383-392.

47. G. Graf, "Analysis of the doppler spectrum of rotating objects", Deutsche Luft-und Raumfahrt, Forschungsbericht 72-46, 1972, 165 pages, DK 535.338.4/538.56.

48. R.F. Harrington, "On the calculation of scattering by conducting cylinders", IEEE Trans. Ant. and Propag. AP-13, (5), 1965, 812-813.

49. R.F. Harrington, 'Time Harmonic Electromagnetic Fields', McGraw Hill Company, New York, 1961.

50. W. Heisenberg, "Über den anschaulichen Inhalt der quantentheoretischen Kinematik und Mechanik", Zeitschrift für Physik, 43, 1927, 172-198.

51. E. Hiatt, T.B.A. Senior and V.H. Weston, 'Studies in radar cross-section XI - Surface roughness and impedance boundary conditions', Univ. of Mich., Dept. Elect. Eng., Radiation Lab., Ann Arbor, Rept. No. 2500-2-T, July 1960.

52. D.A. Hill, "Inverse scattering from a perfectly conducting prolate spheroid in the quasi-static domain", Can. J. Phys. 51, 1973, 219-222.

53. J.D. Hunter, "Electromagnetic scattering by a transversely moving conducting cylinder of arbitrary cross-section", Can. J. Phys. 51, (7), 1973, 699-706.

54. W.A. Imbriale and R. Mittra, 'A two-dimensional inverse scattering problem', Antenna Lab.,Univ. of Illinois, Rept. No. 69-6, May 1969.

55. W.A. Imbriale and R. Mittra, "The two-dimensional inverse scattering problem", IEEE Trans. Ant. and Propag. AP-18, 1972, 632-642.

56. J.E. Jackson, "The P'(f) to N(h) inversion problem in ionospheric soundings", in Ref.89, 4.2-4.14.

57. D.S. Jones, 'The Theory of Electromagnetism', New York, McGraw-Hill, 1961.

58. G. Joos, 'Introduction to Theoretical Physics', Translated from first German edition by Ira M. Freeman, Blackie and Son Limited, London and Glasgow, 1934.

59. E.V. Jull, "An investigation of near-field radiation patterns measured with large antennas", IRE Trans. Ant. and Propag. AP-10, (4), 1962, 363-369.

60. E.V. Jull, "The estimation of aerial radiation patterns from limited near field measurements", Proc. IEE, 110, 1963, 501-506.

61. I. Kay, "The inverse problem for transmission lines", in Ref. 89, 6.2-6.17.

62. R.E. Kell, "On the derivation of bistatic RCS from monostatic measurement", Proc. IEEE, 53, Part I, 1965, 983-992.

63. J.B. Keller, "The inverse scattering problem in geometrical optics and the design of reflectors", IRE Trans. Ant. and Propag. AP-7, 1959, 146-149.

64. E.M. Kennaugh and D.L. Moffat, "Transient and impulse response approximations", Proc. IEEE, 53, Part I, 1965, 893-901.

65. R.W. King, 'Transmission-Line Theory', Dover Public. Inc., New York, 1965.

66. M.A. Leontovich, "Appendix of diffraction, reflection and reflection of radio waves", (13 papers by V.A. Fock, Eds. N. Logan and P. Blacksmith, U.S. Govt. Print Off. Washington, D.C., Rept. No. AD-117, 276.)

67. R.M. Lewis, "Physical optics inverse diffraction", IEEE Trans. Ant. and Propag. AP-17, (3), 1969, 308-314.

68. R.M. Lewis, 'Short pulse inverse diffraction theory', Mitre Corp., Bedford, Mass., MTR-322, Nov. 1966 and supplement Jan.1967.

69. C. Liang and Y.T. Lo, "Scattering by two spheres", Radio Science, 2, (12), 1967, 1481-1495.

70. A.C. Ludwig, "Numerical check on the accuracy of the spherical wave functions", Electronics Letters, 8, (8), 1972, 202-203.

71. T.M. MacRobert, 'Spherical Harmonics', Intern. Ser. of Monographs in Pure and Applied Mathematics, 98, Pergamon Press, New York, (3rd ed.), 1967.

72. C.L. Mateer,"A review of some aspects of inferring the ozone profile by inversion of ultraviolet radiance measurements", in Ref.89, 1.2-1.25.

73. L.G. McAllister, "Acoustical radar sounding of the lower atmosphere", in Ref.89, 2.2-2.11.

74. L. McCulley, "Numerical methods for reduction of topside ionograms", in Ref.89, 4.27-4.36.

75. R.F. Millar, "On the Rayleigh assumption in scattering by a periodic surface II", Proc. Cambridge Philos. Soc., 69, 1971, 217-225.

76. R.F. Millar, "Rayleigh hypothesis in scattering problems", Electronic Letters, 5, (17), 1969, 416-417.

77. R.F. Millar, "Singularities of two-dimensional exterior solutions of the Helmholtz equation", Proc. Cambridge Philos. Soc. 69, 1971, 175-188.

78. R.F. Millar, "Some controversial aspects of scattering by periodic structures", XVII General Assembly of URSI, session VI-5, Warsaw, Aug. 1972.

79. H. Minkowski, "Volumen und Oberfläche", Mathematische Annalen, 57, 1903, 447-495.

80. R. Mittra and P.L. Ransom, "Imaging with coherent fields", presented at the Symp. on Mod. Opts., Polytech. Inst. of Brooklyn, March 1967.

81. R. Mittra and D.R. Wilton, "A numerical approach to the determination of electromagnetic scattering characteristics of perfect conductors", Proc. IEEE, 57, (11), 1969, 2064-2065.

82. H.M. Mitzner, "An integral equation approach to scattering from a body of finite conductivity", Radio Science, 2, (New series), (12), 1967, 1459-1470.

83. H.E. Moses, "Solutions of Maxwell's equations in terms of a spinor notation: The direct and inverse problem", Phys. Review, 113, 1959, 1670-1679.

84. P. Moon and D.E. Spencer, 'Field Theory Handbook', Springer-Verlag, Berlin, 1961.

85. C. Müller, "Electromagnetic radiation patterns and source", IRE Trans. Ant. and Propag. AP-4, (3), 1956, 224-232.

86. C. Müller, "Radiation patterns and radiation fields", J. Rat. Mech. and Anal. 4, 1955, 235-246.

87. R.C. Murphy, 'Inverse scattering by conducting circular cylinders', M.Eng. thesis, McGill Univ., Montreal, P.Q. Canada, 1971.

88. T. Musha, "Electrodynamics of anisotropic media with space and time dispersion", Proc. IEEE, 60, (12), 1972, 1475-1485.

89. Nasa Technical Memorandum, 'Mathematics of Profile Inversion', Proc. of the workshop held at Ames Research Center, Moffett Field, Calif. July 1971.

90. R.G. Newton, "Introduction to the inverse quantum scattering problem", in Ref.89, 5.2-5.13.

91. Louis Nirenberg, "The Weyl and Minkowski problems in differential geometry in the large", Com. on Pure and Applied Math. 6, 1953, 337-394.

92. G.O. Olaofe, "Scattering by two cylinders", Radio Science, 5, (11), Nov. 1970, 1351-1360.

93. E.L. O'Neill and A. Walther, "The question of phase in image formulation", Optica Acta, 63, (10), 1962, 33-40.

94. R.L. Parker, "The Backus-Gilbert method and its application to the electrical conductivity problem", in Ref. 89, 7.21-7.28.

95. R.L. Parker, "The inverse problem of elec. conductivity in the mantle", Geophys. J. Roy. Ast. Soc., 22, 1970, 121-138.

96. A.K. Paul, "The mathematical physical problem of P'(f) to N(h) inversion for anisotropic media", in Ref. 89, 437-449.

97. R.P. Porter, "Diffraction-limited, scalar image formulation with holograms of arbitrary shape", J. Opt. Soc. Am. 60, 1970, 1051-1058.

98. Robert C. Restrick, III, "Electromagnetic scattering by a moving conducting sphere", Radio Science, 3, (12), 1968, 1144-1154.

99. C.D. Rodgers, "Statistical retrieval techniques for sounding the metereological structure of the atmosphere", in Ref.89, 1.26-1.35.

100. H.H. Rosenbrock, "An automatic method for finding the greatest or least value of a function", Computer Journal, 3, Oct. 1960, 175-184.

101. M.R. Rotenberg, R. Bivins, N. Metropolis and J.K. Wooten, Jr., 'The 3-J, and 6-J Symbols', Technology Press M.I.T., Cambridge, Massachusetts.

102. G.T. Ruck, D.E. Barrick, W.D. Stuart and C.K. Krichbaum, ' Radar Cross-Section Handbook', Plenum Press, New York, 1970.

103. S.M. Rytov, "Computation of the skin effect by the perturbation method", Zhur. Eksp. i Teoret. 10, (2), 180-189. [Translation available from K.M. Mitzner].

104. P.C. Sabatier, "Review of the inverse scattering problem at fixed energy in quantum mechanics", in Ref.89, 5.14-5.32.

105. W.K. Saunders, "On solution of Maxwell's equations in an exterior region", Proc. Nat. Aca. Sci., U.S.A., 38, 1952, 342-348.

106. T.B.A. Senior, "Impedance boundary conditions for imperfectly conducting surfaces", Appl. Sci. Res. (Netherlands) 8b, 1960, 418-436.

107. T.B.A. Senior, "Impedance boundary conditions for statistically rough surfaces", Appl. Sci. Res. (Netherlands) 8B, 1960, 437-462.

108. T.B.A. Senior, "A note on impedance boundary conditions", Can. J. Phys. 40, 1962, 663-665.

109. T.B.A. Senior and G.F. Goodrich, "Scattering by a sphere", Proc. IEE (London) III, 1964, 907.

110. L. Shafai, S.J. Towaij and M.A.K. Hamid, "Fast generation of spherical Bessel functions with complex arguments", Electronics Letters, 6, (19), 1970, 612-613.

111. B.D. Sleeman, "The three-dimensional inverse scattering problem for the Helmholtz equation", Proc. Cambridge Phil. Soc. 73, 1973, 477-488.

112. S. Stein, "Addition theorems for spherical wave functions", Quart. Appl. Maths. 19, (1), 1961, 15.

113. D.J. Stigliani, R. Mittra and R.G. Semonin, "Particle-size measurement using forward-scatter holography", J. Opt. Soc. Am. 60, (8), 1970, 1059-1067.

114. J.J. Stoker, "On the uniqueness theorems for the embedding of convex surfaces in three-dimensional space", Com. on Pure and Appl. Mathematics, 3, (3), 1970, 231-257.

115. J.A. Stratton, 'Electromagnetic Theory', McGraw-Hill, New York, 1941.

116. C.T. Tai, 'Dyadic Green's Functions in Electromagnetic Theory', Scranton, Intext Educational Publishers, 1971.

117. C.T. Tai, "On the presentation of Maxwell's theory", Proc. IEEE, 60, (8), 1972, 936-945.

118. W. Trinks, "Zur Vielfachstreuung an kleinen Kugeln", Ann. Phys. Dtsch. 22, 1935, 561.

119. V. Twersky, "Multiple scattering by arbitrary configurations in three-dimensions", J. Math. Phys. 3, 1962, 83.

120. S. Twomey, "The application of numerical filtering to the solution of integral equations encountered in indirect sensing measurements", J. of the Franklin Inst., 279, (2), 1964, 95-109.

121. F.H. Vandenberghe and W.M. Boerner, "A system synthesis approach to the inverse problem of scattering by smooth convex shaped scatterers for the high frequency case", Radio Science, 5, (12), 1972, 1163-1169.

122. F.H. Vandenberghe, 'Aspects of inverse scattering from rotationally symmetric bodies', Ph.D. dissertation, Univ. of Manitoba, Winnipeg, Canada, R3T 2N2, 1972.

123. F.H. Vandenberghe and W.M. Boerner, "On the inverse problem of scattering from a perfectly conducting elliptical cylinder", Can. J. Phys. 50, (17), 1972, 1987-1992.

124. F.H. Vandenberghe and W.M. Boerner, "On the inverse problem of scattering from a perfectly conducting prolate spheroid", Can. J. Phys. 50, (8), 1972, 754-759.

125. H.C. van der Hulst, 'Light Scattering by Small Particles', John Wiley, New York, 1957.

126. J.R. Wait, 'Electromagnetic Waves in Stratified Media, Intern. Ser. of Monogr. on Electromagnetic Waves', Vol. 3, Pergamon Press, The McMillan Co., New York, 1962.

127. J.R. Wait and C.M. Jackson, "Calculations of the bistatic scattering cross-section of a sphere with an impedance boundary condition", Radio Science, J. of Res. Nat. Bur. Stds., 69D, (2), 1965, 299-315.

128. A. Walther, "The question of phase retrieval in optics", Optica Acta, 62, (10), 1962, 41-49.

129. G.N. Watson, 'A Treatise on the Theory of Bessel Functions', Cambridge Univ. Press, New York, 1966.

130. M.R. Weiss, "Inverse scattering in geometrical optics limit', J. Opt. Soc. of America, 58, (11), 1968, 1524-1528.

131. V.H. Weston, "Inverse scattering investigation report No. 1", The Univ. of Michigan Radiation Lab., Rept. No. 8579-1-Q, April 1967.

132. V.H. Weston, "On the inverse problem for a hyperbolic dispersive partial differential equation", J. Math. Phys. 13, (12), 1972, 1952-1956.

133. V.H. Weston, "Theory of absorbers in scattering", IEEE Trans. Ant. and Propag. AP-11, 1963, 578-584.

134. V.H. Weston, "Some special cases of the electromagnetic inverse problem", of Ref.89, 6.48-6.57.

135. V.H. Weston, W.M. Boerner and D.R. Hodgins, 'Inverse scatt. investigation - Quart. reprot no.4', The Univ. of Michigan Radiation Lab. Rept. no. 8579-4-Q, ESD-TR-67-517, IV, Feb. 1968.

136. V.H. Weston and W.M. Boerner, 'Inverse scattering investigation, Final report', Univ. of Michigan, Contract AF-19 (628)-67-C-0190, April 1968.

137. V.H. Weston and W.M. Boerner, "An inverse scattering technique for electromagnetic bistatic scattering", Can. J. Phys. 47, (11), 1969, 1177-1184.

138. V.H. Weston and J.J. Bowman, "Some remarks concerning the design of absorbers in the resonance region", IEEE Trans. Ant. and Propag. AP-13, 1968, 467-468.

139. V.H. Weston, J.J. Bowman and E. Ar, 'Inverse scattering investigation', Final Report, Univ. of Michigan, Contract AF-19 (628)-4884, 1966.

140. V.H. Weston, J.J. Bowman and E. Ar, "On the electromagnetic inverse scattering problem", Archive for Rational Mechs and Analysis, 31, (3), 1968, 199-213.

141. V.H. Weston and R. Hemenger, "High-frequency scattering from a coated sphere", J.Res. Nat. Bur. Stds., 66D, 1962, 237-244.

142. V.H. Weston and R.J. Krueger, "On the inverse problem for a hyperbolic dispersive partial differential equation II", J. Math. Phys. 4, (3), 1973, 406-408.

143. H. Weyl, "Die natürlichen Randwertaufgaben im Aussenraum für Strahlungsfelder beliebiger Dimension,beliebigen Ranges", Math. Z. 56, (12), 1962, 105-119.

144. H. Weyl, "Über die Bestimmung einer geschlossenen konvexen Fläche durch ihr Linienelement", Vierteljahresschrift der naturforschenden Gesellschaft, Zürich, 61, 1916, 40-72.

145. R.A. Wiggins, "Monte Carlo inversion of seismic data", in Ref. 89 , 7.2-7.9.

146. C.H. Wilcox, "An expansion theorem for em fields", J. Rat. Mech. and Anal. 4, 1955, 235-246.

147. D.R. Wilton, "The new numerical approach to the calculation of em properties of two-dimensional bodies of arbitrary cross-section", Ph.D. dissertation, Univ. of Illinois, Urbana, Ill., 1970.

148. D.R. Wilton and R. Mittra, "A new numerical appraoch to the calculation of electromagnetic scattering properties of two-dimensional bodies of arbitrary cross-section", IEEE Trans. Ant. and Propag. AP-20, (3), 1972, 310-317.

149. N.R. Zitron and S.N. Karp, "Higher-order approximations in multiple scattering; II. Three-dimensional scalar cases", J. Math. Phys. 2, 1961, 402.

Additional References:

150. P. Blacksmith, Jr., R.E. Hiatt and R.B. Mack, "Introduction to radar cross-section measurements", Proc. IEEE, 53, (8), 1965, 901-920.

151. J.W. Crispin,Jr. and A.L. Maffett, "Radar cross-section estimation of complex shapes", Proccedings IEEE, 53, Part I, 1965, 972-982.

152. F.G. Friedlander, 'Sound Pulses', London, Cambridge Univ. Press, 1958.

153. A.C. Ludwig, "Calculation of orthogonal function expansions from imperfect data", Technical University of Denmark, Laboratory of Electromagnetic Theory report R-102, 1972.

154. A.C. Ludwig, "Near-field far-field transformations using spherical wave expansions", IEEE Trans., AP-19, 1971, 214-220.

155. C. Müller, 'Mathematical Theory Of Electromagnetic Waves', Springer-Verlag, 1969.

appendix A.1

SCALAR AND VECTOR PRODUCT OPERATIONS ONTO THE FOUR COMPLEMENTARY FORMULATIONS OF THE LEONTOVICH CONDITION

The relationships resulting from scalar and vector product operations of (2.3.1) to (2.3.4) onto one another are presented in detail in this appendix. For convenience of representation, the total magnetic field $\underline{H}_T$ is normalized with respect to the total electric field $\underline{E} = \underline{E}_T$ by the free-space intrinsic impedance Z_0 so that $\underline{H} = Z_0 \underline{H}_T$ and equations (2.3.1) to (2.3.4) assume the following forms [136, 23]:

$$\text{I} : \{[\underline{E} - (\hat{n}\cdot\underline{E})\hat{n}] - \eta\hat{n} \times \underline{H}\} = 0$$

$$\text{II} : \{\underline{E} \times \hat{n} - \eta[\underline{H} - (\hat{n} \cdot \underline{H})\hat{n}]\} = 0$$

$$\text{III} = \text{I}^* : \{[\underline{E}^* - (\hat{n} \cdot \underline{E}^*)\hat{n}] - \eta^*\hat{n} \times \underline{H}^*\} = 0$$

$$\text{IV} = \text{II}^* : \{\underline{E}^* \times \hat{n} - \eta^*[\underline{H}^* - (\hat{n} \cdot \underline{H}^*)\hat{n}]\} = 0$$

Scalar Products

I · I or II · II

$$c_1 = (\underline{E}\cdot\underline{E}) - \eta^2(\underline{H}\cdot\underline{H}) = (\hat{n}\cdot\underline{E})^2 - \eta^2(\hat{n}\cdot\underline{H})^2 \qquad \text{(A1.1)}$$

$$\eta\hat{n}\cdot(\underline{E}\times\underline{H}) = (\hat{n}\cdot\underline{E})^2 - (\underline{E}\cdot\underline{E}) = \eta^2(\hat{n}\cdot\underline{H})^2 - \eta^2(\underline{H}\cdot\underline{H}) \qquad \text{(A1.2)}$$

or

I*·I* or II*·II*

$$c_1^* = (\underline{E}^* \cdot \underline{E}^*) - \eta^{*2}(\underline{H}^*\cdot\underline{H}^*) = (\hat{n}\cdot\underline{E}^*)^2 - \eta^{*2}(\hat{n}\cdot\underline{H}^*)^2 \qquad \text{(A1.3)}$$

$$\eta^*\hat{n}\cdot(\underline{E}^*\times\underline{H}^*) = (\hat{n}\cdot\underline{E}^*)^2 - (\underline{E}^*\cdot\underline{E}^*) = \eta^{*2}(\hat{n}\cdot\underline{H}^*)^2 - \eta^{*2}(\underline{H}^*\cdot\underline{H}^*) \qquad \text{(A1.4)}$$

or

$$c_2^* = (\underline{E}^*\cdot\underline{E}^*) + \eta^{*2}(\underline{H}^*\cdot\underline{H}^*) = [(\hat{n}\cdot\underline{E}^*)^2 + \eta^{*2}(\hat{n}\cdot\underline{H}^*)^2] - 2\eta^*\hat{n}\cdot(\underline{E}^*\times\underline{H}^*)$$

I · II and I*·II*

$$d_1 = 2\eta(\underline{E}\cdot\underline{H}) = 2\eta(\hat{n}\cdot\underline{E})(\hat{n}\cdot\underline{H}) \qquad \text{(A1.5)}$$

$$d_1^* = 2\eta^*(\underline{E}^*\cdot\underline{H}^*) = 2\eta^*(\hat{n}\cdot\underline{E}^*)(\hat{n}\cdot\underline{H}^*)$$

I · I* or II·II*

$$(\hat{n}\times\underline{E})\cdot(\hat{n}\times\underline{E}^*) + \eta\eta^*(\hat{n}\times\underline{H})\cdot(\hat{n}\times\underline{H}^*) + \eta^*\hat{n}\cdot(\underline{E}\times\underline{H}^*) + \eta\hat{n}\cdot(\underline{E}^*\times\underline{H}) = 0 \qquad \text{(A1.6)}$$

or

$$a_2 = (\underline{E}\cdot\underline{E}^*) + \eta\eta^*(\underline{H}\cdot\underline{H}^*) = [(\hat{n}\cdot\underline{E})(\hat{n}\cdot\underline{E}^*) + \eta\eta^*(\hat{n}\cdot\underline{H})(\hat{n}\cdot\underline{H}^*)]$$
$$- \hat{n}\cdot\{\eta(\underline{E}^*\times\underline{H}) + \eta^*(\underline{E}\times\underline{H}^*)$$

$$\hat{n}\cdot\underline{A} = \hat{n}\cdot\{\eta(\underline{E}^*\times\underline{H}) - \eta^*(\underline{E}\times\underline{H}^*)\} = 0 \qquad \text{(A1.7)}$$

$$(\hat{n}\times\underline{E})\cdot(\hat{n}\times\underline{E}^*) - \eta\eta^*(\hat{n}\times\underline{H})\cdot(\hat{n}\times\underline{H}^*) = 0 \qquad \text{(A1.8)}$$

or

$$a_1 = (\underline{E}\cdot\underline{E}^*) - \eta\eta^*(\underline{H}\cdot\underline{H}^*) = (\hat{n}\cdot\underline{E})(\hat{n}\cdot\underline{E}^*) - \eta\eta^*(\hat{n}\cdot\underline{H})(\hat{n}\cdot\underline{H}^*)$$

I·II* or I*·II

$$(\underline{E}\times\underline{E}^*)\cdot\hat{n} + \eta\eta^*(\underline{H}\times\underline{H}^*)\cdot\hat{n} + \eta(\hat{n}\times\underline{H})\cdot(\hat{n}\times\underline{E}^*) - \eta^*(\hat{n}\times\underline{H}^*)\cdot(\hat{n}\times\underline{E}) = 0 \qquad \text{(A1.9)}$$

or

$$b_2 = [\eta(\underline{E}^*\cdot\underline{H}) - \eta^*(\underline{E}\cdot\underline{H}^*)] = [\eta(\hat{n}\cdot\underline{E}^*)(\hat{n}\cdot\underline{H}) - \eta^*(\hat{n}\cdot\underline{E})(\hat{n}\cdot\underline{H}^*)]$$
$$- \hat{n}\cdot\{(\underline{E}\times\underline{E}^*) + \eta\eta^*(\underline{H}\times\underline{H}^*)\}$$

$$\hat{n}\cdot\underline{B} = \hat{n}\cdot\{(\underline{E}\times\underline{E}^*) - \eta\eta^*(\underline{H}\times\underline{H}^*)\} = 0 \qquad \text{(A1.10)}$$

$$\eta(\hat{n}\times\underline{H})\cdot(\hat{n}\times\underline{E}^*) + \eta^*(\hat{n}\times\underline{H}^*)\cdot(\hat{n}\times\underline{E}) = 0 \qquad \text{(A1.11)}$$

or

$$b_1 = \eta(\underline{E}^*\cdot\underline{H}) + \eta^*(\underline{E}\cdot\underline{H}^*) = \eta(\hat{n}\cdot\underline{E}^*)(\hat{n}\cdot\underline{H}) + \eta^*(\hat{n}\cdot\underline{E})(\hat{n}\cdot\underline{H}^*)$$

Vector Products

I x I* or II x II*

$$\hat{n}\cdot\{(\underline{E}x\underline{E}^*) + \eta\eta^*(\underline{H}x\underline{H}^*)\} = \{\eta^*(\hat{n}x\underline{E})\cdot(\hat{n}x\underline{H}^*) - \eta(\hat{n}x\underline{E}^*)\cdot(\hat{n}x\underline{H})\} \quad (A1.12)$$

$$\eta(\hat{n}x\underline{E}^*)\cdot(\hat{n}x\underline{H}) = -\hat{n}\cdot(\underline{E}x\underline{E}^*) = -\eta\eta^*\hat{n}\cdot(\underline{H}x\underline{H}^*) \quad (A1.13)$$

$$\eta^*(\hat{n}x\underline{E})\cdot(\hat{n}x\underline{H}^*) = \hat{n}\cdot(\underline{E}x\underline{E}^*) = \eta\eta^*\hat{n}\cdot(\underline{H}x\underline{H}^*) \quad (A1.14)$$

$$\{\eta^*(\hat{n}x\underline{E})\cdot(\hat{n}x\underline{H}^*) - \eta(\hat{n}x\underline{E}^*)\cdot(\hat{n}x\underline{H})\} = 2\hat{n}\cdot(\underline{E}x\underline{E}^*) = 2\eta\eta^*(\underline{H}x\underline{H}^*)\cdot\hat{n} \quad (A1.15)$$

I x II* and I* x II

$$\hat{n}\{(\hat{n}x\underline{E})\cdot(\hat{n}x\underline{E}^*) + \eta\eta^*(\hat{n}x\underline{H})\cdot(\hat{n}x\underline{H}^*)\} + \eta(\hat{n}x\underline{E}^*)\ x\ (\hat{n}x\underline{H}) + \eta^*(\underline{E}x\underline{H}^*)$$
$$+ \eta^*[(\underline{E}x\underline{H}^*)\ x\ \hat{n}]\ x\ \hat{n} = 0 \quad (A1.16)$$

$$\hat{n}\{(\hat{n}x\underline{E})\cdot(\hat{n}x\underline{E}^*) + \eta\eta^*(\hat{n}x\underline{H})\cdot(\hat{n}x\underline{H}^*)\} + \eta^*(\hat{n}x\underline{E})\ x\ (\hat{n}x\underline{H}^*) + \eta(\underline{E}^*x\underline{H})$$
$$+\eta[(\underline{E}^*x\underline{H})\ x\ \hat{n}]\ x\ \hat{n} = 0 \quad (A1.17)$$

$$\eta(\hat{n}x\underline{E}^*)\ x\ (\hat{n}x\underline{H}) - \eta^*(\hat{n}x\underline{E})\ x\ (\hat{n}x\underline{H}^*) = \hat{n}\cdot[\eta(\underline{E}^*x\underline{H}) - \eta^*(\underline{E}x\underline{H}^*)]\hat{n} = 0 \quad (A1.18)$$

I* x II - I x II*

$$[\eta(\underline{E}^*x\underline{H}) - \eta^*(\underline{E}x\underline{H}^*)] = \hat{n}\ x\ \{[\eta(\underline{E}^*x\underline{H}) - \eta^*(\underline{E}x\underline{H}^*)]\ x\ \hat{n}\} \quad (A1.19)$$

where

$$[\eta(\underline{E}^*x\underline{H}) - \eta^*(\underline{E}x\underline{H}^*)] = [\underline{E}^*x(\underline{E}x\hat{n}) - \underline{E}\ x\ (\underline{E}^*x\hat{n})]$$
$$+ \eta\eta^*\{(\hat{n}\cdot\underline{H})[(\hat{n}x\underline{H}^*)\ x\ \hat{n}] - (\hat{n}\cdot\underline{H}^*)[(\hat{n}x\underline{H})\ x\ \hat{n}]\}$$
$$= [(\underline{E}^*\cdot\hat{n})\underline{E} - (\underline{E}\cdot\hat{n})\underline{E}^*] + \eta\eta^*[(\underline{H}\cdot\hat{n})\underline{H}^* - (\underline{H}^*\cdot\hat{n})\underline{H}]$$
$$= \hat{n}\ x\ [(\underline{E}x\underline{E}^*) - \eta\eta^*(\underline{H}x\underline{H}^*)] \quad (A1.20)$$

$$[(\underline{E}x\underline{E}^*) - \eta\eta^*(\underline{H}x\underline{H}^*)] = \{\eta^*[\underline{E}x(\hat{n}x\underline{H}^*)] - \eta[\underline{H}x(\underline{E}^*x\hat{n})\}$$
$$+ \{(\hat{n}\cdot\underline{E}^*)\underline{E}\ x\ \hat{n} - \eta\eta^*(\hat{n}\cdot\underline{H}^*)\underline{H}\ x\ \hat{n}\}$$
$$= \hat{n}\{[(\underline{E}^*\cdot\underline{H})\eta + \eta^*(\underline{E}\cdot\underline{H}^*)] - \underbrace{[\eta(\hat{n}\cdot\underline{E}^*)(\hat{n}\cdot\underline{H}) + \eta^*(\hat{n}\cdot\underline{E})(\hat{n}\cdot\underline{H}^*)]}\}$$
$$\equiv 0 \quad \text{according to (A1.11)}$$

$$+ \{[\eta(\hat{n}\cdot\underline{E}^*)\underline{H} - \eta(\hat{n}\cdot\underline{H})\underline{E}^*] - [\eta^*(\hat{n}\cdot\underline{E})\underline{H}^* - \eta^*(\hat{n}\cdot\underline{H}^*)\underline{E}]\}$$

$$= [\eta(\underline{E}^*x\underline{H}(- \eta^*(\underline{E}x\underline{H}^*)] \times \hat{n} \qquad \text{(A1.21)}$$

This concludes the derivation of scalar and vector product operations which result into the following important identities according to (A1.17), (A1.10), (A1.18) and (A1.19) to (A1.21)

$$\hat{n}\cdot\underline{A} = \hat{n}\cdot[(\underline{E}x\underline{E}^*) - \eta\eta^*(\underline{H}x\underline{H}^*)] = 0 \qquad \text{(A1.22)}$$

$$\hat{n}\cdot\underline{B} = \hat{n}\cdot[\eta(\underline{E}^*x\underline{H}) - \eta^*(\underline{E}x\underline{H}^*)] = 0 \qquad \text{(A1.23)}$$

$$\underline{A} = (\underline{E}x\underline{E}^*) - \eta\eta^*(\underline{H}x\underline{H}^*) = [\eta(\underline{E}^*x\underline{H}) - \eta^*(\underline{E}x\underline{H}^*)] \times \hat{\underline{n}} = \underline{B} \times \hat{n} \qquad \text{(A1.24)}$$

and

$$\underline{B} = \eta(\underline{E}^*x\underline{H}) - \eta^*(\underline{E}x\underline{H}^*) = \hat{n} \times [(\underline{E}x\underline{E}^* - \eta\eta^*(\underline{H}x\underline{H}^*)] = \hat{n} \times \underline{A} \qquad \text{(A1.25)}$$

Thus $\underline{A}$ and $\underline{B}$ represent two orthogonal vectors which lie in the local tangent plane of the scatterer so that

$$\underline{A} \cdot \underline{B} = 0 \qquad \text{(A1.26)}$$

and its cross product $\underline{D} = \underline{A} \times \underline{B}$ is purely real vector directed along the outward normal $\hat{n}$ of the scatterer.

Further details of derivation are presented in Weston and Boerner [136] and in Boerner and Ahluwalia [23] to which the reader is referred.

appendix A.2

COEFFICIENTS OF EQUATION (3.4.14)

The coefficients of the characteristic equation

$$e_1 \tan^4\psi + e_2 \tan^3\psi + e_3 \tan^2\psi + e_4 \tan\psi + e_5 = 0$$

can be calculated, as is shown in Boerner and Ahluwalia [23] as

$$e_5 = 4(\underline{a}\cdot\underline{d})(\underline{b}\cdot\underline{d})(\underline{d}\cdot\underline{d}) - (\underline{a}\cdot\underline{a})(\underline{b}\cdot\underline{d})(\underline{b}\cdot\underline{d}) - (\underline{b}\cdot\underline{b})(\underline{a}\cdot\underline{d})(\underline{a}\cdot\underline{d}) + 2(\underline{a}\cdot\underline{b})(\underline{a}\cdot\underline{d})(\underline{b}\cdot\underline{d}) \quad \text{(A2.1)}$$

$$e_4 = 8(\underline{a}\cdot\underline{d})(\underline{b}\cdot\underline{d})(\underline{d}\cdot\underline{c}) + 4(\underline{a}\cdot\underline{d})(\underline{d}\cdot\underline{d})(\underline{b}\cdot\underline{c}) + 4(\underline{b}\cdot\underline{d})(\underline{d}\cdot\underline{d})(\underline{a}\cdot\underline{c}) + 2(\underline{a}\cdot\underline{b})(\underline{a}\cdot\underline{d})(\underline{b}\cdot\underline{c}) + 2(\underline{a}\cdot\underline{b})(\underline{b}\cdot\underline{d})(\underline{a}\cdot\underline{c}) - 2(\underline{b}\cdot\underline{b})(\underline{a}\cdot\underline{d})(\underline{a}\cdot\underline{c}) - 2(\underline{a}\cdot\underline{a})(\underline{b}\cdot\underline{d})(\underline{b}\cdot\underline{c}) \quad \text{(A2.2)}$$

$$e_3 = 8(\underline{a}\cdot\underline{d})(\underline{d}\cdot\underline{c})(\underline{b}\cdot\underline{c}) + 8(\underline{b}\cdot\underline{d})(\underline{d}\cdot\underline{c})(\underline{a}\cdot\underline{c}) + 4(\underline{d}\cdot\underline{d})(\underline{b}\cdot\underline{c})(\underline{a}\cdot\underline{c}) + 4(\underline{c}\cdot\underline{c})(\underline{a}\cdot\underline{d})(\underline{b}\cdot\underline{d}) - (\underline{a}\cdot\underline{a})(\underline{b}\cdot\underline{d})(\underline{b}\cdot\underline{d}) - (\underline{b}\cdot\underline{b})(\underline{a}\cdot\underline{d})(\underline{a}\cdot\underline{d}) + 2(\underline{a}\cdot\underline{b})(\underline{a}\cdot\underline{d})(\underline{b}\cdot\underline{d}) - (\underline{a}\cdot\underline{a})(\underline{b}\cdot\underline{c})(\underline{b}\cdot\underline{c}) - (\underline{b}\cdot\underline{b})(\underline{a}\cdot\underline{c})(\underline{a}\cdot\underline{c}) + 2(\underline{a}\cdot\underline{b})(\underline{b}\cdot\underline{c})(\underline{a}\cdot\underline{c}) \quad \text{(A2.3)}$$

$$e_2 = 4(\underline{c}\cdot\underline{c})(\underline{a}\cdot\underline{d})(\underline{b}\cdot\underline{c}) + 4(\underline{c}\cdot\underline{c})(\underline{b}\cdot\underline{d})(\underline{a}\cdot\underline{c}) + 8(\underline{d}\cdot\underline{c})(\underline{b}\cdot\underline{c})(\underline{a}\cdot\underline{c}) + 2(\underline{a}\cdot\underline{b})(\underline{a}\cdot\underline{d})(\underline{b}\cdot\underline{c}) + 2(\underline{a}\cdot\underline{b})(\underline{b}\cdot\underline{d})(\underline{a}\cdot\underline{c}) - 2(\underline{b}\cdot\underline{b})(\underline{a}\cdot\underline{d})(\underline{a}\cdot\underline{c}) - 2(\underline{a}\cdot\underline{a})(\underline{b}\cdot\underline{d})(\underline{b}\cdot\underline{c}) \quad \text{(A2.4)}$$

$$e_1 = 4(\underline{c}\cdot\underline{c})(\underline{b}\cdot\underline{c})(\underline{a}\cdot\underline{c}) - (\underline{a}\cdot\underline{a})(\underline{b}\cdot\underline{c})(\underline{b}\cdot\underline{c}) - (\underline{b}\cdot\underline{b})(\underline{a}\cdot\underline{c})(\underline{a}\cdot\underline{c}) + 2(\underline{a}\cdot\underline{b})(\underline{b}\cdot\underline{c})(\underline{a}\cdot\underline{c}) \quad \text{(A2.5)}$$

where

$$\underline{a} = -j(\underline{E} \times \underline{E}^*), \qquad \underline{b} = -j(\underline{H} \times \underline{H}^*), \qquad \underline{c} = \frac{1}{2}[(\underline{E}^* \times \underline{H}) + (\underline{E} \times \underline{H}^*)]$$

and

$$\underline{d} = \frac{1}{2}j[\underline{E} \times \underline{H}^*) - (\underline{E}^* \times \underline{H})]$$

all being vector quantities.

appendix A.3

COEFFICIENTS OF ADDITION THEOREMS

The possibility of obtaining the em fields in the vicinity of the three-dimensional scatterer accurately and optimally depends upon efficient computation of the translation coefficients $A_{\mu\nu}^{mn}$ and $B_{\mu\nu}^{mn}$ of (5.4.5a) and (5.4.5b). Equations (5.4.5a) and (5.4.5b) involve coefficients $a(m,n,\mu,\nu,p)$ defined by the linearized expansion

$$p_n^m(x)p_\nu^\mu(x) = \sum_p a(m,n,\mu,\nu,p)p_p^{m+\mu}(x) \tag{A3.1}$$

where p extends from $|n-\nu|$ to $|n+\nu|$ with integer steps of 2. The coefficients $a(m,n,\mu,\nu,p)$ in turn are defined by [38]

$$a(m,n,\mu,\nu,p) = (-1)^{m+\mu}(2p+1)\left[\frac{(n+m)!(\nu+\mu)!(p-m-\mu)!}{(n-m)!(\nu-\mu)!(p+m+\mu)!}\right]^{1/2}$$

$$\begin{pmatrix} n & \nu & p \\ 0 & 0 & 0 \end{pmatrix}\begin{pmatrix} n & \nu & p \\ m & & \mu-m-\mu \end{pmatrix} \tag{A3.2}$$

where $\begin{pmatrix} j_1 & j_2 & j_3 \\ m_1 & m_2 & -m_1-m_2 \end{pmatrix}$ is the Wigner 3-j symbol[40,101].Out of many different representations for 3-j symbols, Van der Waerden's definition[40] is the most convenient for the present discussion and is given as

$$\begin{pmatrix} n & \nu & p \\ m & \mu & -m-\mu \end{pmatrix} = (-1)^{n-\nu-m-\mu}$$

$$\left[\frac{(n+\nu-p)!(n-\nu+p)!(-n+\nu+p)!(n+m)!(n-m)!(\nu+\mu)!(\nu-\mu)!(\nu-\mu)!(p+m+\mu)!(p-m-\mu)!}{(n+\nu+p+1)!}\right]^{1/2}$$

$$\sum_k (-1)^k[k!(n+\nu-p-k)!(n-m-k)!(\nu+\mu+k)!(p-\nu+m+k)!(p-n-\mu-k)!]^{-1}$$

(A3.3)

Because of the multitude of factorials appearing in above definition of 3-j symbols, calculation of (5.4.5a) and (5.4.5b) using (A3.3) is highly inefficient. The following three-term recursion formula reduces the computation time considerably

$$a(m,n,\mu,\nu,p)\alpha_p + a(m,n,\mu,\nu,p-2)\alpha_{p-2} + a(m,n,\mu,\nu,p-4)\alpha_{p-4} = 0 \quad \text{(A3.4)}$$

where

$$\alpha_p = -(2p-5)(p+m_3-1)(n+\nu+p+1)(-n+\nu+p)[(p-\nu-3)\mu-m(\nu+1)]$$
$$\{[(p+m_3)(n+\nu-p+1)(n-\nu+p)(\mu(p+\nu)+m(\nu+1))]/$$
$$[(2p+1)(\nu-\mu+1)((m-\mu)p(p-1)-m_3(n-\nu)(n+\nu+1))]\}$$

$$\alpha_{p-2} = (2p-1)(2p-5)(\nu+\mu+1)[(m-\mu)(p-1)(p-2)-m_3(n-\nu+1)(n+\nu+2)]$$
$$-(2p-1)(p-m_3-2)(n+\nu-p+4)(n-\nu+p-3)[\mu(p+\nu)+m(\nu+1)]$$
$$\{[(p+m_3-2)(n+\nu-p+3)(n-\nu+p-2)(\mu(p+\nu-2)+m(\nu+1))]/$$
$$[(2p-3)(\nu-\mu+1)(m-\mu)(p-2)(p-3)-m_3(n-\nu)(n+\nu+1))]\}$$
$$-(2p-5)(p+m_3-1)(n+\nu+p+1)(-n+\nu+p)[(p-\nu-3)\mu-m(\nu+1)]$$
$$\{[(p-m_3-1)(-n+\nu+p-1)(n+\nu+p)(\mu(p-\nu-1)-m(\nu+1))]/$$
$$[(2p-3)(\nu-\mu+1)((m-\mu)p(p-1)-m_3(n-\nu)(n+\nu+1))]\}$$

$$\alpha_{p-4} = -(2p-1)(p-m_3-2)(n+\nu-p+4)(n-\nu+p-3)[\mu(p+\nu)+m(\nu+1)]$$
$$\{[(p-m_3-3)(-n+\nu+p-3)(n+\nu+p-2)(\mu(p-\nu-3)-m(\nu+1))]/$$
$$[(2p-7)(\nu-\mu+1)((m-\mu)(p-2)(p-3)-m_3(n-\nu)(n+\nu+1))]\}$$

In using (A3.4) backward-recursion is used with starting values given by [30].

$$a(m,n,\mu,\nu,n+\nu) = \frac{(2n-1)!!(2\nu-1)!!}{(2n+2\nu-1)!!} \frac{(n+\nu-m_3)!}{(n-m)!(\nu-\mu)!}$$

and

$$a(m,n,\mu,\nu,n+\nu-2) = \frac{(2n+2\nu-3)}{(2n-1)(2\nu-1)(n+\nu-m_3)(n+\nu-m_3-1)}$$

$$\{(n+\nu-1)[n\nu+m\mu(2n+2\nu-1)]-m_3[\nu m(2\nu-1)+n\mu(2n-1)]\}a(m,n,\nu,\mu,n+\nu) \tag{A3.5}$$

For the special case of translation along the axis, the coefficients $A_{\mu\nu}^{mn}$ and $B_{\mu\nu}^{mn}$ attain the simple form

$$A_{\mu\nu}^{mn} = (-1)^m j^{\nu-n} \frac{2\nu+1}{2\nu(\nu+1)} \sum_p j^p [n(n+1)+\nu(\nu+1)-p(p+1)]$$

$$a(m,n,-m,\nu,p)Z_p^r(kd) \tag{A3.6}$$

$$B_{\mu\nu}^{mn} = (-1)^m j^{\nu-n} \frac{(2\nu+1)}{2\nu(\nu+1)} \sum_p j^p (2jmkd)a(m,n,-m,\nu,p)Z_p^{(r)}(kd) \tag{A3.7}$$

where $r = 1$ for exterior expansion and $r = 3$ for interior expansion. The recursion formula for computing $a(m,n,-m,\nu,p)$, as given in Bruning and Lo [31], is

$$\alpha_{p-3}a_{p-4}-(\alpha_{p-2}+\alpha_{p-1}-4m^2)a_{p-2}+\alpha_p a_p = 0 \tag{A3.8}$$

where

$$a_p = a(m,n,-m,\nu,p)$$

$$\alpha_p = c(p)c(-p) \tag{A3.9}$$

and

$$c(p) = \frac{1}{2p+1}\,(n+\nu+p+1)(n-\nu+p) \tag{A3.10}$$

The two starting values are

$$a_{n+\nu} = \frac{(2n-1)!!(2\nu-1)!!}{(2n+2\nu-1)!!}\;\frac{(n+\nu)!}{(n-m)!(\nu+m)!} \tag{A3.11}$$

$$a_{n+\nu-2} = \frac{2n+2\nu-3}{(2n-1)(2\nu-1)(n+\nu)}\,[\nu n-m^2(2n+2\nu-1)]a_{n+\nu} \tag{A3.12}$$

Many other relevant recursion formulae are given in the Appendices of [38,30].

appendix A.4

SUMMARY OF CABAYAN, MURPHY AND PAVLASEK'S ANALYSIS [33]

Application of the Helmholtz theorem [57] to a source-free region outside the minimum circle C (Fig. 4.3) of radius r_a, results in the following integral equation for the far-field pattern function $g(\phi)$

$$g(\phi) = kr_a \int_0^{2\pi} f(\theta) \frac{\partial G}{\partial (kr)} \, d\theta \qquad \text{(A4.1)}$$

where $f(\theta)$ represents the field on the circle C and G is the Green's function of the first kind that vanishes on C and is given by [ ]

$$G(\theta,\phi) = \frac{1}{4j} \sum_n H_n^{(1)}(kr_1)[J_n(kr)+c_n H_n^{(1)}(kr)]\exp[jn(\theta-\phi)] \qquad \text{(A4.2)}$$

where

$$c_n = -J_n(kr_a)/H_n^{(1)}(kr_a) \qquad \text{(A4.3)}$$

The normal derivative $\partial G/\partial(kr)$ at $r = r_a$ is,

$$\left.\frac{\partial G}{\partial (kr)}\right|_{r=r_a} = \frac{1}{2\pi kr_a} \sum \frac{H_n^{(1)}(kr_1)}{H_n^{(1)}(kr_a)} \exp\,[jn(\theta-\phi)] \qquad \text{(A4.4)}$$

Substituting (A4.4) into (A4.1), we obtain

$$g(\phi) = \frac{1}{2\pi} \sum_n \frac{H_n^{(1)}(kr_1)}{H_n^{(1)}(kr_a)} \int_0^{2\pi} f(\theta)\exp[jn(\theta-\phi)] \, d\theta \qquad \text{(A4.5)}$$

Defining a_n and b_n as

$$a_n = \frac{1}{2\pi} \int_0^{2\pi} f(\theta) \exp\,(jn\theta) \, d\theta$$

and

$$b_n = a_n \frac{H_n^{(1)}(kr_1)}{H_n^{(1)}(kr_0)}$$

the far field pattern function becomes

$$g(\phi) = \sum_n b_n \exp(-jn\phi) \qquad \text{(A4.6)}$$

Due to measurement and numerical quadrature errors involved in the reconstruction, an upper bound is inflicted on the number of coefficients to be used in the series expansions of (A4.6). To simplify the analysis, Cabayan et al. introduce operator notation to relate the fields g and f via the operator T

$$g = Tf \qquad \text{(A4.7)}$$

where the operator T is defined by (A4.5).

The numerical form of (A4.7) is written as

$$Ax = y + \varepsilon$$

where A, x and y are the discrete forms of T, f and g, respectively, and ε is the total equivalent error vector.

The eigen-values of this problem can be determined directly for T^*T from the eigen-value equation

$$T^*T\phi_n = \lambda_n \phi_n \qquad \text{(A4.9)}$$

Substitution of T from (A4.5), results into

$$T^*T\phi_n = \frac{1}{2\pi} \sum_n \frac{|H_n^{(1)}(kr_1)|^2}{|H_n^{(1)}(kr_a)|^2} \int_0^{2\pi} \phi_n(\theta)\exp[jn(\theta-\theta')]\, d\theta \qquad \text{(A4.10)}$$

With the trial-eigen-functions given by $\phi_n = \exp(-jn\theta)$, (A4.10) yields the following expression for the eigen-values λ_n

$$\lambda_n = \frac{|H_n^{(1)}(kr_1)|^2}{|H_n^{(1)}(kr_a)|^2} \qquad \text{(A4.11)}$$